

International PhD Program in Neuroscience

XXXV Cycle

**Development of nanomedicines for ophthalmic
drug delivery**

PhD Thesis

Alessia Romeo

Coordinator: Prof. Claudio Bucolo

Tutor: Prof.ssa Teresa Musumeci



Department of Biomedical and Biotechnological Sciences.

University of Catania - Medical School

This project was supported with a fellowship by the International PhD Program in Neuroscience from the University of Catania, School of Medicine (Catania, Italy).

The work for this thesis was carried out in the laboratories of:

Home Institute

Professor Teresa Musumeci

Department of Drug and Health

Sciences, Laboratory of Drug

Delivery Technology

University of Catania

Viale A. Doria, 6, 95125

Catania, Italy

Guest Institute

Professor Romána Zelkó

University of Pharmacy

Department of Pharmacy

Administration

Semmelweis University

Högyes Endre Street 7-9, 1092

Budapest, Hungary

International mobility project partly funded by

Erasmus+ Mobility Network grant



Erasmus+

ABSTRACT	3
CHAPTER I: General Introduction	9
1. NEURODEGENERATIVE OCULAR DISEASES.....	10
2. THE ROLE OF OXIDATIVE STRESS AND MITOCHONDRIAL DYSFUNCTION	11
3. MITOCHONDRIAL DYSFUNCTION IN RETINAL DISEASES	13
4. NEUROPROTECTIVE AGENTS AGAINST OXIDATIVE DAMAGE	17
5. DELIVERY TO THE POSTERIOR EYE SEGMENT: ROUTES OF ADMINISTRATION AND LIMITS	22
6. NANOMEDICINE FOR THE POTENTIAL TREATMENT OF OCULAR DISEASES	30
7.1. Polymeric nanoparticles	34
7.2. Lipid nanoparticles	38
7.3. Hybrid Nanoparticles.....	40
7.4. Nanofibers	42
7. MATERIALS SELECTED IN THIS PROJECT	45
11.1. Polymers.....	45
11.2. Lipids.....	50
8. QUALITY BY DESIGN AND DESIGN OF EXPERIMENT	53
9. AIM OF THE PROJECT	58

CHAPTER II: Ferulic Acid-Loaded Polymeric Nanoparticles for Potential Ocular Delivery	61
CHAPTER III: Melatonin loaded hybrid nanomedicine: DoE approach, optimization and in vitro study on diabetic retinopathy model	84
CHAPTER IV: mPEG-PLGA Nanoparticles Labelled with Loaded or Conjugated Rhodamine-B.....	124
CHAPTER V: Fluorescent Nanosystems for Drug Tracking and Theranostics: Recent Applications in the Ocular Field.....	150
CHAPTER VI: Multilevel statistical optimization: ion pair complexes with flunarizine dihydrochloride encapsulated in nanostructured lipid carriers for potential ocular delivery	188
CHAPTER VII: Electrospun nanofibers for melatonin ocular delivery.....	199
CHAPTER VIII: General Discussion	207
CHAPTER IX: Conclusions	214
CHAPTER IX: References	217
CHAPTER X: Annexes	261
List of Publications and Scientific Contributions.....	262
1. Publications.....	262
2. Conference proceedings.....	263

ABSTRACT

The prevalence of ocular neurodegenerative diseases is growing in the elderly population but also among younger people. These disorders cause impairment and reduction of vision and in the most severe cases lead to irreversible blindness. The etiology is not completely clear, the mechanisms behind the onset of these diseases is currently much discussed. Age and genetic abnormalities are among the most relevant critical factors, but oxidative cellular stress plays a crucial role. Natural molecules such as terpenoid, phenolic and alkaloid compounds have shown excellent antioxidant, anti-radical and anti-inflammatory properties, proving to be excellent neuroprotective agents. Thyroid, pituitary, pancreatic, sexual and neurosteroid hormones have shown antioxidant, anti-apoptotic and anti-inflammatory activities, attracting great interest due to their neuroprotective effect on several models of neuronal degeneration. Calcium channel blockers by restoring homeostasis of neuronal calcium channels, improved neurological damage and were effective in preventing neuronal death.

Despite the benefits of these molecules, their ocular administration shows many challenges to overcome. Increasing the poor drug bioavailability in intraocular tissues is one of the biggest challenges. Recent advances in nanomedicines have contributed to improve drug delivery to the posterior eye segment. Nanosystems have provided manifold advantages, including the ability to improve the delivery of poorly soluble drugs and provide protection against enzymatic degradation. Nanocarrier modifications on the surface allow to bypass ocular barriers, improving penetration and ensuring effective drug delivery to intraocular target tissues. So, the composition of nanocarriers plays a critical role in establishing properties such as drug loading, release profiles and site of action.

Currently, the incorporation of drugs in nanovectors has been shown to improve the amount of drugs delivery to the posterior eye segment.

Ensuring quality, safety and efficacy parameters is necessary to receive regulatory approval for the marketing of new drug delivery devices. For this purpose, it may be useful to follow a rational approach during the design of innovative platforms. The use of systematic methods such as Quality by Design has proven effective in producing nanomedicines with the desired quality parameters. The multivariate statistical approach of Design of Experiment assured successful design and optimization methodologies.

Moreover, tracking nanosystems using fluorescent probes could be an effective and non-invasive strategy to quantify and evaluate drug release and to monitor biodistribution *in vivo*.

Taking into account these considerations, the aim of my doctoral thesis was to explore innovative platforms as ocular drug delivery systems. This thesis focused on the design, optimization, preparation and characterization of polymeric, lipid, hybrid nanoparticles (NPs) and nanofibers aimed to improve ocular delivery, especially targeting the posterior region of the eye. Molecules with a neuroprotective action (ferulic acid, flunarizine dihydrochloride and melatonin) were incorporated with the purpose to produce nanodevices for potential treatment of chronic neurodegenerative diseases such as age-related macular degeneration, diabetic retinopathy and glaucoma.

In **paper I** (*Romeo et al. – Pharmaceutics – 2021*) two types of polymeric NPs (PLA and PLGA) were investigated for the potential intravitreal delivery of ferulic acid. The biodegradable and biocompatible polymers PLA and PLGA with low molecular weights and slow degradation rate were selected to provide sustained release profiles and to improve drug bioavailability in intraocular tissues. This work was based on extensive

technological analyses with the aim of obtaining a NP powder with a simple composition and long-term storage suitable for intravitreal delivery. A preliminary *in vitro* study was performed on empty nanocarriers to assess the absence of cytotoxicity on retinal endothelial and pericyte cells. Different purification techniques were explored to remove traces of surfactant and unencapsulated drug and to make the nanocarriers suitable for *in vitro* and *in vivo* studies. To extend shelf life, the nanosuspensions were lyophilized. The formulations were cryoprotected with 5% (w/v) HP- β -Cyd to maintain physico-chemical properties were maintained after reconstitution of the freeze-dried powder. Thermal and spectroscopic analyses were performed to determine the effective encapsulation of the drug in the polymer matrix. Morphological analyses showed NPs with spherical shape and smooth surface. The nanocarriers showed high encapsulation efficiency (between 64,86 e 75,16%) and controlled release profiles. Our results suggested that the developed carriers could be tested *in vitro* in animal models to evaluate their efficacy compared to the free drug.

In the **paper II** (*Romeo et al – 2022 – Int. J. Pharm.*) an eye drop for melatonin (MEL) delivery to the posterior segment of the eye was designed and optimized. Hybrid NPs were produced from a mucopenetrating PLGA-PEG polymer matrix and a cationic lipid coating with mucoadhesive properties. Simple, reproducible one-step nanoprecipitation was employed to prepare the hybrid NPs. Design and optimization were performed using Design of Experiment (DoE). Preservative addition to the optimized nanosuspension and sterilization by UV exposure were performed to qualify the formulation as an eye drop. Microbiological tests demonstrated the efficacy of the preservative and the sterilization method. The nanosuspension remained stable for up to 6 months under refrigerated storage conditions. The mucoadhesive properties were demonstrated through the mucin

particle method. MEL was released from the nanocarriers with a sustained and prolonged profile. Thermal and spectroscopic analyses confirmed the interaction between the lipid components and the polymer matrix. An *in vitro* model of diabetic retinopathy was used to evaluate the neuroprotective and antioxidant activity of melatonin on human retinal endothelial cells. Ocular tolerability was ascertained by the Draize Test. This study demonstrated a robust and effective delivery nanomedicine for the potential management of neurodegenerative retinal disorders.

In **paper III** (*Craparo et al. – 2021 – Pharmaceuticals*) fluorescent polymer nanosystems were developed as vectors for *in vitro/in vivo* imaging studies. PLGA-PEG was employed as a mucopenetrating polymer. The fluorescent probe Rhodamine B was used to label NPs following two strategies: encapsulation and covalent grafting on the backbone of the copolymer. The systems were extensively characterized in terms of size, polydispersity, surface charge and pegylation density to assess the suitability of the formulations in nose-to-brain delivery. Purification by centrifugation allowed the removal of unencapsulated dye in order to avoid artefacts during data interpretation in tracking studies. Release profiles confirmed the effective entrapment of the fluorescent probe. Cytotoxicity tests on olfactory ensheathing cells and neuronal PC12 cells were conducted to assess the safety of the formulations in brain targeting. The results suggested that the grafting method provided the most stable labelling. Both nanosystems were efficiently internalized into cells, proving to be suitable nanocarriers for possible cell tracking studies. In the published manuscript fluorescent nanosystems with Rhodamine B were studied as drug transport models to explore cellular internalization for potential intranasal administration for brain target. The same carrier could also be investigated to evaluate ocular distribution.

For this reason, a deeply literature study was carried out and allowed to write the **review IV** (*Zingale, Romeo et al. – 2022 – Pharmaceutics*), in which fluorescent nanosystems for diagnostic and theranostic uses in the ocular field manufactured in the last five years were reviewed. A summary of the most widely used fluorescent probes was presented and their classification was drawn up according to the classes to which they belong. Fluorescent nanosystems were discussed on the basis of their polymeric, lipidic, metallic and protein nature. An overview of the use of fluorescent markers in clinical studies and on the market was also discussed. This review showed that the application of fluorescent nanosystems has proven to be a promising strategy for targeting and their use is growing to translate designed nanoformulations into drugs for marketing.

Paper V (*in progress*) aimed to encapsulate flunarizine dihydrochloride in a lipid matrix. The hydrophobic ion-pair technique was employed to modify the salt solubility. The most suitable ion-pair (flunarizine-counterion) complex was investigated by DoE. Citric, oxalic and sorbic organic acids at different molar ratios (1:1, 1:2 and 1:4) were examined. The complex binding efficiency was measured by UV spectrophotometry. The solid-state complexes were analyzed by spectroscopic and calorimetric analysis. Nanostructured lipid carriers (NLCs) were prepared from the solid lipid Gelucire[®] 44/14 and the liquid lipid Miglyol[®] 812. Gelucire[®] 44/14 was selected to provide a sustained drug release profile. A fusion-emulsification preparation method combined with a low-energy injection technique was used to prepare the NLCs. Design and optimization of the nanocarriers was performed using DoE, where different concentrations of the two lipids and of a surfactant mixture were tested.

Paper VI (*in progress*) in collaboration with Professor Romàna Zelkó of Semmelweis University concerns the preparation of nanofiber-based ocular inserts for MEL delivery.

The production of the nanofibers was carried out using the electrospinning technique. Composite nanofibers were prepared from two polymers of different nature, hydrophobic PLA and hydrophilic PVA. Both nanofibers were loaded with MEL at different concentrations (0.1, 0.3 and 0.5 % wt). The addition of the permeation enhancer Tween® 80 (0.5% wt) was investigated. The nanofibers morphology was examined by scanning electron microscopy (SEM). Release profiles was monitored by UV spectrophotometry. Preliminary results showed different dissolution rates of the nanofibers. PVA due to its high solubility in aqueous medium showed immediate MEL release, unlike PLA that provided sustained drug release. The electrospinning technique was effectively used to produce MEL-loaded nanofibers that could be interesting vehicles for MEL ocular delivery.

CHAPTER I: *General Introduction*

1. NEURODEGENERATIVE OCULAR DISEASES

The human eye is a sense organ in intimate connection with the brain so much to be considered as a brain extension. In fact, both the brain and the retina originate from the neural tube and are made up of neurons. Retina, an integral part of the brain, is a tissue of nervous origin that forms the innermost layer of the eyeball. This membrane contains two types of light-sensitive cells, the photoreceptors properly called cones and rods. This structure acts as a transducer, capturing light stimuli, processing them and converting them into bioelectric signals. These are responsible for visual interpretation and are transmitted via the optic nerve fibers to the brain structures of the central nervous system (CNS) (Marchesi et al., 2021).

In order to safeguard the neuronal environment, the eye and the CNS are protected by physiological barriers consisting of non-fenestrated endothelial cells connected by tight junctions, the blood-retinal barrier (BRB) and the blood-brain barrier (BBB) respectively. Any insult to the optic nerve or CNS results in axonal degeneration, resulting in localized oxidative stress, reduction of neurotrophic factors, toxic levels of neurotransmitters and generally disruption of the physiological environment and neurotoxicity. The resulting neurotoxic environment is unsuitable for neuronal regeneration; therefore, chronic eye diseases such as glaucoma, age-related macular degeneration (AMD), diabetic retinopathy (DR) and retinitis pigmentosa (RP) over time can lead to progressive vision loss and irreversible impairment of neurons, whereby the most critical consequence could be irreversible blindness (Jindal, 2015).

Although the molecular basis of neurodegenerative diseases remains unknown, it is clear that the incidence and prevalence of these dysfunctions have multifactorial origins. Age remains the primary risk factor, but there are several etiological determinant causes,

including excitotoxicity, cellular oxidative stress, neuroinflammation, abnormal protein deposition in neuronal tissue, proteolytic degradation, dysregulation of ocular hemodynamic parameters, genetic polymorphisms and aberrant cell signaling pathways (Gupta et al., 2016).

2. THE ROLE OF OXIDATIVE STRESS AND MITOCHONDRIAL DYSFUNCTION

Oxidative stress plays a key role in the onset of inflammatory processes that lead to neuronal degeneration. The main causes of oxidative stress in the ocular structure include three critical factors:

- genetic disorders;
- excessive exposure to oxidative stress factors;
- ageing.

The reason for neurodegenerative diseases are often associated with advanced age is due to morphological and functional alterations in mitochondrial structures. Mitochondrial dysfunctions contribute to the pathogenesis of several neurodegenerative disorders. Mitochondria play several important roles such as ATP production, control of cell metabolism and regulation of programmed cell death. Recent studies have reported that the RPE of the elderly has reduced mitochondria, both in number and size. These cell organelles consist of two membranes, inner and outer, which delimit two distinct regions, the inner mitochondrial space and the matrix where the mitochondrial DNA (mtDNA) is located. The inner membrane is characterized by invaginations (cristae) that, by increasing the surface area, allow efficient packing of the electron transport chain (ETC). The ETC comprises multisubunit complexes (I to IV) involved in the generation of

adenosine triphosphate (ATP) via oxidative phosphorylation. Although under physiological conditions ROS contribute positively in cell signaling, their overproduction leads to imbalances resulting in molecular damage to mtDNA, lipids and proteins.

Mitochondria homeostasis is regulated by multiple processes that preserve their integrity, and the disruption of one of the pathways involved can lead to the onset of various pathologies. The main regulatory processes are fusion, fission, biogenesis, mitophagy and the coordinated expression of nuclear and mitochondrial DNA genes (Ferrington et al., 2020). Under senescent conditions or exposure to oxidative stress factors, mitochondria undergo a progressive decline in metabolic functions. Consequently, their ability to repair mtDNA damage is reduced, and mitochondria become increasingly susceptible to ROS damage. The eye, being a metabolically active structure, is also affected by these dysfunctions. Although the highest metabolic activity occurs on the ocular surface (cornea and conjunctiva) which is the most exposed part of the eye, the inner tissues (retina and optic nerve) are also susceptible due to oxidative stress (Williams, 2008).

The visual system is among the most energy-consuming brain systems. Energy, in terms of ATP, sustains multiple neuronal functions and is generated via two pathways: glycolytic and oxidative metabolism. The most efficient ATP production occurs in the mitochondria via the oxidative pathway. Since energy metabolism is regulated by factors such as blood flow, glucose uptake and oxidative metabolism, deficits make the visual system vulnerable (Wong-riley, 2010).

Among body tissues, the retina and retinal pigment epithelium (RPE) demand the highest oxygen requirements and derive their main energy sources from the mitochondria. Their survival is strictly co-dependent so much that they exchange energy substrates useful for providing vital functions. Therefore, in the case of metabolic deficits, the close

relationship between the two tissues involves damage extension. When blood flow decreases and oxygen levels fall below a critical level in one of the two tissues, the other one also suffers and a hypoxic condition occurs, leading to apoptotic cell death (Bilbao-Malavé et al., 2021).

3. MITOCHONDRIAL DYSFUNCTION IN RETINAL DISEASES

There is growing evidence to support an existing association between mitochondrial dysfunction caused by oxidative stress and retinal degenerations, including DR, AMD and glaucoma (Barot et al., 2011). Although these pathologies share imbalances in mitochondrial dynamics, they affect different subcellular structures (Figure 1).

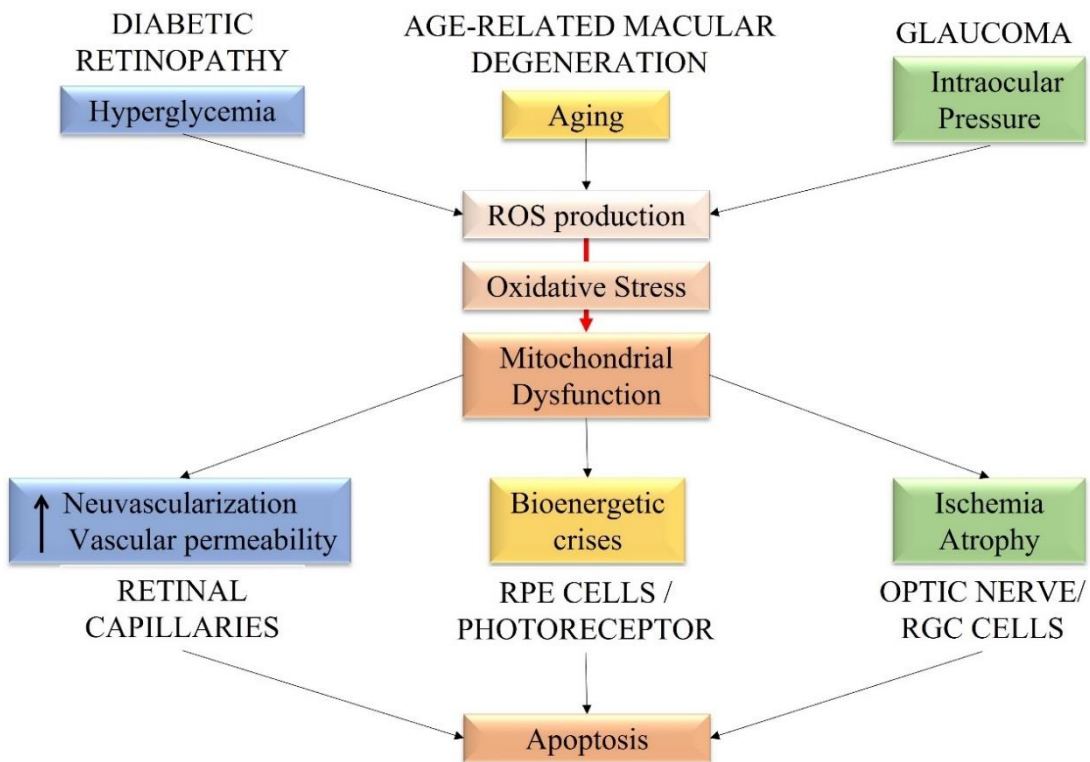


Figure 1. Involvement of stress-induced mitochondrial dysfunction in retinal diseases

To better understand the role of mitochondrial dysregulation on the antioxidant defences of retinal cells, a brief overview is given below to comprehend the mechanistic basis through which oxidative stress could induce retinal damage in these different pathologies. DR is the most common microvascular complication of diabetes mellitus that involves BRB impairment. The manifestation of non-proliferative DR is macular edema, characterized by thickening of the retinal blood vessels, increased capillary permeability and fluid accumulation in the retina. In some cases, progression of the disease leads to proliferative DR, which induces neovascularization. The severity of the disease is correlated with the duration of diabetes, and chronic oxidative stress conditions induced by hyperglycemia, or other risk factors such as hypertension and dyslipidemia, trigger various biochemical and physiological events resulting in microvascular damage and retinal dysfunction. Metabolic disorders caused by hyperglycemia (such as activation of protein kinase C (PKC), advanced glycation end products (AGEs) and increased activity of the polyol pathway) are factors mediating oxidative stress (Barber and Baccouche, 2017). Cytosolic ROS are critical mediators in the activation of several pathways implicated in the pathogenesis of DR. Chronic ROS overproduction in the retina results in: downregulation of antioxidant enzymes expression, release of proinflammatory cytokines and vascular endothelial growth factor (VEGF) and premature apoptosis of retinal cells (Kowluru and Abbas, 2003)(Madsen-Bouterse et al., 2010)(Kan et al., 2017) (Masuda et al., 2017)(Cecilia et al., 2019)(Ain et al., 2020). Therefore, it is obvious that hyperglycemia-induced oxidative stress is a critical instigator of mitochondrial dysfunction which leads to the onset of DR.

AMD is the leading cause of visual disability. Manifestations in the early stages are the appearance of small drusen (yellow deposits of lipids and proteins under the retina) and

RPE focal anomalies; AMD in advanced stages can evolve into dry (atrophic) AMD characterized by photoreceptor and RPE atrophy, or wet (neovascular) AMD characterized by choroidal neovascularization. Both atrophic and exudative forms lead to severe impairment of visual function (Mitchell et al., 2018). It is an etiologically complex multifactorial disease with numerous epidemiological risk factors, some modifiable (e.g., body mass index, cigarette smoking, lipidemia and cholesterolemia levels, hypertension, and an antioxidant-poor diet), others non-modifiable, related to genotype (sex, ethnicity, and age). Age, as the name of the disease itself indicates, is the primary risk factor; with ageing, mitochondria suffer both structural (such as partial or total loss of mitochondrial cristae) and functional (due to the imbalance between antioxidant and ROS levels) alterations, resulting in damage to mtDNA. (Kasahara et al., 2005)(Somasundaran et al., 2020). The RPE, which in physiological conditions obtains energy entirely via the oxidative pathway of mitochondria, is forced to obtain its energy demand from glucose generated by glycolysis. This bioenergetic crisis is responsible for photoreceptor and RPE cell death (Marazita et al., 2016).

In addition to risk factors, genetic susceptibilities known to contribute to the etiology of AMD were identified in individuals with polymorphisms of a protein localized on the mitochondrial membrane or point mutations in mtDNA (Jones et al., 2004)(Kanda et al., 2007)(Fritsche et al., 2008)(De Angelis et al., 2017).

Although the connection between ROS overproduction, functional and structural alterations of mitochondria in the RPE and lesions/mutations of mtDNA have been described, the mechanisms of onset and progression of AMD need further investigation.

Glaucoma is a neurodegenerative disease of the optic nerve. Death of retinal ganglion cells (RGCs) and their axons leads to progressive loss of visual function. Mitochondria

are densely distributed around the optic nerve where oxygen demand is elevated. For this reason, they provide a high ATP requirement to ensure proper function (Bristow et al., 2002). The main risk factor for glaucoma is increased intraocular pressure (IOP). In a study conducted by Ju et al. was demonstrated that high-hydrostatic pressure environment induces fission and alteration of the cristae on the external membrane of RGC cell mitochondria resulting in apoptosis (Ju et al., 2007)(Chrysostomou et al., 2013). However, the control of this parameter alone does not exclude disease progression. Age is also a risk factor, and as we have seen above, mitochondrial function tends to decline with age, suggesting mitochondrial involvement in the disease (Lee et al., 2011). Mitochondria function may also be impaired by mechanical stress and acute systemic hypotension. A higher incidence/prevalence of glaucoma was observed in individuals where low systemic arterial pressure combined with high IOP and reduced ocular perfusion pressure coexisted. Reduced ocular blood flow to the optic nerve head causes oxidative stress damage, which results in axon ischemia and RGC atrophy (Costa et al., 2014).

Genetic susceptibility also plays an important role in glaucomatous pathogenesis. Genetic mutations in mtDNA or nuclear DNA coding for mitochondrial proteins could contribute to the development of functional/structural alterations in mitochondria, increasing susceptibility to RGC loss in glaucoma (Cipolat et al., 2006)(Chen et al., 2006)(So et al., 2008)(Zanna et al., 2008) (Mariappan et al., 2009)(Goto et al., 2009)(Wolf et al., 2009)(Bougaki et al., 2010).

In summary, oxidative stress and associated mitochondrial dysfunction (congenital or acquired) are critical factors implicated in the pathophysiology of neurodegenerative retinal diseases. Thus, counteracting stress could be a very useful therapeutic goal.

4. NEUROPROTECTIVE AGENTS AGAINST OXIDATIVE DAMAGE

Despite neurodegenerative diseases representing a major global problem, the current pharmacological treatments suffer from limitations that have prompted research towards the development of innovative neuroprotective therapies. Neuroprotection is a therapeutic approach which can change the progression of these conditions. Neuroprotective agents can prevent cell death, restore the function and number of damaged neurons and so delay disease progression (Monteiro et al., 2017). As we have seen, oxidative stress plays a key role in triggering mitochondrial damage. Since the pathogenesis of neurodegenerative diseases is partially attributed to mitochondrial alterations, functional repair of mitochondria should be considered a potential treatment approach. So an appropriate strategy to improve the course of such retinal degenerations could be to maximize the protection of mitochondria against oxidative damage (Williams, 2008).

This hypothesis is supported by the neuroprotective effect that antioxidants have shown in reducing the negative effects of oxidative stress in such pathogenic conditions (Komeima et al., 2006). Currently, the literature showed an increased interest in natural compounds, hormones and calcium channel blockers (CCBs).

Natural products with antioxidant and anti-inflammatory properties are potential candidates as neuroprotective agents for the management of neurodegenerative disorders (Sharifi-Rad et al., 2020). Phenolic compounds are the most common secondary metabolites of plants and are classified into phenolic acids, flavonoids, tannins and stilbenes (Alara et al., 2021). Phenolic acids are the most popular bioactive compounds and are gaining increasing interest in the prevention and treatment of neurological diseases due to their antioxidant, anti-radical and neuroprotective properties (Szwajgier et al., 2017). Phenolic acids can be distinguished into two classes: benzoic acid (gallic

acid and cinnamic acid (ferulic and coumaric acid) derivatives. Cinnamic acid and its derivatives exhibit anti-inflammatory properties that are attributed to their ability to suppress the production of inflammation mediators such as the cytokines IL-6, IL-1 β , and TNF- α , prostaglandin E2, and the enzymes COX-1 and COX-2 (Alam et al., 2016).

The neuroprotective effects of ferulic acid (FA) were tested in ischemia/reperfusion-induced brain injury, where the molecule was able to contrast oxidative stress-mediated apoptosis (Cheng et al., 2008)(Ren et al., 2017).

Given its promising neuroprotective properties, FA has recently been investigated for the management of ocular neurodegenerative diseases. Administration of this polyphenol showed protective effects on several models, including: retinal degeneration, injury, inflammation, and hyperglycemia of the human retinal pigmented epithelial cell line (ARPE-19 cells) and retinitis pigmentosa (RP) (Kohno et al., 2020)(Sun et al., 2021)(Zhu et al., 2022). The application of natural antioxidant molecules such as FA has proven to be a suitable strategy to inhibit the cell death cascade and protect the integrity of ocular tissues from oxidative injury. For this reason, FA was selected as one of the active molecules to be delivered in the following thesis project.

Recent studies have highlighted potential neuroprotective effects of hormones, arousing growing interest in their use as agents in the management of neurodegenerative diseases. Several preclinical studies reported that thyroid, pituitary, pancreatic and several sex hormones, some also known as neurosteroids as they are produced by brain cells, showed neuroprotective activities (Shin et al., 2004) (Duarte et al., 2008)(Sanders et al., 2010)(Fanne et al., 2011)(Mancini et al., 2013)(Bunevicius et al., 2015)(Toro-Urrego et al., 2016)(Céspedes Rubio et al., 2018)(Peng et al., 2018).

The protective effects of neurosteroids have also been demonstrated at the retinal level in models of ischemia-reperfusion-induced damage (Bucolo and Drago, 2004).

The production and levels of neurosteroids are in turn regulated by another hormone, melatonin. Melatonin is a neurohormone secreted by the pineal gland involved in the regulation of many biological functions such as circadian rhythm, energy metabolism and hormone secretion (Cipolla-Neto et al., 2022). In this regard, it has been extensively studied as a potential neuroprotective agent, becoming one of the most widely used substances in recent years. This hormone is also released from extra-pineal tissues (such as the brain, lens, ciliary body and retina), where, it is generated in response to stress factors and acts as an antioxidant and anti-inflammatory agent (Tan et al., 2007).

The synthesis of this molecule takes place in the mitochondria, whose physiological functions are preserved by the beneficial properties locally exerted by this molecule (Tan et al., 2013). By preserving the mitochondrial membrane potential, melatonin prevents release of cytochrome c into the cytoplasm and consequently inhibits apoptotic processes (Yang et al., 2015). Numerous experimental trials have tested the antioxidant, anti-apoptotic and anti-inflammatory properties of melatonin on ischemic stroke models, and its neuroprotective action has been confirmed (Chern et al., 2012)(Li et al., 2014)(Paredes et al., 2015)(Wu et al., 2017)(Zhao et al., 2018).

In recent decades, the beneficial properties of melatonin have also been exploited in the treatment and prevention of neurodegenerative eye diseases. Melatonin's ability to prevent oxidative damage and associated mitochondrial dysfunction has proven to be a useful approach in the management of AMD, where the molecule has been able to preserve the viability of RPE cells (Yi et al., 2005)(Mehrzadi et al., 2020). In addition to regulating neurosteroid levels, melatonin exerts control on the expression of

inflammatory cytokines (IL-6 and TNF- α) and pathological VEGF secretion in the retina; therefore, melatonin could be an effective therapeutic resource in counteracting neovascularization in proliferative DR (Ferreira de Melo et al., 2020).

Several studies have evaluated the influence of melatonin on IOP modulation. It was found that IOP and melatonin follow inverse circadian rhythms, during the day melatonin levels are low while IOP is high, vice versa during the night. This relationship was confirmed by studies showing that melatonin levels were significantly altered in the course of ocular diseases such as glaucoma (Alkozi et al., 2020). Investigations in animal models and clinical studies proved that melatonin administration was effective in IOP regulation (Musumeci et al., 2013)(Carracedo-Rodríguez et al., 2020). Furthermore, neuroprotection of ocular hypertension lesions has shown added efficacy to the therapeutic benefits of this molecule in the management of glaucomatous diseases (Gubin et al., 2021). Collectively, these mechanisms could be useful in protecting neurons from oxidative insults and subsequent neurodegenerative diseases; therefore, melatonin was the second active molecule selected for this thesis work.

Another class of neuroprotective drugs are calcium channel blockers (CCBs). Calcium signaling pathways play a crucial role in neuronal function, actively participating in synaptic transmission. During ageing or in case of neurodegenerative diseases, neurons suffer from energetic disorders, which also adversely affect neuronal Ca²⁺ signaling (Brini et al., 2014).

The neuronal energy source is exclusively ATP produced by the mitochondria; when mitochondrial oxidative phosphorylation is impaired, neurons do not obtain energy from glycolysis. The energy homeostasis of the mitochondria is regulated by calcium levels, and in case of impairment they signal an increased energy demand (Duchen, 2012).

When mitochondrial calcium levels increase, this generates an overload which mitochondria cannot counterbalance with ATP production, resulting in structural damage to the mitochondrial membrane and cell death. Thus, in neurodegenerative diseases, there is a strong dependency between mitochondrial dysfunction and Ca^{2+} dysregulation (Calì et al., 2012). Calcium homeostasis in neurons can be regulated by L-type calcium channels, activated at high voltage, or T-type calcium channels activated at low voltage (Wildburger et al., 2009).

Recent studies in different models of neuronal injury have successfully demonstrated that pharmacological interventions that modulate calcium levels, such as CCBs, attenuated the increase in intracellular Ca^{2+} resulting in reduced neurological damage and neuroprotective effects (Bancila et al., 2011)(Yagami et al., 2004)(Yamada et al., 2006). Flunarizine is dual L/T-type CCBs. This molecule was effective in protecting neuronal cells from retinal neurotoxicity in a model of ocular hypertension-induced ischemia/reperfusion (Torii et al., 2000).

Since over 30 years, flunarizine has been extensively investigated in the ophthalmic field for its neuroprotective properties. Previous studies investigated these properties and proved the ability of this diphenylalkylamine to reduce light-induced degeneration of photoreceptors and improve the RGCs survival when deprived of neuronal growth factor (NGF) (Edward et al., 1991)(Eschweiler and Bähr, 1993).

Flunarizine is also known to block sodium channels and modulate NMDA secretion; these additional beneficial effects provide support for the use of this drug in diseases affecting RGCs (Osborne et al., 2002). Therefore, flunarizine was selected to be investigated as a neuroprotective agent for ocular degeneration.

Despite the many beneficial effects of these molecules, they should be able to overcome the anatomical limitations of the ocular structures to exert therapeutic action in the posterior eye segment.

5. DELIVERY TO THE POSTERIOR EYE SEGMENT: ROUTES OF ADMINISTRATION AND LIMITS

Various therapeutic options are available to deliver active molecules to the posterior eye segment, including topical, periocular (subconjunctival, sub-tenon, peribulbar, retrobulbar, and posterior juxta-scleral injection), systemic and intravitreal routes (Varela-Fernández et al., 2020). However, each route of administration presents protective barriers, static and dynamic, that molecules must overcome to reach target tissues. The anatomical characteristics of each barrier and their permissiveness to the passage of active molecules - according to their molecular weight, solute charge, lipophilicity, and molecular radius - are briefly listed below.

- *Pre-corneal barrier*: this is the first barrier that an eye drop applied topically to the ocular surface encounters. When the drop is instilled, it mixes with the tear fluid overlying the cornea and conjunctiva. The dynamics of tear fluid flow was first studied by Mishima et al. using fluorescein as an indicator. The study showed that the drug deposition in the conjunctival sac of a healthy subject in an upright position has a maximum capacity of 30 μL , the rest being drained at a flow rate of about 1 $\mu\text{L}/\text{min}$, which causes it to drain towards the nasolacrimal duct (Mishima et al., 1966). This quota of drained drug constitutes the percentage of non-productive absorption and contributes to side effects. Another fraction of the

instilled compound is rapidly removed from the ocular surface due to ocular blinking.

- *Corneal barrier*: if the compound crosses the precorneal barriers, it encounters the cornea, which consists of five layers. Starting from the most anterior region consists of lipophilic corneal epithelium that can be crossed by hydrophobic compounds, Bowman's layer, hydrophilic corneal stroma made up of a fibrous structure that affects the permeability of large molecules and constitutes 90% of the corneal thickness, Descemet's membrane, and hydrophobic corneal endothelium (Espana and Birk, 2020). The crossing of this complex structure depends on the physico-chemical characteristics of the molecules, such as molecular weight and lipophilicity. Epithelium and endothelium permit the passage of small lipophilic molecules with a molecular weight < 500 Da, while the crossing of the stroma is mainly dependent on the molecular weight (Edwards and Prausnitz, 2001).

Only small molecules with optimal lipophilicity (2-3 log D) can effectively permeate the cornea (Huang et al., 1983). Another influential parameter is the charge of the solute, cationic compounds that bind to the negatively charged corneal surface permeate more easily (Liaw et al., 1992). Another obstacle to transcorneal diffusion is provided by efflux transporters on the membrane of corneal cells, which further reduce permeation through the aqueous humor (Chen et al., 2013).

- *Aqueous humor*: is a liquid contained in the anterior eye segment between the cornea and the crystalline lens. In order to preserve the blood-aqueous barrier, aqueous humor prevents the diffusion of high molecular weight molecules

through Schlemm's canal, a venous vessel responsible for draining the aqueous humor (Braakman et al., 2016).

- *Conjunctival-scleral barrier*: the conjunctiva consists of an external stratified squamous epithelium permeable by hydrophilic compounds. This epithelium is vascularized, therefore, only compounds that avoid systemic absorption from the conjunctival vessels can permeate the conjunctiva. The conjunctiva permits the transit of higher molecular weight molecules (up to 20 kDa) (Huang et al., 1989). Larger molecules show lower permeation, which is why macromolecules such as anti-VEGF are preferentially administered by intravitreal injections. The succeeding barrier is the sclera, which is more permissive to hydrophilic compounds compared to the cornea and conjunctiva (Prausnitz, 1998). Molecular weight, on the other hand, appears to be a less predictive permeability parameter than molecular radius. A study by Ambati et al showed that at equal molecular weight, a globular protein with a molecular radius of 5.23 nm permeated better than a linear dextran but with a higher molecular radius (8.25 nm) (Ambati et al., 2000). The trans-scleral permeability is also influenced by the compound charge. The extracellular matrix of the sclera consists of collagen fibrils and negatively charged glycoproteins, but contrary to the cornea, here the passage of positively charged solutes is hindered by electrostatic binding (Maurice and Polgar, 1977).
- *Crystalline lens*: this lens can act as a drug reservoir for the anterior chamber of the eye. The crystalline lens allows the diffusion of water-soluble molecules, but this process is compromised by ageing because the diffusion coefficient decreases, hindering the transport of molecules (Pescosolido et al., 2016).

- *Vitreous barrier:* the vitreous body is a gelatinous connective tissue that constitutes about 80% of the eyeball. It is composed of 98% water and the rest of collagen fibers that form a three-dimensional network within which hyaluronic acid is contained. Inside the vitreous body, two types of barriers can be distinguished, anatomical and physiological (Peynshaert et al., 2018). The anatomical barrier consists of the vitreous structure itself, which acts as a static barrier. The permeation of this static barrier does not depend so much on the size of the particles, as the pore size is large enough to allow small molecules and antibodies to pass through, but on the surface charge. Positively charged particles could be trapped within the vitreous by interaction with negatively charged vitreous components (Käsdorf et al., 2015). The physiological (or dynamic) barrier is regulated by the flow and clearance processes that occur in the vitreous. The vitreous body flow is subject to convective motions regulated by the pressure difference between the front and back of this structure (Park et al., 2005). These fluxes are critical in determining the half-life of molecules in the eye. Small and lipophilic molecules are eliminated from the posterior side via the BRB to the retinal and choroidal blood circulation in a short time, large and hydrophilic molecules instead follow the anterior route via aqueous humor flows and uveal blood circulation and persist in the vitreous for longer times (Kidron et al., 2012).
- *Blood-ocular barrier:* is a highly selective structure for crossing molecules and comprises two barriers, blood-aqueous barrier and BRB. The blood-aqueous barrier consists of the vascular endothelium of the iris and Schlemm's canal and the epithelium of the ciliary body and is more permissive than the BRB (Yang et al., 2020). The BRB consists of the retinal vessel endothelium (inner BRB) and

the RPE (outer BRB), both of which are characterized by tight junctions that restrict the passage to the retina of orally or intravenously administered drugs, particularly hydrophilic compounds, and macromolecules (Kansara and Mitra, 2006). Also here, molecular radius is the most influential permeation factor for retinal penetration; permeability decreases significantly as molecular radius increases (Pitkänen et al., 2005). Regarding lipophilicity, lipophilic compounds cross the RPE via the transcellular pathway, while hydrophilic molecules cross it through the tight junctions of the paracellular pathway (Diaz-Coranguez et al., 2017). Thus, retinal permeation is elevated for lipophilic molecules and the rate of diffusion increases as the molecular radius decreases.

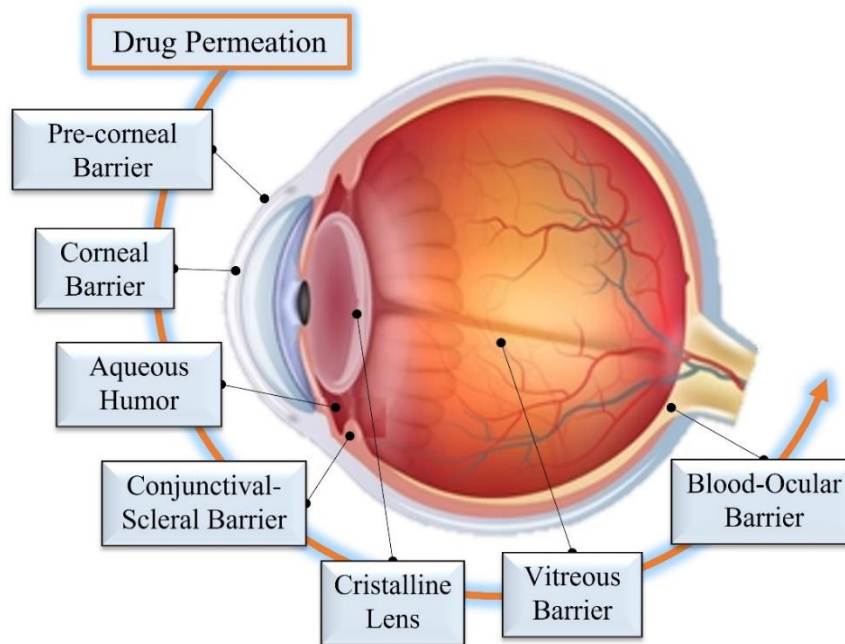


Figure 2. Structure of eye and physiological barriers

The routes of administration to target the posterior eye segment are distinguished in invasive and non-invasive routes. Invasive methods of administration include intravitreal injections/implants, which allow drugs to be administered directly into the vitreous, and periorbital injections/implants, which reach around the target site. Although intravitreal

injection is administered directly to the vitreous body, it does not ensure that the full dose of drug is available for pharmacological effect, since the injected drug must overcome the above-mentioned barriers to reach the target sites (Tavakoli et al., 2020). Although these are invasive methods, the incidence of risks associated with these techniques (retinal detachment, cataracts, increased IOP and endophthalmitis) is low even with repeated administrations (Lai et al., 2015). Endophthalmitis, for example, was effectively prevented by prophylaxis with topical antibiotics (Sampat and Garg, 2010). An advantage of intravitreal administration is to moderate systemic exposure and limit side effects.

Periocular routes are an alternative to intravitreal delivery, considered to be a good compromise between the absence of pain associated with injection and the efficiency of delivery to the posterior segment, particularly the external retina. Among the periocular delivery routes, the subconjunctival one is considered the least invasive (Janoria et al., 2007). The drug administered through the periocular pathways is applied close to the sclera and passes through one of three routes: the direct trans-scleral pathway, the systemic circulation through the choroid and the anterior pathway (tear film, cornea, aqueous humor, and vitreous humor). The trans-scleral penetration route allows the vitreous to be reached by passing through the sclera, choroid, RPE and retina (Ghate and Edelhauser, 2006). Although the positioning of these medicines may be visible from the outside, being away from the visual axis does not interfere with the patient's visual function (Kompella et al., 2021). A major limitation of this method consists in the high washout of the drug, which must cross several physiological barriers (static, dynamic and metabolic) to reach target sites at therapeutically effective concentrations. Therefore, providing protection to the drug against degradation and clearance could partially improve the therapeutic efficiency of this route of administration (Hiral J Shah, 2014).

The posterior eye segment can also be reached via the systemic route (oral or intravenous route). Drugs absorbed in the circulation can reach the choroid via blood vessels, but due to BRB and first-pass metabolism the amount of bioavailable drug in the target tissue is limited ($< 2\%$) (Weng et al., 2017). High drug concentrations are required to pass the BRB, but on the other hand could cause systemic side effects (Hosoya et al., 2011).

The non-invasive route for excellence is topical application. This route is used to treat disorders affecting both segments of the eye, anterior and posterior. Although the instillation of eye drops is a painless, simple practice that the patient can self-administer and guarantees a rapid effect, there are several disadvantages. After application, the tear film (pre-corneal barrier) is the first obstacle that the eye drops encounter. Here, enzymatic degradation, binding to tear proteins, short contact time with the ocular surface, poor corneal penetration, rapid tear turnover and nasolacrimal drainage to the systemic circulation all limit tissue bioavailability (Sebbag et al., 2020). The residual amount of eye drops must overcome subsequent tissue barriers and non-productive systemic absorption at the level of the conjunctiva, which represent additional obstacles. Consequently, only a small percentage ($< 5\%$) of administered drug is absorbed and available to reach intraocular tissues (Djebli et al., 2017). Thus, to maintain an effective drug regimen, the patient is obliged to correctly adhere to the therapy by applying regular and frequent doses of medication. Poor compliance is especially controversial for patients approaching new therapies (Reardon et al., 2011). Due to the chronicity of posterior eye segment disorders, sustained drug delivery is required in most cases. Due to the unique anatomy and physiology of the eye, administration to the posterior eye segment remains a complex challenge for the pharmaceutical industry.

Sustained drug release formulations could maintain constant drug levels at the site of action and partly provide a solution to this problem (Abdelkader and G. Alany, 2012). Sustained drug release could improve the patient's quality of life and bring added benefits for both topical and intravitreal routes. For topical applications it could reduce washout, non-productive absorption, and consequently systemic side effects (Kaur and Kanwar, 2002). In the case of intraocular delivery, which requires frequently repeated injections to maintain therapeutic levels, it could reduce the economic costs of hospitalization. Other strategies proposed to improve ocular delivery is the modification of formulation parameters to develop systems with increased bioavailability and reduced side effects. Among the methods proposed to increase drug penetration through barriers include the addition of solubility or permeability enhancers of active molecules, viscosity or mucoadhesive agents, vasoconstrictors, prodrugs and nanotechnology (Lanier et al., 2021).

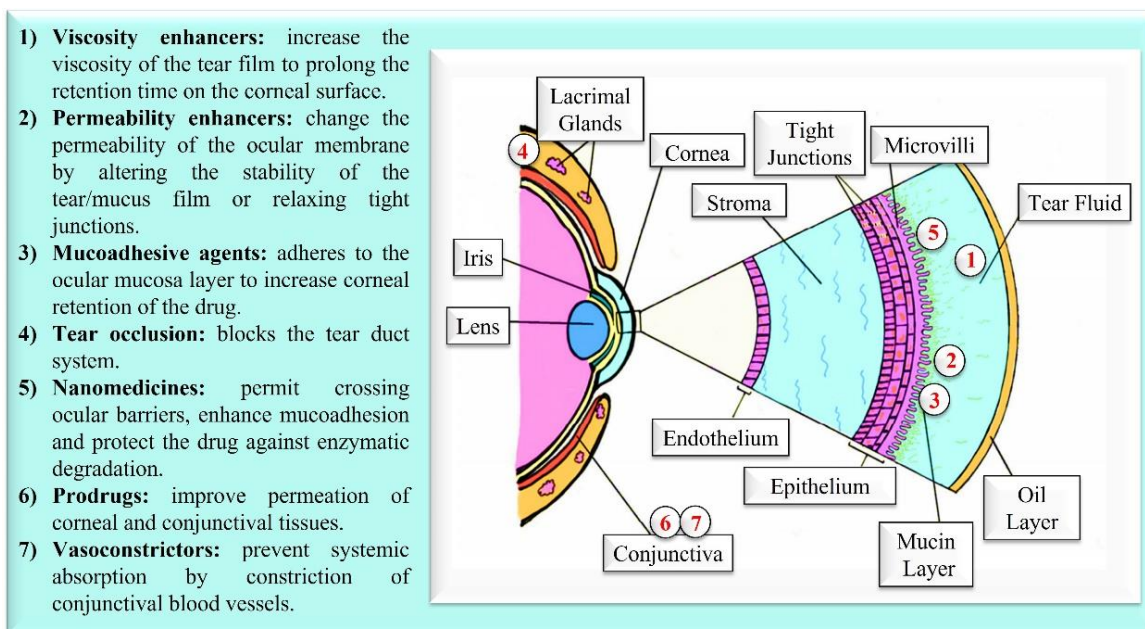


Figure 3. Schematic diagram of various methods to enhance ocular drug bioavailability. Adapted from Lanier et al., 2021.

6. NANOMEDICINE FOR THE POTENTIAL TREATMENT OF OCULAR DISEASES

Most drugs used in the ocular field are lipophilic molecules with a low solubility in water, additives that enhance solubility could be useful to improve the eye drops performance. To date, several techniques have been used to increase the solubility of poorly soluble drugs in tear fluid. Drug-cyclodextrin inclusion complexation has been effective in improving not only aqueous solubility of drugs, but also stability, permeability and bioavailability (Kim et al., 2020)(Senjoti et al., 2020).

The incorporation of drugs into nanocarriers has opened a new window for modifying drug properties. In this regard, the rational development of nanocarriers for therapy and imaging in recent decades has contributed significantly to improving the results of ocular delivery to the posterior segment. These nanosystems could provide an effective and promising alternative for the management and diagnosis of ophthalmic diseases through the ocular pathways. Various pharmaceutical strategies have been investigated to overcome the limitations of ocular barriers and improve drug permeability to intraocular tissues. The benefits of nanotechnology are manifold, their use has been useful in improving drug aqueous solubility, stability, protection against chemical and physical degradation (Gunasekaran et al., 2014). Furthermore, by modulating physico-chemical and functional properties such as size, composition, and surface properties of nanocarriers, it is possible to influence the fate, permeation, distribution and clearance of therapeutics. Nanocarriers with a size between 50 and 400 nm limited ocular irritation and were able to cross physiological barriers providing effective delivery (Silva et al., 2021).

Modification of the surface properties through the addition of mucoadhesive agents, viscosifiers, penetration enhancers and polymers responsive to external stimuli (pH, temperature, and ions) facilitated the penetration of precorneal barriers (Sai et al., 2020). The protection provided by these modifications against tear drainage reduced systemic absorption and side effects, and improved retention time on the corneal surface and transcorneal penetration. This design strategy offered several advantages that, collectively, ensured effective drug delivery to target tissues (Wang et al., 2018).

The composition of nanosystems plays an important role for encapsulation efficiency, loading and release pattern of the drug (Razavi et al., 2022). Various materials have been used to develop delivery systems with predictable release profiles. Polymers have a crucial role in the functionalization of drug release from nanodevices that are highly dependent on degradation mechanisms under physiological conditions. Depending on the desired application, the most suitable polymers can be selected to provide a pertinent degradability rate with the desired release profile, immediate or sustained (Visan et al., 2021). With these arrangements, it is possible to enhance adhesion and permeation to ocular tissues, provide targeted delivery and ensure controlled and sustained therapeutic effects, all of which are crucial factors in increasing drug activity and bioavailability compared to conventional drug delivery systems (Weng et al., 2017). The ability to improve delivery to intraocular tissues reduces both non-productive systemic absorption and adverse effects (Liu et al., 2012).

A variety of nanocarriers have been developed for posterior segment delivery, such as polymeric and lipid NPs, hybrid NPs, nanogels, liposomes, nanoemulsions, micelles, dendrimers and nanofibers. Table 1 lists some examples of nanomedicines designed to treat neurodegenerative diseases affecting the posterior eye segment.

Table 1. Management of neurodegenerative diseases affecting the posterior eye segment using nanomedicines. PubMed database was used to perform the search that did not include time ranges. The keywords used were "nanoparticles," "nanofibers," "ocular", "posterior eye segment" and "neurodegenerative diseases."

Disease	Type of system	Administration route	Encapsulated Drug	Excipients	Reference
Glaucoma	Polymeric NPs	Topical	Melatonin	PLGA PLGA-PEG Tween® 80	(Musumeci et al., 2013)
	Polymeric NPs	Topical	Timolol	Chitosan Hyaluronic acid	(Wadhwa et al., 2010)
	Polymeric NPs	Topical	Tetrandrine	Bovine serum albumin Chitosan	(Radwan et al., 2022)
	SLN NLC	Topical	Brimonidine	Glyceryl monostearate Poloxamer® P 188 Castor oil	(El-Salamouni et al., 2018)
	SLN	Topical	Melatonin	Softisan 100 Didodecylmethyl amonium bromide Stearic acid Palmitic acid	(Leonardi et al., 2015)
	SLN	Topical	Timolol	Phospholipon 90G	(Attama et al., 2009)
	Core-shell type Hybrid NPs	Topical	Brinzolamide	PLGA PVA Soybean phosphatidylcholine Cholesterol	(Zhou et al., 2020)
	Dendrimer-based nanofibers	Topical	Brimonidine	Polyamidoamine dendrimers conjugated mPEG poly(ethylene oxide)	(Lancina et al., 2017)
	In situ gelling nanofibers film	Conjunctival sac	Timolol	PVA Poloxamer® P 407	(Andreadis et al., 2022)
	Implant of coaxial or uniaxial fibers	Topical	Acetazolamide	PCL Poloxamer® P 407 poly (ethylene-co-vinyl acetate)	(Morais et al., 2021)
DR	Polymeric NPs	Topical	IL-12	PLGA PVA	(Zeng et al., 2019)
	Polymeric NPs	Subconjunctival	Bevacizumab	PLGA Chitosan PVA	(Pandit et al., 2021)

	Polymeric NPs	IVT injection	Fenofibrate	PLGA PVA	(Qiu et al., 2019)
	SLN	Topical	Pilocarpine	Stearic acid Sodium taurodeoxycholate Purified egg lecithin	(Cavalli et al., 1995)
	SLN	IVT injection	Etoposide	Gelucire® 44/14 Compritol® 888 ATO Tween® 80 Mannitol	(Ahmad et al., 2019)
	SLN	IVT injection	siRNA	Softisan® 100 Didecylmethylammonium bromide Tween® 80	(Amadio et al., 2016)
AMD	Polymeric NPs	Topical	Sirolimus	PLGA PVA Chitosan	(Suri et al., 2021)
	Polymeric NPs	IVT injection	Resveratrol	PLGA	(Bhatt et al., 2020)
	Polymeric NPs	IVT injection	Axitinib	PLGA PVA	(Narvekar et al., 2019)
	SLN	Topical	Atorvastatin	Compritol® 888 ATO Phospholipon 90 Poloxamer® P 188 PEG 400	(Yadav et al., 2020)
	SLN	Topical	Lutein	Gelucire® 44/14 Tween 80	(Sunny Shah et al., 2022)
		Core-shell type Hybrid NPs	Topical	Moxifloxacin	Chitosan Cholesterol Hyaluronic acid 1,2-dipalmitoyl-sn-glycerol-3-phosphoethanolamine Egg phospholipid
Intraocular inflammation	Insert	Conjunctival sac	Fluocinolone Acetonide	PCL	(Singla et al., 2019)
	Insert	Conjunctival sac	Triamcinolone Acetonide	Eudragit S100 Zein Chitosan PVP PVA	(Mirzaeei et al., 2018)

	Insert	Conjunctival sac	Triamcinolone Acetonide	Poly(1,4-butylene succinate inulin α,β -poly(N-2-hydroxyethyl)-D,L-aspartamide heparin	(Di Prima et al., 2019)
Retinal delivery	Core-shell type Hybrid NPs	IVT injection	-	Chitosan Hyaluronic acid Cholesterol 1,2-dioleoyl-sn-glicerol-3-phosphoethanolamine	(Gan et al., 2013)
Gene therapy	Core-shell type Hybrid NPs	Topical	pDNA model	Egg phospholipid Chitosan Egg phospholipid Cholesterol 1,2-dioleoyl-3-trimethylammonium-m-propane	(Jiang et al., 2012)

The following sections will provide applications of the nanosystems investigated in this thesis project.

7.1. Polymeric nanoparticles

Polymeric NPs are particle systems with an average diameter between 10 and 1000 nm.

Such nanoscale size facilitates permeation to intraocular tissues (Chen et al., 2018).

NPs can be prepared from polymeric materials of natural or synthetic origin. Natural polymers of animal or plant source often used in ophthalmic preparations are chitosan, hyaluronic acid, sodium alginate and sodium carboxymethyl cellulose. However, due to batch-to-batch variations, synthetic polymers have attracted particular interest due to their reproducibility in production. Among the synthetic polymers used for ocular delivery are polylactic acid (PLA), poly(lactic-co-glycolic acid) (PLGA), poly(ethylene glycol) (PEG), polyoxamers (Pluronic), poly(ϵ -caprolactone) (PCL), poly(vinyl alcohol) (PVA) and polyvinylpyrrolidone (PVP).

All these synthetic polymers have excellent biocompatibility and safety and have been approved by the Food and Drug administration (FDA) for drug delivery and other clinical applications. An added value of these polymers is their biodegradability; the body metabolically decomposes them into non-toxic products. For ocular implants, the use of these biodegradable compounds has been a revolution, as it has eliminated the need for surgery to remove them (Kimura and Ogura, 2001).

To deliver the colloidal nanosuspension to the intraocular tissues, direct administration to the posterior segment (intravitreal or subretinal injection) can be used, or if the topical route is preferred, systems with functionalized surfaces provide a longer retention time and more effective permeation (Lynch et al., 2019).

The surface engineering of NPs allows them to satisfy the most suitable requirements for the intended application. Nevertheless, it should be highlighted that some polymers by themselves exhibit mucoadhesive or mucopenetrating characteristics. By modulating the surface charge of NPs, it is possible to obtain cationic particles with mucoadhesive properties, which are immobilized within the mucus gel layer, or anionic or uncharged particles with mucopenetrating properties, which easily diffuse through the mucous membranes (Netsomboon and Bernkop-Schnürch, 2016).

Permeation enhancers are mucopenetrating molecules that can improve the passage of poorly permeable membranes such as the cornea. These molecules act through three mechanisms: by altering the precorneal barrier (tear film and mucous layer), loosening tight junctions, and modifying lipid bilayers of epithelial cell membranes (Moiseev et al., 2019). NPs consisting of PLGA, PCL, poloxamers, and chitosan polymers showed effective transcorneal permeation and improved drug ocular bioavailability (Valls et al., 2008)(Yeh et al., 2011).

In contrast, agents with mucoadhesive properties are advantageous for providing prolonged retention times on the ocular mucosa. Alginate, hyaluronic acid, cellulose derivatives, chitosan, and poloxamers are known for mucoadhesive properties and prolonged contact time with corneal tissues and conjunctival epithelium (Bíró and Aigner, 2019).

In addition to being mucopenetrating agents, poloxamers also exhibit mucoadhesive characteristics; they are thermosensitive polymers that undergo thermal gelation in the temperature range 25-35 °C. The sol-gel transition of poloxamers is concentration-dependent; therefore, the total polymer content may need to be increased to contrast the dilution effect of tear fluid (Edsman et al., 1998). High initial concentrations (>3% w/v) can cause hyperglycemia in the eye or gel formation at room temperature. To overcome these limitations and exploit the benefits of such polymers, poloxamers are often used in combination with cellulose derivatives (Kurniawansyah et al., 2020).

PEG is an uncharged hydrophilic polymer that exhibits a dual character depending on molecular weight. Low molecular weight PEG coatings (≤ 5 kDa) conferred mucopenetrating properties to the systems, conversely by increasing the molecular weight of polymer the NPs were immobilized in mucus due to steric interactions of the PEG chains with mucus (Lai et al., 2009).

PVA also showed ambivalent properties, dependent on the degree of hydrolysis and the type of coating (covalent or non-covalent) with the NP surface. NPs with non-covalent coating and degree of hydrolysis between 75-95 % promoted mucus crossing, conversely those that were non-covalently bonded possessed mucoadhesive properties (Popov et al., 2016).

Polymer NPs can deliver active molecules on their surface by adsorption/ entrapment, or within the polymer matrix by encapsulation (Chen et al., 2018). The disposition of the drug in NPs is one parameter that influences release kinetics, Usually the burst effect occurs when the drug is located close to the surface. However, the parameters that influence burst release profiles depend on several impact factors. Burst release is accentuated by the low molecular weight of the polymer, the high porosity of the polymer matrix, the small diameter of the NPs, the aliphatic properties of the drug (hydrophobic drugs with high affinity for the polymer matrix follow a slow initial release), the encapsulation efficiency, and the initial drug loading (Rodrigues de Azevedo et al., 2017). The parameters that influence release kinetics mainly depend on polymer degradation mechanisms. Drug release from polymer matrices can occur by polymer diffusion, degradation, or a combination of the two. If the drug is well immobilized inside the matrix, release will depend on polymeric erosion. Polymer degradation can be bulk, when it involves hydrolysis of the entire matrix and not occurring at a constant rate, or superficial, when it starts from the outermost layers and proceeds at a constant rate allowing more predictable drug release kinetics (Burkersroda et al., 2002). Parameters that influence the degradation rate include, for example, the molecular weight and degree of crystallinity of the polymer, the composition of the copolymer, the nature of the incubation medium, the presence of specific enzymes, and the autocatalysis induced by the acid degradation products (Bohr et al., 2017)(Azimi et al., 2014).

Methods to design ocular delivery devices based on polymeric NPs are innumerable, and tuning key parameters such as size, charge and functionalization of surface, choice of polymers, suspension media and route of administration is useful to develop appropriate carriers for the desired therapeutic target.

7.2. Lipid nanoparticles

Lipid NPs are divided into two classes: solid lipid nanoparticles (SLNs) and nanostructured lipid carriers (NLCs). SLNs constitute the first generation of lipid-based NPs and range from 50-1000 nm in average diameter (Goyal et al., 2016). SLNs are composed of solid lipids melting at temperatures above 40 °C such as triglycerides, partial glycerides, fatty acids, steroids, and waxes. They offer numerous advantages such as the ability to encapsulate hydrophilic and lipophilic drugs and preparation methods suitable for industrial scale-up not needing organic solvents. The starting materials are biodegradable, biocompatible, and provide excellent in vivo tolerability (Wang et al., 2018). SLNs possess mucoadhesive properties which facilitate interaction with the ocular mucosa and promote trans-scleral absorption due to enhanced phagocytosis of epithelial cells. Drug delivery by SLNs ensured high therapeutic levels in intraocular tissues (vitreous body and retina), resulting as ideal carriers for delivery to the posterior segment (Chetoni et al., 2016).

In addition to their ability to cross barriers, lipid carriers promote delivery and release to the target site to improve therapeutic efficacy. Delivery of chemotherapeutic drugs in SLNs has shown superior effects compared with conventional delivery, reducing side effects and improving drug delivery to the target site (Ahmad et al., 2019).

Despite this, such systems show poor loading capacity (~25 % of the lipid matrix), initial burst release for hydrophilic drugs, and high drug expulsion during the storage period attributable to the lipids polymorphic transitions (Bachu et al., 2018).

To overcome the limitations associated with SLN, second-generation of lipid NPs consisting of a mixture of solid and liquid lipids, have been developed, the NLC. The addition of liquid lipids allows systems to contain a greater amount of drug and prevents

polymorphic changes during storage (Vieira et al., 2020). By controlling the composition of the mixture between solid and liquid lipids, it is possible to modulate the encapsulation efficiency and release profiles, resulting in better performance compared with SLNs. In addition, liquid lipids also provide NLCs with superior capabilities in terms of corneal retention and penetration than previous generation (Balguri et al., 2016).

To further enhance absorption to intraocular tissues, both lipid carriers have been effectively coated with cationic lipids (e.g., cetyltrimethylammonium bromide (CTAB), dimethyldihydecylammonium bromide (DDAB)) to increase electrostatic interaction with the anionic ocular surface, or with mucopenetrating polymers (such as chitosan and PEG) to obtain greater transcorneal penetration (Joana F. Fangueiro et al., 2014)(Fangueiro et al., 2016)(Luo et al., 2011)(Lakhani et al., 2019).

In addition to increasing the interaction with the corneal epithelium, the coating with hydrophilic polymers confers the nanocarriers "stealth" effect which prevents interactions with degradative enzymes, oxidative agents and opsonins in the blood serum. The steric barrier that polymers form on the surface of NPs makes them "invisible" to phagocytes. The reduced clearance and increased circulation time contribute to increased therapeutic efficacy (Salmaso and Caliceti, 2013).

Generally, lipid-based preparations are ideal candidates for delivery to the posterior eye segment because of their nontoxicity, scalability of industrial production, facilitated corneal penetration, and improved bioavailability of poorly water-soluble and poorly permeable drugs (BCS class II and IV) (Teixeira et al., 2017). These advantages could be attributed to the use of GRAS (Generally Recognized as Safe) lipid components with high solubilizing properties (Battaglia et al., 2016).

7.3. Hybrid Nanoparticles

Lipid-polymer hybrid nanoparticles (LPHNs) are next-generation NPs that combine the biomimetic benefits of lipid NPs with the structural benefits of polymer NPs to overcome the challenges associated with the individual carriers. They generally consist of a biodegradable polymeric core that provides high drug loading, controlled and sustained drug release profiles, and a lipid coating shell that improves corneal tissue penetration, confers stability and biocompatibility (Jose et al., 2018).

The polymer core and the lipid shell interact through covalent interactions if the polymer core is hydrophilic, conversely through noncovalent interactions (electrostatic, hydrophobic, and Van der Waals forces) if polymer core is hydrophobic (Mendoza et al., 2019). Based on the structural organization of the lipid and polymer components, several classes of LPHNs are distinguished: polymer core lipid shell, core-shell type LPHN, erythrocyte membrane-camouflaged polymeric NP, monolithic LPHN e polymer-caged liposomes (Mohanty et al., 2020). These carriers offer advantages in the control of average particle size, good physical and plasma stability, high loading of both hydrophilic and hydrophobic drugs, easy formulation with biodegradable polymers and lipids, controlled and sustained drug release kinetics, and physiological, biocompatible, and biodegradable improved properties. The application of such systems has been useful for targeting specific targets, for siRNA delivery, for bioimaging, and for delivery of drugs alone or in combination. In fact, the hybrid nature of these carriers allows simultaneous delivery of water-soluble drugs, in the polymer matrix, and water-insoluble drugs, in the lipid shell (Aryal et al., 2010).

LPHNs also show a combination of attributes between lipid and polymer NPs in drug release kinetics. The release profiles from LPHNs are affected by the size of the carriers,

the choice of starting components, the solubility of the drug, its disposition into the NP, and the type of encapsulation, physical or chemical (Saurabh Shah et al., 2022). Lipophilic molecules that interact with lipid coating result in high drug loading and prolonged release profiles (Cheow and Hadinoto, 2011). Regarding drug disposition, the release profiles of drugs physically encapsulated in the polymeric core are governed by the degradative mechanisms of the polymer, the drug diffusion through the matrix, and the thickness of the lipid layer, which slows the degradation rate by limiting the water uptake into the LPHNs (Hadinoto et al., 2013). Instead, the drug release profiles of chemically encapsulated molecules depend on linker hydrolysis (Dave et al., 2019). Generally, LPHNs provide sustained release kinetics over time. For example, Shi et al. were able to achieve long-term gene silencing by siRNA release sustained for more than one month (Shi et al., 2014).

The lipid coating provides several advantages to the robust core polymer structure. In addition to acting as a biocompatible shield and barrier against rapid drug release, it also limits drug transport to the external environment during the preparation phase of LPHNs, enhancing drug encapsulation. Another key role of the lipid layer is as an anchor function for ligands used to engineer the surface of LPHNs (Cheow and Hadinoto, 2011).

The possibility of surface functionalization adds further benefits to LPHNs, and the most commonly used moiety in these systems is PEG again. In addition to the well-known mucopenetrating, mucoadhesive, and stealth effects, the lipid-PEG external layer permits further LPHNs engineerization with target ligands such as antibodies, peptides, aptamers, and small molecule (J. M. Chan et al., 2011)(Hu et al., 2010). Hyaluronic acid, for example, has been used as a ligand to target the CD44 receptor, which under inflammatory conditions is overexpressed in epithelial cells of the cornea, conjunctiva

and RPE (Gan et al., 2013)(Liu et al., 2018). Surface charge also plays a critical role in the performance of LPHNs in vivo. Cationic lipids have been used to form a shell on LPHNs able to enhance ocular gene transfection efficiency (Jiang et al., 2012). Negative particles with diameter <200 nm showed increased internalization, cellular uptake and prolonged circulation times in the target tissue (Duan et al., 2017).

Due to their manifold advantages, LPHNs have emerged as promising delivery systems in the ocular field.

7.4. Nanofibers

Nanofibers present diameters in the nanometric range between 1 and 100 nm. The high surface area-to-volume ratio increases the drug loading capacity; nanofibers with diameters of 100 nm can provide up to 1000 m²/gr of surface area (Deepak et al., 2018). They are produced from high viscosity fluid polymers by the process of electrospinning. Polymeric solutions can be obtained by heating melting or dissolution in appropriate solvents. The application of high voltage (between 5-30 kV) results in the elongation of polymer solutions electrified by a metal needle acting as an electrode, giving a conical shape known as a Taylor cone (Taylor and A, 1969). The jet coming out of the needle is accelerated by the electric field and directed toward the collector. In the process, the solvents used during preparation evaporate, and the resulting solid fibers can be collected by the collector (Islam et al., 2019). The electrospinning process is highly flexible, offering the advantage of modulating critical process parameters to obtain nanofibers for the desired application. The morphology and diameter of the resulting nanofibers are controlled by three factors:

- polymer solution parameters (viscosity, surface tension, conductivity, molecular weight and polymer concentration);
- process conditions (voltage, flow rate and distance between the needle and the collector);
- environmental conditions (temperature and relative humidity).

Regarding polymer solution parameters, polar solvents and ionic compounds can increase the electrical conductivity and thus reduce the diameter of nanofibers, vice versa to surface tension, which generally betters the electrospinning process when the values are not too high (Haider et al., 2018). Viscosity is a critical parameter for a successful spinning procedure. Molecular weight and polymer concentration are both influential factors on viscosity, and an increase in them is proportional to an increase in viscosity. Generally spinning processes of polymer solutions with viscosities between 1 and 20 poise and surface tension of 35-55 dynes/cm resulted in smooth, uniform nanofibers (Huang et al., 2003). One strategy to optimize these parameters is the use of surfactants. Adding surfactants to the polymer solution could increase electrical conductivity, reduce surface tension, and increase viscosity (Jia and Qin, 2013). Uniform and small-diameter nanofibers were obtained using different surfactants (cationic, anionic, and nonionic) (Zeng et al., 2003).

Process parameters are similarly critical. Nanofibers with small diameters were obtained by applying high tensions; however, very high tension values failed for proper evaporation of the solvent and resulted in nanofibers with larger diameters (Bhardwaj and Kundu, 2010). Slow flow rates allowed an effective solvent removal and were useful for obtaining uniform and thin nanofibers (Sun et al., 2019). Solvent evaporation is also affected by distance; generally long distances resulted in small, uniform and without

morphological imperfections fibers. Although too long distances reduced the effect of the electric field and resulted in fibers elongation (Hekmati et al., 2013).

The electric field and consequently the spinning process are also influenced by environmental parameters. Generally, humidity lower than 25% resulted in smooth nanofibers without imperfections, while values higher than 30% resulted in pores formation on the surface (Hu et al., 2014). Temperature influenced two effects (solvent evaporation and viscosity) that adjusted the diameter in opposite ways. High temperatures on the one hand slowed solvent evaporation and prolonged the solidification time of nanofibers, on the other hand reduced the viscosity and improved the elongation of the polymer solution, resulted in thin fibers (De Vrieze et al., 2009).

So, despite these expedients, there are no always applicable rules, but each spinning process must be optimized by finding the right balance among critical parameters according to the investigated polymer.

Commonly used polymers can be natural (chitosan, fibronectin, collagen, gelatin, silk and ethyl cellulose), synthetic (PLA, PLGA, PVA and PVP) or a combination of both. Unique physical properties such as high elastic modulus, porosity, high contact time with ocular tissues, biodegradability, and biocompatibility make polymeric nanofibers ideal carriers for the treatment of ocular diseases. Nanofiber-based inserts are receiving a great attention, these are biodegradable and bioerodible devices with controlled drug release profiles and prolonged contact times on the ocular surface (Omer and Zelkó, 2021).

Surface modifications of the nanofibers, such as the addition of penetration enhancers/mucosal agents or the selection of the most suitable polymers, can bring additional benefits to these delivery devices.

Coating biopolymers like natural polysaccharides (inulin and heparin) and semisynthetic polyamino acids (α,β -poly(N-2-hydroxyethyl)-D,L-aspartamide) in addition to providing biomimetic properties were able to impart mucoadhesive properties to the nanofibrous inserts to increase permeation through the corneal tissue (Di Prima et al., 2019).

HP- β -CD as penetration enhancer and sodium alginate as mucoadhesive agent were used to coating nanofibers for ocular inserts (Polat et al., 2020). Although cyclodextrin increased corneal drug penetration, resulted in swelling of polymer fibers and burst drug release in the first two days followed by slow and continuous release up to 7 days. In addition to being ruled by variables such as diameter, porosity, geometry and morphology, the release kinetics of nanofibers also depend on diffusion, osmosis and erosion mechanisms of the polymer structure (Patrojanasophon et al., 2020).

Prolonged release profiles and the use of biodegradable materials are great advantages to reduce the frequency of administration and to improve patient compliance (Gelb et al., 2022). Special attention could be focused on the use of nanofiber-based ocular inserts for the treatment of chronic ocular diseases of the posterior eye segment.

7. MATERIALS SELECTED IN THIS PROJECT

Material selection is critical to obtain formulations suitable for the intended application. In this project, selected polymers and lipids were designed to improve ocular targeting of proposed nanocarriers. These materials show promising and interesting characteristics as reported in the following paragraphs.

11.1. Polymers

The investigated polymers for nanosystem development in this thesis were PLA, PLGA, PLGA-PEG and PVA (Figure 4). These FDA-approved synthetic polymers for ocular use

are characterized by predictable properties (Allyn et al., 2022). By varying molecular weights, structure, composition and copolymers, it is possible to regulate a wide range of properties (degradation rates, physical and mechanical properties) that affect the characteristics of nanosystems (size, degradation, solubility and dissolution rate) (Song et al., 2018).

Their design advantages and the extensive exploration of these polymers for small-molecule ocular delivery were the reasons behind the selection.

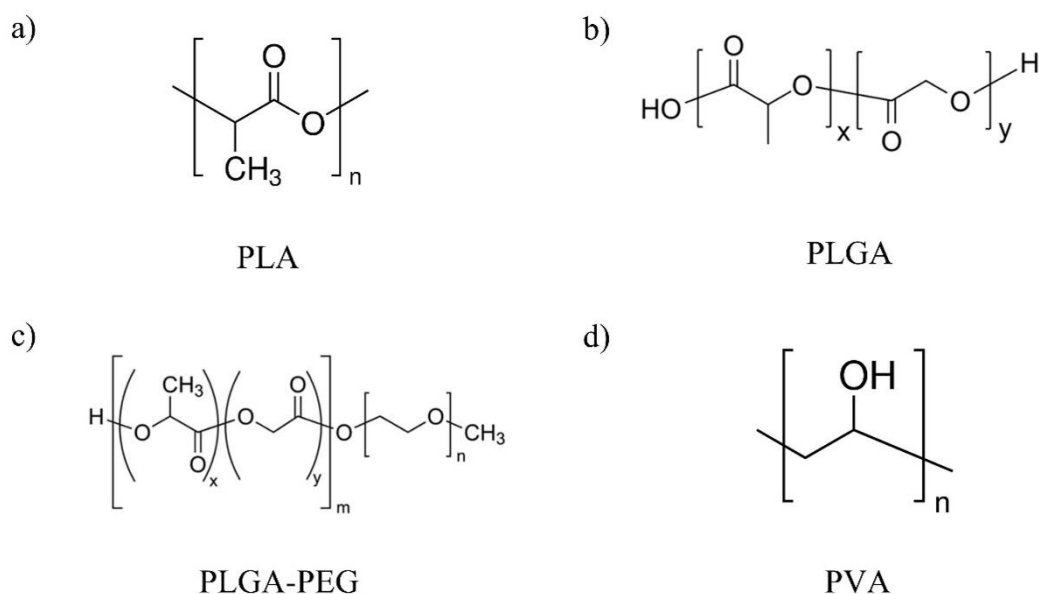


Figure 4. Chemical structure of a) Poly-lactic acid (PLA), b) poly-lactic-co glycolic acid (PLGA), c) polyethylene glycol-poly lactic acid-co-glycolic acid (PLGA-PEG) and d) polyvinyl alcohol (PVA).

PLA is a high-strength thermoplastic polyester polymer that exhibits desirable manufacturing properties. It is synthesized from renewable sources such as cornstarch, potato starch and sugarcane. Bacterial fermentation is used to produce lactic acid, which by removal of water is converted in the lactide dimer (Martinez Villadiego et al., 2022). Dimer polymerization can produce three stereoisomeric structures: D-PLA, L-PLA and DL-PLA. The DL-PLA stereoisomer possesses high mechanical stability, slow degradation rates, and excellent biodegradable and biocompatible properties as to be used

for the preparation of intravitreal implants (Morita et al., 1998)(Fialho and Da Silva Cunha, 2005). The slow degradation of PLA was exploited to develop Brimo DDS[®], an intravitreal implant for brimonidine delivery that recently completed phase 2 clinical trials (Kuppermann et al., 2021).

The production of DL-PLA-based NPs for ocular drug delivery has also warranted promising results, showing prolonged release profiles and improved intraocular bioavailability (Ibrahim et al., 2012)(Giannavola et al., 2003).

PLA can be copolymerized with polyglycolic acid to form PLGA. Degradation of these polyesters occurs by hydrolysis and leads to the formation of nontoxic byproducts, such as lactic and glycolic acids, which are cleared from the body through the Krebs cycle as water and carbon dioxide (Zou et al., 2009). During the copolymerization step, the lactide:glycolide monomer ratios can be regulated to produce PLGA with controlled physico-chemical properties (Tamboli et al., 2011). Degradation times and hydrophobicity of polymers can be optimized by modifying monomer ratios. Higher lactide contents exhibit a slower degradation rate of the matrix, resulting in more sustained drug release profiles (Janoria and Mitra, 2007). In addition, degradation rates are affected by the molecular weight of the polymer. Polymers with higher molecular weights degrade faster compared to those with lower molecular weights (Wu and Wang, 2001). Molecular weight also influences drug loading efficiency. For both of the polyesters discussed here, it was shown that lower molecular weights resulted in higher drug encapsulation efficiency (Basarkar et al., 2007). Therefore, in this study to improve encapsulation efficiency and obtain sustained release profiles, we opted for PLA and PLGA at low molecular weights, 10000-18000 and 4000-15000 respectively. To pursue the same goal, PLGA with lactide:glycolide ratio 75:25 was selected.

The hydrophobic features of these polymers have been used to improve drug delivery both via the topical route, as they facilitate permeation through the ocular mucosa, and via the intravitreal route, as they reduce drug diffusion away from the target tissue and provide controlled release (Duvvuri et al., 2007)(Herrero-Vanrell and Molina-Martinez, 2007)(Sah et al., 2017)(Swetledge et al., 2021). These advantages have made PLGA an attractive polymer as an ocular delivery carrier. Intravitreal implants of PLGA (Ozurdex® 46-47 and Durysta® 48) have been approved for the treatment of neurodegenerative retinal diseases such as diabetic macular edema and glaucoma (A. Chan et al., 2011)(Shirley, 2020). Both implants provided a controlled release of drug for 4-6 months, overcoming the challenges associated with frequent eyedrop administrations otherwise required to manage chronic conditions.

PLGA can in turn be copolymerized with PEG chains to further control physical, chemical, and mechanical properties such as stability, biodegradation, loading, and drug release. PEG is a hydrophilic polymer composed of repeated monomeric subunits of ethylene oxide. It possesses excellent solubility in both organic and hydrophilic solvents (Place et al., 2009). Again, the properties of the PLGA-PEG copolymer can be influenced by the molecular weight and relative concentrations of the starting units (Pannuzzo et al., 2020). As seen previously according to the molecular weight of PEG it was possible to obtain mucoadhesive or mucopenetrating properties (Lai et al., 2009). Therefore, with the aim of improving the corneal penetration by topical formulation, PLGA-PEG copolymer with PEG unit molecular weight of 5 kDa was selected in this project.

Conjugation of PEG to PLGA reduces its hydrophobicity. Increased hydrophilicity improves cell adhesion and confers stealth properties to the nanosystems, reducing clearance and prolonging the half-life in circulation of the nanosystems. PEG coatings

sterically stabilize particles, prevent aggregation, and improve drug encapsulation by providing a barrier against drug release. PEG coating density influences cellular uptake and minimizes adhesive interactions between particles and mucins, improving penetration in biological matrices like ocular mucosa (Galindo et al., 2022)(Gonzalez-Pizarro et al., 2019). The PEG addition imparts new chemical and physical properties to the polymers, giving additional advantages.

PVA is a thermoplastic, odorless, colorless, and water-soluble polymer. The synthesis of this polymer is obtained from the polymerization of vinyl acetate free radicals resulting in the formation of vinyl polyacetate. Hydrolysis of the acetate groups causes the production of PVA. The hydrolysis process is not always complete; PVA can be obtained at different degrees of hydrolysis: partially (80-98.5%), highly (<98.5%) and completely hydrolyzed (Gaaz et al., 2015). In addition to the degree of hydrolysis, a wide range of molecular weights (20000-400000) are available, depending on chain length and reaction conditions (acidic or basic) (De Merlis and Schoneker, 2003). Hydrolysis levels and molecular weights affect the physico-chemical properties and water solubility, however, PVA dissolution requires prolonged times and high temperatures (< 100 °C). The hydroxyl groups on the side chains allow the polymer to self-crosslink to form hydrogels with soft and elastic texture, tensile strength and high flexibility. The physical properties of PVA hydrogels similar to human tissue make it highly biocompatible (Jiang et al., 2011). The absence of toxic effects and excellent cell adhesion have made it a widely used polymer for several biochemical applications (Yang et al., 2004). In addition, the appealing properties have been widely exploited in the current year for the development of nanofibers, in situ gelling nanofiber films, and nanofiber-based implants for ocular delivery (Taghe et al., 2022)(Mirzaeei and Barfar, 2022)(Andreadis et al., 2022).

11.2. Lipids

Lipids have desirable attributes for the development of nanomedical products. Lipids can self-assemble to form biologically inert NPs coatings or structures. This property prevents the formation of nonspecific bonds with other biomolecules and consequently increases the specificity of targeting (Mashaghi et al., 2013). Their attractive properties make them ideal components for nanodevices. Here, the lipids selected for the development of the proposed nanosystems were CTAB, DDAB, Gelucire[®] 44/14 e Miglyol[®] 812 (Figure 5).

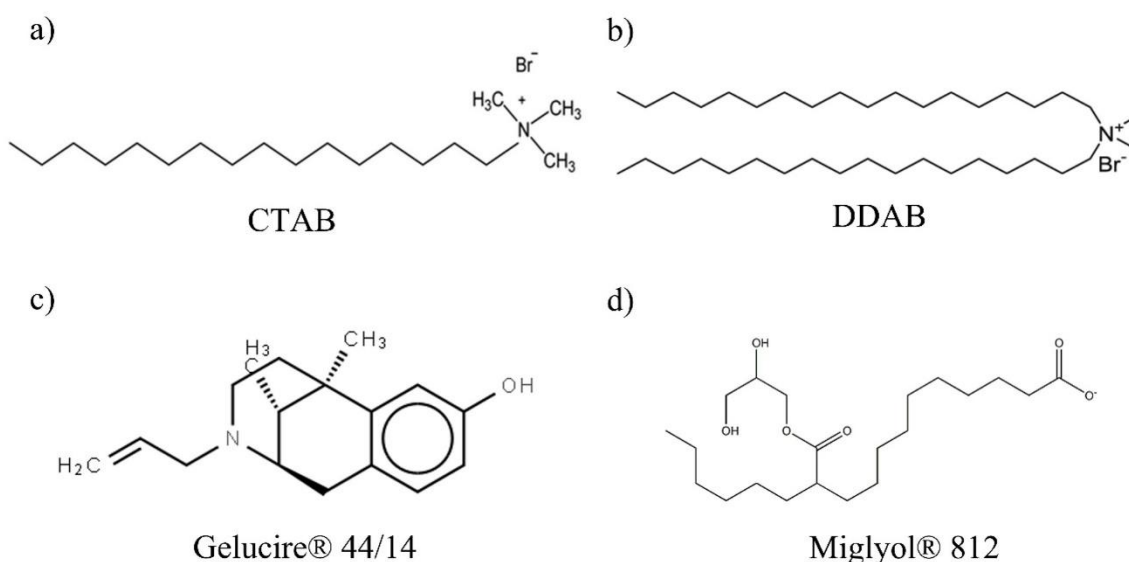


Figure 5. Chemical structure of a) Cetyltrimethylammonium bromide (CTAB), b) Didodecyldimethylammonium bromide (DDAB), c) Gelucire[®] 44/14 and d) Miglyol[®] 812.

CTAB and DDAB are two cationic lipids also known as surfactants, with structures of quaternary ammonium salts. They are amphiphilic molecules, consisting of a hydrophilic polar head and a hydrophobic nonpolar tail consisting of a long alkyl chain. CTAB has a single chain with 16 carbon atoms, while DDAB has a double chain with 18 carbon atoms which provides greater lipophilicity (Joana F Fangueiro et al., 2014). The use of these cationic lipids as a coating confers to the particles high positive zeta potential (ZP). Cationically charged systems are more likely to penetrate cells by endocytosis or fusion with the membrane. The electrostatic interaction that is generated with the negative

charges of cell membranes enhances adhesion to biomembranes and thereby bioavailability (Basarkar et al., 2007). In addition to increasing bioavailability, external surface charges also improve plasmid loading. These features provided by CTAB and DDAB have been exploited in numerous studies with the aim of increasing the immunogenicity of DNA vaccines and gene transfection (Date et al., 2011)(Russo et al., 2013)(Oyewumi et al., 2016)(Khodaei et al., 2021). The advantages of discussed cationic lipids have also been used as an approach to improve mucoadhesion and prolong the retention time of nanosystems in the eye (Leonardi et al., 2015)(Almeida et al., 2015)(Hassan et al., 2018)(Baig et al., 2020)(Bonaccorso et al., 2021a). In addition, electrostatic repulsion at positive ZP values increased the stability of suspended particles. CTAB concentrations between 0.5 and 1% wt are predictors of good stability (Joana F Fanguero et al., 2014). The single or double chains of lipids affected the physico-chemical properties of the nanosystems. For example, when CTAB was used as a coating for lipid NPs a better encapsulation efficiency was achieved due to the higher degree of crystallinity than DDAB (Joana F Fanguero et al., 2014). While lipid coating of PLA nanosystems with double chain DDAB provided better packing of the outer layer and higher ZP values than CTAB, leading to the formation of stable, well-defined, spherical-shaped and sustained-release nanodevices (Carbone et al., 2016). This phenomenon could be attributed not only to the different chemical structure but also to the different lipophilicity of the two lipids. In this project, lipid coating was applied to NPs of PLGA-PEG. Considering the dual lipophilic/hydrophilic nature of the selected polymer, both lipids were investigated as NP shells.

Gelucire[®] 44/14 is a semisolid lipid consisting of a mixture of monoglycerides, diglycerides, triglycerides, and fatty acid esters of polyethylene glycol (Da Fonseca

Antunes et al., 2013). This lipid is often used for preparation of lipid NPs for ocular drug delivery. It is an absorption enhancer employed to increase corneal permeation (Li et al., 2008)(Liu et al., 2011)(Sunny Shah et al., 2022). Gelucire[®] 44/14 also improves the absorption of poorly soluble drugs and provides extended release profiles (Liu et al., 2016). The absorption capacity of this lipid is related to drug molecular weight. Drugs with higher molecular weights (10000 Da) showed better absorption compared the ones with lower weights (H. Zhang et al., 2014). Increased drug absorption, prolonged corneal adhesion, and sustained release give to this lipid unique advantages in terms of drug bioavailability.

Miglyol[®] 812 is a clear, slightly yellowish liquid lipid. It consists of a mixture of medium-chain triglycerides (caprylic and capric fatty acids) extracted from palm oil endosperm and/or coconut plants. Although the choice of solid lipids is varied, Miglyol[®] 812 is the most commonly used liquid lipid for the production of NLC to be administered ocularly (Yu et al., 2019)(W. Zhang et al., 2014)(Zhang et al., 2013)(Tian et al., 2013). Miglyol[®] 812 improved solubility of hydrophobic molecules and encapsulation efficiency in NLC (Souto et al., 2004). When mixed with Gelucire[®] 44/14, it reduced the melting point of the solid lipid (from 44 °C to 38-40 °C), suggesting that it could promote faster melting. In addition, by tuning the proportions between the solid and liquid lipid, it is possible to modulate the release from the lipid matrix (Ortiz et al., 2021). NLCs consisting of Gelucire[®] 44/14 and Miglyol[®] 812 applied topically improved drug bioavailability to the retina, resulting in promising vehicles for the treatment of posterior eye segment diseases (Platania et al., 2019).

8. QUALITY BY DESIGN AND DESIGN OF EXPERIMENT

The European Medicines Agency (EMA) publishes scientific guidelines on medicinal products for human use harmonized by the International Conference on Harmonization of Technical Requirements for Registration of Pharmaceuticals for Human Use (ICH). Designing formulations in accordance with ICH guidelines will ensure that products with the required quality, safety and efficacy parameters can be produced. Therefore, applications for commercial authorization of quality-designed medicines are welcomed by EMA. Quality, as well as efficacy and safety, are key criteria for drug approval and must be ensured at all stages of drug production starting from design (Kumar and Vishal Gupta, 2015). Identifying, explaining, and managing the sources of variability that affect the design, development, and production phases of medicines is the first step for quality assurance. To rationally process these steps, the use of statistical, mathematical, and systematic methods is helpful.

The systematic approach of Quality by Design (QbD) in chemical production control was introduced by the Food and Drug Administration (FDA) in 2005. In the ICH Q8 guidelines, QbD is defined as *“A systematic approach to pharmaceutical development that begins with predefined objectives and emphasizes product and process understanding and process control, based on sound science and quality risk management”* (EMA, 2009).

This approach can also be applied to nanotechnology to obtain nanocarriers with the desired quality through robust design processes. The adoption of QbD begins with the identification of the quality target product profile (QTTP). QTTP is a prospective summary of the quality characteristics of the medicament that ideally should be achieved to assure the desired quality. Examples of QTTP in nanomedicine are drug release,

stability, and intended dosage form (Bonaccorso et al., 2021b). Second, it is necessary to determine which parameters affect QTTP and which critically affect it. These parameters are known as critical quality attributes (CQA), critical material attributes (CMA), and critical process parameters (CPP).

CQA are chemical, physical, biological, microbiological properties and characteristics that must fall within a specific range for a product to be of acceptable grade. In the case of nanomedicine, they include physico-chemical characteristics of particles such as size, polydispersion, surface charge, pH, rheological behavior, encapsulation, drug loading capacity, and so on (Rawal et al., 2019).

CMA are not defined by the ICH guidelines, but can be described as the physico-chemical, biological or microbiological characteristics of the input materials (type, concentration, purity of polymers/lipids, etc.). CMA must also fall within a certain range to ensure product quality, because small variations in the quality of a material have a major impact on CQA and formulation quality (Namjoshi et al., 2020).

CPPs also affect CQA; these are process parameters that in turn must be controlled to ensure a quality production process. These are operational parameters (pressure, speed, temperature, flow, etc.) that influence processes such as melting, mixing, filtering, drying, and precipitation. Identifying CPPs is important to understand and control the manufacturing processes that affect the quality of the final formulation (EMA, 2009).

Previous knowledge observed by practitioners in manufactured batches and literature filtering of similar products allow identification of critical attributes and parameters (Pallagi et al., 2015). The next step after identifying CQAs, CMAs, and CPPs is the delineation of the design space, defined by the ICH Q8 guidelines as “*The multidimensional combination and interaction of input variables (e.g., material*

attributes) and process parameters that have been demonstrated to provide assurance of quality”.

The correct parameters selection guides the construction of an appropriate design space to research the desired QTTP (EMA, 2009). Figure 6 shows the QbD approach culminating in the achievement of QTTP.

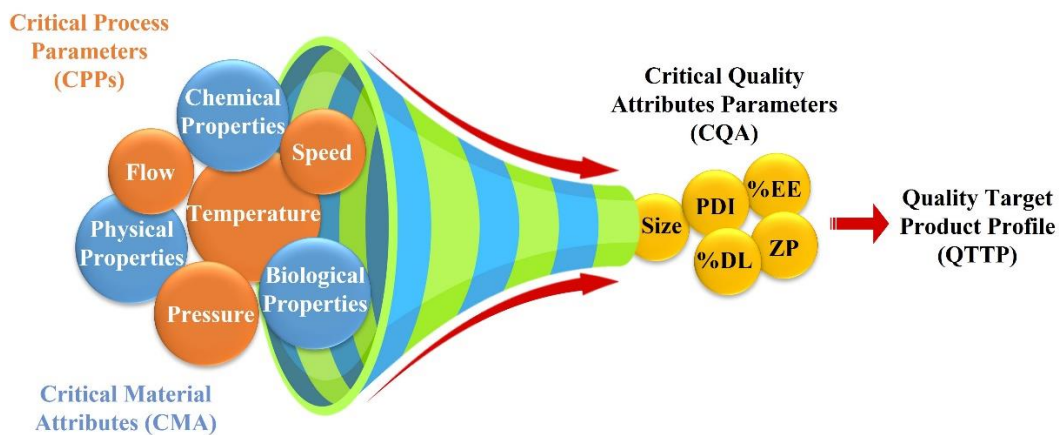


Figure 6. Components of QbD approach

Designing experiments to obtain the final product with the desired quality could require excessive time and cost and the preparation of unnecessary batches. Over decades, traditional approaches such as OVAT (One Variable at A Time) and OFAT (One Factor at A Time) have been used to study the influence of one variable at a time. In addition to the large number of experiments to be performed, the limitation of this approach was non-observation of the influence of interactions between variables (Arora et al., 2016).

Design of Experiment (DoE) is a multivariate approach methodology that overcomes the drawbacks of traditional approaches. This approach through a small number of rationally planned experiments yields maximum results. DoE allows the experimenter to observe how multiple input variables (X_1, X_2) or interactions between variables (X_1X_2) affect the measured response (Y). Input variables, also referred to as "independent variables," can be qualitative (categorical) or quantitative (numerical) and are investigated by the

experimenter at different levels in a space known as "experimental domain." The measured response variables are referred to as "dependent variables." The number of experiments to be performed depends on the number of variables and levels investigated. The planned experiments involve five steps, as shown in Figure 7.

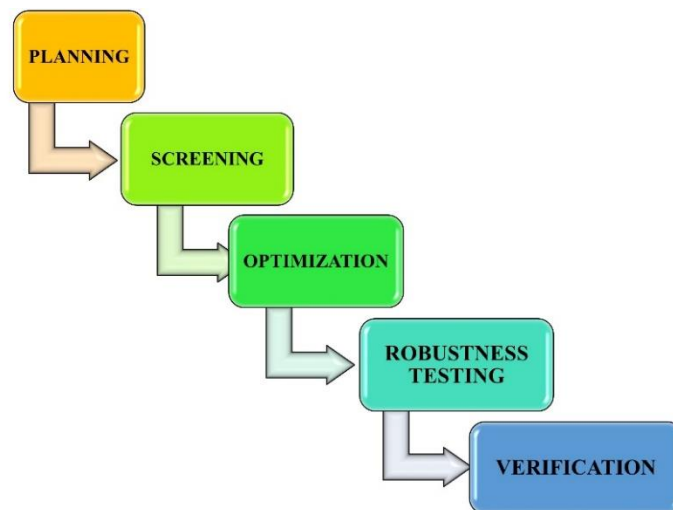


Figure 7. Steps to plan experiments

1. *Planning*: before performing experiments and data collection, it is necessary to plan the course of experimentation, assess time, available resources, and integrate prior knowledge to proceed to the experimental phase. This step involves identification of the variables and levels to be investigated and the selection of the appropriate responses to be measured. For example, if some factors (polymer concentration, viscosity, etc.) present levels that result in unfavorable outcomes, the experimental domain range must be modified (Bonaccorso et al., 2021c).
2. *Screening*: used to identify critical factors that significantly influence process responses and to remove irrelevant factors. Parameters that are intended to be kept constant are also selected during this step. Full Factorial Design (FFD) is

useful in screening to identify the most significant variables to study (Tavares Luiz et al., 2021);

3. *Optimization*: to achieve the desired goal, the best combination of the factors investigated must be determined. The pursuable objectives are maximize, minimize, target, within range. Response surface methodology (RSM) is used in this step to analyze the response relative to the variables (Musumeci et al., 2019);
4. *Robustness Testing*: used to identify sources of variation outside the control of the investigator, also known as "noise factors" (e.g., humidity, temperature). Making the process insensitive to these factors improve the robustness of the design (Bonaccorso et al., 2021b);
5. *Verification*: involves validation of method by experimental tests to confirm the predictivity of the methodology. Calculating the error between the experimental and predicted data allows the prediction accuracy of the model to be evaluated (Bonaccorso et al., 2020).

The application of RSM methodology in optimization is gaining increasing interest in the field of nanotechnology; it has been used to optimize polymeric and lipid NPs or nanofibers (Nair et al., 2020)(Ismail et al., 2019)(Rivelli et al., 2021)(Subramaniam et al., 2020).

This is a promising statistical tool for analyzing multivariate processes. The data collected in the experimental phase are processed to produce different mathematical models (linear, quadratic, cubic, or two-factor interaction). The model that best fits the data is subjected to analysis of variance (ANOVA) to test reliability and adequacy to navigate the design space. The selected model outlines the shaping of the response surface. 3D graphs and

contour plots generated help to identify changes in response in accordance with the investigated factors. This tool permits to find the ideal "window" of operability (Breig and Luti, 2021).

RSM use is advantageous for achieving nanocarriers with desirable quality, as long as the steps preceding optimization (planning and screening) are carried out with appropriate logic. However, it remains true that the investigator's knowledge of the parameters, processes, formulations, and design methodologies underlies a successful DoE application.

9. AIM OF THE PROJECT

The treatment of neurodegenerative eye diseases presents a significant great challenge in the field of ophthalmic drugs. Static and dynamic ocular protective barriers hinder drug delivery into intraocular tissues. Molecules used for the management of such diseases often exhibit poor solubility and consequently mild tissue permeation. As a result, dose/response profiles are generally very poor. In addition, patient adherence to treatment is a critical condition for therapeutic success in disease management. However, these drawbacks have often been overcome through advances in nanotechnology to date. Positive results have been achieved with the development of nanomedicines that have been able to jointly provide effective delivery devices and ensure patient compliance. Mucoadhesion and mucopenetration enhancers have proven to be effective agents for circumventing ocular barriers and improving intraocular bioavailability of administered drugs. Sustained drug release profiles have made it easier for patients to maintain therapeutic regimens.

Based on the listed advantages, the goal of my thesis was to develop innovative platforms to improve the delivery of active molecules to the posterior segment of the eye. Polymeric, lipid and hybrid nanocarriers intended for different routes of administration were studied to achieve this purpose. In detail, the study was conducted as described below:

- (i) Development of polymeric NPs (PLA and PLGA) for potential FA intravitreal delivery. Preliminary cytotoxicity testing on empty carriers, characterization studies and physicochemical stability of the systems. Evaluation of purification efficacy of different techniques employed. Study of the influence of the two matrices on FA release profiles;
- (ii) Design and optimization of melatonin-loaded mucoadhesive LPHNs for topical application. The cationic lipid shell was exploited to prolong the retention time on the ocular surface to improve bioavailability. A preservative and sterilization were employed to prolong the storage life of the nanosuspension. Release experiments were followed for 8 days. In vitro tests on a diabetic retinopathy model and Draize assay were conducted to evaluate neuroprotective/antioxidant efficacy and ocular tolerability, respectively;
- (iii) Production of fluorescent PLGA-PEG NPs for in vitro and in vivo cell tracking labeled by two different techniques: encapsulation and grafting of the fluorophore on polymer backbone. Evaluation of in vitro cytotoxicity on olfactory ensheathing cell lines and neuronal cells to assess a potential application for the treatment of neurodegenerative disorders by nose-brain delivery;

- (iv) Review on fluorescent nanosystems for diagnostic and theranostic applications in the ocular field. Overview of fluorescent molecules and nanosystems classified according to their nature (lipidic, polymeric, metal-based, and protein-based) commonly used in ocular applications. Summary of fluorescent nanosystems found in clinical trials and in the marketplace;
- (v) Design and optimization of ion-pair in combination with NLC to improve the incorporation of FLN dichlorhydrate in lipid carrier systems;
- (vi) Production of melatonin-loaded nanofibers (PLA and PVA) by electrospinning technique for the development of ocular inserts. Spectroscopic characterization and in vitro release profiles were compared for the two types of produced nanofibers.

CHAPTER II: *Ferulic Acid-Loaded Polymeric Nanoparticles*
for Potential Ocular Delivery

Article

Ferulic Acid-Loaded Polymeric Nanoparticles for Potential Ocular Delivery

Alessia Romeo¹, Teresa Musumeci^{1,2,*}, Claudia Carbone^{1,2}, Angela Bonaccorso¹, Simona Corvo¹, Gabriella Lupo^{3,*}, Carmelina Daniela Anfuso³, Giovanni Puglisi¹ and Rosario Pignatello^{1,2}

¹ PhD in Neurosciences, Department of Drug and Health Sciences, University of Catania, viale A. Doria 6, 95125 Catania, Italy; alessia.romeo@phd.unict.it (A.R.); ccarbone@unict.it (C.C.); abonaccorso@unict.it (A.B.); simona.corvo09@gmail.com (S.C.); puglisig@unict.it (G.P.); r.pignatello@unict.it (R.P.)

² NANO-i, Research Centre for Ocular Nanotechnology, University of Catania, viale A. Doria 6, 95125 Catania, Italy

³ Department of Biomedical and Biotechnological Sciences, University of Catania, 95127 Catania, Italy; daniela.anfuso@unict.it

* Correspondence: teresa.musumeci@unict.it (T.M.); gabriella.lupo@unict.it (G.L.)

Abstract: Ferulic acid (FA) is an antioxidant compound that can prevent ROS-related diseases, but due to its poor solubility, therapeutic efficacy is limited. One strategy to improve the bioavailability is nanomedicine. In the following study, FA delivery through polymeric nanoparticles (NPs) consisting of polylactic acid (NPA) and poly(lactic-co-glycolic acid) (NPB) is proposed. To verify the absence of cytotoxicity of blank carriers, a preliminary in vitro assay was performed on retinal pericytes and endothelial cells. FA-loaded NPs were subjected to purification studies and the physico-chemical properties were analyzed by photon correlation spectroscopy. Encapsulation efficiency and in vitro release studies were assessed through high performance liquid chromatography. To maintain the integrity of the systems, nanoformulations were cryoprotected and freeze-dried. Morphology was evaluated by a scanning electron microscope. Physico-chemical stability of resuspended nanosystems was monitored during 28 days of storage at 5 °C. Thermal analysis and Fourier-transform infrared spectroscopy were performed to characterize drug state in the systems. Results showed homogeneous particle populations, a suitable mean size for ocular delivery, drug loading ranging from 64.86 to 75.16%, and a controlled release profile. The obtained systems could be promising carriers for ocular drug delivery, legitimating further studies on FA-loaded NPs to confirm efficacy and safety in vitro.

Keywords: antioxidant; PLA; PLGA; retinal pericytes; endothelial cell; controlled release

1. Introduction

Oxidative stress is able to involve morphological and functional alterations to retinal tissues, playing a key role in the onset and progression of retinal diseases, such as age-related macular degeneration (AMD), glaucoma, diabetic retinopathy (DR), and retinal vein occlusion (RVO) [1]. Recent clinical studies have demonstrated the potential health benefits obtained with the consumption of fruit and vegetables rich in phytochemicals, such as polyphenols, on visual function. Thanks to the pluriphar-macological effects, these molecules might be able to slow down and prevent the progression of the aforementioned pathologies [2,3].

The most attractive polyphenol effects in these diseases are wielded on oxidative stress pathways, where they are able to suppress the harmful effect of the reactive oxygen species (ROS) [4]. For this reason, antioxidant molecules are gaining importance as a promising therapeutic strategy in treatment/prevention of eye chronic

disease. A comparative study regarding the properties of various antioxidants including ascorbic acid, ferulic acid (FA), α -tocopherol and β -carotene, has shown that FA is the most efficient among the tested antioxidants [5,6]. Thanks to its phenolic nucleus and an extended side chain conjugation, this substance can act as a potent antioxidant in both isolated membranes and intact cells, because it is able to form a resonance-stabilized phenoxy radical, thereby inhibiting lipid peroxidation and ROS production.

FA (4-hydroxy-3-methoxycinnamic acid) is a phenolic compound and a notable biological and structural component of the plant cells. It is one of the most abundant phenolic acids in plants and might be found in high concentration in food such as whole grains (1–3 mg/100 g), fruits, and vegetables (800 mg/100 g) [7]. FA exhibits a wide spectrum of beneficial activity for human health, it was tested *in vitro* for its potential anti-inflammatory, anticancer, neuroprotective, anti-angiogenesis effects and was tested *in vivo* on mice for its antidiabetic, anticancer, antiapoptotic, and antioxidant properties [8]. Despite this, poor solubility of FA in aqueous solution remains a major limit for its bioavailability. In recent years, in order to overcome this problem and to improve the drug dissolution rate, many strategies were developed such as the drug complexation with hydroxypropyl- β -cyclodextrin (HP- β -CD), the inclusion in platforms composed of cocrystal, micelles, and nanogels, and the encapsulation in nanostructured lipid carriers (NLC) or chitosan NPs [9–16].

The use of biodegradable polymeric particles has been extensively studied to increase bioavailability, prolong controlled drug release, and avoid repeated ocular administration [17]. The use of polymeric NPs include many advantages, such as good control on size and size distribution, reduce clearance time, and protection and retention of the drug that improves bioavailability in intraocular or extraocular tissues [18]. Polymers frequently used to develop NPs for ocular delivery include poly(lactic acid) (PLA), poly(lactic acid)/poly(lactic-co-glycolic acid) (PLGA), polycaprolactone (PCL), and hyaluronic acid [19]. Despite this, to date, no study has been conducted on PLA or PLGA NPs for ocular delivery of FA. The use of PLA/PLGA carriers for ocular drug delivery (ODD) is sustained by their biocompatibility and biodegradability [18,20,21]. In a work by Gupta et al., sparfloxacin loaded in PLGA-NPs was administered to rabbits, showing to improve the residence time at the corneal surface with respect to conventional eye drops. *In vivo* studies of this formulation signaled that PLGA-NPs have a good stability and ocular tolerance. Moreover, *in vivo* degradation of PLGA mainly happens by hydrolysis, resulting in nontoxic lactic and glycolic acids, which enter to the tricarboxylic acid cycle to be metabolized in water, carbon dioxide, and energy [22]. A study conducted by Bourges et al. on PLA NPs showed that a single intravitreal injection in rats allows the system in retinal pigment epithelium (RPE) cells to be found, even after 4 months. Histology demonstrated the anatomical integrity of the injected eyes and the absence of toxic effects [17]. Administration by intravitreal injection has also been shown to be safe with PLA/PLGA microspheres, so the systems can be considered suitable for the treatment of diseases affecting the posterior segment of the eye [23]. In addition, several studies on polymeric nanoparticles (NPs) have used intravitreal injection as a route of administration, so the nanocarriers designed and discussed here could be used for this purpose [24–27].

The aim of this study was to prepare and characterize FA-PLA and PLGA NPs for potential ocular delivery, evaluating their physico-chemical, technological properties suitable for the selected site of administration, and a preliminary *in vitro* study was performed. The two unloaded nanocarriers were subjected to *in vitro* cell viability

studies on primary endothelial cells and primary retinal pericytes to assess the absence of cytotoxicity. The two nanoformulations were loaded with the drug and investigated to determine the mean size, polydispersity index (PDI), zeta potential (ZP), pH, osmolarity, encapsulation efficiency (EE), and release profile until 48 h. Centrifugation and dialysis were carried out to eliminate both surfactant and the unloaded drug, and to select the most efficient purification method. The final formulations were cryoprotected and freeze-dried both to prevent premature drug release and to avoid hydrolysis of the polymeric material from the aqueous suspension. NPs morphology was assessed by SEM analysis. To evaluate the stability after resuspension, physico-chemical parameters were monitored during 28 days of storage at 5 °C. Freeze-dried samples were subjected to thermal analysis through differential scanning calorimetry (DSC) and FT-IR spectroscopy.

2. Materials and Methods

2.1 Materials

Trans-Ferulic acid, Resomer[®] R 202 H, acid terminated, Mw 10.000–18.000 (PLA), Resomer[®] RG 752 H, acid terminated, lactide:glycolide 75:25, Mw 4.000–15.000 (PLGA), and Tween[®] 80 were supplied by Merck (Milan, Italy). Ethanol (96% purity) was obtained from J.T.Baker (Deventer, The Netherlands). Acetone and dialysis membrane (molecular weight cut off (Mwco) 3000 Da, diameter 11.5 mm; Spectra/Por[®]) were purchased from VWR International PBI Srl (Milan, Italy). Hydroxypropyl- β -cyclodextrin was obtained from Roquette Freres (Lestrem, France). Deionized water was used for all the preparations.

2.2 Preparation of Unloaded Nanoparticles

Nanoprecipitation technique was applied to prepare PLA (NPA) and PLGA (NPB) NPs with slight modification of a previously reported process [28]. PLA or PLGA polymer (3.6 mg/mL) was dissolved in acetone. The organic phase (5 mL) was poured, drop by drop, into 10 mL of water/ethanol mixture (1:1), containing 0.05% (*w/v*) Tween[®] 80, under magnetic stirring (500 rpm) at room temperature, thus forming a milky colloidal suspension. The organic solvents were removed under vacuum by a rotavapor (Buchi) at 40 °C.

2.3 Physico-Chemical Characterization

The particle size (Z-ave) and the polydispersity index (PDI) were determined by photon correlation spectroscopy (PCS). PCS was performed using a Zetasizer Nano ZS90 (Malvern Instruments Ltd., Malvern, England) and the experiments were carried out using a 4 mW He-Na laser beam with a 633 nm wavelength. The following parameters were used for these experiments: temperature 25 °C, medium refractive index 1.330, medium viscosity 1.0 mPa s, and dielectric constant value 80.4. The analysis of a sample consisted of 3 sets of measurements, and the results are expressed as mean size \pm standard deviation (SD). Each sample was analyzed into disposable sizing cuvettes (DTS 0012).

Zeta potential (mV) was measured using the same instrument. Electrophoretic mobility for each sample was revealed at 25 °C, using the Smoluchowski constant with a value of 1.5 to obtain the corresponding ZP values.

2.4 Osmolarity and pH

The osmolarity of NPs was analyzed by freezing point depression (FPD) using a digital osmometer (Osmomat 030, Gonotec, Berlin, Germany) and as calibration

solutions distilled water and sodium chloride 0.9%. The value reported for each sample is the mean of 3 different measurements. The determination of pH was carried out using a pH-meter at 25 °C (Checket, Hanna Instrument, Woonsocket, RI, USA) which was calibrated before each use with 3 buffer solutions at pH 4.01 ± 0.02 ; 7.00 ± 0.02 and 10.00 ± 0.02 . Three measurements were made for each sample.

2.5 *In Vitro* Cytotoxicity Test of Unloaded Nanoparticles

2.5.1 Cell Cultures

Primary cultures of microvascular pericytes were obtained from bovine retinas as already described [29]. Briefly, the cells were homogenized and filtered through a nylon filter (80 μm). Phosphate-buffered saline (PBS) at pH 7.4 was supplemented with collagenase-dispase and bovine serum albumin, at concentrations of 1 mg/mL and 0.5%, respectively. The micro-vessels were immersed in the PBS solution for 20 min and maintained at 37 °C. The homogenate was centrifuged for 10 min at 1000x g. The isolated cells were plated in Dulbecco's Modified Essential Medium (DMEM) supplemented with 20% fetal bovine serum (FBS), 2 mM glutamine, 100 U/mL penicillin and 100 $\mu\text{g}/\text{mL}$ streptomycin. Culture plates were previously covered with a thin layer of gelatin. At confluence, the cells were trypsinized and seeded in new petri dishes in DMEM at 10% fetal bovine serum.

Bovine microvascular endothelial cells (BMVEC) were purchased from Sigma (Milan, Italy) and fed with Ham's F10 medium supplemented with 10% FBS, 80 $\mu\text{g}/\text{mL}$ heparin,

2.5.2 MTT Assay

Pericyte and endothelial cells were seeded in 96-well plates at a cell density of 1.5×10^4 per well. 3-[4,5-dimethylthiazol-2-yl]-2,5-diphenyl tetrasodium bromide (MTT) (Chemicon, Temecula, CA, USA) was used to perform the cell viability assays. Prior to treatment, cells were incubated at a temperature of 37 °C overnight and then treated for 24 h and 48 h in the absence (control) or the presence of NPA and NPB (0.25–5 mg/mL). After incubation periods, 10 μL of MTT reagent (5 mg/mL) was added to each well and the cells were incubated at 37 °C for a further 3 h. Formazan crystals were solubilized under constant agitation with 100 μL of DMSO for 10 min. The absorbance was detected at a wavelength of 570 nm with plate reader (Synergy 2-bioTek). All experiments were performed at least 6 times in triplicate.

2.6 FA-Loaded Nanoparticles

FA-loaded NPs were obtained with the same procedure described in Section 2.2. The active compound (1% *wt/wt*, drug/polymer) was added to the organic phase and the preparation proceeded as described above [30,31].

2.7 Purification Steps

Nanosystems were subjected to purification by two methods: dialysis and centrifugation, with the aim of removing any residual surfactant or unloaded drugs. The removal of unstructured polymer chains in the nanocarriers was not considered, as their molecular weight is higher than the cut-off of that the dialysis membrane used. In order to observe any physico-chemical properties variation due to purification processes, the NPs suspensions were monitored in terms of mean size, PDI, and surface charge, before and after the purification phases. Centrifugation was performed with a Thermo-scientific SL 16R Centrifuge (Thermo Scientific Scientific Inc., Waltham, MA, USA) at 15,777xg for 1 h at 8 °C. The obtained supernatants were collected for high performance liquid chromatography (HPLC) analysis, pellets were resuspended in water

and characterized through PCS analysis. For dialysis, previously hydrated cellulose membranes (Mwco 3000 Da, diameter 11.5 mm; Spectra/Por®) were used. Membranes containing the colloidal suspensions were immersed in 500 mL of distilled water. Dialysis of each sample (NPA-FA and NPB-FA) was performed with different frequencies of water changes per hour (L/h). In the first case equal to 0.5 L/h (2.5 L in 5 h with 5 water changes) and in the second equal to 1 L/h (3 L in 3 h with 6 water changes). Dialyzed samples were collected and centrifuged at 15,777xg for 1 h at 8 °C; the obtained supernatants were then analyzed by HPLC, pellets were resuspended and subjected to PCS analysis.

2.8 Encapsulation Efficiency

The percentage of the encapsulated FA into the polymeric matrix of NPs was determined both after centrifugation and after dialysis performed with frequency of water changes of 0.5 and 1 L/h. Samples, including those purified by dialysis, were centrifuged in order to obtain separation of pellet from supernatant. The obtained supernatants were analyzed by HPLC to evaluate the drug concentration; each amount of the sample was quantified by measuring the UV absorbance at 320 nm. The EE was calculated by the difference between the amount of drug entrapped inside the NPs and the total quantity of drug employed to prepare the nanosystems, according the following equation [32]:

$$\text{Purification efficacy (\%)} = \frac{\mu\text{g FA in supernatant}}{(\mu\text{g FA}_{\text{tot}} - \mu\text{g encapsulated FA})} \times 100$$

2.9 Yield of Purification Process

The dialysis purification yield was calculated to select the most efficient method to remove unencapsulated FA from the systems. Purification efficiency was expressed as the percentage amount of dialyzed FA compared with the unencapsulated amount. Dialyzed samples were collected and centrifuged. The concentration of FA in the obtained supernatants was quantified by HPLC analysis, by measuring UV absorbance at 320 nm. The percentage of purification was calculated using the following equation:

$$\text{Purification efficacy (\%)} = \frac{\mu\text{g FA in supernatant}}{(\mu\text{g FA}_{\text{tot}} - \mu\text{g encapsulated FA})} \times 100$$

Each experiment was performed in triplicate and the results represent the mean \pm SD.

2.10 Stability Study of Resuspended Cryoprotected Freeze-Dried Formulations

The suspensions of purified NPs were mixed in a 1:1 ratio with 10% (*w/v*) of HP- β -Cyd to achieve a final cryoprotectant concentration of 5% (*w/v*). The resulting formulations were frozen and freeze-dried for 24 h (Freeze Dryer Edwards Modulyo, Akribis Scientific Limited, Knutsford, Cheshire, UK). The resuspended cryoprotected freeze-dried NPs were analyzed to evaluate potential changes over time of Z-Ave, PDI, ZP, osmolarity, and pH. The analyses were conducted on the NPs lyophilized powder, resuspended with the same volume of water lost during the drying phase [33]. After reconstitution, the above parameters were analyzed (zero time), after that, all of the formulations were stored in the refrigerator (5 °C) and tests were run again after 7, 14, 21, and 28 days.

2.11 *In Vitro* Release Profile of FA-Loaded NPs

The *in vitro* drug diffusion profiles of non-encapsulated FA solution (in PBS, pH 7.4) and the release profiles of drug-loaded NPs (NPA-FA and NPB-FA) were evaluated. The amount of FA released from NPs was measured after centrifugation of the samples, performed at 15,777xg rpm at 8 °C for 1 h; the obtained supernatants were subjected to HPLC analysis, the pellets were resuspended in a 5% (*w/v*) of HP- β -Cyd solution and freeze-dried. Lyophilized NPs were resuspended in 1 mL of PBS pH 7.4 [34]. The suspensions were placed into a cellulose membrane dialysis tubing (Mwco 3.5 kDa, flat width 18 mm, diameter 11.5 mm; Spectra/Por® Dialysis Membrane) and incubated in 19 mL of medium (PBS, pH 7.4), which was maintained under magnetic stirring at 37 °C, up to 48 h. Release medium (500 μ L) was sampled at predetermined time points (0, 1, 2, 3, 4, 5, 6, 7, 8, 24, and 48 h) and immediately replaced with the same volume of fresh medium, to maintain the sink condition. FA concentration in the collected samples was quantified by HPLC analysis. Release study was performed in triplicate for each formulation. The release curve was drawn according to the average and SD of 3 values at each moment.

2.12 HPLC Analysis

HPLC analysis was performed at room temperature using a 1050 Hewlett-Packard instrument (Hewlett-Packard, Milan, Italy) equipped with a 20 μ L injection valve Rheodyne 7125 (Rheodyne Inc., Cotati, CA, USA) and a UV-VIS detector (Hewlett-Packard, Milan, Italy). Mobile phase consisted of a mixture of 81:19 (*v/v*) acetonitrile:acetic acid (2% *v/v*). Stationary phase was a 4.6x15 cm C 18 column (Waters, Milan, Italy). Effluent was monitored at a wavelength of 320 nm, with a flow rate of 1 mL/min. The standard calibration curves were prepared at different dilutions of FA in methanol. The linear regression coefficient determined in the range 0.05–10 μ g/mL was 0.9997. No interference resulting from other components was observed.

2.13 Scanning Electron Microscopy (SEM)

NPs morphology was assessed by SEM study. The samples were prepared for the electron microscope with a spin-coating procedure at 500 rpm for 1 min with a Suss Microtech instrument and left to dry in air for a few hours. To ensure good conductivity, all of the samples were then coated with 5 nm of gold sputtering at a pressure of 10⁻³ mbar with an Emitech K500X equipment. The SEM were acquired at a low voltage of 3 KV with an InLens detector by using a Field Gemini microscope from Zeiss.

2.14 Thermal Analysis of Unloaded and FA-Loaded Cryoprotected Freeze-Dried Nanosuspensions

A DSC1 Star System apparatus (Mettler Toledo, Schwerzenbach, Switzerland) was used to perform calorimetric analyses. The DSC detection system consisted of a Mettler Full Range ceramic sensor (FRS5) with 56 thermocouples and a high sensitivity sensor (HSS8) with 120 thermocouples. The signal time constants were respectively equal to 1.8 and 3.1 s, while the digital resolution of the measurement signal was 16.8 million points. The sampling rate was maximum 50 values/s. Calorimetric resolution and sensitivity of FRS5 and HSS8 sensors, determined through the TAWN test, were respectively between 0.12–0.20 and 11.9–56.0. Each DSC scan had an accuracy of 0.2 K, a precision of ± 0.02 K, and a resolution of ± 0.00006 K. Optiplex 3020 software at Mettler Star® Dell was used for the data acquisition. DSC aluminum pans (40 μ L) were filled with pure FA, pure polymers, cryoprotectant, cryoprotected freeze-dried empty NPs (NPA and NPB), as well as loaded with FA (NPA-FA and NPB-FA) before sealing. All

samples were submitted to heating and cooling cycles in the temperature range 20–200 °C at a scanning rate of 5 °C/min (heating) and 10 °C/min (cooling).

2.15 FT-IR Spectroscopy Measurements

Pure FA, pure polymers, cryoprotectant, cryoprotected freeze-dried empty NPs (NPA and NPB) and loaded with FA (NPA-FA and NPB-FA) were analyzed using FT-IR spectrophotometer (Perkin-Elmer Spectrum RX I, Waltham, MA, USA). The instrument was equipped with an attenuated total reflectance (ATR) accessory and a diamond window and zinc selenide crystal (diamond/ZnSe). The dried samples were mixed with potassium bromide (KBr anhydrous of FT-IR grade) to obtain a homogeneous mixture, which was compressed into 1 mm pellets. The background was acquired from pure KBr pellet. For each sample, 20 scans were collected over the range of 400–4000 cm^{-1} at a resolution of 2 cm^{-1} at room temperature.

2.16 Statistical Analysis

All results are reported as mean \pm SD. The results were analyzed using one-way ANOVA followed by Tukey–Kramer multiple comparisons test; differences between groups were considered significant for a p -value < 0.05 . The t -test was used to calculate the statistical significance in the MTT assay; the percentages obtained relative to the control group were considered not significant for $p > 0.05$, significant for $p < 0.05$, very significant for $p < 0.01$ and extremely significant for $p < 0.001$.

3. Results and Discussion

In the present study, NPs have been produced by a solvent displacement technique. Tween 80, a non-ionic surfactant, was added in order to reduce the dynamic interfacial tension and to increase the steric repulsion between NPs [28]. Its non-ionic nature allows it to be included in the ophthalmic formulations, but this is acceptable since it does not induce strong eye irritation [35]. The concentration chosen for the emulsifier (0.05% w/v) was selected because it is considered a suitable amount both for obtaining small diameter particles and for the demonstrated ocular safety and tolerability [28,36].

3.1 Influence of Unloaded NPs Concentration on Cell Viability of Primary Cultures of Micro-Capillaries Pericytes and Endothelial Cells

An NPs system proposed for ocular administration must be able to deliver the active agent without compromising the viability of the host cells. To assess if NPA or NPB could induce cytotoxicity, MTT bioassay was performed on primary cultures of microcapillaries pericytes and endothelial cells. Unloaded NPs were studied at different concentrations (0.25–5 mg/mL) to evaluate the effect on cell viability and the potential application of these systems as FA nanocarriers for ocular therapy.

Figure 1 shows cell viability vs NPs concentration (mg/mL). An important consideration is that cell viability strictly depended on the type of cell line as well as on the concentration tested. The results obtained from the analysis of NPA and NPB carriers on BMVEC were plotted as a function of the incubation time, which is equal to 24 (Figure 1A) and 48 h (Figure 1B). Regarding the data obtained at 24 h, the cells incubated with NPA and NPB showed a high viability ($>90\%$) in the concentration range 0.25–1 mg/mL. Viability at 48 h follows the same trend, with no significant reduction.

The evidence of a more marked reduction is observable for NPA at higher concentrations. From the statistical analysis of the data, it emerged that the decrease in viability compared to the control recorded for NPA at 2.5 mg/mL oscillates between significant (24 h) and very significant (48 h), it is instead extremely significant at 5 mg/mL. For NPB, the amount of reduction was significant at 2.5 mg/mL and very significant at 5 mg/mL. Therefore, although NPB in the safe range 0.25–1 mg/mL have the lowest cell viability rates, at higher concentrations, they show a less pronounced, although still toxic, reduction. Pursuant to ISO 10993-5, percentages of cell viability above 70% are considered an absence of cytotoxicity [37]. The results obtained showed that the highest concentrations (2.5–5 mg/mL), for both samples and times examined were cytotoxic, resulting in a reduction in viability >30%.

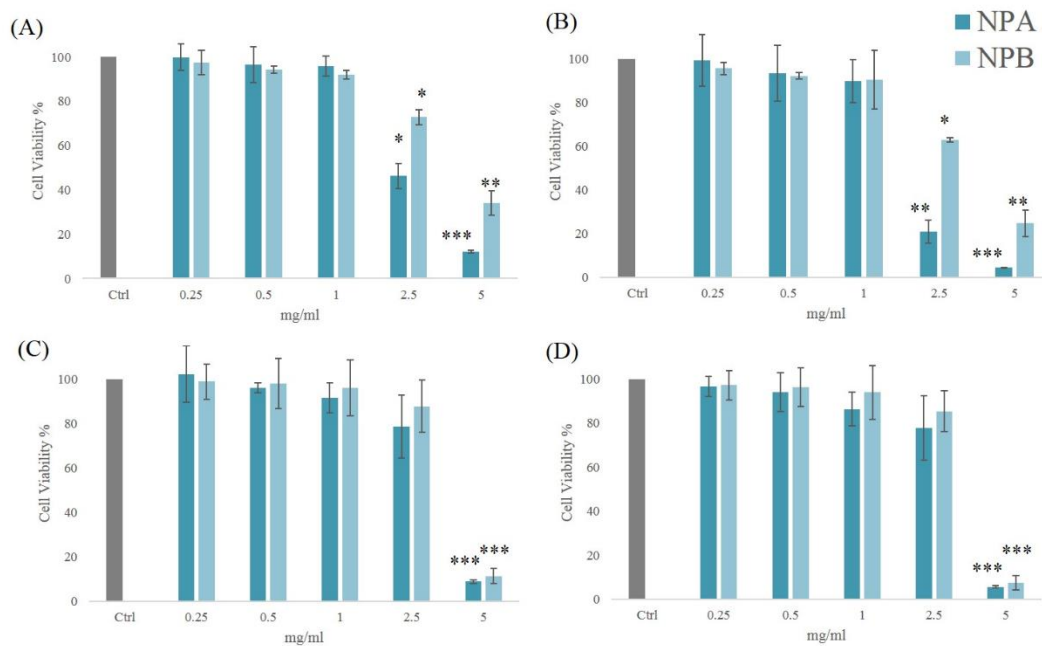


Figure 1. Cytotoxicity of NPA and NPB NPs on primary endothelial cells after (A) 24 h and (B) 48 h of incubation and on primary retinal pericytes cells after (C) 24 h and (D) 48 h of incubation at different concentrations (5; 2.5; 1; 0.5; 0.25 mg/mL). Three independent experiments were performed in sixfold. Error bars depict the S.D. of the mean. *t*-test was used to calculate statistical significance of the percentages obtained versus control group. [ns = not significant ($p > 0.05$); * = significant ($p < 0.05$); ** = very significant ($p < 0.01$); *** = extremely significant ($p < 0.001$)].

The analysis of NPs on RMP incubated for 24 h showed the absence of toxicity in the concentration range 0.25–2.5 mg/mL for both systems studied (Figure 1C). NPB showed higher viability percentages on the concerned cell line with respect to the NPA. Similar data with the same safety interval were obtained also for cells incubated for 48 h (Figure 1D). Analysis revealed that both formulations at the highest concentration (5 mg/mL) were cytotoxic, resulting in an extremely significant reduction in cell viability.

From the results obtained, it was observed that NPA and NPB showed similar behavior on both cell lines. In detail, absence of cytotoxicity was observed in pericyte cell lines with a wider concentration range (0.25–2.5 mg/mL) than in endothelial cells (0.25–1 mg/mL). Endothelial cells and pericytes are essential components of the microvessel wall. Pericytes play several roles in the retinal vascular system, from controlling flow to maintaining microcirculation integrity [38,39]. Pericytes work co-dependently with

endothelial cells, to which they also provide mechanical support. Among the activities that pericytes regulate are the proliferation and migration of endothelial cells, as well as the production of cytokines for the immune response [40–42].

In vivo, therefore, contact and interactions between pericytes and endothelial cells act on different levels of control. Similar results were reported in a study conducted on human pericytes and endothelial cells, where differences in cell lines cultured solitary and in co-culture were observed. The results showed that DNA synthesis of endothelial cells in single culture was reduced by 30% compared to cells co-cultured with pericytes. Therefore, in vitro co-culture studies should be more reliable and predictive in the evaluation of biological cellular responses [43].

3.2 Influence of the Purification Process on Physico-Chemical Properties of Nanocarriers

As shown by the physico-chemical characterization of formulated systems (Table 1), the particle size ranged between 158 and 219 nm, thus, NPs were obtained [44,45]. In particular, the mean particle size of unloaded NPs was ~158–170 nm and of FA-loaded NPs was ~178–219 nm. The particle size distribution was very narrow in all cases (PDI less than 0.3), corresponding to monodispersed systems [46].

Table 1. Mean size, PDI, zeta potential (ZP), osmolarity and pH of loaded (NPA-FA, NPB-FA) and unloaded (NPA, NPB) nanoparticles. Data represent mean standard deviation (SD), $n = 3$.

Sample	Mean Size (nm) \pm SD	PDI \pm SD	ZP (mV) \pm SD	Osmolarity \pm SD (mOsm/kg)	pH \pm SD
NPA	170.400 \pm 5.781	0.128 \pm 0.028	-39.00 \pm 1.40	-	-
NPA-FA	178.600 \pm 0.289	0.056 \pm 0.035	-33.70 \pm 1.31	258.3 \pm 0.023	7.30 \pm 0.533
NPB	158.700 \pm 1.700	0.130 \pm 0.023	-29.70 \pm 0.90	-	-
NPB-FA	219.300 \pm 2.751	0.207 \pm 0.028	-23.80 \pm 2.22	265.6 \pm 0.027	7.33 \pm 0.495

The ZP of NPs was strongly negative, ranging between 23.8 ± 2.22 to 39.0 ± 1.40 mV. The negative ZP values could be attributed to the presence of terminal carboxylic groups of the polymers, which confer to the matrix of a negative surface charge [28,47,48].

The ZP value showed a reduction of 6 mV in absolute value when the drug was incorporated into the systems, probably due to its precipitation on the surface on NPs. The selection of the organic solvent and its evaporation played a crucial role in this process. Acetone can diffuse into the continuous phase and temporarily increase the drug solubility. As a result, when the organic solvent was completely evaporated, FA could precipitate and deposit onto the NP surface, masking their surface charge [49]. The results of osmolarity values of the obtained formulations showed the achievement of isoosmolar systems with the tear fluid and pH values of 7.3, which fall within the ocular tolerability range.

In order to evaluate the influence of purification methods on the physico-chemical properties of the obtained systems and to select the appropriate process for these nanocarriers, we characterized NPA-FA and NPB-FA before and after the purification processes (Figure 2). The results obtained showed that both formulations subjected to the centrifugation process endured an increase in mean size, passing from 178.6 to 325 nm for

NPA-FA and from 219.3 to 357.2 nm for NPB-FA. This increase should be attributed to the speed used during the centrifugation, which is able to generate collision forces between NPs. The mechanical induced stress leads to the formation of non-redispersible aggregates, according to Sari et al. [50]. After centrifugation the samples showed an increase in PDI reaching values of 0.649 and 0.769 respectively for NPA-FA and NPB-FA. The increase in polydispersity confirmed that high speed used during the centrifugation process caused the formation of aggregates. ZP of both centrifuged NPs showed a reduction of about ten mV. This decrease is a result of the aggregation phenomena that cannot keep the surface properties of NPs unaltered, probably due to the reduction in the total surface area [51].

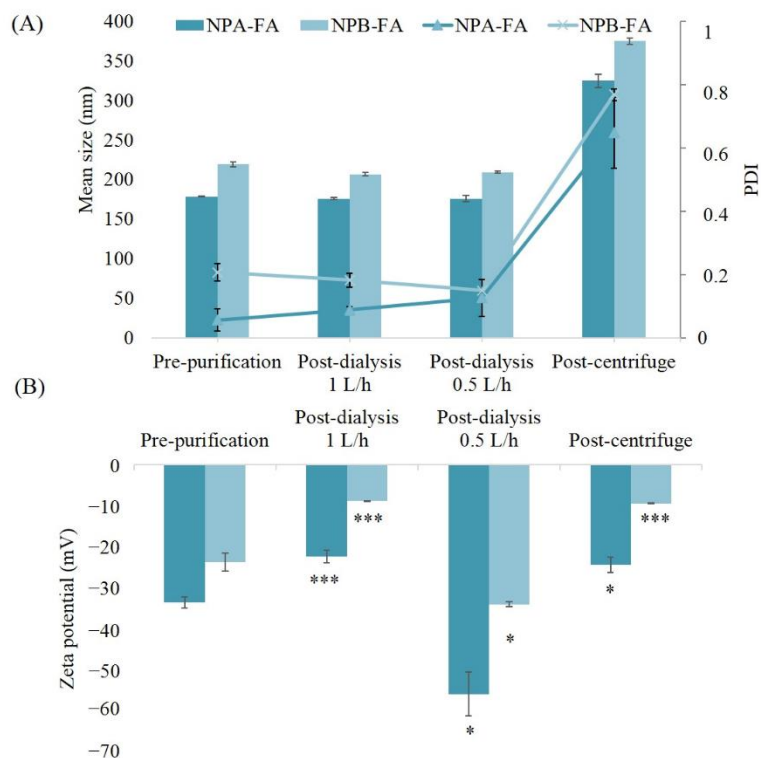


Figure 2. Mean size, PDI (A) and zeta potential (B) of the samples NPA-FA and NPB-FA. *t*-test was used to calculate statistical significance of the percentages obtained versus control group. [ns = not significant ($p > 0.05$); * = significant ($p < 0.05$); *** = extremely significant ($p < 0.001$)].

No significant variation was highlighted in the average dimensions of NPs which remained rather constant after the dialysis process. Systems obtained after dialysis maintained a low PDI value (<0.2).

For dialyzed samples, significant changes on ZP (p -value <0.05) were observed based on the volumes of water exchanged per hour. As reported in Figure 2, a reduction in ZP values can be observed for samples dialyzed against 1 L/h. This result could be due to the further adsorption of the unloaded drug onto the surface of NPs. Moreover, the higher frequency of water exchange avoids the formation of possible surfactant micelles that could entrap the free drug and prevent its diffusion through the membrane. The ZP values of the samples dialyzed against 0.5 L/h of water showed an increase in absolute value of this parameter. The reason for this could be an increase in the osmotic pressure in the dialysis solution. It has been shown that the osmotic pressure of a non-ionic aqueous surfactant solution in the micellar region increases with increasing concentration of the surfactant [52]. In our case, lower frequency of water exchanges (0.5 L/h) may lead

to increased surfactant concentration in the dialysis medium forming micelle. The formation of micelle could sequestrate a fraction of the unloaded drug. The difference in osmotic pressure that was generated in the dialysis medium could hinder the progressive diffusion of the surfactant molecules from the nanodispersion, preventing proper dialysis of the samples [53].

In fact, to support this hypothesis and to evaluate the influence of frequency of water exchanges on dialysis efficacy, a comparison of obtained data was made (Table 2). The results showed that the dialysis technique, which allows a better purification yield of drug (>50%) and is able to remove the greater percentage of FA, is that performed with a frequency of water changes equal to 1 L/h. Samples dialyzed against 0.5 L/h of water showed lower purification efficiency. The reason for this could be a sequestration of the drug from the surfactant micelles present in dialysis medium [54]. In regard to the reasons for the major purification of NPB-FA, this could be attributed to the lipophilic nature of drug. Consequently, the fact that FA is less related to the PLGA polymer, which has hydrophilic groups in its structure, is retained less from NPB-FA [55]. The poor affinity of drug for this type of polymer could reduce its solubilization inside the matrix, therefore a higher amount of drug could remain adsorbed on the NPB-FA surface. Thanks to the ease with which FA is removed from the surface of PLGA based NPs, a higher dialysis percentage may have been obtained [56].

Table 2. Purification efficiency (%) of NPA-FA and NPB-FA referred to the purification processes using the dialysis method performed with frequency of water exchanges of 0.5 and 1 L/h.

Sample	Frequency of Water Changes (L/h)	Purification Efficiency (%) ± SD
NPA-FA	1	28.60 ± 0.211
	0.5	24.13 ± 0.015
NPB-FA	1	53.29 ± 2.258
	0.5	30.00 ± 0.785

3.3 Encapsulation Efficiency and In Vitro Release Profile of FA-Loaded Nanocarriers

The entrapment efficiency of FA (1% *wt/wt*) in the NPs prepared by the nanoprecipitation method was calculated for both purification methods investigated. The results are shown in Table 3. The EE obtained for centrifuged systems ranged from 64.86 to 75.16%, respectively for NPB-FA and NPA-FA. For dialyzed samples, the percentages showed higher values ranging from 81 to 90% and it was observed that by subtracting the non-dialyzed amounts of drug (Table 2), the results were identical to those obtained for the samples purified by centrifugation. Therefore, the efficiency obtained for the dialyzed samples was defined as ‘apparent EE’, consisting of the encapsulated drug, plus the amount of FA not removed by dialysis.

It was demonstrated that the encapsulation yield depends on several factors, such as: the solvent miscibility in the aqueous phase, the precipitation speed rate which leads to polymer solidification, and the drug solubility into the polymer used [57].

Table 3. Encapsulation efficiency (%) of NPA-FA and NPB-FA and apparent encapsulation efficiency (%) of NPA-FA and NPB-FA referred to the purification processes using the dialysis method performed with frequency of water exchanges of 0.5 and 1 L/h.

Sample	Encapsulation Efficiency (%) \pm SD	Frequency of Water Changes (L/h)	Apparent Encapsulation Efficiency (%) \pm SD
NPA-FA	75.16 \pm 5.148	1	89.36 \pm 0.085
		0.5	90.22 \pm 0.007
NPB-FA	64.86 \pm 6.357	1	81.27 \pm 0.792
		0.5	89.46 \pm 0.276

The values obtained could be related to the high solvent miscibility in the continuous phase. It has been shown that if the solvent has a good miscibility, such as in acetone, a very fast solidification of the polymer may occur during the evaporation step. Especially for a hydrophobic drug, a rapid solidification is advantageous in order to obtain high EE, because the dense polymeric shell that is obtained acts as a diffusion barrier for the drug [54]. Additionally, faster hardening can be observed when the volume ratio of continuous to dispersed phase increased (as in our case where a 2:1 ratio is used), which could result in fast solidification of the systems and so improve the effectiveness of encapsulation [58].

NPB-FA showed a lower drug loading than NPA-FA made up of PLA polymer. The lower EE could be attributed to the lower ability of a drug interaction with the polymer. This capacity depends on the drug interaction with the matrix, therefore the more of the drug that is akin to the polymer, the greater the amount of encapsulated FA will be [59].

PLA polymer has a greater hydrophobicity with respect to PLGA, which instead contain a glycol portion in its structure, which provides hydrophilic properties to the polymer [49].

Release curves of pure drug and FA-loaded NPs are shown in Figure 3. More than 80% of FA powder released quickly in 2 h under PBS conditions (pH = 7.4). The release rate was similar to a straight line between 0 and 2 h, then the slope tends to decrease. After 8 h, the drug concentration was almost unchanged, suggesting that FA was completely released into the solution.

As shown in the graph, the slope in the NPs release curves is reduced compared to the pure drug, indicating that the encapsulation of the drug was able to provide a more prolonged release over time. FA release from the NPs in the first 2 h was about 23% for both systems. This premature release could be due to the amount of unloaded FA that was not removed through dialysis. The release profile then increased gradually, reaching about 50% after 4 h from NPB-FA and 5 h from NPA-FA. The FA concentration increased to the theoretical maximum concentration in 48 and 24 h for NPA-FA and NPB-FA, respectively.

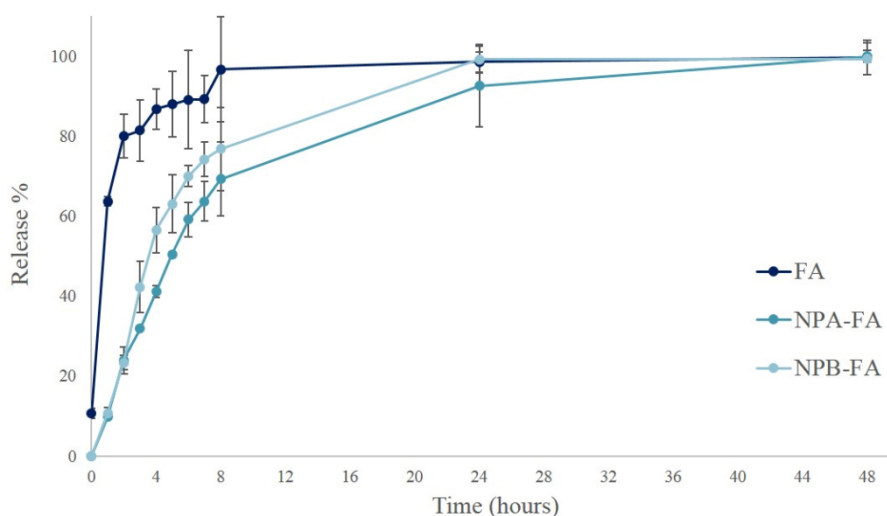


Figure 3. *In vitro* release profiles of pure drug, NPA-FA and NPB-FA in phosphate buffered solution (pH 7.4) at 37 °C.

Although both curves show similar trends, NPA-FA releases lower drug concentrations over time than NPB-FA. The release profile of a drug is governed by its partitioning between the polymer matrix and the aqueous release medium [60]. The difference in release rates could therefore be attributed to the nature of the investigated matrices. NPA-FA, which has demonstrated higher EE, showed a relatively lower drug release than NPB-FA containing a hydrophilic portion in the matrix composition. A similar behavior was observed in a study by Panyam et al., which demonstrated a close correlation between drug release profiles and the degree of hydrophilia of the polymer matrix [49]. The release process is controlled by the degradation rate of the polymer [61,62]. During this process the drug diffuses through the hydrated polymer matrix to the release medium. The water uptake into the systems relaxes the polymer chains and increases the rate of diffusion of drug molecules [63]. Therefore, a higher release rate is justified for NPB-FA particles more hydrophilic than NPA-FA.

3.4 Stability Studies on Resuspended Freeze-Dried FA-Loaded NPs

Liquid polymeric nanosuspensions have some limitations related to the integrity of the formulations. Among these, a recurring phenomenon is the formation of undesirable degradation products generated by hydrolysis of the polymeric material [64,65]. Another limitation of nanosuspensions has been reported about the possibility of premature release of the encapsulated drug [66]. To exceed the above limits, samples were converted from aqueous suspensions to dried powders through the freeze-drying process. However, the freezing and drying steps for removing water from nanosystems subject them to various stresses, so cryoprotective agents are usually added to the formulation with the aim to preserve the structure and morphology of colloidal systems and increase their stability during storage [67,68]. Carbohydrates are among the most commonly used adjuvants able to prevent aggregation phenomena. A good quality lyophilized product is characterized by quick and easy reconstitution, as well as by maintaining the particle size [69]. In our previous studies it was demonstrated that an elegant cake appearance and a short reconstitution time were achieved when

5% (w/v) of HP- β -Cyd was employed as cryoprotectant, because, thanks to its cyclic structure, it is able to be easily absorbed onto the NPs surface during the sublimation step, ensuring also an easy reconstitution of the dried material [28,68]. Furthermore, the concentration of cryoprotectant used is able to provide a dispersion of NPs with an adequate tonicity for ocular administration [70]. SEM scans of cryoprotected and freeze-dried empty and FA-loaded NPs are shown in Figure 4. Results showed NPs with a spherical shape, smooth surface, and a reduced average-diameter compared to pre-lyophilization values, as reported in Table 1.

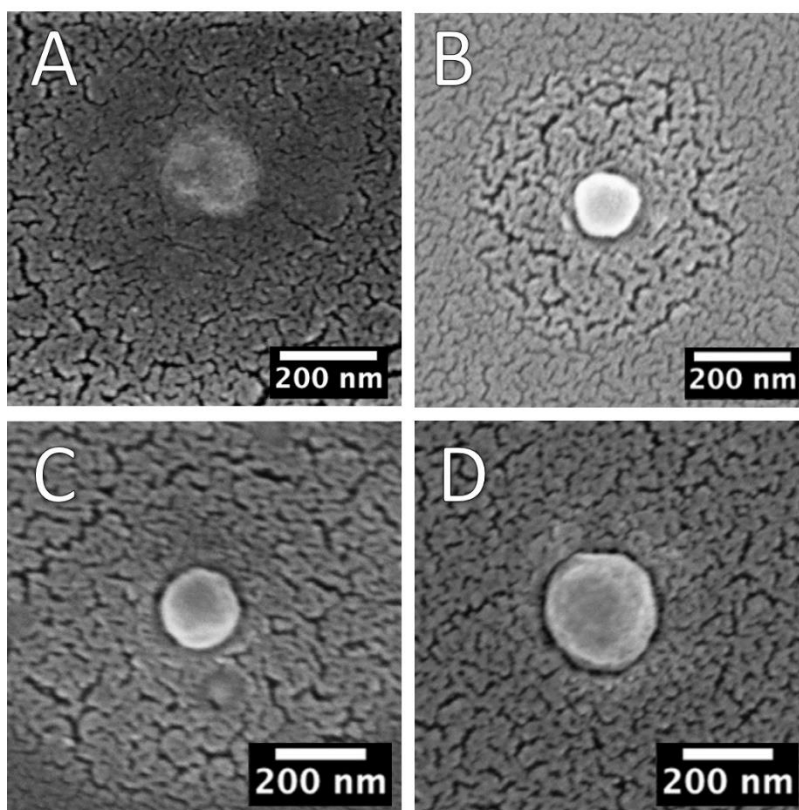


Figure 4. SEM micrographies of: (A) NPA (B) NPB-FA (C) NPB and (D) NPB-FA.

The results obtained from the stability studies conducted on lyophilized systems resuspended with distilled water and stored at refrigeration temperature have shown a chemical-physical stability almost unchanged over time. The data collected are shown in Figure 4. PCS analysis provided further confirmation of the reduction in the mean size of the systems (Figure 5A), which remained stable during the storage time considered. In addition, the PDI of all the analyzed formulations maintained constant values, always below 0.2 (Figure 5B). From the analysis of the ZP (Figure 5C) it is possible to observe a slight decrease in this parameter over the course of 28 days, despite the fact that the surface charge of the systems always remains greater than 20.5 mV. In general, dispersions with high absolute values of ZP are considered stable because the electrical repulsion between the charges of the NPs is able to reduce the aggregation capacity of systems [61,71]. Therefore, NP formulations were found to be physically stable, and aggregation of colloidal particles was probably prevented due to adequate values of ZP. Figure 5D, E show respectively measurements of osmolarity and pH values of the NPs suspensions, whose variations over time have proved to be practically irrelevant.

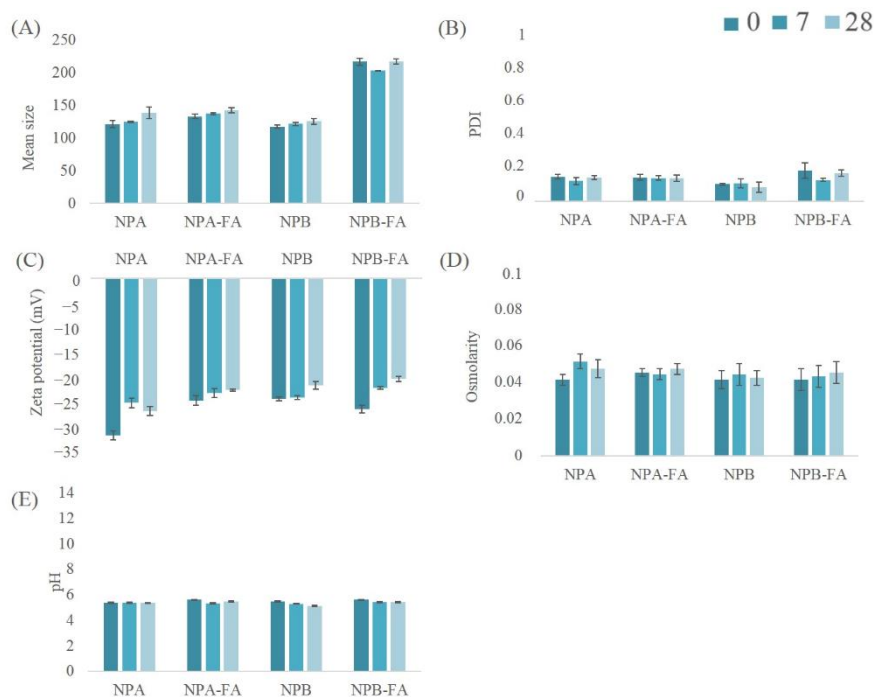


Figure 5. Mean size (A) index of polydispersion (B) zeta potential (C) osmolarity (D) and pH (E) of the samples stored at 5 °C.

3.5 Thermal and Infrared Analyses of Cryoprotected and Freeze-Dried Nanoparticles

In order to investigate the polymorphic states and crystallinity of the materials used during the preparation and of the cryoprotected and lyophilized formulations, we conducted a DSC study. The NPs made of PLA are represented in Figure 6A, those produced with PLGA are represented in Figure 7A.

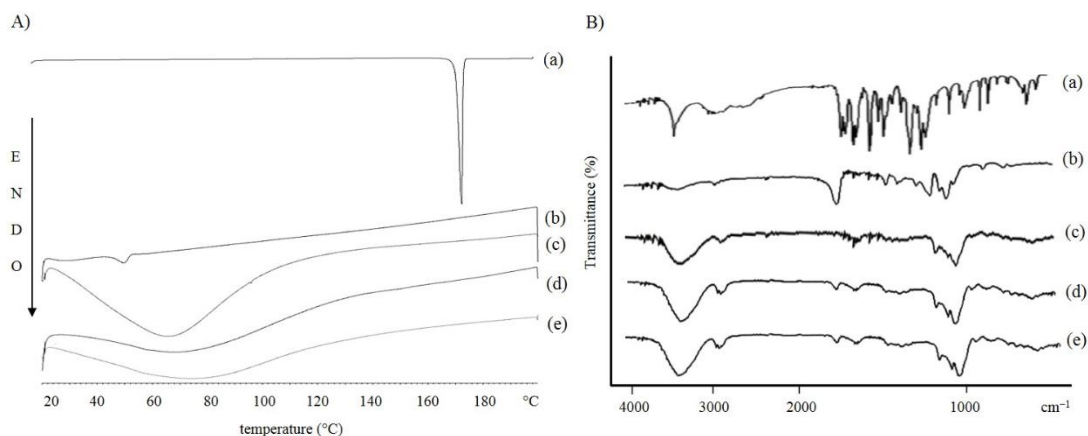


Figure 6. (A) DSC and (B) FT-IR curves of FA (a) PLA polymer (b) HP-β-CD (c) unloaded NPA (d) and FA-loaded NPA nanoparticles (e).

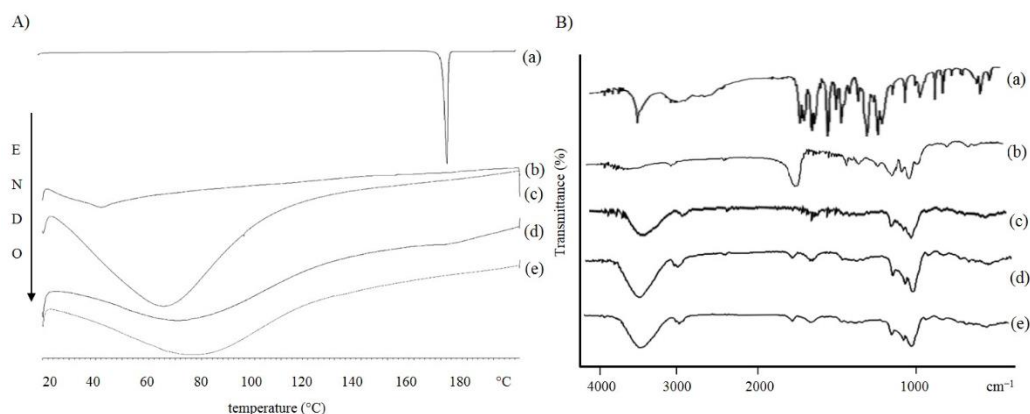


Figure 7. (A) DSC and (B) FT-IR curves of FA (a) PLGA polymer (b) HP-β-CD (c) unloaded NPB (d) and FA-loaded NPB nanoparticles (e).

As shown in the curves (a) of both graphs, the melting point of FA is 172.3 °C, which represents the characteristic endothermic peak of the drug [72]. The disappearance of the characteristic endothermic FA peak in the thermograms of FA-loaded NPs [Figures 6A and 7A(e)] demonstrates that the drug could be successfully entrapped in the amorphous state within the formulated systems. As expected, the polymer thermograms show characteristic peaks between 40–50 °C [73].

Regarding the DSC thermograms of the cryoprotected freeze-dried NPs, no obvious melting process occurred. This could be due to the presence of cryoprotectants. It has been shown that cryoprotectant molecules act through water substitution. The stabilization of NPs could be explained as the formation of hydrogen bonds between the polar groups on the polymer surface and the cryoprotectant molecules, resulting in the loss of water [64]. HP-β-CD has a relatively high glass transition temperature (T_g). When it is arranged around the NPs, it changes the collapse temperature of the systems. This results in a shorter primary drying phase during lyophilization. The obtained amorphous structures are characterized by a low aggregation capacity which prevents the formation of agglomerates during the freeze-drying process [74,75].

FT-IR spectroscopic analysis was performed to identify the functional groups of the materials used in the preparation and the chemical interactions that could have occurred in the formulated carriers. The spectra of the raw materials and cryoprotected and freeze-dried NPs, empty and loaded with FA, were scanned. The results are shown in Figures 5B and 6B. The FA showed a peak at 3436 cm⁻¹ typical for -OH stretching vibrations, the absorption bands in the range 2968–3016 cm⁻¹ corresponded to the presence of the alkane groups. The band at 1690 cm⁻¹ was observed for the C=O carbonyl group and the band at 1277 cm⁻¹ for the C-O group. The signals at 1619 and 1517 cm⁻¹ were related to the vibration of the aromatic ring, while the peak at 1205 cm⁻¹ is typical for C-OH stretching and finally, the band at 1035 cm⁻¹ for methoxide O-CH₃ stretching. The polymer spectra also showed characteristic absorption bands. The broad bands at 3400 cm⁻¹ are typical for hydroxyl groups, the bands at 2997 cm⁻¹ corresponding to the vibration for C-H alkane groups, the characteristic stretching peaks for C=O carbonyl group are shown at 1751 and 1761 cm⁻¹ for PLA and PLGA, respectively. The bands between 1300 and 1400 cm⁻¹ were characteristic for C-H alkane groups bending vibration and the bands in the region between 1272 and 1048 cm⁻¹ were characteristic for C-O vibration. Cryoprotectant FT-IR spectrum showed an absorption band at 3420 cm⁻¹ for -OH stretching vibration, a peak at 2933 cm⁻¹ for alkane group vibration, and a signal at 1157 cm⁻¹ for C-O vibration.

Cryoprotected and freeze-dried NPs scans, empty and loaded with FA, confirmed the results obtained from the thermal analysis, which showed a similar trend to cryoprotectant. In the infrared spectra of PLA (Figure 5B) and PLGA (Figure 6B) NPs, all of the characteristic peaks of FA disappeared, while the cryoprotectant typical peaks were detected at 3400 cm^{-1} for -OH group, at 2900 cm^{-1} for alkane group and the bands in the region between 1035–1157 cm^{-1} for C-O groups. In addition, a characteristic polymer peak at 1750 cm^{-1} for carbonyl group was detected. An interesting feature of the NPs spectra was the appearance of a peak at 1650 cm^{-1} , attributable to the H-O-H bending band, which suggested a possible chemical interaction between the cryoprotectant and the polymer matrix.

Therefore, it could be stated that NPs consist of a polymeric matrix in which the drug was present in a dispersed form and partially exposed on the surface, while the external area of the matrix is covered by a cryoprotective layer capable of maintaining the integrity of the nanosystems.

4. Conclusions

In this work, the synthesis of empty PLA (NPA), PLGA (NPB), and polymeric NPs loaded with FA was developed for ophthalmic applications. The obtained systems were characterized by PCS analysis, data show homogeneous particle populations with a $\text{PDI} < 0.2$, with adequate dimension for ophthalmic administration and a strongly negative ZP, which reduces the probability of obtaining aggregates.

To obtain suitable formulations for *in vitro* or *in vivo* studies, different purification techniques were analyzed. Centrifugation proved to be the least suitable method because it involves heterogeneous and non-redispersible aggregate formation. Dialysis on the other hand, did not affect the dimensional parameters or PDI values for both frequencies of water changes tested. Purification efficacy was also evaluated in terms of drug removed. Dialysis, which allows a high FA purification yield, was performed with a frequency of water changes equal to 1 L/h. The formulations were characterized in terms of osmolarity and pH, making them suitable for ocular administration with well tolerated pH (7.3) and isotonic osmolarity values with the tear fluid between 258–265 mOsm/Kg. The tolerability of the blank carriers was confirmed by cell viability assays. NPA and NPB showed no toxic effect in the concentration range 0.25–1 mg/mL on endothelial cells, while on pericytes, NPs were safe at a higher concentration range of 0.25–2.5 mg/mL. However, further studies would be required to ascertain the toxicity of polymeric carriers *in vivo*. The encapsulation effectiveness was also assessed for both loaded formulations (NPA-FA, NPB-FA) with drug entrapment yields of 75.16 and 64.86%, respectively. The results of *in vitro* release studies showed that obtained systems are able to provide a controlled FA release up to 48 h. Using 5% (*w/v*) HP- β -cyclodextrin as cryoprotective agent, the polymeric carrier systems can be freeze-dried, ensuring good physical-chemical properties upon reconstitution and over 28 days. From the results of morphological analysis, the nanoparticles showed a spherical and smooth surface. Thermal and spectroscopic analyses confirmed that the drug was encapsulated within the polymer matrix. Hypothesis made on the *in vitro* biological tests must be confirmed with further studies which must also be conducted on FA-loaded NPs, although the obtained results may not be correlated with results of the *in vivo* studies where cellular homeostasis is governed by multiple factors.

Author Contributions: Conceptualization, A.R. and T.M.; methodology, validation, project

administration, T.M.; writing—original draft preparation, investigation, data curation, A.R.; software, writing—original draft preparation, data curation, A.B.; validation, writing—review and editing, C.C.; investigation, visualization, S.C.; formal analysis, validation, data curation, G.L. and C.D.A.; validation and supervision, G.P. and R.P. All authors have read and agreed to the published version of the manuscript.

Funding: Alessia Romeo has been supported by the International Ph.D. program in Neuroscience, University of Catania, Italy.

Institutional Review Board Statement: Not applicable.

Informed Consent Statement: Not applicable.

Data Availability Statement: The data presented in this study are available on request from the corresponding author.

Acknowledgments: The manuscript was supported by University of Catania (Programma Ricerca di Ateneo unict 2020-2022- Linea 2; Project NanoRET). The authors are grateful to Research Centre on Ocular Nanotechnology (NANO-i) from the University of Catania for his technical assistance. Authors are grateful to Maria José Lo Faro for her collaboration to perform SEM studies.

Conflicts of Interest: The authors declare no conflict of interest.

References

1. Masuda, T.; Shimazawa, M.; Hara, H. Retinal Diseases Associated with Oxidative Stress and the Effects of a Free Radical Scavenger (Edaravone). *Oxidative Med. Cell. Longev.* **2017**, *2017*, 9208489. [[CrossRef](#)]
2. Xu, Z.; Sun, T.; Li, W.; Sun, X. Inhibiting effects of dietary polyphenols on chronic eye diseases. *J. Funct. Foods* **2017**, *39*, 186–197. [[CrossRef](#)]
3. London, D.S.; Beezhold, B. A phytochemical-rich diet may explain the absence of age-related decline in visual acuity of Amazonian hunter-gatherers in Ecuador. *Nutr. Res.* **2015**, *35*, 107–117. [[CrossRef](#)] [[PubMed](#)]
4. Soobrattee, M.; Neerghen, V.; Luximon-Ramma, A.; Aruoma, O.; Bahorun, T. Phenolics as potential antioxidant therapeutic agents: Mechanism and actions. *Mutat. Res. Mol. Mech. Mutagen.* **2005**, *579*, 200–213. [[CrossRef](#)]
5. Trombino, S.; Serini, S.; Di Nicuolo, F.; Celleno, L. Antioxidant Effect of Ferulic Acid in Isolated Membranes and Intact Cells: Synergistic Interactions with α -Tocopherol, β -Carotene, and Ascorbic Acid. *J. Agric. Food Chem.* **2004**, *52*, 2411–2420. [[CrossRef](#)]
6. Joshi, G.; Perluigi, M.; Sultana, R.; Agrippino, R.; Calabrese, V.; Butterfield, D.A. In Vivo protection of synaptosomes by ferulic acid ethyl ester (FAEE) from oxidative stress mediated by 2,2-azobis (2-amidino-propane) dihydrochloride (AAPH) or $\text{Fe}^{2+}/\text{H}_2\text{O}_2$: Insight into mechanisms of neuroprotection and relevance to oxidative stress-related neurodegenerative disorders. *Neurochem. Int.* **2006**, *48*, 318–327. [[CrossRef](#)]
7. De Paiva, L.B.; Goldbeck, R.; Dos Santos, W.D.; Squina, F.M. Ferulic acid and derivatives: Molecules with potential application in the pharmaceutical field. *Braz. J. Pharm. Sci.* **2013**, *49*, 395–411. [[CrossRef](#)]
8. Gohil, K.J.; Kshirsagar, S.B.; Sahane, R.S. Ferulic acid – A comprehensive pharmacology of an important bioflavonoid. *Int. J. Pharm. Sci. Res.* **2012**, *3*, 700–710.
9. Panwar, R.; Sharma, A.K.; Kaloti, M.; Dutt, D.; Pruthi, V. Characterization and anticancer potential of ferulic acid-loaded chitosan nanoparticles against ME-180 human cervical cancer cell lines. *Appl. Nanosci.* **2016**, *6*, 803–813. [[CrossRef](#)]
10. Júnior, J.V.C.; dos Santos, J.A.B.; Lins, T.B.; Batista, R.S.D.A.; Neto, S.A.D.L.; Oliveira, A.D.S.; Nogueira, F.H.A.; Gomes, A.P.B.; de Sousa, D.P.; de Souza, F.S.; et al. A New

- Ferulic Acid–Nicotinamide Cocrystal With Improved Solubility and Dissolution Performance. *J. Pharm. Sci.* **2020**, *109*, 1330–1337. [[CrossRef](#)]
11. Li, L.; Liu, Y.; Xue, Y.; Zhu, J.; Wang, X.; Dong, Y. Preparation of a ferulic acid–phospholipid complex to improve solubility, dissolution, and B16F10 cellular melanogenesis inhibition activity. *Chem. Cent. J.* **2017**, *11*, 26. [[CrossRef](#)]
 12. Rezaei, A.; Varshosaz, J.; Fesharaki, M.; Farhang, A.; Jafari, S.M. Improving the solubility and In Vitro cytotoxicity (anticancer activity) of ferulic acid by loading it into cyclodextrin nanosponges. *Int. J. Nanomed.* **2019**, *14*, 4589–4599. [[CrossRef](#)]
 13. Wang, J.; Cao, Y.; Sun, B.; Wang, C. Characterisation of inclusion complex of trans-ferulic acid and hydroxypropyl- β -cyclodextrin. *Food Chem.* **2011**, *124*, 1069–1075. [[CrossRef](#)]
 14. Grimaudo, M.A.; Amato, G.; Carbone, C.; Diaz-Rodriguez, P.; Musumeci, T.; Concheiro, A.; Alvarez-Lorenzo, C.; Puglisi, G. Micelle-nanogel platform for ferulic acid ocular delivery. *Int. J. Pharm.* **2020**, *576*, 118986. [[CrossRef](#)]
 15. Zhang, Y.; Li, Z.; Zhang, K.; Yang, G.; Wang, Z.; Zhao, J.; Hu, R.; Feng, N. Ethyl oleate-containing nanostructured lipid carriers improve oral bioavailability of trans-ferulic acid as compared with conventional solid lipid nanoparticles. *Int. J. Pharm.* **2016**, *511*, 57–64. [[CrossRef](#)] [[PubMed](#)]
 16. Carbone, C.; Caddeo, C.; Grimaudo, M.A.; Manno, D.E.; Serra, A.; Musumeci, T. Ferulic Acid-NLC with Lavandula Essential Oil: A Possible Strategy for Wound-Healing? *Nanomaterials* **2020**, *10*, 898. [[CrossRef](#)]
 17. Bourges, J.-L.; Gautier, S.E.; Delie, F.; Bejjani, R.A.; Jeanny, J.-C.; Gurny, R.; Benezra, D.; Behar-Cohen, F.F. Ocular Drug Delivery Targeting the Retina and Retinal Pigment Epithelium Using Polylactide Nanoparticles. *Investig. Ophthalmol. Vis. Sci.* **2003**, *44*, 3562–3569. [[CrossRef](#)] [[PubMed](#)]
 18. Sur, S.; Rathore, A.; Dave, V.; Reddy, K.R.; Chouhan, R.S.; Sadhu, V. Recent developments in functionalized polymer nanoparticles for efficient drug delivery system. *Nano-Struct. Nano-Objects* **2019**, *20*, 100397. [[CrossRef](#)]
 19. Prajapati, S.K.; Jain, A.; Jain, S.; Tirth, B.; College, P. Biodegradable polymers and constructs: A novel approach in drug delivery. *Eur. Polym. J.* **2019**, *120*, 109191. [[CrossRef](#)]
 20. Imperiale, J.C.; Acosta, G.B.; Sosnik, A. Polymer-based carriers for ophthalmic drug delivery. *J. Control. Release* **2018**, *285*, 106–141. [[CrossRef](#)]
 21. Yandrapu, S.K.; Upadhyay, A.K.; Petrash, J.M.; Kompella, U.B. Nanoparticles in Porous Microparticles Prepared by Supercritical Infusion and Pressure Quench Technology for Sustained Delivery of Bevacizumab. *Mol. Pharm.* **2013**, *10*, 4676–4686. [[CrossRef](#)]
 22. Gupta, H.; Aqil, M.; Khar, R.K.; Ali, A.; Bhatnagar, A.; Mittal, G. Sparfloxacin-loaded PLGA nanoparticles for sustained ocular drug delivery. *Nanomed. Nanotechnol. Biol. Med.* **2010**, *6*, 324–333. [[CrossRef](#)]
 23. Rong, X.; Yuan, W.; Lu, Y. Safety evaluation of poly (lactic-co-glycolic acid)/poly (lactic acid) microspheres through intravitreal injection in rabbits. *Int. J. Nanomed.* **2014**, *9*, 3057–3068. [[CrossRef](#)] [[PubMed](#)]
 24. Mayol, L.; Silvestri, T.; Fusco, S.; Borzacchiello, A.; De Rosa, G.; Biondi, M. Drug micro-carriers with a hyaluronic acid corona toward a diffusion-limited aggregation within the vitreous body. *Carbohydr. Polym.* **2019**, *220*, 185–190. [[CrossRef](#)]
 25. Andrés-Guerrero, V.; Zong, M.; Ramsay, E.; Rojas, B.; Sarkhel, S.; Gallego, B.; de Hoz, R.; Ramírez, A.I.; Salazar, J.J.; Triviño, A.; et al. Novel biodegradable polyesteramide microspheres for controlled drug delivery in Ophthalmology. *J. Control. Release* **2015**, *211*, 105–117. [[CrossRef](#)]
 26. Arranz-Romera, A.; Davis, B.; Bravo-Osuna, I.; Esteban-Pérez, S.; Molina-Martínez, I.; Shamsher, E.; Ravindran, N.; Guo, L.; Cordeiro, M.; Herrero-Vanrell, R. Simultaneous co-delivery of neuroprotective drugs from multi-loaded PLGA microspheres for the treatment of glaucoma. *J. Control. Release* **2019**, *297*, 26–38. [[CrossRef](#)]

27. Peters, T.; Kim, S.-W.; Castro, V.; Stingl, K.; Strasser, T.; Bolz, S.; Schraermeyer, U.; Mihov, G.; Zong, M.; Andres-Guerrero, V.; et al. Evaluation of polyesteramide (PEA) and polyester (PLGA) microspheres as intravitreal drug delivery systems in albino rats. *Biomaterials* **2017**, *124*, 157–168. [[CrossRef](#)] [[PubMed](#)]
28. Musumeci, T.; Ventura, C.; Giannone, I.; Ruozi, B.; Montenegro, L.; Pignatello, R.; Puglisi, G. PLA/PLGA nanoparticles for sustained release of docetaxel. *Int. J. Pharm.* **2006**, *325*, 172–179. [[CrossRef](#)]
29. Lupo, G.; Anfuso, C.D.; Ragusa, N.; Strosznajder, R.P.; Walski, M.; Alberghina, M. t-Butyl hydroperoxide and oxidized low density lipoprotein enhance phospholipid hydrolysis in lipopolysaccharide-stimulated retinal pericytes. *Biochim. Biophys. Acta (BBA)-Mol. Cell Biol. Lipids* **2001**, *1531*, 143–155. [[CrossRef](#)]
30. Musumeci, T.; Bucolo, C.; Carbone, C.; Pignatello, R.; Drago, F.; Puglisi, G. Polymeric nanoparticles augment the ocular hypotensive effect of melatonin in rabbits. *Int. J. Pharm.* **2013**, *440*, 135–140. [[CrossRef](#)]
31. Musmade, K.P.; Deshpande, P.B.; Musmade, P.B.; Maliyakkal, M.N.; Kumar, A.R.; Reddy, M.S.; Udupa, N. Methotrexate-loaded biodegradable nanoparticles: Preparation, characterization and evaluation of its cytotoxic potential against U-343 MGa human neuronal glioblastoma cells. *Bull. Mater. Sci.* **2014**, *37*, 945–951. [[CrossRef](#)]
32. Hou, D.; Hu, S.; Huang, Y.; Gui, R.; Zhang, L.; Tao, Q.; Zhang, C.; Tian, S.; Komarneni, S.; Ping, Q. Preparation and In Vitro study of lipid nanoparticles encapsulating drug loaded montmorillonite for ocular delivery. *Appl. Clay Sci.* **2016**, *119*, 277–283. [[CrossRef](#)]
33. Abdelwahed, W.; Degobert, G.; Stainmesse, S.; Fessi, H. Freeze-drying of nanoparticles: Formulation, process and storage considerations. *Adv. Drug Deliv. Rev.* **2006**, *58*, 1688–1713. [[CrossRef](#)]
34. Yu, A.; Shi, H.; Liu, H.; Bao, Z.; Dai, M.; Lin, D.; Lin, D.; Xu, X.; Li, X.; Wang, Y. Mucoadhesive dexamethasone-glycol chitosan nanoparticles for ophthalmic drug delivery. *Int. J. Pharm.* **2020**, *575*, 118943. [[CrossRef](#)] [[PubMed](#)]
35. Gonzalez-Mira, E.; Egea, M.A.; Souto, E.B.; Calpena, A.C.; García, M.L. Optimizing flurbiprofen-loaded NLC by central composite factorial design for ocular delivery. *Nanotechnology* **2010**, *22*, 045101. [[CrossRef](#)] [[PubMed](#)]
36. Leonardi, A.; Bucolo, C.; Romano, G.L.; Platania, C.B.M.; Drago, F.; Puglisi, G.; Pignatello, R. Influence of different surfactants on the technological properties and In Vivo ocular tolerability of lipid nanoparticles. *Int. J. Pharm.* **2014**, *470*, 133–140. [[CrossRef](#)]
37. Standard, I. *Biological Evaluation of Medical Devices. Part 5: Tests for In Vitro Cytotoxicity*; ISO 10993-5:2009; International Organization for Standardization (ISO): Geneva, Switzerland, 2009.
38. Frank, R.N.; Turczyn, T.J.; Das, A. Pericyte coverage of retinal and cerebral capillaries. *Investig. Ophthalmol. Vis. Sci.* **1990**, *31*, 999–1007.
39. Choi, S.H.; Chung, M.; Park, S.W.; Jeon, N.L.; Kim, J.H.; Yu, Y.S. Relationship between Pericytes and Endothelial Cells in Retinal Neovascularization: A Histological and Immunofluorescent Study of Retinal Angiogenesis. *Korean J. Ophthalmol.* **2018**, *32*, 70–76. [[CrossRef](#)]
40. Sims, D.E. Experimental Biology 2000 Symposium on Capillaries: How their structure and function can alter to meet tissue demands-Diversity within Pericytes. *Clin. Exp. Pharmacol. Physiol.* **2000**, *27*, 836–841.
41. Yan, Q.; Sage, E.H. Transforming growth factor- β 1 induces apoptotic cell death in cultured retinal endothelial cells but not pericytes: Association with decreased expression of p21waf1/cip1. *J. Cell. Biochem.* **1998**, *70*, 70–83. [[CrossRef](#)]
42. Huang, H. Pericyte-Endothelial Interactions in the Retinal Microvasculature. *Int. J. Mol. Sci.* **2020**, *21*, 7413. [[CrossRef](#)] [[PubMed](#)]
43. Tarallo, S.; Beltramo, E.; Berrone, E.; Porta, M. Human pericyte-endothelial cell interactions in co-culture models mimicking the diabetic retinal microvascular

- environment. *Acta Diabetol.* **2012**, *49*, 141–151. [[CrossRef](#)]
44. Zielińska, A.; Carreiró, F.; Oliveira, A.; Neves, A.; Pires, B.; Venkatesh, D.; Durazzo, A.; Lucarini, M.; Eder, P.; Silva, A.; et al. Polymeric Nanoparticles: Production, Characterization, Toxicology and Ecotoxicology. *Molecules* **2020**, *25*, 3731. [[CrossRef](#)]
 45. Ma, X.; Williams, R.O. Polymeric nanomedicines for poorly soluble drugs in oral delivery systems: An update. *J. Pharm. Investig.* **2018**, *48*, 61–75. [[CrossRef](#)]
 46. Liu, H.; Wang, L.; Yang, T.; Zhang, G.; Huang, J.; Sun, J.; Huo, J. Optimization and evaluation of fish oil microcapsules. *Particuology* **2016**, *29*, 162–168. [[CrossRef](#)]
 47. Cao, J.; Choi, J.-S.; Oshi, M.A.; Lee, J.; Hasan, N.; Kim, J.; Yoo, J.-W. Development of PLGA micro- and nanorods with high capacity of surface ligand conjugation for enhanced targeted delivery. *Asian J. Pharm. Sci.* **2019**, *14*, 86–94. [[CrossRef](#)] [[PubMed](#)]
 48. Vieira, S.M.; Michels, L.R.; Roversi, K.; Metz, V.G.; Moraes, B.K.; Piegas, E.M.; Freddo, R.J.; Gundel, A.; Costa, T.D.; Burger, M.E.; et al. A surface modification of clozapine-loaded nanocapsules improves their efficacy: A study of formulation development and biological assessment. *Colloids Surf. B Biointerfaces* **2016**, *145*, 748–756. [[CrossRef](#)]
 49. Panyam, J.; Williams, D.; Dash, A.; Labhsetwar, V.; Leslie-Pelecky, D. Solid-state Solubility Influences Encapsulation and Release of Hydrophobic Drugs from PLGA/PLA Nanoparticles. *J. Pharm. Sci.* **2004**, *93*, 1804–1814. [[CrossRef](#)]
 50. Sari, D.P.; Utami, T.S.; Arbianti, R.; Hermansyah, H. The effect of centrifugation speed and Chitosan-Sodium Tripolyphosphate ratio toward the nanoencapsulation of Sambiloto (*Andrographis paniculate*) for the formulation of Hepatitis B drug. *IOP Conf. Ser. Earth Environ. Sci.* **2018**, *105*, 012112. [[CrossRef](#)]
 51. Choi, K.-O.; Aditya, N.; Ko, S. Effect of aqueous pH and electrolyte concentration on structure, stability and flow behavior of non-ionic surfactant based solid lipid nanoparticles. *Food Chem.* **2014**, *147*, 239–244. [[CrossRef](#)]
 52. Xiao, J.; Li, W. Study on osmotic pressure of non-ionic and ionic surfactant solutions in the micellar and microemulsion regions. *Fluid Phase Equilib.* **2008**, *263*, 231–235. [[CrossRef](#)]
 53. Wong, C.K.; Stenzel, M.H.; Thordarson, P. Non-spherical polymersomes: Formation and characterization. *Chem. Soc. Rev.* **2019**, *48*, 4019–4035. [[CrossRef](#)]
 54. Wischke, C.; Schwendeman, S.P. Principles of encapsulating hydrophobic drugs in PLA/PLGA microparticles. *Int. J. Pharm.* **2008**, *364*, 298–327. [[CrossRef](#)] [[PubMed](#)]
 55. Zduńska, K.; Dana, A.; Kolodziejczak, A.; Rotsztejn, H. Antioxidant Properties of Ferulic Acid and Its Possible Application. *Ski. Pharmacol. Physiol.* **2018**, *31*, 332–336. [[CrossRef](#)] [[PubMed](#)]
 56. Frasco, M.F.; Almeida, G.M.; Santos-Silva, F.; Pereira, M.D.C.; Coelho, M.A.N. Transferrin surface-modified PLGA nanoparticles- mediated delivery of a proteasome inhibitor to human pancreatic cancer cells. *J. Biomed. Mater. Res. Part A* **2014**, *103*, 1476–1484. [[CrossRef](#)]
 57. Vineeth, P.; Vadaparathi, P.R.R.A.O.; Kumar, K.; Babu, B.D.J.; Rao, A.V.; Babu, K.S. Influence of organic solvents on nanoparticle formation and surfactants on release behaviour in-vitro using costunolide as model anticancer agent. *Int. J. Pharm. Pharm. Sci.* **2014**, *6*, 638–645.
 58. Li, W.; Anderson, K.W.; Mehta, R.C.; Deluca, P.P. Prediction of solvent removal profile and effect on properties for peptide-loaded PLGA microspheres prepared by solvent extraction/evaporation method. *J. Control. Release* **1995**, *37*, 199–214. [[CrossRef](#)]
 59. Govender, T. PLGA nanoparticles prepared by nanoprecipitation: Drug loading and release studies of a water soluble drug. *J. Control. Release* **1999**, *57*, 171–185. [[CrossRef](#)]
 60. Babu, C.; Kumara Babu, P.; Sudhakar, K.; Subha, M.C.S.; Chowdoji Rao, K. Aripiprazole loaded PLGA nanoparticles for controlled release studies: Effect of co-polymer ratio. *Int. J. Drug Deliv.* **2014**, *6*, 151–155. [[CrossRef](#)]
 61. Jin, X.; Asghar, S.; Zhu, X.; Chen, Z.; Tian, C.; Yin, L.; Ping, Q.; Xiao, Y. In Vitro and In Vivo evaluation of 10-hydroxycamptothecin- loaded poly (n-butyl cyanoacrylate) nanoparticles prepared by miniemulsion polymerization. *Colloids Surf. B Biointerfaces* **2018**, *162*, 25–34.

- [CrossRef]
62. Choi, K.-O.; Aditya, N.; Ko, S. Preparation and characterization of fentanyl-loaded PLGA microspheres in vitro release profiles. *Food Chem.* **2002**, *234*, 195–203. [CrossRef]
 63. Budhian, A.; Siegel, S.J.; Winey, K.I. Controlling the In Vitro release profiles for a system of haloperidol-loaded PLGA nanoparticles. *Int. J. Pharm.* **2008**, *346*, 151–159. [CrossRef] [PubMed]
 64. Mohammady, M.; Mohammadi, Y.; Yousefi, G. Freeze-Drying of Pharmaceutical and Nutraceutical Nanoparticles: The Effects of Formulation and Technique Parameters on Nanoparticles Characteristics. *J. Pharm. Sci.* **2020**, *109*, 3235–3247. [CrossRef] [PubMed]
 65. Fonte, P.; Soares, S.; Costa, A.; Andrade, J.C.; Seabra, V.; Reis, S.; Sarmiento, B. Effect of cryoprotectants on the porosity and stability of insulin-loaded PLGA nanoparticles after freeze-drying. *Biomatter* **2012**, *2*, 329–339. [CrossRef]
 66. Saez, A.; Guzmán, M.; Molpeceres, J.; Aberturas, M. Freeze-drying of polycaprolactone and poly(D,L-lactic-glycolic) nanoparticles induce minor particle size changes affecting the oral pharmacokinetics of loaded drugs. *Eur. J. Pharm. Biopharm.* **2000**, *50*, 379–387. [CrossRef]
 67. Bonaccorso, A.; Musumeci, T.; Carbone, C.; Vicari, L.; Lauro, M.R.; Puglisi, G. Revisiting the role of sucrose in PLGA-PEG nanocarrier for potential intranasal delivery. *Pharm. Dev. Technol.* **2017**, *23*, 265–274. [CrossRef] [PubMed]
 68. Musumeci, T.; Vicari, L.; Ventura, C.A.; Gulisano, M.; Pignatello, R.; Puglisi, G. Lyoprotected Nanosphere Formulations for Paclitaxel Controlled Delivery. *J. Nanosci. Nanotechnol.* **2006**, *6*, 3118–3125. [CrossRef]
 69. Bozdog, S.; Dillen, K.; Vandervoort, J.; Ludwig, A. The effect of freeze-drying with different cryoprotectants and gamma-irradiation sterilization on the characteristics of ciprofloxacin HCl-loaded poly(D,L-lactide-glycolide) nanoparticles. *J. Pharm. Pharmacol.* **2010**, *57*, 699–707. [CrossRef]
 70. Parra, A.; Mallandrich, M.; Clares, B.; Egea, M.A.; Espina, M.; García, M.L.; Calpena, A.C. Design and elaboration of freeze-dried PLGA nanoparticles for the transcorneal permeation of carprofen: Ocular anti-inflammatory applications. *Colloids Surf. B Biointerfaces* **2015**, *136*, 935–943. [CrossRef] [PubMed]
 71. Shakeri, F.; Shakeri, S.; Hojjatoleslami, M. Preparation and Characterization of Carvacrol Loaded Polyhydroxybutyrate Nanoparticles by Nanoprecipitation and Dialysis Methods. *J. Food Sci.* **2014**, *79*, N697–N705. [CrossRef]
 72. Carbone, C.; Campisi, A.; Musumeci, T.; Raciti, G.; Bonfanti, R.; Puglisi, G. FA-loaded lipid drug delivery systems: Preparation, characterization and biological studies. *Eur. J. Pharm. Sci.* **2014**, *52*, 12–20. [CrossRef] [PubMed]
 73. Zvonar, A.; Kristl, J.; Kerc, J.; Grabnar, P.A. High celecoxib-loaded nanoparticles prepared by a vibrating nozzle device. *J. Microencapsul.* **2009**, *26*, 748–759. [CrossRef] [PubMed]
 74. Zu, Y.; Wu, W.; Zhao, X.; Li, Y.; Wang, W.; Zhong, C.; Zhang, Y.; Zhao, X. Enhancement of solubility, antioxidant ability and bioavailability of taxifolin nanoparticles by liquid antisolvent precipitation technique. *Int. J. Pharm.* **2014**, *471*, 366–376. [CrossRef] [PubMed]
 75. Chow, S.F.; Wan, K.Y.; Cheng, K.K.; Wong, K.W.; Sun, C.C.; Baum, L.; Chow, A.H.L. Development of highly stabilized curcumin nanoparticles by flash nanoprecipitation and lyophilization. *Eur. J. Pharm. Biopharm.* **2015**, *94*, 436–449. [CrossRef] [PubMed]

CHAPTER III: *Melatonin loaded hybrid nanomedicine: DoE approach, optimization and in vitro study on diabetic retinopathy model*



Melatonin loaded hybrid nanomedicine: DoE approach, optimization and *in vitro* study on diabetic retinopathy model

Alessia Romeo^a, Angela Bonaccorso^{a,c}, Claudia Carbone^{a,c}, Gabriella Lupo^c, Carmelina Daniela Anfuso^c, Giovanni Giurdanella^c, Cinzia Caggia^{b,d}, Cinzia Randazzo^{b,d}, Nunziatina Russo^d, Giovanni Luca Romano^c, Claudio Bucolo^c, Milena Rizzo^a, Giovanni Tosi^e, Jason Thomas Duskey^e, Barbara Ruozi^e, Rosario Pignatello^{a,b}, Teresa Musumeci^{a,b,*}

^a Department of Drug and Health Sciences, University of Catania, Viale A. Doria, 6 - 95125 Catania, Italy

^b NANO-i, Research Centre for Ocular Nanotechnology, University of Catania, Viale A. Doria 6, 95125 Catania, Italy

^c Department of Department of Biomedical and Biotechnological Sciences, University of Catania, Via S. Sofia 97, 95123 Catania, Italy

^d Department of Agriculture, Food and Environment (Di3A), University of Catania, Via S. Sofia 100, 95123 Catania, Italy

^e Department of Life Sciences, Nanotech Lab, Te.Far.T.I., University of Modena & Reggio Emilia, Via Campi 103, Modena 41125, Italy

A B S T R A C T

Melatonin (MEL) is a pleiotropic neurohormone of increasing interest as a neuroprotective agent in ocular diseases. Improving the mucoadhesiveness is a proposed strategy to increase the bioavailability of topical formulations. Herein, the design and optimization of MEL-loaded lipid-polymer hybrid nanoparticles (mel-LPHNs) using Design of Experiment (DoE) was performed. LPHNs consisted of PLGA-PEG polymer nanoparticles coated with a cationic lipid-shell. The optimized nanomedicine showed suitable size for ophthalmic administration (189.4 nm; PDI 0.260) with a positive surface charge (+39.8 mV), high encapsulation efficiency (79.8 %), suitable pH and osmolarity values, good mucoadhesive properties and a controlled release profile. Differential Scanning Calorimetry and Fourier-Transform Infrared Spectroscopy confirmed the encapsulation of melatonin in the systems and the interaction between lipids and polymer matrix. Biological evaluation in an *in vitro* model of diabetic retinopathy demonstrated enhanced neuroprotective and antioxidant activities of mel-LPHNs, compared to melatonin aqueous solution at the same concentration (0.1 and 1 μ M). A modified Draize test was performed to assess the ocular tolerability of the formulation showing no signs of irritation. To the best of our knowledge, this study reported for the first time the development of mel-LPHNs, a novel and safe hybrid platform suitable for the topical management of retinal diseases.

1. Introduction

Melatonin (N-acetyl-5-methoxytryptamine, MEL) is a pleiotropic neurohormone of promising interest in the treatment of eye diseases. Several studies have demonstrated its antioxidant, anti-angiogenic, anti-inflammatory, anti-apoptotic and hypotensive properties in neurodegenerative ocular diseases (Lundmark et al., 2006, Martínez-Águila et al., 2021). Due to its countless beneficial effects, this molecule is gaining increasing interest as a neuroprotective agent (Yu et al. 2021). Despite its advantages, high-dose intravitreal administration of MEL may be inappropriate for compromising both the morphology and function of retinal cells. In this regard, to reduce the toxic effects on retinas, it may be useful to develop controlled release carriers to be topically applied (Tao et al., 2020). Bessone et al. found that topical instillation of MEL encapsulated in ethylcellulose nanoparticles provides an efficient neuroprotection of retinal ganglion cells (RGCs) (Bessone et al., 2020). It is worth to note that melatonin regulates changes in

neurosteroids levels, these latter are neuroprotective for the retinal tissue (Bucolo and Drago, 2004). After topical administration on rabbit eyes, Musumeci et al., reported a prolonged hypotensive effect when MEL was delivered in PLGA-PEG nanoparticles (NPs), compared to a drug aqueous solution at the same concentration, suggesting a potential application of nanosystems for glaucoma treatment (Musumeci et al., 2013). In addition, it has been shown that the desired pharmacological effect of the drug occurred when topical administration is instilled at micromolar concentrations. Initially, almost all the administered drugs (>99%) would reside outside the posterior segment, towards which they would be progressively released to reach the inner retinal structures at nanomolar concentrations, sufficient to induce a neuroprotective effect (Martínez-Águila et al., 2016, Dal Monte et al., 2020). Topically administered formulations for the treatment of diseases affecting the eye posterior segment are the most convenient but also the most complicated. The main obstacle is the limited residence time of the drug on the corneal surface, which reduces absorption (Scheive et al., 2021). There are many factors that trigger this problem, including rapid tear turnover, blinking, nasolacrimal drainage, and systemic absorption. As a result, the amount of drug that is bioavailable within the eye is less than 5% and penetration into intraocular tissues is less than 0.001% (Gaudana et al., 2009, Agrahari et al., 2016, Varela-Fernández et al., 2020).

A promising strategy to improve bioavailability is to prolong the corneal retention using systems with mucoadhesive properties that increase corneal residence time (Wang et al., 2017). Nanomedicines with mucoadhesive properties have been proposed to overcome these challenges such as niosomes, liposomes, nanostructured lipid carriers and polymeric nanoparticles (Silva et al., 2021).

From the comparison between the two different matrices, lipid and polymer-based, both classes present advantages and limitations in terms of physico-chemical properties (Hadinoto et al., 2013, Date et al., 2018). To overcome these limits and obtain nanomedicine characterized by the advantages of both matrices, such as a high encapsulation efficiency and a well-controlled release kinetics, a new generation of NPs has been designed, the lipid-polymer hybrid nanoparticles (LPHNs) (Mukherjee et al., 2019). Based on their structure, these hybrid systems are classified as: (i) monolithic LPHNs, consisting of a polymeric matrix inside which lipid molecules are dispersed; (ii) biomimetic LPHNs, designed with a polymeric matrix coated with erythrocyte membrane; (iii) polymer -caged liposomes, consisting of a liposomal matrix with polymers on the surface; (iv) core-shell type LPHNs, possessing a structure characterized by a polymer core coated with a lipid shell (Date et al., 2018). To date, several applications of LPHNs have been reported such as delivery of antibiotic drugs, chemotherapeutics, diagnostics contrast agents, and gene therapy agents (Aryal et al., 2010, Liu et al., 2010, Zhong et al., 2010, Aryal et al., 2011, Cheow et al., 2011, Kandel et al., 2011, Aryal et al., 2012, Cheow and Hadinoto, 2012, Mieszawska et al., 2012, Wang et al., 2012, Aryal et al., 2013, Fang et al., 2014, Feng et al., 2014, Lee et al., 2014, Agrawal et al., 2015, Gao et al., 2015, Evangelopoulos et al., 2016, Yan et al., 2016, Zhang et al., 2016).

This new generation of NPs has also been used for ocular drug delivery. Diebold et al. designed chitosan/phospholipid LPHNs with mucoadhesive properties for drug delivery to the anterior eye segment by topical application (Diebold et al., 2007); Gan et al., reported hyaluronic acid-functionalized LPHNs to increase delivery to the retinal pigment epithelium (RPE) targeted after intravitreal injection (Gan et al., 2013); analogous systems administered topically showed permeation confined to the superficial eye layers (cornea and conjunctiva). Here for the first time, the topical

application of LPHNs was investigated for potential retinal delivery. The common choices of biodegradable polymers included polylactic-co-glycolic acid (PLGA), polycaprolactone (PCL) and their copolymers with polyethylene glycol (PEG) due to their biocompatibility, biodegradability, non-toxicity and previous use in several FDA-approved therapeutic products (Zhang and Zhang, 2010). The commonly used lipids in the preparation of LPHNs include cholesterol, phosphatidylcholine, 1,2-dioleoyl-sn-glycero-3-phosphoethanolamine (DOPE), 1,2-dioleoyl-3-trimethylammonium-propane (DOTAP), 1,2-dioleoyl-sn-glycero-3-phosphocholine (DOPC) and lipid-PEG materials such as 1,2-distearoyl-sn-glycero-3-phosphoethanolamine-polyethylene glycol (DSPE-PEG) (Sengupta et al., 2005, Zheng et al., 2010, Su et al., 2011). It should be noted that the addition of PEG always occurs by conjugation with the lipid, used as an anchor point (Chan et al., 2009). To our knowledge, the use of pegylated copolymers is a rare approach, to date exclusively employed for siRNA delivery in cationic hybrid systems. In this case, the cationic lipids were exploited to allow binding to the negatively charged siRNA and PEG portions to allow extended circulation time by eluding reticuloendothelial system (RES) uptake (Yang et al., 2012, Khodaei et al., 2021). With the aim of prolonging corneal retention time, the novelty of this work was the design of hybrid nanoparticles consisting of a PLGA-PEG copolymer, to exploit the PEG mucopenetrating agent action, and two cationic lipids, used to enhance mucoadhesion through electrostatic interaction with the anionic ocular mucosa. Selected cationic lipids have been previously used in ophthalmic pharmaceutical formulations, cetyltrimethylammonium bromide (CTAB) and didodecyldimethylammonium bromide (DDAB) (Fangueiro et al., 2014, Almeida et al., 2015, Leonardi et al., 2015, Carbone et al., 2016).

The present study was aimed to design and optimize MEL-loaded LPHNs (mel-LPHNs) using the single-step nanoprecipitation method. The optimization of nanocarriers was performed using the statistical experimental design approach, setting up a 3-level factorial design (independent variables: MEL and lipids concentrations; dependent variables: zeta potential (ZP) and encapsulation efficiency (%EE)). The selected final nanomedicine was deeply investigated in terms of physico-chemical, mucoadhesive properties, and release profile. Solid-state thermal and infrared analysis were done on the produced mel-LPHNs. Their morphology was investigated by transmission electron microscopy (TEM), and stability studies were carried out following ICH QA(R2) guidelines. *In vitro* and *in vivo* tests were performed after a UV-radiation process to obtain adequate sterilization, hence microbiological assays were carried out. The antioxidant and neuroprotective activities of delivered MEL was assayed *in vitro* on a model of glucose-induced diabetic retinopathy on Human Retinal Endothelial cells (HREC). Draize test was performed to evaluate the ocular tolerability of the formulation.

2. Materials and methods

2.1 Materials

MEL (powder <98%), poly(ethylene glycol) methyl ether-block-poly(lactide-co-glycolide) (PEG average Mn 5000, PLGA Mn 55000), poly(D,L-lactide-co-glycolide)acid terminated (lactide:glycolide 75:25, Mw 4,000-15,000), polyoxyethylene sorbitan monooleate (Tween 80®), CTAB (cetyltrimethylammonium bromide), DDAB (didodecyldimethylammonium bromide), dibasic sodium phosphate, benzalkonium

chloride ($\geq 95.0\%$), glycerol, and mucin from porcine stomach type II were purchased from Merck Life Science S.r.l. (Milan, Italy). Ethanol (96% purity) and acetone were obtained from Honeywell (Monza, Italy). Acetonitrile 200 for UV was kindly supplied by Romil Ltd. (Cambridge, UK). All other chemical reagents, solvents used for HPLC analysis, and deionized water were of analytical grade.

2.2 Experimental design

The experimental design was created using Design-Expert® software (version 11 Stat-Ease Inc., Minneapolis, MN, USA). Response surface quadratic model using I-optimal design was performed to optimize mel-LPHNs and investigate the correlation between responses and factors (Bonaccorso et al., 2021). The design was composed of three independent variables such as MEL (X_1), CTAB (X_2) and DDAB (X_3) concentrations at three coded levels as shown in Table 1.

Table 1. Factors and the corresponding levels investigated during the I-optimal design.

Coded Factors	Coded levels		
	low	medium	high
X_1 : MEL conc. (% wt/wt)	1	3	5
X_2 : CTAB conc. (% w/v)	0	0.25	0.50
X_3 : DDAB conc. (% w/v)	0	0.25	0.50

According to the design, 18 formulations were prepared, and the effect of the factors was studied on the mel-LPHNs ZP (Y_1) and %EE (Y_2) which were chosen as response variables. The order of the experiments was randomized to avoid experimental bias. The nonlinear computer-generated quadratic model for design can be expressed as the following second-order polynomial:

$$R = b_0 + b_1 X_1 + b_2 X_2 + b_3 X_3 + b_{12} X_1 X_2 + b_{13} X_1 X_3 + b_{23} X_2 X_3 + b_{11} X_1^2 + b_{22} X_2^2 + b_{33} X_3^2$$

where R is response, b_0 is intercept, b_1 – b_{33} are regression coefficients computed from the observed values of R from experiments, and X_1 , X_2 and X_3 are independent variables. The terms ($X_1 X_2$, $X_1 X_3$ and $X_2 X_3$) and (X_1^2 , X_2^2 and X_3^2) represent the interaction and quadratic terms, respectively (Kalam et al., 2013).

The obtained responses were subjected to model fitting using analysis of variance (ANOVA), and the best model fit was selected based on statistical parameters such as standard deviation (SD), R^2 and the lack of fit. Numerical and graphical optimizations, through three-dimensional (3D) response surface plots, were performed to generate maximum desirability, which correspond to the geometric mean of all individual desirability for each response. Finally, the optimized formulation was selected from the design space and used for further investigations.

2.2 Nanoparticles preparation

2.3.1. Hybrid nanoparticles preparation

A modified nanoprecipitation method was used as a single-step technique to prepare mel-LPHNs (Musumeci et al., 2013). Briefly, PLGA-PEG (3 mg/mL) and MEL

(1, 3, 5 % drug-to-polymer w/w ratio) were dissolved in the organic phase (acetone). The aqueous phase composed of a water/ethanol solution (1:1, v/v) containing 0.1 % w/v Tween 80® and different concentrations of the employed lipids (0, 0.25, 0.5 % w/v) was placed in a capped vial and heated to 70 °C to ensure lipids melting. The organic phase was then added dropwise to the aqueous phase at room temperature under magnetic stirring, obtaining a milky colloidal suspension. The organic solvent was removed under vacuum by a rotavapor (Buchi R111) at 40 °C. The formulations were purified through centrifugation (12000 rpm) for 1 hour at 8 °C, using a Thermo Scientific SL16R, equipped with a FiberLite™ F15-6x100y fixed angle-rotor (Thermo Scientific Scientific Inc., Waltham, Massachusetts, USA). The obtained pellet was resuspended with the same volume of the aqueous phase as the pre-purification phase. Both unpurified and purified samples were characterized according to the mean diameters provided by the instrument as Z-Ave, size distributions (polydispersity index, PDI) and ZP

2.3.2 Preparation of P-NPs and P-PEG-NPs

To perform mucoadhesion studies (in section 2.10 below), MEL-loaded P-NPs/P-PEG-NPs were prepared from PLGA and PLGA-PEG diblock copolymer, respectively. The nanoprecipitation method was used as previously reported (Musumeci et al., 2013). Briefly, PLGA or PLGA-PEG (3 mg/mL) and MEL (1%, drug-to-polymer weight ratio) were dissolved in acetone. The organic phase was added dropwise under constant agitation (500 rpm) at room temperature into the aqueous phase (water/ethanol 1:1 v/v containing 0.1% w/v Tween® 80) until a milky suspension was obtained. Organic solvents were removed under vacuum (Buchi R111) at 40 °C. The nanosystems were purified by different techniques. P-NPs consisting of the PLGA polymer were subjected to dialysis with a water change rate of 1 L/h; according to our previous findings, the purification of P-NPs by centrifugation resulted in the formation of heterogeneous, non-redispersible aggregates (Romeo et al., 2021). P-PEG-NPs were purified by centrifugation (12000 rpm) for 1 h at 8 °C using the Thermo Scientific SL16R centrifuge (Thermo Scientific Inc., Waltham, Massachusetts, USA) followed by resuspension of the pellet in water. The obtained P-NPs and P-PEG-NPs nanosuspensions were subjected to the mucin particle method.

2.4 Physico-chemical characterization and %EE of the designed mel-LPHNs

Photon correlation spectroscopy (PCS) was performed using Zetasizer Nano S90 (Malvern Ins. Ltd., Malvern, UK), to determine the particle size, PDI and ZP of mel-LPHNs. The experiments were carried out by measuring the intensity changes of scattered light, at 25 °C, using a 4 mW He-Ne laser operating at 633 nm, with a detection angle of 90°. Each sample was measured in triplicate and the results are expressed as mean ± SD. %EE of mel-LPHNs was measured through spectrophotometry (UH5300 UV-visible spectrophotometer, Hitachi, Chiyoda, Japan). The MEL-loaded nanosuspensions (1, 3, 5 % wt/wt) were centrifuged at 12000 rpm for 1 h at 8 °C (Thermo Fischer Scientific Inc., USA). The supernatant solution was separated while the NP pellet was dissolved in 1 mL of acetonitrile. The concentration of MEL in the samples was quantified from absorbance measurements at a λ_{max} of 278 nm against the standard calibration curve that was linear in the concentrations range 10-50 µg/mL ($R^2 = 0.9989$).

$$EE (\%) = \frac{\text{amount of drug in the pellet}}{\text{total amount of drug}} \times 100$$

2.5 Osmolarity and pH adjustment of the selected mel-LPHNs

To make the optimized mel-LPHNs formulation adequate for ophthalmic administration, a suitable resuspension medium, consisting of water for injectable preparations with the addition of glycerol (2.6 % w/v) as an osmotic agent and benzalkonium chloride (0.01 % w/V) as a preservative, was prepared (Ahuja et al., 2008, Badr et al., 2021). To assess the fitness of the selected medium, pH and osmolarity values were measured after mel-LPHNs resuspension.

The osmolarity of mel-LPHNs was measured by freezing point depression (FPD) using a digital osmometer (Osmomat 030, Gonotec, Berlin, Germany). The determination of pH was carried out at 25 °C using a pH-meter (Seven Compact™ S210, Mettler Toledo S.p.A, Milano, Italy). Analyses were performed in triplicate and results are expressed as mean ± SD. The adjusted resuspension medium was used for subsequent characterization studies.

The resulting optimized mel-LPHNs was sterilized by UV irradiation (250-270 nm) for 30 min before *in vitro* and *in vivo* studies.

2.6 Morphological characterization and *in vitro* release profile of the selected mel-LPHNs

The morphology and shape of mel-LPHNs were analyzed by TEM as previously reported (Duskey et al., 2021). Briefly, mel-LPHNs were diluted 1:100 (v/v) in deionized water. A drop of diluted suspensions was placed on a 200-mesh formvar copper grid (TABB Laboratories Equipment, Berks, UK). Excess water was removed by drying at room temperature. Images were acquired using a Nova NanoSEM 450 (FEI, Hillsboro, OR, USA) transmission electron microscope operating at 30 kV with the spot set to 1.5 using a STEM II detector in Field free mode.

The *in vitro* release behavior of mel-LPHNs and MEL aqueous solution in phosphate buffered saline (PBS; pH 7.4) was evaluated through dialysis bag method. The amount of drug released from mel-LPHNs was measured after samples centrifugation, performed at 12000 rpm at 8 °C for 1 h; the pellet was resuspended in 1 mL of PBS, pH 7.4 and the suspension was transferred into dialysis tube (Spectra/Por® membranes, MWCO 3.5 kDa). The latter was incubated in 19 mL of medium (PBS, pH 7.4), maintained under magnetic stirring at 37 °C for up to 8 days. At predetermined time points (0, 1, 2, 3, 4, 5, 6, 7, 8, 24, 48, 72, 96, 120, 168 and 192 h), 500 µL of the release solution was withdrawn and replaced with the same volume of fresh buffer. The concentration of MEL was quantified by High-Performance Liquid Chromatography (HPLC): a 20-µL sample was injected into a LiChrospher® RP-18 HPLC column (15 cm × 3.2 mm; 5 µm) at room temperature, at a flow rate of 1 mL/min, with a run time of 6 min, and MEL was detected at a retention time of 4.3 min and a wavelength of 230 nm. The mobile phase was composed of acetonitrile:water (55:45). The standard calibration curve prepared at different dilutions of MEL in the mobile phase was linear in the concentration range of 0.005-1 µg/mL (R² = 0.9987). Release studies were performed in triplicate for each formulation.

2.7 Differential Scanning Calorimetric Analysis (DSC)

Thermal analyses were performed for raw materials such as neat MEL, PLGA-PEG, CTAB, DDAB and freeze-dried mel-LPHNs using a DSC1 Star System apparatus (Mettler Toledo, Schwerzenbach, Switzerland) equipped with a Poly-Science temperature controller (PolyScience, Illinois, USA). The DSC detection system consists of ceramic Mettler Full Range (FRS5, with 56 thermocouples) and High Sensitivity (HSS8, with 120 thermocouples) sensors. Calorimetric resolution and sensitivity of sensors, determined through the TAWN test, were respectively between 0.12 - 0.20 and 11.9 - 56.0. Each scan has an accuracy of ± 0.2 °K and a precision of ± 0.02 °K. Here, 3 mg of each sample were accurately weighed and placed into 40 μ L aluminum crucible and sealed using an aluminum lid by a sealing machine. Samples were submitted to DSC analysis by setting a heating cycle followed by cooling in the temperature range of 20-160 °C, with a scan rate of 5 °C/min (heating cycle) and 10 °C/min (cooling cycle). The obtained transition temperature data was extrapolated from the peak areas with the Mettler STARe Evaluation software system installed on Optiplex3020 DELL.

2.8 Fourier-Transform Infrared Spectroscopy (FTIR) measurement

Infrared analyses were performed for neat MEL, PLGA-PEG polymer, CTAB, DDAB and mel-LPHNs. Absorption spectra were recorded using an FT-IR spectrophotometer (Perkin-Elmer Spectrum RX I, Waltham, MA, USA) equipped with a diamond window and a zinc selenide crystal (diamond/ZnSe) and an attenuated total reflectance (ATR) accessory. All samples were cast on NaCl plates except MEL analyzed by the KBr disk method. Data were collected in the wavenumber range 400-4000 cm^{-1} and each measured spectrum was averaged from 20 scans with a resolution of 2 cm^{-1} at room temperature.

2.9 Stability evaluation of optimized mel-LPHNs

Stability evaluation of the optimized batch of the optimized and selected mel-LPHNs suspension was determined by measuring the physico-chemical properties of the nanosuspension stored for a period of six months at different temperatures and relative humidity (RH). The formulations were stored at refrigeration temperature ($5\text{ °C} \pm 3\text{ °C}$) and under accelerated conditions ($40\text{ °C} \pm 2\text{ °C} / 75 \pm 5\%$ RH) according to the International Conference on Harmonization (ICH) guidelines (QA(R2)) (EMA, 2003). Batches were kept refrigerated or stored in an environmental simulation chamber to keep constant climatic conditions (Binder GmbH, Tuttlingen, Germany). Samples were withdrawn at different intervals (0, 1, 2, 3, 4, 5, 6 months) and evaluated for Z-Ave, PDI, ZP and osmolarity. The %EE was assessed at the beginning, after 3 months and at the end of the storage time. All measurements were made in triplicate and all data were expressed as mean \pm SD.

2.10 In vitro NPs mucoadhesive evaluation by mucin particle method

In this study, the potential mucoadhesive properties of the optimized mel-LPHNs was evaluated by the mucin particle method (Bonaccorso et al., 2018, Pai et al., 2019). NPs uncoted and coated with cationic lipids were analyzed in presence of mucin, with the aim of exploring and comparing the mucoadhesive propensity of the studied

nanosystems. In detail, NPs with different external shells were analyzed: hydrophobic consisting of PLGA polymer (P-NPs), hydrophilic composed of a PLGA-PEG matrix (P-PEG-NPs) and PLGA-PEG/cationic lipids (mel-LPHNs).

Briefly, an accurately weighed amount of mucin was dispersed in phosphate buffer pH 6.8 to obtain 0.25 and 0.5 % w/v solutions. Then, 1 mL of mucin solution was mixed with an equal amount of the respective nanosuspension and vortex-mixed for 1 min. Samples were incubated at 37 °C for 1 and 24 h, and finally, to assess NP/mucin interaction, PCS analysis was performed using the Zetasizer Nano S90, as described above. Controls (Ctrl), consisting of mucin, P-NPs, P-PEG-NPs, and mel-LPHN dispersions in phosphate buffer (pH 6.8) were also treated and measured in the same way. Analyses were performed in triplicate for each sample.

2.11 Microbiological test to evaluate sterilization process

Microbiological analyses were performed according to the European Pharmacopoeia (01/2005:20601), at laboratory of Food Microbiology of the Department of Agriculture, Food and Environment (Di3A), University of Catania.

As reported in the official protocol, both the validation and sterility tests were performed. In details the following strains: *Clostridium sporogenes* ATCC 11437, *Pseudomonas aeruginosa* ATCC 9027, *Staphylococcus aureus* ATCC 25213, *Bacillus subtilis* ATCC 19659, *Candida albicans* ATCC 1023 and *Aspergillus flavus* ATCC 16883 were used. Based on official guidelines, the analytical procedure was validated by performing a validation test, which is designed to verify the absence of substances inhibiting the growth of microorganisms in the product to be examined. In this regard, in order to ensure the viability of the selected target strains, the strains were cultivated in appropriate media and conditions. In details, the strains were previously inoculated and incubated at the optimal growth conditions. *C. sporogenes*, *P. aeruginosa* and *S. aureus* were inoculated in Thioglycollate medium (L-cystine 0.5 g; agar 0.75 g; glucose monohydrate/anhydrous 5.5 g; yeast extract 5 g; pancreatic digest of casein 15 g; sodium thioglycollate 0.5 g; resazurin sodium solution 1 g/L freshly prepared; water R to 1000 mL; the pH of medium, after sterilization, was set to 7.1 ± 0.2) and incubated for 3 days at the optimal growth conditions. *B. subtilis*, *C. albicans* and *A. flavus* were inoculated into TSB Triptic Soy Broth (TSB, Oxoid, Italy) medium and incubated for 3-4 days at the optimal growth conditions. The media were considered suitable when a clear growth was observed. The validation test was performed using three samples of mel-LPHNs: one previously subjected to UV treatment for 30 min, one did not UV-treat, and the last one treated with UV light, opened and analyzed after 28 days (shelf-life for multi-dose eye drop) before the analyses. Fresh cultures of target strains, obtained as above, were dissolved into a sterile saline solution (0.9 w/v of NaCl) and transferred into 1 mL of each mel-LPHNs samples, to reach a final density of 100 Colony Forming Units (CFU). One mL of the obtained mixture was filtered through a 0.45 µm membrane and the membranes were subsequently placed into a suitable agar medium. A positive control of each strain was performed. After the incubation, a clearly visible growth of microorganisms was obtained comparable to the positive control test, highlighting that the samples did not possess any antimicrobial activity under the test conditions or that such activity has been satisfactorily eliminated. In parallel with the validation test, the sterility test was carried out using the technique of membrane filtration by direct inoculation of the standardized microbial culture with the mel-LPHNs samples.

Appropriate negative controls were included. After filtration, the whole membrane was transferred to the culture medium and incubated for 15 days. During the incubation time, the plates were examined to detect microbial growth, at regular intervals.

2.12 *In vitro* biological assessment

2.12.1 Cell viability assay

Cell viability was assessed in an *in vitro* model of diabetic retinopathy by the 3-[4,5-dimethylthiazol-2-yl]-2,5-diphenyl tetrasodium bromide (MTT assay). HRECs were cultured in the presence of a normal concentration of glucose (5 mM, NG), or treated with a high concentration of glucose (25 mM, HG) for 48h in order to mimic a hyperglycemic insult, in the presence or absence of 0.1 and 1 μ M of LPHNs, 0.1 and 1 μ M of mel-LPHNs or 0.1 and 1 μ M of pure MEL. At the end of treatments, 20 μ L of 5 mg/mL MTT were added to the medium that was then incubated for 4 h at 37 °C. The supernatants were replaced with 150 μ L of DMSO to dissolve the precipitate. The absorbance of the mixtures was determined at 570 nm in a plate reader (VariosKan, Thermo Fisher Scientific, Waltham, MA, USA) (Lupo et al., 2019).

2.12.2 ROS determination

ROS production was detected by a spectrophotometric evaluation of a dichlorodihydro-fluorescein diacetate (DCFH-DA) fluorescent probe. After the treatments of HREC reported in section 2.11.1., cells were incubated with 25 μ M 2',7'-dichlorodihydrofluorescein diacetate (DCFDA) in a buffer solution at 37 °C for 30 min. Then, DCFDA was replaced with 100 μ L of medium and the ROS concentration was measured by VarioskanTM (λ_{ex} = 495 nm, λ_{em} = 529 nm) (Giurdanella et al., 2022).

2.13 *Draize Test*

2.13.1 Animals

Male New Zealand albino rabbits (2.0-2.5 kg) were purchased from Envigo (Udine, Italy). Animals were housed under standard conditions with food and water provided ad libitum in a light- controlled room and set temperature and humidity. Animal care and experimental procedures were carried out according to the ARVO Statement for the Use of Animals in Ophthalmic and Vision Research. Protocols were approved by the Institutional Animal Care and Use Committee of the University of Catania (project #886).

2.13.2 Ocular tolerability

The potential ocular irritancy and/or damaging effects of unloaded formulation and MEL-ladden formulation were evaluated according to a modified Draize's test (4 animals/group) (Leonardi et al., 2014, Puglia et al., 2018). Analysis was carried out using a slit lamp (mod. 4179 T Sbisà, Florence, Italy). Congestion, swelling, and discharge of the conjunctiva were graded on a scale from 0 to 3 (0 = normal; 1, 2 and 3 = discrete, moderate and intense dilatation of conjunctival vessels, respectively), 0 to 4 (0 = normal; 1, 2, 3 and 4 = discrete, moderate, intense, intense + lid closure conjunctival swelling, respectively), and 0 to 3 (0 = normal; 1, 2 and 3 = discrete, moderate and intense

discharge, respectively). Iris hyperemia was graded on a scale from 0 to 4 (0 = normal, 1 = discrete dilatation of iris vessels; 2 = moderate dilatation of iris vessels; 3 = intense iridal hyperemia with flare in the anterior chamber; 4 = intense iridal hyperemia with flare in the anterior chamber and presence of fibrinous exudates). Corneal opacity was graded on a scale from 0 to 4 (0 = normal, 1 = some spots of opacity; 2 = diffuse cortical opacity; 3 = cortical and nuclear opacity; 4 = intense opacity plus posterior subcapsular opacity). Formulations (30 μ L) were topically administered in the right eye every 30 min for 6 h (12 treatments). At the end of the treatment, two observations at 10 min and 6 h were carried out to evaluate the ocular tissues. Observations were made by two independent observers in a masked way. Methylene blue staining was used to evaluate the corneal integrity, which allows an accurate determination of the extent of epithelial damage because of its poor diffusion through the stromal layer of the cornea. Intraocular pressure (IOP) was measured at baseline and at the end of treatment (after 6 h) using Bio-Rad Tono-Pen XL tonometer.

2.14 Statistical analysis

All experiments were carried out in triplicate and results presented as mean \pm SD. A single factor ANOVA was used to compare the treatments, where differences between groups were considered significant for a p-value < 0.05 . The T-test was used to calculate the statistical significance in mucoadhesion studies; the obtained values were considered not significant for p-value > 0.05 , significant for p-value < 0.05 , very significant for p-value < 0.01 and extremely significant for p-value < 0.001 respective to the control group.

3. Results and Discussion

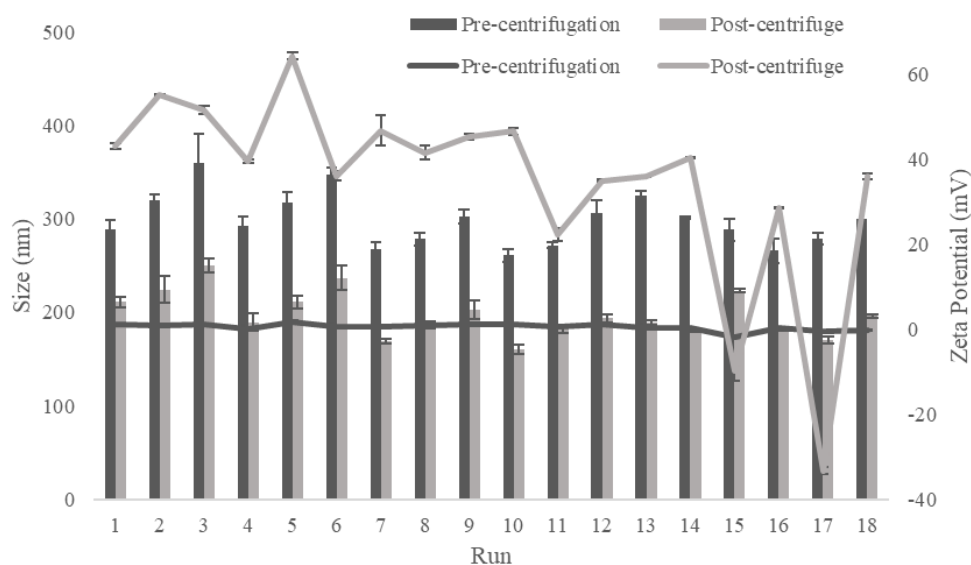
In order to improve the absorption of a topically administered drug loaded nanomedicine, one strategy could be to increase interactions with biological substrates by modifying the surface properties of NPs (Rabinovich-Guilatt et al., 2004). Our novel nanotechnology was developed with cationic lipids and PEG as a mucus penetrating agent to synergistically promote corneal retention and mucoadhesion of nanocarriers. Currently, for the preparation of LPHNs two methods are mainly followed, two-step and single-step. The first involves that the polymer core and the lipid coating are prepared separately, and the two components are then incubated together to obtain the core-shell structure. Beyond the requirement of longer preparation times, the limitation of this technique lies in the incubation phase, during which part of the drug could be expelled from the matrix before the lipid coating forms on the surface. Instead, the single-step method is quick, simple, and reproducible, since it involves the self-assembly of the lipid coating on the polymer matrix in a single step, making this technique suitable for industrial scale-up (Zhang et al., 2008). Thus, the one-step emulsification-solvent evaporation or nanoprecipitation, with slight modifications, preparation techniques were used. The emulsification-solvent evaporation method has two variants, single or double emulsion, used respectively to encapsulate water-insoluble and water-soluble drugs. While the nanoprecipitation technique is limited to water-insoluble drugs, briefly, the polymer and drug are solubilized in a water-miscible organic solvent (e.g., acetone or acetonitrile) and then added dropwise under magnetic stirring into the aqueous phase containing lipids (Cheow and Hadinoto, 2011). The organic phase in contact with the

aqueous phase would result in the polymer coiling in the NPs and self-assembly of the lipid monolayer. To date, the development of self-assembled LPHNs has been used to prepare nanosystems with different applications such as the delivery of anti-cancer agents (vincristine sulphate, methotrexate, paclitaxel and siRNA) for breast or prostate cancer. To the best of our knowledge, this technique has not been used until now to prepare LPHNs for ophthalmic administration (Ling et al., 2008, Zhang et al., 2010, Yang et al., 2012, Garg et al., 2015, Godara et al., 2020). To produce mel-LPHNs, nanoprecipitation using the single-step method was employed. This method has several operational advantages, such as the use of highly biocompatible solvents; in our case acetone and ethanol used in the preparation belong to class 3 according to the ICH solvent toxicity scale and present very low risks for human health. In addition, the chosen method allows the use of low concentrations of surfactant, in our case 0.1% Tween®80 (w/v) which is highly tolerated for ophthalmic use (Leonardi et al., 2015).

3.1 Experimental design: effect of independent variables on Zeta Potential and Encapsulation Efficiency

For a rational design of the systems, a preliminary investigation was conducted to select the independent variables, the factors to be kept constant and the output responses. From the know-how of the research group, it was decided to maintain certain factors constant: the polymer concentration (3 mg/mL), the surfactant concentration (0.1 % w/v) and the ratio between the aqueous and organic phases (1:1). Once the constant parameters were established, the independent variables and their levels were introduced to construct the experimental design (Table 1). The choice of lipids and the concentrations to be investigated within the design space were made based on data available in the literature (on Science Direct database from 2014 to August 2021 accessed). The consulted papers reported that the use of the cationic lipids CTAB and DDAB could improve retention time, drug penetration through the cornea, and thus ocular bioavailability (Sánchez-López et al., 2017, Hassan et al., 2018). Particular attention was focused on Fangueiro et al. investigations who demonstrated that an ocular formulation could be safe and biocompatible when the lipid concentration did not exceed 0.5 % w/v (Fangueiro et al., 2014, Fangueiro et al., 2016). This concentration was set as a high coded level in the experimental design. Particle size, PDI and ZP were measured for the 18 runs before and after the purification step. The mean size of purified mel-LPHNs ranged from 160.3 to 250.4 nm, while the PDI varied from 0.222 to 0.442. The influence of the investigated factors on particle size and PDI was not noticeable by varying mel-LPHNs composition, so these parameters were measured for our knowledge, but data were not included in the experimental design. From the collected data, we found that purification systematically contributed to a decrease in size and a shift in ZP from neutral to positive values (Supplementary Figure 1).

Pre-centrifugation neutral values could be attributed partly to the excess non-ionic surfactant, which was removed by purification, and partly to the PEG chains that provide a negative charge, neutralized by the cationic lipids (Conte et al., 2019, Cortés et al., 2021). The reason of occurred modifications could be attributed to the conformation of the flexible PEG chains. A previous study showed that before purification PEG chains extended into the brush-like conformation, and the applied centrifugation force would induce a conformational change resulting in mushroom-like chains (Craparo et al., 2021).



Supplementary Figure 1. Mean size (nm) (bars) and Zeta potential (mV) (lines) of 18-runs of MEL-loaded LPHNs (mel-LPHNs) before and after the purification step.

A diagram of the assumed hypothesis is shown in Figure 1. Switching from the brush to the mushroom conformation, a strong reduction of the hydrodynamic diameter (> 100 nm) and a change of the ZP towards positive values were observed. It has been hypothesized that the mushroom conformation may allow the heads of lipid-shell to emerge on the surface, providing a positive charge to the hybrid nanocarriers (Zhang et al., 2008).

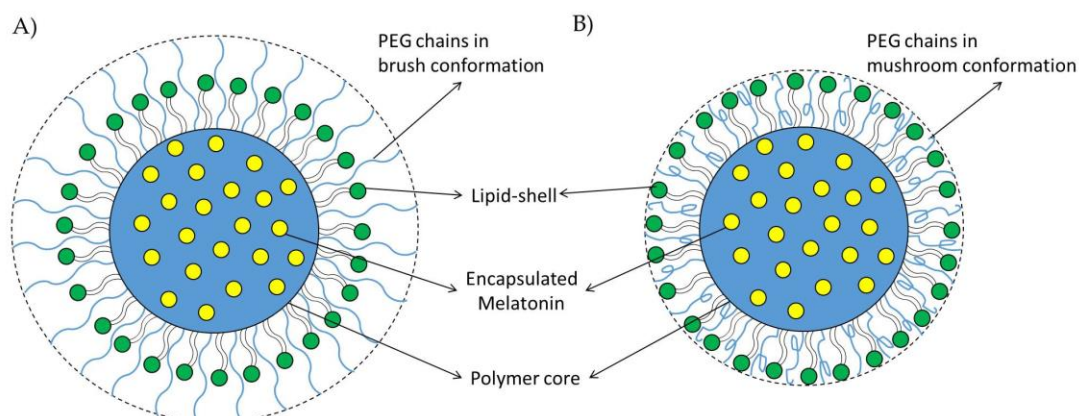


Figure 1. Conformations of MEL-loaded-LPHNs (mel-LPHNs) before (a) and after (b) centrifugation purification processes.

NP optimization was performed by applying I-optimal design to minimize experimental runs. As proposed by the software the response variables were observed experimentally for 18 runs; the obtained data referred to purified samples and were expressed as mean \pm SD in Table 2.

Table 2. Composition and observed responses in I-optimal design for MEL-loaded LPHNs (mel-LPHNs).

Run	Independent Variables ^a			Dependent Variables ^b	
	X ₁	X ₂	X ₃	Y ₁	Y ₂
1	1	0.50	0	43.08 ± 0.643	79.19 ± 9.560
2	3	0	0.25	55.10 ± 0.404	29.52 ± 2.015
3	3	0.25	0.50	51.50 ± 0.971	30.75 ± 1.336
4	1	0.50	0.25	39.50 ± 0.458	86.15 ± 5.346
5	1	0	0.50	64.30 ± 0.781	83.81 ± 1.591
6	3	0.50	0	36.10 ± 1.070	33.12 ± 2.786
7	5	0	0.50	46.80 ± 3.670	18.18 ± 4.773
8	3	0.25	0.50	41.60 ± 1.610	31.24 ± 7.509
9	1	0.50	0.25	45.30 ± 0.586	68.04 ± 5.827
10	3	0	0.25	46.60 ± 0.839	15.44 ± 0.799
11	5	0.25	0	22.30 ± 1.520	14.18 ± 1.209
12	1	0.25	0	35.00 ± 0.265	74.36 ± 0.014
13	5	0.25	0.25	35.90 ± 0.100	18.83 ± 0.566
14	5	0.25	0.25	40.30 ± 0.153	18.11 ± 1.344
15	3	0	0	-9.81 ± 2.210	16.31 ± 0.467
16	3	0.25	0	28.60 ± 0.100	27.05 ± 0.269
17	5	0	0	-33.20 ± 0.924	16.91 ± 0.926
18	5	0.50	0.50	36.00 ± 0.700	24.31 ± 0.021

^aIndependent variables: X₁ = [MEL]; X₂ = [CTAB]; X₃ = [DDAB].

^bDependent variables: Y₁ = Zeta Potential (mV) ± SD; Y₂ = Encapsulation Efficiency (%) ± SD.

The input data were processed for different mathematical models. Reducing the model by removing non-significant terms helped to increase its accuracy. The adequacy of the models was assessed by means of ANOVA (Table 3). The lower the SD value, the better the model describes the response. As shown in Table 3, the lowest SD values were obtained for the quadratic model (8.26 and 6.44, for Y₁ and Y₂ responses, respectively). The highest R², which describes how well the model fits the data, was achieved for the quadratic model (0.9389 and 0.9723 for Y₁ and Y₂, respectively). The fit of the models was assessed by applying the lack-of-fit test. The proposed ideal model should have an insignificant lack-of-fit. Therefore, the significant lack-of-fit results for the linear and two factor interaction (2FI) models showed that they were not adequate. The test was not significant for the quadratic model. The statistical results revealed that the quadratic model would be the recommended model as it can describe the effect of the variables on the responses well compared to the other models. The coefficients of the reduced polynomial models were assessed by ANOVA to measure significance (Table 4).

Table 3. Models summary statistics of response and lack of fit test to select the satisfactory model to fit data.

Source	Y ₁ (ZP)				Y ₂ (%EE)			
	SD	R ²	Lack of fit		SD	R ²	Lack of fit	
			F value	P value			F value	P value
Linear	17.18	0.5380	14.41	0.0102	12.39	0.8207	2.86	0.1612
2FI	12.46	0.8093	8.16	0.0302	13.49	0.8330	3.77	0.1086
Quadratic	8.26	0.9389	3.90	0.1081	6.44	0.9723	0.26	0.8894

2FI= Two factor interaction model.

Table 4. Analysis of variance results.

Polinomyal term	Zeta Potential		Encapsulation Efficiency	
	Coeff. estimate	P value	Coeff. estimate	P value
Model		Quadratic ^a		Quadratic ^a < 0.0001
X ₁	-5.27	0.0939	-29.95	< 0.0001
X ₂	2.68	0.3681		
X ₃	10.21	0.0042		
X ₁ X ₂	12.87	0.0060		
X ₁ X ₃	6.50	0.0967		
X ₂ X ₃	-20.61	0.0002		
X ₁ ²			22.16	< 0.0001
X ₂ ²				
X ₃ ²	-16.65	0.0039		
R ²		0.9202		0.9509
Adjusted R ²		0.8644		0.9444
Predicted R ²		0.6652		0.9293
AP		17.3859		23.4276
F value		16.48		145.35

^aReduced quadratic model.

AP = Adequate Precision

The Fisher's variation (F-value) and the probability value (p-value) suggested the significance of the model. A p-value < 0.05 indicates that the significance of the model is high. As shown in Table 4 the F-value, p-value and R²-value revealed that the quadratic model was adequate and satisfactorily explained the data for both ZP (Y₁) and %EE (Y₂). Another useful parameter for assessing the significance of the model is the adequate precision (AP). AP is a measure of the signal-to-noise ratio, so a value greater than 4 is desirable (Mandlik and Ranpise, 2017). AP > 4 was obtained for responses Y₁ (17.4) and Y₂ (23.4), confirming that the model was adequate to navigate the selected design space and the signal of all responses was satisfactory (Niizawa et al., 2019).

For the ZP (Y₁), the predicted R² (0.6652) and adjusted R² (0.8644) are in reasonable agreement, as the difference is less than 0.2. The F-value (16.48) and p-value (0.0001) implied the significance of the model. The equation of the reduced quadratic model generated for the NPs ZP (Y₁) is shown in equation 1. The estimated coefficients represented the influence that each individual variable exerted on the response,

indicating a synergistic (with positive signs) or adverse (with negative signs) relationship between the variables.

$$ZP = 48.07 - 5.27 \times X_1 + 2.68 \times X_2 + 10.21 \times X_3 + 12.87 \times X_1X_2 + 6.50 \times X_1X_3 - 20.61 \times X_2X_3 - 16.65 \times X_3^2 \quad (1)$$

The significant model terms regarding ZP were X_3 , X_1X_2 , X_2X_3 and X_3^2 . The term X_3 affected the response both individually as a linear term, as a quadratic term and in combination. This indicates that the effect of DDAB concentration on the ZP of NPs was more pronounced than that of CTAB (Sinha et al., 2015). The term that mainly influenced the ZP response (Y_1) was X_2X_3 , referring to the interaction between the two cationic lipids CTAB and DDAB. This interaction term shows how ZP varied when the variables were changed simultaneously. ZP increased proportionally as the concentration of the two lipids increased. A study by Carbone et al showed that the magnitude of the ZP is directly proportional to the concentration of lipids used in the preparation (Carbone et al., 2012). The interaction effects of the terms on the ZP are shown in the 3D response surface plots and the 2D contour plots (Figure 2). From the response surface plots of the X_2X_3 interaction (Figure 2E and 2F), it was observed that negative ZP values were obtained when the systems were formulated in the absence of the lipids (run 15, Table 2). The 3D response surface plots and contour plots of the X_1X_2 (Figure 2A and 2B) and AC (Figure 2C and 2D) interactions showed that low ZP values were obtained at high drug concentrations and low concentrations of the respective lipids.

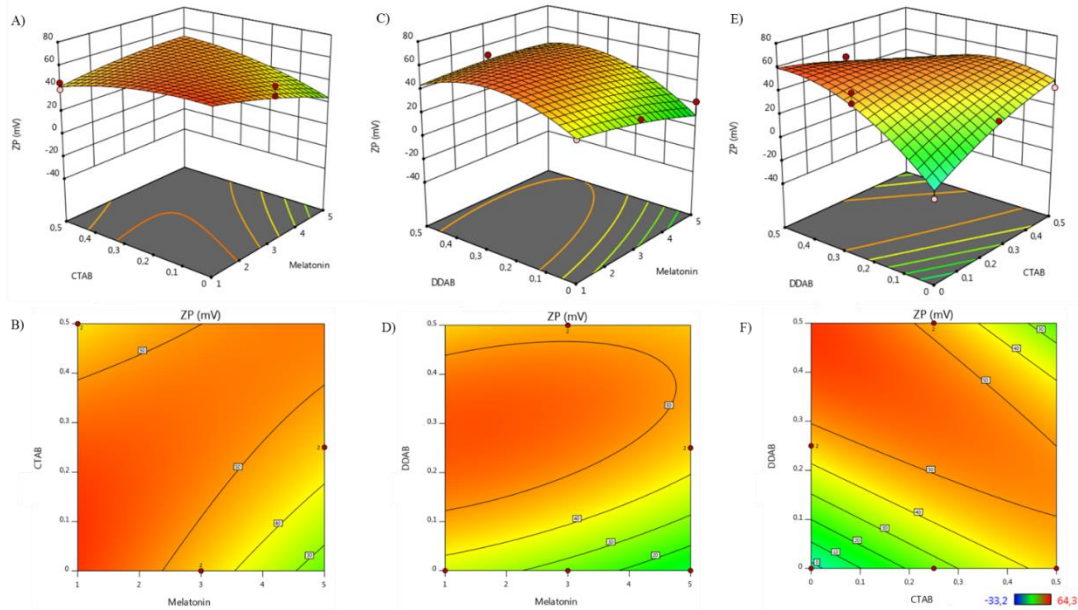


Figure 2. 3D surface (A) and contour plot (B) of the effect of X_1 : MEL concentration (% w/v) versus X_2 : CTAB concentration (% w/v); 3D surface (C) and contour plot (D) of the effect of X_1 : MEL concentration (% w/v) versus X_3 : DDAB concentration (% w/v); 3D surface (E) and contour plot (F) of the effect of X_2 : CTAB concentration (% w/v) versus X_3 : DDAB concentration (% w/v) on the mel-LPHNs zeta potential.

Regarding the %EE of mel-LPHNs, the reduced quadratic model fit with respect to its p-value (<0.0001) as shown in Table 4. The F-value of 145.35 implied that the model was significant. The predicted R^2 of 0.9293 is in reasonable agreement with the adjusted

R² of 0.9444. The mathematical relationship between the independent variable and the %EE for mel-LPHNs is given by the following equation.

$$\%EE = 26.20 - 29.95 \times X_1 + 22.16 \times X_1^2 \quad (2)$$

Among all formulations, the highest %EE equal to 86.15 ± 5.346 % was found for run 4 and the lowest %EE of 14.18 ± 1.209 % was obtained for run 11 (Table 2). Data obtained from ANOVA analysis revealed that X_1 and X_1^2 were the most significant model terms; the other non-significant terms were removed following the stepwise regression procedure, indicating that cationic lipids concentration did not affect %EE. From the equation it is clearly shown that the MEL concentration plays a highly significant role for the %EE. The estimated coefficient for X_1 was negative, showing that a decrease in MEL concentration corresponded to a proportional increase in %EE. The low yield of %EE when the drug concentration was increased could be due to poor availability of polymer to encapsulate MEL (Surwase et al., 2017). The 3D response surface plots and 2D contour plots are shown in Figure 3.

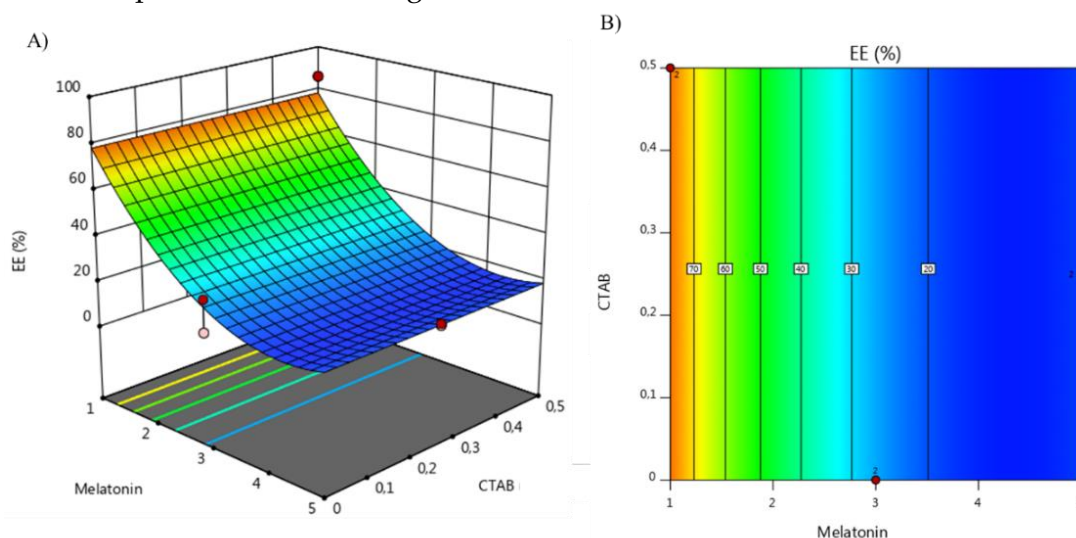


Figure 3. 3D surface (A) and contour plot (B) of the effect of X_1 : MEL concentration (% wt/wt) versus X_2 : CTAB concentration (% w/v) on the mel-LPHNs encapsulation efficiency.

The reliability of the reduced mathematical models obtained through the response surface methodology was validated through the formulation optimization. The goals of the candidate formulation were applied for each significant response and were reported in Table 5. The parameters assigned for the desired formulation were a maximized ZP to obtain NPs with a strong positive surface charge and a %EE with a target value of 86.15, the highest achieved during the 18-run experimental phase. The formulation with the highest desirability index (0.838) was selected and validated experimentally. The optimized formulation was composed by MEL = 1 %wt/wt, CTAB = 0.427% w/v and DDAB = 0.341% w/v. The observed experimental data were compared with the values predicted by the software revealing a good correlation, as demonstrated by the error percentage <4 (Table 6).

Table 5. NPs optimization.

Independent Variables ^a	Goals	Lower limit	Upper limit
X ₁ (% wt/wt)	Minimize	1	5
X ₂ (% w/v)	Maximize	0	0.5
X ₃ (% w/v)	Maximize	0	0.5
Dependent Variables ^b			
Y ₁ (mV)	Maximize	-33.2	64.3
Y ₂ (%)	Target (86.15)	14.18	86.15

^aIndependent variables: X₁ = [MEL]; X₂ = [CTAB]; X₃ = [DDAB].

^bDependent Variables: Y₁ = Zeta potential (mV); Y₂ = Encapsulation efficiency (%).

These findings confirmed the robustness of the DoE, and the reliability of the model used. The optimized formulation with size of (189.40 ± 1.96 nm), particle size distribution of (0.260 ± 0.009), ZP (39.8 ± 1.7 mV) and %EE (79.85 ± 13.039 %) was subjected to further physico-chemical and biological investigation.

Table 6. Results of dependent variables obtained from the optimized formulation: Predicted, Observed values and error percentage.

	Predicted value	Observed value ^a	Error % ^b
Y ₁ (mV)	41.305	39.800 ± 1.700	4
Y ₂ (%)	78.480	79.850 ± 13.039	2

^aMEL-loaded LPHNs (mel-LPHNs) Y₁ = Zeta potential (mV) ± SD; Y₂ = Encapsulation efficiency ± SD (%); n=3;

^bAbsolute Predicted Error = |(Obs.value-Pred.value) / Pred.value| *100

3.2 Physico-chemical properties of optimized mel-LPHNs

As reported above, the optimized mel-LPHNs were 323.40 ± 10.81 nm in the pre-purification phase, which after centrifugation was reduced to ~190 nm. The PDI remained rather unchanged, varying from 0.276 ± 0.023 to 0.260 ± 0.009 corresponding to monodispersed systems. NPs with a size of less than 250 nm and a PDI close to 0.25 have been shown to be good candidates for ophthalmic delivery (Gupta et al., 2010). The surface charge (ZP) moved from neutral (0.087 ± 0.107 mV) to positive values (39.800 ± 1.700 mV). Nanocarriers with positive ZP values (+36.86 mV) were able to enhance electrostatic interactions with the anionic corneal surface layers, showing excellent mucoadhesive properties, an effective requirement for increasing ocular drug bioavailability (Manchanda et al., 2017). The pH and osmolarity measurements of the unpurified systems were carried out in deionized water, with values equal to 5.040 ± 0.105 and 0.034 ± 0.003 mOsm/ kg, respectively. To make the eye drops suitable for ophthalmic administration, the purified mel-LPHN pellet was resuspended in a medium consisting of water for injectable preparations with the addition of a non-ionic excipient, glycerol (2.6 % w/v). NaCl, the tonicity agent of first choice, was excluded from this study because its ionic nature destabilized the nanosuspension by reducing the ZP value close to neutral (data not reported). According to international standards, multidose

ophthalmic formulations should mandatorily contain a preservative to prevent microbial contamination (Datta et al., 2017). Benzalkonium chloride was added as a preservative to obtain a final product with the desirable microbiological properties (0.01 % w/v). The preservative concentration used was approved by the EMA for the absence of irritation and ocular damage and was also reported that its addition to the formulation improved corneal permeation (Ahuja et al., 2008, EMA, 2017). In addition, *in vivo* cytotoxicity studies on monkeys and rabbits showed that following repeated topical applications (for up to 52 weeks, up to 8 times/ day) eye drops containing benzalkonium chloride (0.01% w/v) showed no signs of irritation (Okahara et al. - 2013). The purified nanosuspension showed pH values close to neutral (6.330 ± 0.020) and an isotonic osmolarity similar to tear fluid (0.296 ± 0.001 mOsm/Kg). The designed systems consisted of three structural components (figure 1): a hydrophobic polymeric core of PLGA with a hydrophilic PEG corona (PLGA-PEG) and a cationic lipid monolayer at the interface between the hydrophobic core and the hydrophilic corona as suggested by other authors (Zhang et al., 2008). The self-assembly of the coating layer is induced by hydrophobic interactions, where the hydrophobic lipid tails are attached to the polymer core and the hydrophilic heads are directed to the external side (Mukherjee et al., 2019). TEM analysis of the nanosuspension confirmed a core-shell type spherical NPs with moderately polydispersed particle size distribution (Figure 4A). The core-shell structure is highlighted in the peripheral region of mel-LPHNs by a ring with higher electronic density than the polymer core, which showed a more marked gray coloration (Figure 4B) (Li et al., 2017).

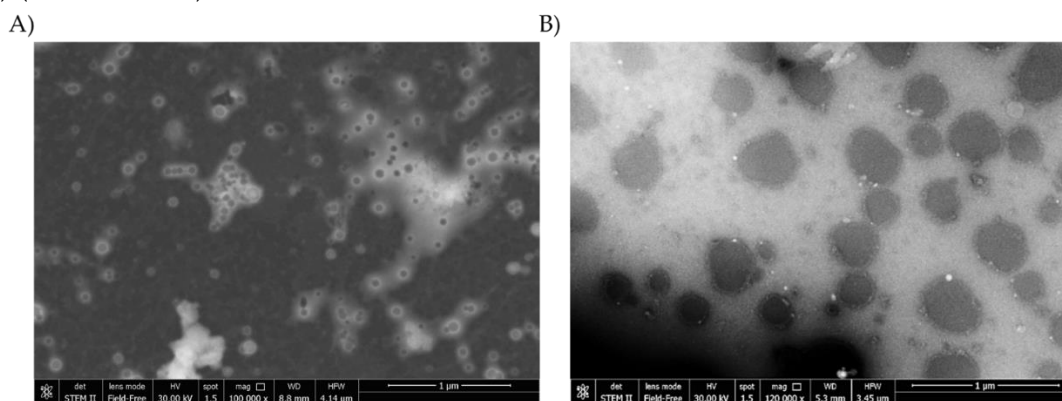


Figure 48. (A) TEM image of MEL-loaded LPHNs (mel-LPHNs) at low magnification, and (B) TEM image of MEL-loaded LPHNs (mel-LPHNs) at high magnification showing core-shell structure. Image B was obtained from cryoprotected (10 % w/v sucrose) and freeze-dried MEL-loaded LPHNs (mel-LPHNs), ongoing cryoprotection studies.

3.3 Release profile of hybrid nanoparticles

The *in vitro* drug release capacity of mel-LPHNs was investigated in PBS at physiological conditions (pH 7.4, 37 °C) for 8 days. The free MEL suspension was compared with the respective optimized nanomedicine. The *in vitro* release profiles of MEL in solution and MEL-loaded LPHNs are shown in figure 5.

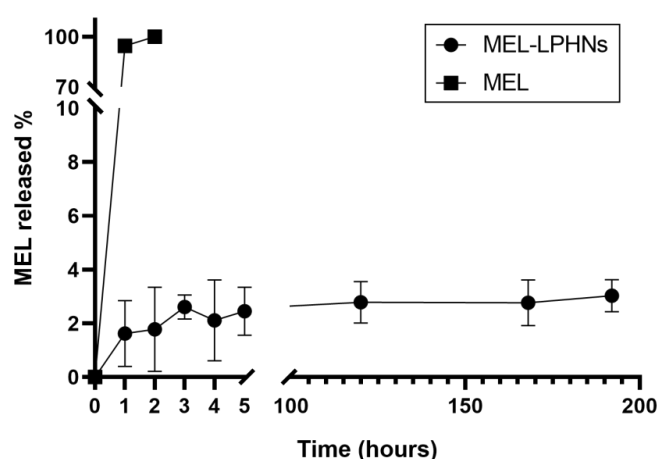


Figure 5. *In vitro* release profiles of the neat drug and MEL-loaded LPHNs (mel-LPHNs) in phosphate buffered solution (pH 7.4) at 37 °C. Each point represents the mean value of three different experiments \pm S.D.

Almost 99% of the drug was recovered in the receiving phase from the MEL solution within 1 h, indicating that drug could diffuse freely through the dialysis bag, while mel-LPHNs showed a controlled and sustained release of MEL. Lack of any initial burst release indicated that there was no drug located at the surface of the NPs, rather it was trapped into the polymer matrix (Afshari et al., 2014). Mel-LPHNs released a small percentage (approximately 2%) of their load over 8 days, resulting in a slow and continuous release typical of this type of nanomedicine, i.e., hybrid nanosystems. In this regard, it is well known that polymers play a key role, but on the other hand it has been widely reported that the role of the lipid monolayer is equally important (Sivadasan et al., 2021). Previous studies on LPHNs have shown that lipids have a dual barrier function, acting both against the diffusion of the drug to the outside and against the penetration of water to the inside (Zhao et al., 2015). Reducing water permeation should also decrease the rate of degradation of the polymer matrix. As a result, the slow degradation of the systems could provide a controlled release for longer time (Tahir et al., 2017, Yalcin et al., 2018). A sustained and prolonged release profile is the main goal for MEL nanocarriers, which for this purpose has been encapsulated in different vehicles; according to a recent study by Liang et al., the neuroprotective effect of MEL on RPE cells was found to be effective only after prolonged (more than 72 h) exposure of MEL (0.1-200 μ M) compared to short-term (less than 24 h) administration (Liang et al., 2004). In this regard, examples of systems designed for the controlled release of MEL were ethylcellulose NPs and hybrid nanocapsules, which showed a release profile trend overlapping with that obtained in our study, linear and constant over time (Carbone et al., 2016, Bessone et al., 2020). In addition, the percentage of MEL released by the mel-LPHNs, equal to a concentration of 1 μ M, was the same that (as presented in sections 3.8.1 and 3.8.2 below) was effective in the *in vitro* studies.

3.4 Thermal and infrared analysis

A DSC study was conducted to investigate the status of raw materials and optimized mel-LPHNs, the results are shown in figure 6A. The thermogram of pure MEL (curve a) showed the endothermic transition at 118 °C, which corresponded to the characteristic melting peak of the drug (Topal et al., 2015). No noticeable endothermic

event was detected in the polymer DSC profile (curve b). In the thermograms of the two lipids the thermotropic liquid crystalline character, typical of quaternary ammonium salts, was highlighted. The two endothermic events observed in curves (c) and (d) showed the sequence of lipid mesophases in response to increasing temperature. The first endothermic event indicated the phase transition of the lipid from a highly ordered crystalline solid state to a crystalline liquid state, where conformational melting of the long aliphatic chains occurred. The first transition was detected at 75 and 62 °C for CTAB and DDAB respectively. The second endothermic event indicated the phase transition from crystalline to isotropic liquid, where all spatial order was completely lost. This second transition represented the melting of the head-groups and corresponds to the melting temperature of the lipids, which was detected at 105 and 70 °C for CTAB and DDAB, respectively (Margomenou Leonidopoulou, 1988, Doktorovova et al., 2011). No peak attributable to MEL was observed in the thermogram of the optimized mel-LPHNs (curve e), confirming that the drug was totally encapsulated in the formulated systems. Endothermic events in the curve of the mel-LPHNs occurred at 45 and 97 °C, showing peaks shifted to new positions. The detected flexures could suggest a possible interaction between the polymeric and lipidic entities (Das et al., 2019).

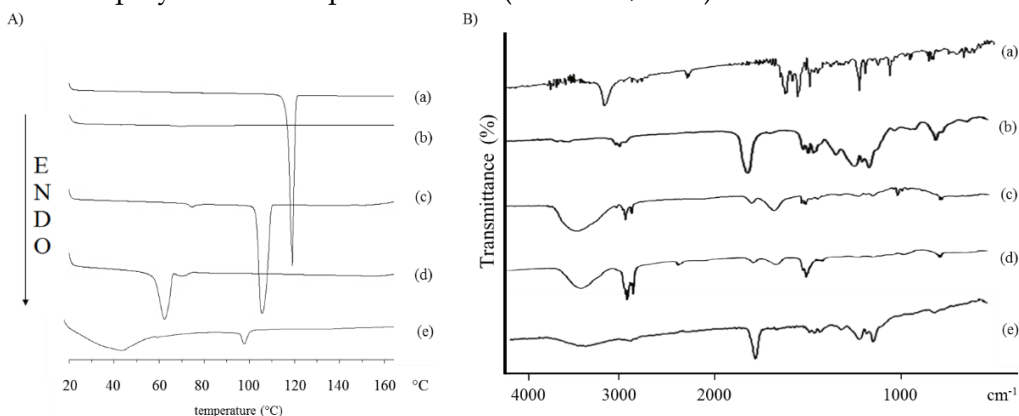


Figure 6. DSC (A) and FT-IR (B) curves of MEL (a), PLGA-PEG polymer (b), CTAB (c) DDAB (d) and MEL-loaded LPHNs (mel-LPHNs) (e).

FT-IR spectroscopy was used to understand the nature of the molecular interactions that may take place in the structuring of the mel-LPHNs and to determine the chemical variations of the functional groups. Pure materials and mel-LPHNs were scanned. The results are shown in figure 6B. MEL showed a typical stretching vibration peak for N-H group at 3303 cm^{-1} , an identifying vibration peak for C=O amidic carbonyl group at 1628 cm^{-1} , an N-H bending signal at 1559 cm^{-1} and characteristic stretching vibration signals for C-N group at 1212 and 1041 cm^{-1} (Topal et al., 2015). The polymer spectra also showed characteristic absorption bands. The absorption band at 3645 cm^{-1} was attributed to the terminal hydroxyl groups, the bands at 3000 cm^{-1} were due to the vibration of the C-H alkane fractions, the stretching peak assigned for C=O stretch of the lactide and glycolide structures was identified at 1759 cm^{-1} and the bands in the region between 1000 and 1400 cm^{-1} were identifying the vibration for C-OR, C-C and C-O groups (Mirakabad et al., 2016). The lipid spectra showed a similar trend. A strong and broad band that can be attributed to the stretching vibrations of the ammonium group was detected at 3645 and 3414 cm^{-1} for CTAB and DDAB, respectively. The peaks displayed at 2916 - 2848 cm^{-1} for CTAB and 2922 - 2852 cm^{-1} for DDAB represented two different C-H band vibrations of the CH_2 group. The signals at 1634 and 1635 cm^{-1} were indicative of the asymmetric stretching vibration of $\text{N}^+\text{-CH}_3$, for CTAB and DDAB, respectively; while the symmetric

vibration signals for methylene group were detected at 1461 and 1466 cm^{-1} , for CTAB and DDAB (Quan et al., 2015, Ain et al., 2020). In the spectrum of the optimized formulation of mel-LPHNs, the absorption peaks of lipids and polymers were found to be shifted to slightly lower frequencies than those of pure substances. Typical lipid signals were detected in the high-frequency region of the spectrum. A broad absorption band typical of the stretching vibration for lipid ammonium group was detected at 3430 cm^{-1} , a signal at 2903 cm^{-1} was attributed to the CH_2 group vibration and a peak at 1455 cm^{-1} was assigned to the symmetrical stretching vibration of the $\text{N}^+\text{-CH}_3$ group. The detection of the ammonium group could confirm the arrangement of the lipid monolayer with the hydrophilic heads directed towards the external environment (Hadinoto et al., 2013). Signals that belonged to the polymer were identified in the low-frequency region of the spectrum. A 1757 cm^{-1} peak was associated with the carbonyl group, and the identification regions for C-O groups were observed in the region between 1172-1093 cm^{-1} . The FT-IR spectra of the mel-LPHNs appeared to be the overlap of the spectra of PLGA-PEG and the two lipids, CTAB and DDAB. The characteristic peaks of the lipids were observed in the spectra of the mel-LPHNs, indicating that CTAB and DDAB successfully modified surface of polymeric NPs (Mishra et al., 2017, Lu et al., 2019). The characteristic signals of MEL had completely disappeared in the spectrum of mel-LPHNs demonstrating an effective incorporation of the drug into the polymer matrix.

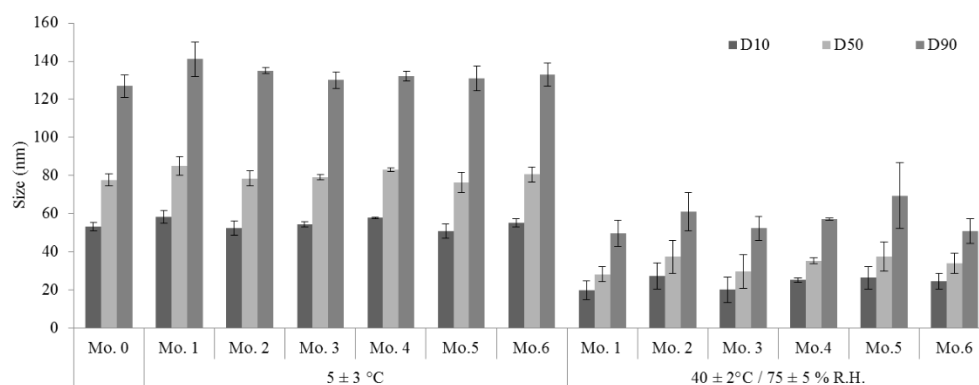
3.5 Stability under storage conditions

Physical and chemical stability is an essential parameter for ensuring the appropriate storage of NPs. Stability studies were performed on optimized mel-LPHNs under two different storage conditions. The sample was divided into two batches and stored at a refrigerated temperature ($5\text{ }^\circ\text{C} \pm 3\text{ }^\circ\text{C}$) or in a climatic chamber ($40\text{ }^\circ\text{C} \pm 2\text{ }^\circ\text{C} / 75 \pm 5\% \text{ RH}$). The results of the physical and chemical stability of the optimized formulation in various time intervals are shown in Table 7. Storage of the mel-LPHNs at $40\text{ }^\circ\text{C}/75\% \text{ RH}$ resulted in a significant change in particle size, from $101.6 \pm 2.4\text{ nm}$ when freshly prepared to $129.6 \pm 86.940\text{ nm}$ after 3 months, to $81.2 \pm 10.310\text{ nm}$ at the end of the sixth month of storage. This change was associated with a significant increase in PDI from 0.117 ± 0.021 to 0.526 ± 0.085 . Storage under accelerated conditions led to an extremely significant ($p < 0.001$) increase in zeta potential from 22 mV to 45 mV and a decrease in MEL content ($>5\%$), above the threshold of the acceptance criteria of the ICH QA(R2) guidelines.

Table 7. Effect of refrigerated ($5 \pm 3\text{ }^\circ\text{C}$) and accelerated ($40 \pm 2\text{ }^\circ\text{C} / 75 \pm 5\% \text{ RH}$) storage conditions on mean particle size, PDI, ZP, osmolarity and encapsulation efficiency of MEL-loaded LPHNs (mel-LPHNs). Each value is the mean \pm SD of three estimations.

Condition	Time (month)	Size (nm) \pm SD	PDI \pm SD	ZP (mV) \pm SD	Osmolarity (Osm/kg) \pm SD	%EE \pm SD
Starting	0	101.6 ± 2.442	0.117 ± 0.021	22.2 ± 3.14	0.296 ± 0.001	78.3 ± 0.012
Refrigerated	3	103.3 ± 2.606	0.126 ± 0.009	24.1 ± 1.00	0.302 ± 0.006	77.34 ± 0.009
	6	105.3 ± 4.143	0.116 ± 0.020	22.9 ± 0.23	0.312 ± 0.011	76.59 ± 0.008
Accelerated	3	129.6 ± 86.94	0.526 ± 0.085	44.4 ± 4.61	0.316 ± 0.003	72.54 ± 0.010
	6	81.2 ± 10.310	0.407 ± 0.122	45.9 ± 2.65	0.329 ± 0.009	68.59 ± 0.012

The observed variations in the samples stored at the higher temperature could be attributed to changes in the polymorphic state of the lipid layer. An endothermic event close to the storage temperature was recorded in the thermogram of mel-LPHNs (Figure 6A, curve e). Lipids are highly polymorphic, and the predominant form depends on intrinsic factors (structure and hydration rate of the molecule) and extrinsic factors (temperature, pressure, ionic strength and pH of the medium) (Lewis and McElhaney, 2013). The energetic input of heat, provided during the storage time, could induce crystalline reorientation of the lipid shell (Makoni et al., 2019). The conversion of lipids into different polymorphic forms could be responsible, in addition to the increased expulsion of MEL from the systems, for changes in the surface charges (Vivek et al., 2007). It has been shown that temperature causes disturbances in the electric double layer (EDL) around the NPs, reflected in changes in the ZP value (Salunkhe et al., 2016). The EDL of a NP can be considered as a layer of liquid molecules at the interface with the particle surface, consequently the hydrodynamic dimensions of the suspended NPs could also be related to the electrical elements of the double layer (i.e., resistance, capacitance, and relaxation frequency) (Tillman and Hill, 2007, Yao et al., 2016). D10, D50 and D90 values of samples stored at 40 °C indicate that on average 10%, 50% and 90% of particles in each population are smaller than 25, 35 and 55 nm respectively (Supplementary Figure 2). These sizes are smaller compared to mel-LPHNs analyzed after fresh preparation (50, 80 and 140 nm, respectively), which remain unchanged in samples stored at refrigerated temperatures.



Supplementary Figure 2. Particle size distribution (D10, D50, and D90) of MEL-loaded LPHNs (mel-LPHNs) stored at different conditions for 6 months. Error bars represent SD ($n = 3$).

Low temperature storage has prevented the polymorphic transition (Bertoni et al., 2021). In comparison, the groups at 5 °C were stable, with unchanged physico-chemical properties after six months of storage. The MEL content decreased around 2%, remaining within the threshold accepted by the guidelines. The optimized formulation was stable under refrigerated storage conditions.

3.6 Mucoadhesive evaluation: influence combining cationic lipid and PEG portion on mucin binding

In these experiments an evaluation of the mucoadhesive properties of mel-LPHNs was performed in comparison with two other NPs, the three investigated NPs differed for external shells: hydrophobic (P-NPs), hydrophilic (P-PEG-NPs) and cationic/PEG (mel-LPHNs). The experiment was performed by varying the mucin

concentration (0.25 and 0.5 %w/v) and incubation time (1 and 24 h). Interactions between mucin and other entities can be due to various forces such as the occurrence of hydrogen, electrostatic, hydrophobic, and/or covalent bonds (Eliyahu et al., 2018). Electrostatic interactions play a key role in mucoadhesive mechanisms (Li et al., 2016). At a physiological pH, glutamate and aspartate residues in mucin undergo ionization, which provides the structure a negative charge (Pai et al., 2019).

Mucoadhesiveness was assessed by monitoring variations in the mean diameter and ZP of NPs incubated with mucin (de Campos et al., 2004, Shen et al., 2009, Ammar et al., 2012). Mucin showed a bimodal size distribution with particle populations in the order of 200 and 2000 nm. The average size of the native P-NPs, P-PEG-NPs and mel-LPHNs were approximately 418, 135 and 200 nm. Their size increased to 494, 397 and 343 nm, respectively, after 24 h of incubation with mucin (Figure 7A-7B). Statistical analysis of the collected data showed that the mean size of NPs incubated with mucin suffered a significant increase in size with $p < 0.001$ in the case of mel-LPHNs and $p < 0.01$ for P-PEG-NPs respectively. Incubation of P-NPs with mucin did not significantly influence their size ($p > 0.05$). Furthermore, it was observed that the increase in size was proportional to the increase in mixed mucin concentration. While the incubation time was not an influential parameter on the final mean size of the NPs. The significant increase of mean size occurred when pegylated and hybrid systems were incubated with mucin, indicating that interaction between the components had taken place. It was noticed that the average size after incubation was in the ideal size range (200-500 nm) for interaction with the mucosa (Hejjaji et al., 2018).

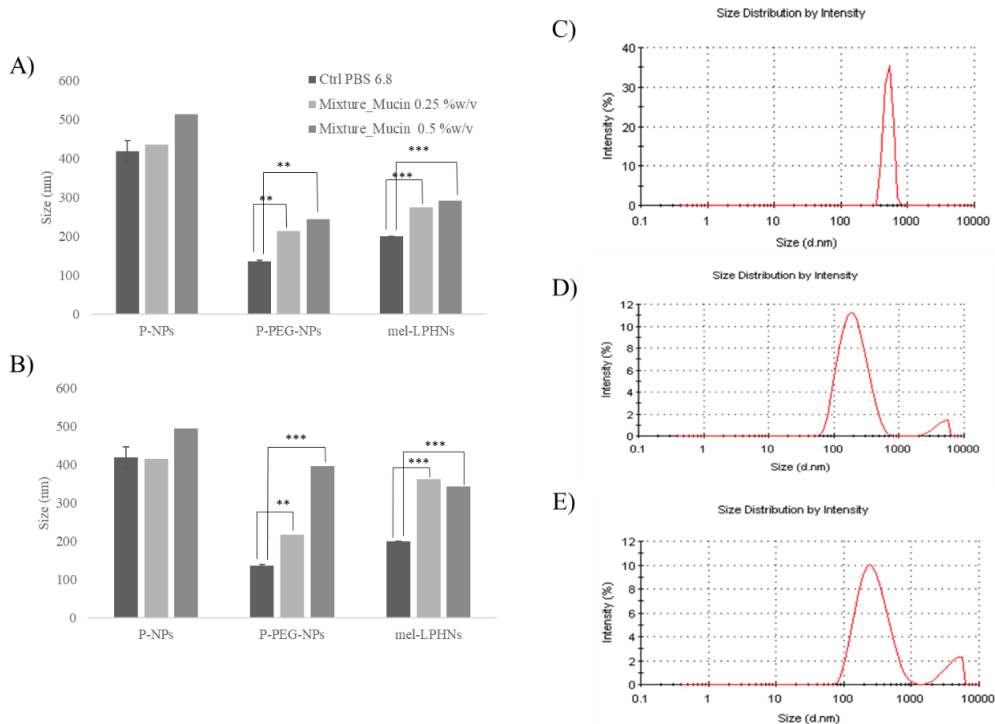


Figure 7. Mean size (nm) of P-NPs, P-PEG-NPs and MEL-loaded LPHNs (mel-LPHNs) in phosphate buffer at pH 6.8 (Ctrl) and in mucin mixture at different concentration (0.25 and 0.5 w/v) after 1 (A) and 24 (B) hours of incubation at 37 °C. Each value was the mean of three experiment \pm SD; T-test was used to calculate statistical significance of the percentages obtained versus control group [ns=not significant ($P > 0.05$); * = significant ($P < 0.05$); ** = very significant ($P < 0.01$); *** = extremely significant ($P < 0.001$)]. Size distribution by intensity of P-NPs (C), P-PEG-NPs (D) and MEL-loaded LPHNs (mel-LPHNs) (E) suspensions after incubation in mucin mixture.

The increase in size was not only attributed to the mucin bound on the NPs, but also to the aggregates formed by the extended interaction of mucin protein between the particles (Boya et al., 2017). Therefore, it was useful to analyze the size distribution of the mixtures. From size distribution graphs, it was possible to observe that both the mel-LPHNs and P-PEG-NPs (Figure 7E - 7D) showed a very heterogeneous distribution, with the presence of two peaks in size distribution, one attributed to the average size of the mucin-coated NPs and the other due to the aggregates of mucin and NPs. The second peak was not detected in the case of the mixture composed of mucin and P-NPs (Figure 7C).

Morris et al. demonstrated that variation in the size of NPs was correlated with variation in ZP (Morris et al., 2013). Accordingly, NP-mucin interactions were further confirmed by ZP measurements. Figure 8 shows the changes in ZP after incubation of the NPs with mucin. The ZP of the mucin particles was negative, around -5 mV. Before incubation with mucin, the ZP values of the native P-NPs, P-PEG-NPs and mel-LPHNs were -4.7 -1.1 and +1.8 mV. The surface charges were -4.8, -6.1 and -5.3 mV, respectively, after incubation with mucin. The ZP values of the observed mixtures were close to the ZP of plain mucin, confirming that the interaction took place (Klemetsrud et al., 2013). The magnitude of ZP reduction was significant for mel-LPHNs ($p < 0.001$) and for P-PEG-NPs ($p < 0.05$). The increased interaction shown by mel-LPHNs compared with P-PEG-NPs could suggest greater mucoadhesion (Hejjaji et al., 2018).

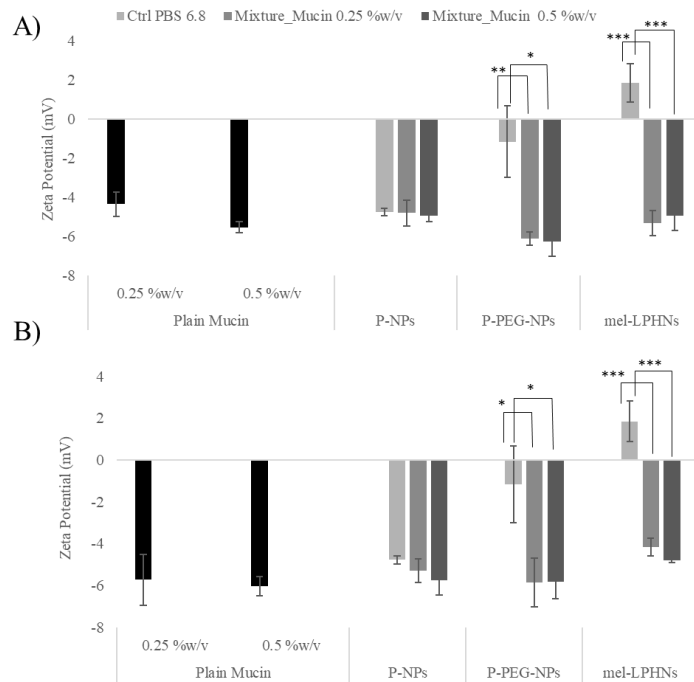


Figure 89. Zeta potential (mV) of P-NPs, P-PEG-NPs and MEL-loaded LPHNs (mel-LPHNs) in phosphate buffer at pH 6.8 (Ctrl) and in mucin mixture at different concentration (0.25 and 0.5 w/v) after 1 (A) and 24 (B) hours of incubation at 37 °C. Three independent experiments were performed and error bars depict SD of the mean; T-test was used to calculate statistical significance of the percentages obtained versus control group [ns=not significant ($P > 0.05$); * = significant ($P < 0.05$); ** = very significant ($P < 0.01$); *** = extremely significant ($P < 0.001$)]

The adhesive forces produced during incubation of P-PEG-NPs with mucin could be attributed to the hydrogen bonds. The enhanced interaction of mel-LPHNs with mucin could be promoted by electrostatic interactions in addition to hydrogen bonds

(Mainardes et al., 2010, Mazzarino et al., 2012). Electrostatic interactions could occur between the protonated amino groups (N^+-CH_3) of lipids and the carboxylate (COO^-) or sulfonate (SO_3^-) groups of mucin (Hejjaji et al., 2018).

From the results, it is evident that mucin significantly modified the surface charge of hybrid systems from positive to negative values, which was required for interaction with the corneal surface of the eye (D'Angelo et al., 2015). This could be great evidence of the good mucoadhesive properties of mel-LPHNs. Mucoadhesiveness between mucin and the designed hybrid systems is desirable to prolong the contact time with the mucous layer surface, and thus could improve absorption as proved by other authors (Silva et al., 2013, Dudhani and Kosaraju, 2010).

3.7 Microbiological analyses

Mel-LPHNs were sterilized by UV exposure for 30 min prior to *in vitro/in vivo* studies. To evaluate the efficacy of the sterilizing treatment and the added preservative, the formulation was subjected to a microbiological assay. The sterility of mel-LPHNs samples, differently treated, was evaluated. According to the European Pharmacopoeia, based on performed validation test, results highlighted that both UV treated and untreated samples, showed a clearly visible growth of the selected target microorganisms (data not shown). The only exception was observed for mel-LPHN samples analyzed 28 days after opening, where no growth of *B. subtilis*, *C. albicans* or *A. flavus* (data not shown) was observed. This finding could be related to the presence of the antimicrobial benzalkonium chloride in the mel-LPHNs samples which was activated after opening. Lastly, the sterility test carried out by direct inoculation of the standardized microbial culture together with the mel-LPHNs samples. After 15 days of incubation, showed no evidence of microbial growth.

3.8 Biological evaluation of empty/melatonin-loaded LPHNs in an "in vitro" model of diabetic retinopathy and in vivo tolerability test on rabbits

3.8.1 Protective effects on HG-treated HREC

As previously shown, LPHN-based carriers could provide beneficial effects to the therapeutic potential of MEL for the treatment of ocular diseases. In fact, these systems ensure an effective drug delivery due to a prolonged interaction between the cationic lipid shell and the anionic ocular mucosa. Moreover, the low percentage of drug (2% corresponding to a concentration of 1 μ M) released in a controlled and prolonged profile from mel-LPHNs reduced MEL-induced cytotoxicity, highlighting its therapeutic benefits (Elsaid et al., 2016). The capability of the nanoparticles to improve the efficacy of the melatonin in prevent the glycemic insult on HRECs has been evaluated by treating the cells with high concentrations of glucose and mel-LPHNs, at the same time (Xie et al., 2014, Jiang et al., 2012).

As reported in Fig 9, 48h of treatment with HG reduced HREC cell viability by about 40% ($p < 0.01$) as a consequence of glucose toxicity (Giurdanella et al., 2020). The treatment with 0.1 and 1 μ M of control LPHNs did not change HREC viability highlighting their delivery potential with no detrimental effects both in normal and in HG conditions. Incubation with HG in the presence of 0.1 and 1 μ M of mel-LPHNs counteracted HG-mediated cell viability reduction in a dose dependent manner. In fact, the presence of 0.1 and 1 μ M Mel-LPHNs restored cell viability by about 30% ($p < 0.01$)

and 80% ($p < 0.001$) in comparison to HG-treated HREC, respectively. Mel-LPHNs were (significantly, $p < 0.05$) more effective in the protection of HREC against HG damage than neat MEL. In fact, the free drug was only able to partially prevent cell viability reduction (in a very statistically significant manner, $p < 0.01$) at a dose of 1 μM in HG-treated HREC. No changes were observed in cell viability of co-treated HREC with NG and tested systems compared to the NG-treated cells.

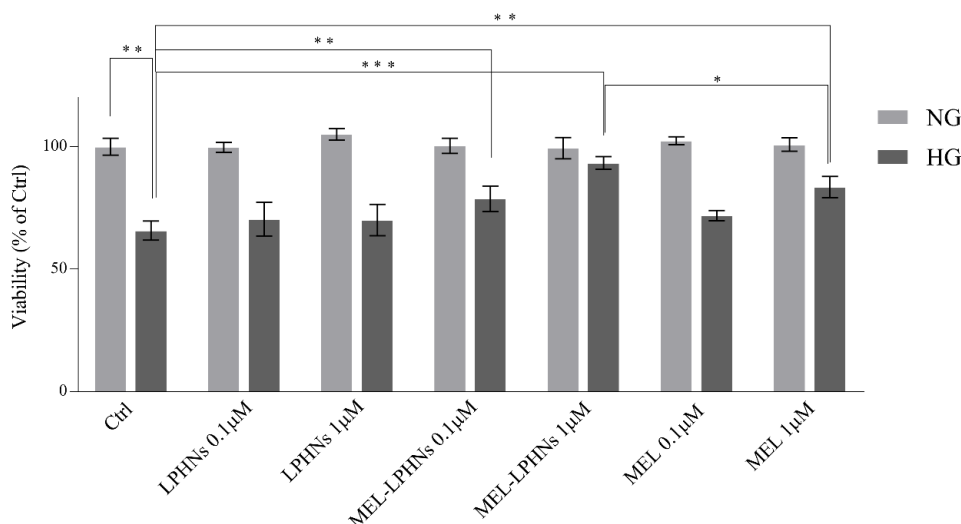


Figure 910. Determination of cell viability (MTT assays) in HREC stimulated with normal glucose (5 mM, Ctrl) or with high glucose (25 mM) with or without 0.1 and 1 μM of LPHNs, 0.1 and 1 μM of MEL-loaded LPHNs (mel-LPHNs) or 0.1 and 1 μM of MEL for 48h. Values are expressed as mean \pm SD of three independent experiments. Two-way ANOVA, followed by Tukey's test was used to calculate statistical significance of the obtained values. [* = significant ($P < 0.05$); ** = very significant ($P < 0.01$); *** = extremely significant ($P < 0.001$)].

3.8.2 Antioxidant effects on HG-treated HREC

MEL was described to protect endothelial cells against hyperglycemic insult by preventing glucose-induced reactive oxygen species (ROS) production at concentrations ranging from 0.1 to 5 μM (Tiong et al., 2020, Wang et al., 2021). To support cell viability data, we further investigate the antioxidant action of neat MEL or loaded LPHNs. Results from these experiments are reported in Fig 10. Compared to NG-treated cells, HREC stimulated with HG showed a very significant increase in ROS levels of about 2-fold, however, the presence of 0.1 and 1 μM mel-LPHNs reverted the HG-mediated ROS production to about 30% ($p < 0.01$) and 65% ($p < 0.001$), respectively, in comparison to HG-treated HREC. According to cell viability data, only the higher concentration of pure MEL was able to partially prevent the enhanced ROS levels induced by HG, reducing their amount by about 35% ($p < 0.01$) in comparison to HG-stimulated HREC. These data highlighted that mel-LPHNs reverted ROS production in HG-induced HREC more effectively ($p < 0.01$) than pure MEL. No remarkable changes in ROS production were observed in co-treated cells with HG and 0.1 and 1 μM of LPHNs compared to HG-treated HREC; the presence of LPHNs, mel-LPHNs or pure MEL in NG conditions did not modify the rate of ROS production in comparison to NG-stimulated cells.

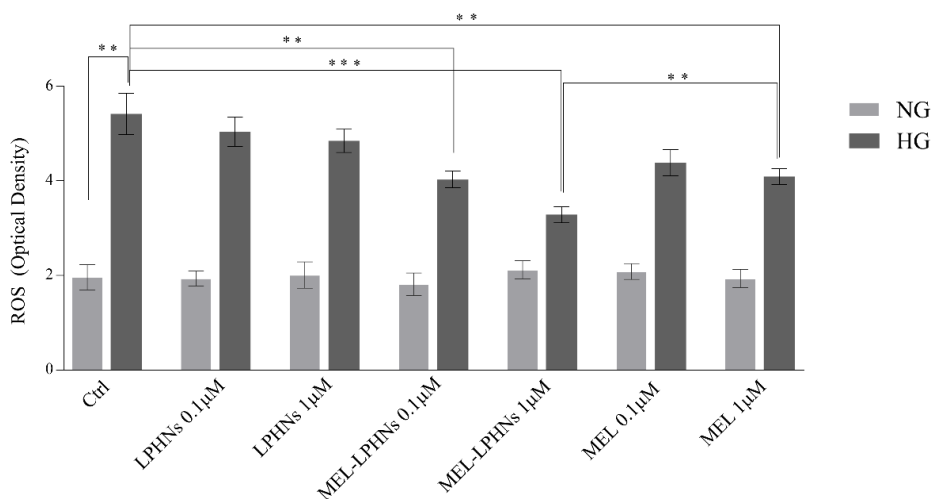


Figure 10. Evaluation of reactive oxygen species (ROS) using the DCFH-DA in HREC stimulated with normal glucose (5 mM, Ctrl) or with high glucose (25 mM) with or without 0.1 and 1 μ M of LPHNs, 0.1 and 1 μ M of MEL-loaded LPHNs (mel-LPHNs) or 0.1 and 1 μ M of MEL for 48h. Values are expressed as mean \pm SD of three independent experiments. Two-way ANOVA, followed by Tukey's test was used to calculate statistical significance of the obtained values. [** = very significant ($P < 0.01$); *** = extremely significant ($P < 0.001$)].

3.9 Tolerability test on rabbits

Both unloaded and mel-LPHNs formulations, were well-tolerated and the score for each parameter was zero at all times of observations (not shown). No changes were also observed for IOP values.

4. Conclusion

Non-invasive topical ocular delivery targeting the posterior segment of the eye remains a challenge due to the numerous barriers protecting the eye. Here, with the need to improve drug delivery to the retina, minimize frequency of administration and provide controlled and sustained drug release, the design of hybrid cationic nanovectors for topical administration has been proposed. The synthesis of hybrid nanoparticles combining polymeric and lipid materials has proved successful in incorporating MEL and resulted in high-performance vehicles. mel-LPHNs showed ideal requirements for an eye drop formulation. The particles consisted of homogeneous populations, with adequate size, optimal pH and osmolarity values and a positive zeta potential, which provided good mucoadhesive properties. Thermal and infrared analysis suggested the incorporation of MEL into the mel-LPHNs and the successful interaction of the lipids with the polymer matrix. The optimized formulation was stable for 6 months under refrigerated storage conditions. According to Ph. Eur., the mel-LPHNs samples met the sterility test. No differences were found between the UV treated and untreated samples, while the preservative addition confirmed the desired effect against some the above listed microorganisms. *In vitro* and *in vivo* studies confirmed that the systems showed no signs of cytotoxicity or ocular irritation. *In vitro* studies also showed that loading of MEL into mel-LPHNs improve its effectiveness in preventing HG-evoked oxidative stress and cell damage in HREC. Taken together, these findings suggested that our novel hybrid NPs could represent a promising strategy for topical MEL delivery in the treatment of ocular pathology.

CRedit authorship contribution statement

T.M., A.R., conceived the study (Conceptualization); Ci.C., C.R., N.R., performed microbiological assay (Methodology, Investigation, Formal analysis); G.L., D. A., G.G., performed studies on *in vitro* model of diabetic retinopathy (Methodology, Investigation, Formal analysis); A.R., M.R., Cl.C., performed HPLC analysis and analyzed the data (Methodology, Investigation, Formal analysis); G.R., C.B. performed *in vivo* study on rabbits (Methodology, Investigation, Formal analysis); R.B., G.T., J.T.D. performed morphological study (Methodology, Investigation, Formal analysis); A.R., A.B., T.M., conceptualized and developed NPs (Conceptualization, Methodology); A.R. and A.B. produced and characterized chemico-physical features of NPs (Methodology, Investigation); T.M., R.P., oversaw and coordinated responsibility for all research activities and their performance and provided experimental advice throughout the work (Supervision and Project administration); T.M., C.B., secured the funding (Funding acquisition); A.R., T.M., wrote the paper (Writing - Original draft, Writing - Review & Editing); all the authors edited and reviewed the paper (Writing - Review & Editing).

Declaration of Competing Interest

The authors declare that they have no known competing financial interests or personal relationships that could have appeared to influence the work reported in this paper.

Acknowledgements

The authors are grateful to the Research Centre on Ocular Nanotechnology (NANO-*i*) of the University of Catania for his technical assistance.

A.R. has been supported by the International Ph.D. program in Neuroscience, University of Catania, Italy. A.B. is a researcher at the University of Catania within the EU-funded PON REACT project (Azione IV.4 - "Dottorati e contratti di ricerca su tematiche dell'innovazione", nuovo Asse IV del PON Ricerca e Innovazione 2014-2020 "Istruzione e ricerca per il recupero – REACT – EU"; Progetto "Approcci terapeutici innovativi per il targeting cerebrale di farmaci e materiale genico", CUP E65F21002640005).

Funding

The manuscript was supported by University of Catania (Programma Ricerca di Ateneo 2020-2022, Linea 2; Project NanoRET and (partially) project 3N-ORACLE) and Italian Minister of University grant (PRIN 2020FR7TCL). A.R. was supported by the International Ph.D. program in Neurosciences, University of Catania, Italy.

References

- Afshari, M., Derakhshandeh, K., Hosseinzadeh, L., 2014. Characterisation, cytotoxicity and apoptosis studies of methotrexate-loaded PLGA and PLGA-PEG nanoparticles. *Journal of Microencapsulation* 31, 239–245. <https://doi.org/10.3109/02652048.2013.834991>
- Agrahari, Vibhuti, Mandal, A., Agrahari, Vivek, Trinh, H.M., Joseph, M., Ray, A., Hadji, H., Mitra, R., Pal, D., Mitra, A.K., 2016. A comprehensive insight on ocular pharmacokinetics. *Drug Delivery and Translational Research* 6, 735–754. <https://doi.org/10.1007/s13346-016-0339-2>
- Agrawal, U., Chashoo, G., Sharma, P.R., Kumar, A., Saxena, A.K., Vyas, S.P., 2015. Tailored polymer-lipid hybrid nanoparticles for the delivery of drug conjugate: Dual strategy for brain targeting. *Colloids and Surfaces B: Biointerfaces* 126, 414–425. <https://doi.org/10.1016/j.colsurfb.2014.12.045>
- Ahuja, M., Dhake, A.S., Sharma, S.K., Majumdar, D.K., 2008. Topical ocular delivery of NSAIDs. *AAPS Journal* 10, 229–241. <https://doi.org/10.1208/s12248-008-9024-9>

- Ain, N., Anas, A., Fen, Y.W., Yusof, N.A., Alia, N., Omar, S., 2020. Cetyltrimethylammonium Bromide / Hydroxylated Graphene Quantum Dots Thin Film for Potential. *Materials* 13, 16.
- Almeida, H., Amaral, M., Lobao, P., Frigerio, C., Sousa Lobo, J., 2015. Nanoparticles in Ocular Drug Delivery Systems for Topical Administration: Promises and Challenges. *Current Pharmaceutical Design* 21, 5212–5224. <https://doi.org/10.2174/1381612821666150923095155>
- Ammar, H.O., El-Nahas, S.A., Ghorab, M.M., Salama, A.H., 2012. Chitosan/cyclodextrin nanoparticles as drug delivery system. *Journal of Inclusion Phenomena and Macrocyclic Chemistry* 72, 127–136. <https://doi.org/10.1007/s10847-011-9950-5>
- Aryal, S., Hu, C.M.J., Zhang, L., 2011. Polymeric nanoparticles with precise ratiometric control over drug loading for combination therapy. *Molecular Pharmaceutics* 8, 1401–1407. <https://doi.org/10.1021/mp200243k>
- Aryal, S., Hu, C.M.J., Zhang, L., 2010. Combinatorial drug conjugation enables nanoparticle dual-drug delivery. *Small* 6, 1442–1448. <https://doi.org/10.1002/sml.201000631>
- Aryal, S., Jack Hu, C.M., Fu, V., Zhang, L., 2012. Nanoparticle drug delivery enhances the cytotoxicity of hydrophobic-hydrophilic drug conjugates. *Journal of Materials Chemistry* 22, 994–999. <https://doi.org/10.1039/c1jm13834k>
- Aryal, S., Key, J., Stigliano, C., Ananta, J.S., Zhong, M., Decuzzi, P., 2013. Engineered magnetic hybrid nanoparticles with enhanced relaxivity for tumor imaging. *Biomaterials* 34, 7725–7732. <https://doi.org/10.1016/j.biomaterials.2013.07.003>
- Badr, M.Y., Abdulrahman, N.S., Schatzlein, A.G., Uchegbu, I.F., 2021. A polymeric aqueous tacrolimus formulation for topical ocular delivery. *International Journal of Pharmaceutics* 599, 120364. <https://doi.org/10.1016/j.ijpharm.2021.120364>
- Bertoni, S., Passerini, N., Albertini, B., 2021. Liquid lipids act as polymorphic modifiers of tristearin-based formulations produced by melting technologies. *Pharmaceutics* 13. <https://doi.org/10.3390/pharmaceutics13071089>
- Bessone, C.D.V., Martinez, S.M., Luna, J.D., Marquez, M.A., Ramírez, M.L., Allemandi, D.A., Carpentieri, Á.R., Quinteros, D.A., 2020. Neuroprotective effect of melatonin loaded in ethylcellulose nanoparticles applied topically in a retinal degeneration model in rabbits. *Experimental Eye Research* 200. <https://doi.org/10.1016/j.exer.2020.108222>
- Bonaccorso, A., Musumeci, T., Carbone, C., Vicari, L., Lauro, M.R., Puglisi, G., 2018. Revisiting the role of sucrose in PLGA-PEG nanocarrier for potential intranasal delivery. *Pharmaceutical Development and Technology* 23, 265–274. <https://doi.org/10.1080/10837450.2017.1287731>
- Bonaccorso, A., Russo, G., Pappalardo, F., Carbone, C., Puglisi, G., Pignatello, R., Musumeci, T., 2021. Quality by design tools reducing the gap from bench to bedside for nanomedicine. *European Journal of Pharmaceutics and Biopharmaceutics* 169, 144–155. <https://doi.org/10.1016/j.ejpb.2021.10.005>
- Boya, V.N., Lovett, R., Setua, S., Gandhi, V., Nagesh, P.K.B., Khan, S., Jaggi, M., Yallapu, M.M., Chauhan, S.C., 2017. Probing mucin interaction behavior of magnetic nanoparticles. *Journal of Colloid and Interface Science* 488, 258–268. <https://doi.org/10.1016/j.jcis.2016.10.090>

Bucolo, C., Drago, F., 2004. Effects of neurosteroids on ischemia-reperfusion injury in the rat retina: Role of σ 1 recognition sites. *European Journal of Pharmacology* 498, 111-114. <https://doi.org/10.1016/j.ejphar.2004.06.067>

Carbone, C., Manno, D., Serra, A., Musumeci, T., Pepe, V., Tisserand, C., Puglisi, G., 2016. Innovative hybrid vs polymeric nanocapsules: The influence of the cationic lipid coating on the "4S." *Colloids and Surfaces B: Biointerfaces* 141, 450-457. <https://doi.org/10.1016/j.colsurfb.2016.02.002>

Carbone, C., Tomasello, B., Ruozi, B., Renis, M., Puglisi, G., 2012. Preparation and optimization of PIT solid lipid nanoparticles via statistical factorial design. *European Journal of Medicinal Chemistry* 49, 110-117. <https://doi.org/10.1016/j.ejmech.2012.01.001>

Chan, J.M., Zhang, L., Yuet, K.P., Liao, G., Rhee, J.W., Langer, R., Farokhzad, O.C., 2009. PLGA-lecithin-PEG core-shell nanoparticles for controlled drug delivery. *Biomaterials* 30, 1627-1634. <https://doi.org/10.1016/j.biomaterials.2008.12.013>

Cheow, W.S., Chang, M.W., Hadinoto, K., 2011. The roles of lipid in anti-biofilm efficacy of lipid-polymer hybrid nanoparticles encapsulating antibiotics. *Colloids and Surfaces A: Physicochemical and Engineering Aspects* 389, 158-165. <https://doi.org/10.1016/j.colsurfa.2011.08.035>

Cheow, W.S., Hadinoto, K., 2012. Lipid-polymer hybrid nanoparticles with rhamnolipid-triggered release capabilities as anti-biofilm drug delivery vehicles. *Particuology* 10, 327-333. <https://doi.org/10.1016/j.partic.2011.08.007>

Cheow, W.S., Hadinoto, K., 2011. Factors affecting drug encapsulation and stability of lipid-polymer hybrid nanoparticles. *Colloids and Surfaces B: Biointerfaces* 85, 214-220. <https://doi.org/10.1016/j.colsurfb.2011.02.033>

Conte, C., Dal Poggetto, G., Swartzwelter, B.J., Esposito, D., Ungaro, F., Laurienzo, P., Boraschi, D., Quaglia, F., 2019. Surface exposure of peg and amines on biodegradable nanoparticles as a strategy to tune their interaction with protein-rich biological media. *Nanomaterials* 9. <https://doi.org/10.3390/nano9101354>

Cortés, H., Hernández-Parra, H., Bernal-Chávez, S.A., del Prado-Audelo, M.L., Caballero-Florán, I.H., Borbolla-Jiménez, F. v., González-Torres, M., Magaña, J.J., Leyva-Gómez, G., 2021. Non-ionic surfactants for stabilization of polymeric nanoparticles for biomedical uses. *Materials* 14. <https://doi.org/10.3390/ma14123197>

Craparo, E.F., Musumeci, T., Bonaccorso, A., Pellitteri, R., Romeo, A., Naletova, I., Cucci, L.M., Cavallaro, G., Satriano, C., 2021. Mpeg-plga nanoparticles labelled with loaded or conjugated rhodamine-b for potential nose-to-brain delivery. *Pharmaceutics* 13. <https://doi.org/10.3390/pharmaceutics13091508>

Dal Monte, M., Cammalleri, M., Amato, R., Pezzino, S., Corsaro, R., Bagnoli, P., Rusciano, D., 2020. A topical formulation of melatonergic compounds exerts strong hypotensive and neuroprotective effects in a rat model of hypertensive glaucoma. *International Journal of Molecular Sciences* 21, 1-26. <https://doi.org/10.3390/ijms21239267>

D'Angelo, I., Casciaro, B., Miro, A., Quaglia, F., Mangoni, M.L., Ungaro, F., 2015. Overcoming barriers in *Pseudomonas aeruginosa* lung infections: Engineered nanoparticles for local delivery of a cationic antimicrobial peptide. *Colloids and Surfaces B: Biointerfaces* 135, 717-725. <https://doi.org/10.1016/j.colsurfb.2015.08.027>

- Das, L., Kaurav, M., Pandey, R.S., 2019. Phospholipid-polymer hybrid nanoparticle-mediated transfollicular delivery of quercetin: prospective implement for the treatment of androgenic alopecia. *Drug Development and Industrial Pharmacy* 45, 1654–1663. <https://doi.org/10.1080/03639045.2019.1652635>
- Date, T., Nimbalkar, V., Kamat, J., Mittal, A., Mahato, R.I., Chitkara, D., 2018. Lipid-polymer hybrid nanocarriers for delivering cancer therapeutics. *Journal of Controlled Release* 271, 60–73. <https://doi.org/10.1016/j.jconrel.2017.12.016>
- Datta, S., Baudouin, C., Brignole-Baudouin, F., Denoyer, A., Cortopassi, G.A., 2017. The eye drop preservative benzalkonium chloride potently induces mitochondrial dysfunction and preferentially affects LHON mutant cells. *Investigative Ophthalmology and Visual Science* 58, 2406–2412. <https://doi.org/10.1167/iovs.16-20903>
- de Campos, A.M., Diebold, Y., Carvalho, E.L.S., Sánchez, A., Alonso, M.J., 2004. Chitosan nanoparticles as new ocular drug delivery systems: In vitro stability, in vivo fate, and cellular toxicity. *Pharmaceutical Research* 21, 803–810. <https://doi.org/10.1023/B:PHAM.0000026432.75781.cb>
- Diebold, Y., Jarrín, M., Sáez, V., Carvalho, E.L.S., Orea, M., Calonge, M., Seijo, B., Alonso, M.J., 2007. Ocular drug delivery by liposome-chitosan nanoparticle complexes (LCS-NP). *Biomaterials* 28, 1553–1564. <https://doi.org/10.1016/j.biomaterials.2006.11.028>
- Doktorovova, S., Shegokar, R., Rakovsky, E., Gonzalez-Mira, E., Lopes, C.M., Silva, A.M., Martins-Lopes, P., Muller, R.H., Souto, E.B., 2011. Cationic solid lipid nanoparticles (cSLN): Structure, stability and DNA binding capacity correlation studies. *International Journal of Pharmaceutics* 420, 341–349. <https://doi.org/10.1016/j.ijpharm.2011.08.042>
- Dudhani, A.R., Kosaraju, S.L., 2010. Bioadhesive chitosan nanoparticles: Preparation and characterization. *Carbohydrate Polymers* 81, 243–251. <https://doi.org/10.1016/j.carbpol.2010.02.026>
- Duskey, J.T., Ottonelli, I., Rinaldi, A., Parmeggiani, I., Zambelli, B., Wang, L.Z., Prud'homme, R.K., Vandelli, M.A., Tosi, G., Ruozi, B., 2021. Tween® preserves enzyme activity and stability in PLGA nanoparticles. *Nanomaterials* 11. <https://doi.org/10.3390/nano11112946>
- Eliyahu, S., Aharon, A., Bianco-Peled, H., 2018. Acrylated chitosan nanoparticles with enhanced mucoadhesion. *Polymers (Basel)* 10, 1–17. <https://doi.org/10.3390/polym10020106>
- Elsaid, N., Jackson, T.L., Elsaid, Z., Alqathama, A., Somavarapu, S., 2016. PLGA microparticles entrapping chitosan-based nanoparticles for the ocular delivery of ranibizumab. *Molecular Pharmaceutics* 13, 2923–2940. <https://doi.org/10.1021/acs.molpharmaceut.6b00335>
- EMA, 2017. Questions and answers on benzalkonium chloride used as an excipient in medicinal products for human use 44, 3.
- EMA, 2003. ICH Topic Q1A (R2): Stability Testing of New Drug Substances and Products. Handbook of Pharmaceutical Manufacturing Formulations. <https://doi.org/10.1201/9781420048452-7>
- Evangelopoulos, M., Parodi, A., Martinez, J.O., Yazdi, I.K., Cevenini, A., van de Ven, A.L., Quattrocchi, N., Boada, C., Taghipour, N., Corbo, C., Brown, B.S., Scaria, S., Liu, X., Ferrari, M., Tasciotti, E., 2016. Cell source determines the immunological impact of biomimetic nanoparticles. *Biomaterials* 82, 168–177. <https://doi.org/10.1016/j.biomaterials.2015.11.054>

- Fang, D.L., Chen, Y., Xu, B., Ren, K., He, Z.Y., He, L.L., Lei, Y., Fan, C.M., Song, X.R., 2014. Development of lipid-shell and polymer core nanoparticles with water-soluble salidroside for anti-cancer therapy. *International Journal of Molecular Sciences* 15, 3373–3388. <https://doi.org/10.3390/ijms15033373>
- Fangueiro, J.F., Andreani, T., Egea, M.A., Garcia, M.L., Souto, S.B., Silva, A.M., Souto, E.B., 2014. Design of cationic lipid nanoparticles for ocular delivery: Development, characterization and cytotoxicity. *International Journal of Pharmaceutics* 461, 64–73. <https://doi.org/10.1016/j.ijpharm.2013.11.025>
- Fangueiro, J.F., Calpena, A.C., Clares, B., Andreani, T., Egea, M.A., Veiga, F.J., Garcia, M.L., Silva, A.M., Souto, E.B., 2016. Biopharmaceutical evaluation of epigallocatechin gallate-loaded cationic lipid nanoparticles (EGCG-LNs): In vivo, in vitro and ex vivo studies. *International Journal of Pharmaceutics* 502, 161–169. <https://doi.org/10.1016/j.ijpharm.2016.02.039>
- Feng, Q., Yu, M.Z., Wang, J.C., Hou, W.J., Gao, L.Y., Ma, X.F., Pei, X.W., Niu, Y.J., Liu, X.Y., Qiu, C., Pang, W.H., Du, L.L., Zhang, Q., 2014. Synergistic inhibition of breast cancer by co-delivery of VEGF siRNA and paclitaxel via vaptotide-modified core-shell nanoparticles. *Biomaterials* 35, 5028–5038. <https://doi.org/10.1016/j.biomaterials.2014.03.012>
- Gan, L., Wang, J., Zhao, Y., Chen, D., Zhu, C., Liu, J., Gan, Y., 2013. Hyaluronan-modified core-shell liponanoparticles targeting CD44-positive retinal pigment epithelium cells via intravitreal injection. *Biomaterials* 34, 5978–5987. <https://doi.org/10.1016/j.biomaterials.2013.04.035>
- Gao, D.Y., Lin, T.T., Sung, Y.C., Liu, Y.C., Chiang, W.H., Chang, C.C., Liu, J.Y., Chen, Y., 2015. CXCR4-targeted lipid-coated PLGA nanoparticles deliver sorafenib and overcome acquired drug resistance in liver cancer. *Biomaterials* 67, 194–203. <https://doi.org/10.1016/j.biomaterials.2015.07.035>
- Garg, N.K., Singh, B., Sharma, G., Kushwah, V., Tyagi, R.K., Jain, S., Katare, O.P., 2015. Development and characterization of single step self-assembled lipid polymer hybrid nanoparticles for effective delivery of methotrexate. *RSC Advances* 5, 62989–62999. <https://doi.org/10.1039/c5ra12459j>
- Giurdanella, G., Longo, A., Distefano, A., Olivieri, M., Cristaldi, M., Cosentino, A., Agafonova, A., Caporarello, N., Lupo, G., Anfuso, C.D., 2022. The anti-inflammatory effect of the β 1-adrenergic receptor antagonist metoprolol on high glucose treated human microvascular retinal endothelial cells. *Cells* 11. <https://doi.org/10.3390/cells11010051>
- Giurdanella, G., Lupo, G., Gennuso, F., Conti, F., Furno, D. lo, Mannino, G., Anfuso, C.D., Drago, F., Salomone, S., Bucolo, C., 2020. Activation of the VEGF-A/ERK/PLA2 axis mediates early retinal endothelial cell damage induced by high glucose: New insight from an in vitro model of diabetic retinopathy. *International Journal of Molecular Sciences* 21, 1–19. <https://doi.org/10.3390/ijms21207528>
- Godara, S., Lather, V., Kirthanashri, S. v., Awasthi, R., Pandita, D., 2020. Lipid-PLGA hybrid nanoparticles of paclitaxel: Preparation, characterization, in vitro and in vivo evaluation. *Materials Science and Engineering C* 109, 110576. <https://doi.org/10.1016/j.msec.2019.110576>
- Gupta, H., Aqil, M., Khar, R.K., Ali, A., Bhatnagar, A., Mittal, G., 2010. Sparfloxacin-loaded PLGA nanoparticles for sustained ocular drug delivery. *Nanomedicine: Nanotechnology, Biology, and Medicine* 6, 324–333. <https://doi.org/10.1016/j.nano.2009.10.004>

- Hadinoto, K., Sundaresan, A., Cheow, W.S., 2013. Lipid-polymer hybrid nanoparticles as a new generation therapeutic delivery platform: A review. *European Journal of Pharmaceutics and Biopharmaceutics* 85, 427–443. <https://doi.org/10.1016/j.ejpb.2013.07.002>
- Hassan, D.H., Abdelmonem, R., Abdellatif, M.M., 2018. Formulation and characterization of carvedilol leciplex for glaucoma treatment: In-vitro, ex-vivo and in-vivo study. *Pharmaceutics* 10. <https://doi.org/10.3390/pharmaceutics10040197>
- Hejjaji, E.M.A., Smith, A.M., Morris, G.A., 2018. Evaluation of the mucoadhesive properties of chitosan nanoparticles prepared using different chitosan to tripolyphosphate (CS:TPP) ratios. *International Journal of Biological Macromolecules* 120, 1610–1617. <https://doi.org/10.1016/j.ijbiomac.2018.09.185>
- Jiang, T., Chang, Q., Zhao, Z., Yan, S., Wang, L., Cai, J., Xu, G., 2012. Melatonin-Mediated Cytoprotection against Hyperglycemic Injury in Müller Cells. *PLoS ONE* 7, 1–8. <https://doi.org/10.1371/journal.pone.0050661>
- Kalam, M.A., Sultana, Y., Ali, A., Aqil, M., Mishra, A.K., Aljuffali, I.A., Alshamsan, A., 2013. Part I: Development and optimization of solid-lipid nanoparticles using Box-Behnken statistical design for ocular delivery of gatifloxacin. *Journal of Biomedical Materials Research - Part A* 101 A, 1813–1827. <https://doi.org/10.1002/jbm.a.34453>
- Kandel, P.K., Fernando, L.P., Ackroyd, P.C., Christensen, K.A., 2011. Incorporating functionalized polyethylene glycol lipids into reprecipitated conjugated polymer nanoparticles for bioconjugation and targeted labeling of cells. *Nanoscale* 3, 1037–1045. <https://doi.org/10.1039/c0nr00746c>
- Khodaei, M., Rostamizadeh, K., Taramchi, A.H., Monirinasab, H., Fathi, M., 2021. DDAB cationic lipid-mPEG, PCL copolymer hybrid nano-carrier synthesis and application for delivery of siRNA targeting IGF-1R into breast cancer cells. *Clinical and Translational Oncology* 23, 1167–1178. <https://doi.org/10.1007/s12094-020-02507-3>
- Klemetsrud, T., Jonassen, H., Hiorth, M., Kjøniksen, A.L., Smistad, G., 2013. Studies on pectin-coated liposomes and their interaction with mucin. *Colloids and Surfaces B: Biointerfaces* 103, 158–165. <https://doi.org/10.1016/j.colsurfb.2012.10.012>
- Lee, J.Y., Yang, H., Yoon, I.N.S., Kim, S.B., Ko, S.H., Shim, J.S., Sung, S.H., Cho, H.J., Kim, D.D., 2014. Nanocomplexes based on amphiphilic hyaluronic acid derivative and polyethylene glycol-lipid for ginsenoside Rg3 delivery. *Journal of Pharmaceutical Sciences* 103, 3254–3262. <https://doi.org/10.1002/jps.24111>
- Leonardi, A., Bucolo, C., Drago, F., Salomone, S., Pignatello, R., 2015. Cationic solid lipid nanoparticles enhance ocular hypotensive effect of melatonin in rabbit. *International Journal of Pharmaceutics* 478, 180–186. <https://doi.org/10.1016/j.ijpharm.2014.11.032>
- Leonardi, A., Bucolo, C., Luca, G., Bianca, C., Platania, M., Drago, F., Puglisi, G., Pignatello, R., 2014. Influence of different surfactants on the technological properties and in vivo ocular tolerability of lipid nanoparticles. *International Journal of Pharmaceutics* 470, 133–140. <https://doi.org/10.1016/j.ijpharm.2014.04.061>
- Lewis, R.N.A.H., McElhaney, R.N., 2013. Membrane lipid phase transitions and phase organization studied by Fourier transform infrared spectroscopy. *Biochimica et Biophysica Acta - Biomembranes* 1828, 2347–2358. <https://doi.org/10.1016/j.bbamem.2012.10.018>

- Li, Q., Xia, D., Tao, J., Shen, A., He, Y., Gan, Y., Wang, C., 2017. Self-Assembled Core-Shell-Type Lipid-Polymer Hybrid Nanoparticles: Intracellular Trafficking and Relevance for Oral Absorption. *Journal of Pharmaceutical Sciences* 106, 3120–3130. <https://doi.org/10.1016/j.xphs.2017.05.029>
- Li, X., Muller, R.H., Keck, C.M., Bou-Chacra, N.A., 2016. Mucoadhesive dexamethasone acetate-polymyxin B sulfate cationic ocular nanoemulsion - Novel combinatorial formulation concept. *Pharmazie* 71, 327–333. <https://doi.org/10.1691/ph.2016.5190>
- Liang, F.Q., Green, L., Wang, C., Alssadi, R., Godley, B.F., 2004. Melatonin protects human retinal pigment epithelial (RPE) cells against oxidative stress. *Experimental Eye Research* 78, 1069–1075. <https://doi.org/10.1016/j.exer.2004.02.003>
- Ling, G., Zhang, P., Zhang, W., Sun, J., Meng, X., Qin, Y., Deng, Y., He, Z., 2010. Development of novel self-assembled DS-PLGA hybrid nanoparticles for improving oral bioavailability of vincristine sulfate by P-gp inhibition. *Journal of Controlled Release* 148, 241–248. <https://doi.org/10.1016/j.jconrel.2010.08.010>
- Liu, Y., Li, K., Pan, J., Liu, B., Feng, S.S., 2010. Folic acid conjugated nanoparticles of mixed lipid monolayer shell and biodegradable polymer core for targeted delivery of Docetaxel. *Biomaterials* 31, 330–338. <https://doi.org/10.1016/j.biomaterials.2009.09.036>
- Lu, B., Lv, X., Le, Y., 2019. Chitosan-modified PLGA nanoparticles for control-released drug delivery. *Polymers (Basel)* 11. <https://doi.org/10.3390/polym11020304>
- Lundmark, P.O., Pandi-Perumal, S.R., Srinivasan, V., Cardinali, D.P., 2006. Role of melatonin in the eye and ocular dysfunctions. *Visual Neuroscience* 23, 853–862. <https://doi.org/10.1017/S0952523806230189>
- Lupo, G., Cambria, M.T., Olivieri, M., Rocco, C., Caporarello, N., Longo, A., Zanghi, G., Salmeri, M., Foti, M.C., Anfuso, C.D., 2019. Anti-angiogenic effect of quercetin and its 8-methyl pentamethyl ether derivative in human microvascular endothelial cells. *Journal of Cellular and Molecular Medicine* 23, 6565–6577. <https://doi.org/10.1111/jcmm.14455>
- M. Scheive, S.Y. and A.R.H., 2021. The utility and risks of therapeutic nanotechnology in the retina. *Therapeutic Advances in Ophthalmology* 13, 1–16. <https://doi.org/https://doi.org/10.1177/25158414211003381>
- Mainardes, R.M., Khalil, N.M., Gremião, M.P.D., 2010. Intranasal delivery of zidovudine by PLA and PLA-PEG blend nanoparticles. *International Journal of Pharmaceutics* 395, 266–271. <https://doi.org/10.1016/j.ijpharm.2010.05.020>
- Makoni, P.A., Kasongo, K.W., Walker, R.B., 2019. Short term stability testing of efavirenz-loaded solid lipid nanoparticle (SLN) and nanostructured lipid carrier (NLC) dispersions. *Pharmaceutics* 11. <https://doi.org/10.3390/pharmaceutics11080397>
- Manchanda, S., Sahoo, P.K., 2017. Topical delivery of acetazolamide by encapsulating in mucoadhesive nanoparticles. *Asian Journal of Pharmaceutical Sciences* 12, 550–557. <https://doi.org/10.1016/j.ajps.2017.04.005>
- Mandlik, S.K., Ranpise, N.S., 2017. Implementation of experimental design methodology in preparation and characterization of zolmitriptan loaded chitosan nanoparticles. *International Current Pharmaceutical Journal* 6, 16–22. <https://doi.org/10.3329/icpj.v6i3.32684>

- Margomenou Leonidopoulou, 1988. Thermal behavior of some long-chain di-n-dodecyl quaternary ammonium salts. *Thermochimica Acta* 134, 49–54.
- Martínez-Águila, A., Fonseca, B., de Lara, M.J.P., Pintor, J., 2016. Effect of Melatonin and 5-Methoxycarbonylamino-N-Acetyltryptamine on the Intraocular Pressure of Normal and Glaucomatous Mice. *Journal of Pharmacology and Experimental Therapeutics* 357, 293–299. <https://doi.org/10.1124/jpet.115.231456>
- Martínez-águila, A., Martín-gil, A., Carpena-torres, C., Pastrana, C., Carracedo, G., 2021. Influence of circadian rhythm in the eye: Significance of melatonin in glaucoma. *Biomolecules* 11, 1–25. <https://doi.org/10.3390/biom11030340>
- Mazzarino, L., Travelet, C., Ortega-Murillo, S., Otsuka, I., Pignot-Paintrand, I., Lemos-Senna, E., Borsali, R., 2012. Elaboration of chitosan-coated nanoparticles loaded with curcumin for mucoadhesive applications. *Journal of Colloid and Interface Science* 370, 58–66. <https://doi.org/10.1016/j.jcis.2011.12.063>
- Mieszawska, A.J., Gianella, A., Cormode, D.P., Zhao, Y., Meijerink, A., Langer, R., Farokhzad, O.C., Fayad, Z.A., Mulder, W.J.M., 2012. Engineering of lipid-coated PLGA nanoparticles with a tunable payload of diagnostically active nanocrystals for medical imaging. *Chemical Communications* 48, 5835–5837. <https://doi.org/10.1039/c2cc32149a>
- Mirakabad, F.S.T., Akbarzadeh, A., Milani, M., Zarghami, N., Taheri-Anganeh, M., Zeighamian, V., Badrzadeh, F., Rahmati-Yamchi, M., 2016. A Comparison between the cytotoxic effects of pure curcumin and curcumin-loaded PLGA-PEG nanoparticles on the MCF-7 human breast cancer cell line. *Artificial Cells, Nanomedicine and Biotechnology* 44, 423–430. <https://doi.org/10.3109/21691401.2014.955108>
- Mishra, R., Mishra, S., Upadhyay, C., Prakash, R., 2017. DDAB-Triggered, Size-Sorted, Instant Phase-Switching of Silver Nanoparticles. *ChemistrySelect* 2, 3028–3034. <https://doi.org/10.1002/slct.201602012>
- Morris, G.A., Kök, S.M., Harding, S.E., Adams, G.G., 2013. Polysaccharide drug delivery systems based on pectin and chitosan. *Biotechnology and Genetic Engineering Reviews* 27, 257–284. <https://doi.org/10.1080/02648725.2010.10648153>
- Mukherjee, A., Waters, A.K., Kalyan, P., Achrol, A.S., Kesari, S., Yenugonda, V.M., 2019. Lipid-polymer hybrid nanoparticles as a next generation drug delivery platform: State of the art, emerging technologies, and perspectives. *International Journal of Nanomedicine* 14, 1937–1952. <https://doi.org/10.2147/IJN.S198353>
- Musumeci, T., Bucolo, C., Carbone, C., Pignatello, R., Drago, F., Puglisi, G., 2013. Polymeric nanoparticles augment the ocular hypotensive effect of melatonin in rabbits. *International Journal of Pharmaceutics* 440, 135–140. <https://doi.org/10.1016/j.ijpharm.2012.10.014>
- Niizawa, I., Espinaco, B.Y., Zorrilla, S.E., Sihufe, G.A., 2019. Natural astaxanthin encapsulation: Use of response surface methodology for the design of alginate beads. *International Journal of Biological Macromolecules* 121, 601–608. <https://doi.org/10.1016/j.ijbiomac.2018.10.044>
- Okahara, A., Kawazu, K., 2013. Local toxicity of benzalkonium chloride in ophthalmic solutions following repeated applications. *Journal of Toxicological Sciences* 38, 531–537. <https://doi.org/10.2131/jts.38.531>

- Pai, R. v., Monpara, J.D., Vavia, P.R., 2019. Exploring molecular dynamics simulation to predict binding with ocular mucin: An in silico approach for screening mucoadhesive materials for ocular retentive delivery systems. *Journal of Controlled Release* 309, 190–202. <https://doi.org/10.1016/j.jconrel.2019.07.037>
- Puglia, C., Blasi, P., Ostacolo, C., Sommella, E., Bucolo, C., Platania, C.B.M., Romano, G.L., Geraci, F., Drago, F., Santonocito, D., Albertini, B., Campiglia, P., Puglisi, G., Pignatello, R., 2018. Innovative nanoparticles enhance N-palmitoylethanolamide intraocular delivery. *Frontiers in Pharmacology* 9, 1–7. <https://doi.org/10.3389/fphar.2018.00285>
- Quan, G., Pan, X., Wang, Z., Wu, Q., Li, G., Dian, L., Chen, B., Wu, C., 2015. Lactosaminated mesoporous silica nanoparticles for asialoglycoprotein receptor targeted anticancer drug delivery. *Journal of Nanobiotechnology* 13, 1–12. <https://doi.org/10.1186/s12951-015-0068-6>
- Rabinovich-Guilatt, L., Couvreur, P., Lambert, G., Dubernet, C., 2004. Cationic vectors in ocular drug delivery. *Journal of Drug Targeting* 12, 623–633. <https://doi.org/10.1080/10611860400015910>
- Romeo, A., Musumeci, T., Carbone, C., Bonaccorso, A., Corvo, S., Lupo, G., Anfuso, C.D., Puglisi, G., Pignatello, R., 2021. Ferulic acid-loaded polymeric nanoparticles for potential ocular delivery. *Pharmaceutics* 13. <https://doi.org/10.3390/pharmaceutics13050687>
- Salunkhe, S.S., Bhatia, N.M., Bhatia, M.S., 2016. Implications of formulation design on lipid-based nanostructured carrier system for drug delivery to brain. *Drug Delivery* 23, 1306–1316. <https://doi.org/10.3109/10717544.2014.943337>
- Sánchez-López, E., Espina, M., Doktorovova, S., Souto, E.B., García, M.L., 2017. Lipid nanoparticles (SLN, NLC): Overcoming the anatomical and physiological barriers of the eye – Part II - Ocular drug-loaded lipid nanoparticles. *European Journal of Pharmaceutics and Biopharmaceutics* 110, 58–69. <https://doi.org/10.1016/j.ejpb.2016.10.013>
- Sengupta, S., Eavarone, D., Capila, I., Zhao, G., Watson, N., Kiziltepe, T., Sasisekharan, R., 2005. Temporal targeting of tumour cells and neovasculature with a nanoscale delivery system. *Nature* 436, 568–572. <https://doi.org/10.1038/nature03794>
- Shen, J., Wang, Y., Ping, Q., Xiao, Y., Huang, X., 2009. Mucoadhesive effect of thiolated PEG stearate and its modified NLC for ocular drug delivery. *Journal of Controlled Release* 137, 217–223. <https://doi.org/10.1016/j.jconrel.2009.04.021>
- Silva, B., São Braz, B., Delgado, E., Gonçalves, L., 2021. Colloidal nanosystems with mucoadhesive properties designed for ocular topical delivery. *International Journal of Pharmaceutics* 606. <https://doi.org/10.1016/j.ijpharm.2021.120873>
- Silva, N.C., Silva, S., Sarmento, B., Pintado, M., 2013. Chitosan nanoparticles for daptomycin delivery in ocular treatment of bacterial endophthalmitis. *Drug Delivery* 22, 885–893. <https://doi.org/10.3109/10717544.2013.858195>
- Sinha, R., Roychoudhury, J., Palit, P., Ali, N., 2015. Cationic liposomal sodium stibogluconate (ssg), a potent therapeutic tool for treatment of infection by ssg-sensitive and resistant leishmanidionovani. *Antimicrobial Agents and Chemotherapy* 59, 334–354. <https://doi.org/10.1128/AAC.03305-14>
- Sivadasan, D., Sultan, M.H., Madkhali, O., Almoshari, Y., Thangavel, N., 2021. Polymeric lipid hybrid nanoparticles (Plns) as emerging drug delivery platform—a comprehensive review of

their properties, preparation methods, and therapeutic applications. *Pharmaceutics* 13. <https://doi.org/10.3390/pharmaceutics13081291>

Su, X., Fricke, J., Kavanagh, D.G., Irvine, D.J., 2011. In vitro and in vivo mRNA delivery using lipid-enveloped pH-responsive polymer nanoparticles. *Molecular Pharmaceutics* 8, 774–787. <https://doi.org/10.1021/mp100390w>

Surwase, S.S., Munot, N.M., Idage, B.B., Idage, S.B., 2017. Tailoring the properties of mPEG-PLLA nanoparticles for better encapsulation and tuned release of the hydrophilic anticancer drug. *Drug Delivery and Translational Research* 7, 416–427. <https://doi.org/10.1007/s13346-017-0372-9>

Tahir, N., Madni, A., Balasubramanian, V., Rehman, M., Correia, A., Kashif, P.M., Mäkilä, E., Salonen, J., Santos, H.A., 2017. Development and optimization of methotrexate-loaded lipid-polymer hybrid nanoparticles for controlled drug delivery applications. *International Journal of Pharmaceutics* 533, 156–168. <https://doi.org/10.1016/j.ijpharm.2017.09.061>

Tao, Y., Hu, B., Ma, Z., Li, H., Du, E., Wang, G., Xing, B., Ma, J., Song, Z., 2020. Intravitreal delivery of melatonin affects the retinal neuron survival and visual signal transmission: in vivo and ex vivo study. *Drug Delivery* 27, 1386–1396. <https://doi.org/10.1080/10717544.2020.1818882>

Tillman, P., Hill, J.M., 2007. Determination of nanolayer thickness for a nanofluid. *International Communications in Heat and Mass Transfer* 34, 399–407. <https://doi.org/10.1016/j.icheatmasstransfer.2007.01.011>

Tiong, Y.L., Ng, K.Y., Koh, R.Y., Ponnudurai, G., Chye, S.M., 2020. Melatonin inhibits high glucose-induced ox-LDL/LDL expression and apoptosis in human umbilical endothelial cells. *Hormone Molecular Biology and Clinical Investigation* 41. <https://doi.org/10.1515/hmbci-2020-0009>

Topal, B., Çetin Altındal, D., Gümüşderelioglu, M., 2015. Melatonin/HP β CD complex: Microwave synthesis, integration with chitosan scaffolds and inhibitory effects on MG-63CELLS. *International Journal of Pharmaceutics* 496, 801–811. <https://doi.org/10.1016/j.ijpharm.2015.11.028>

Varela-Fernández, R., Díaz-Tomé, V., Luaces-Rodríguez, A., Conde-Penedo, A., García-Otero, X., Luzardo-álvarez, A., Fernández-Ferreiro, A., Otero-Espinar, F.J., 2020. Drug delivery to the posterior segment of the eye: Biopharmaceutic and pharmacokinetic considerations. *Pharmaceutics* 12, 1–39. <https://doi.org/10.3390/pharmaceutics12030269>

Vivek, K., Reddy, H., Murthy, R.S.R., 2007. Investigations of the effect of the lipid matrix on drug entrapment, in vitro release, and physical stability of olanzapine-loaded solid lipid nanoparticles. *AAPS PharmSciTech* 8. <https://doi.org/10.1208/pt0804083>

Wang, B., Li, J., Bao, M., Chen, R., Li, H., Lu, B., Chen, M., Huang, D., Zhang, Y., Gao, F., Shi, G., 2021. Melatonin Attenuates Diabetic Myocardial Microvascular Injury through Activating the AMPK/SIRT1 Signaling Pathway. *Oxidative Medicine and Cellular Longevity* 2021. <https://doi.org/10.1155/2021/8882130>

Wang, J., Zhao, F., Liu, R., Chen, J., Zhang, Q., Lao, R., Wang, Z., Jin, X., Liu, C., 2017. Novel cationic lipid nanoparticles as an ophthalmic delivery system for multicomponent drugs: Development, characterization, in vitro permeation, in vivo pharmacokinetic, and molecular dynamics studies. *International Journal of Nanomedicine* 12, 8115–8127. <https://doi.org/10.2147/IJN.S139436>

- Wang, Y., Kho, K., Cheow, W.S., Hadinoto, K., 2012. A comparison between spray drying and spray freeze drying for dry powder inhaler formulation of drug-loaded lipid-polymer hybrid nanoparticles. *International Journal of Pharmaceutics* 424, 98–106. <https://doi.org/10.1016/j.ijpharm.2011.12.045>
- Xie, M., Hu, A., Luo, Y., Sun, W., Hu, X., Tang, S., 2014. Interleukin-4 and melatonin ameliorate high glucose and interleukin-1 β stimulated inflammatory reaction in human retinal endothelial cells and retinal pigment epithelial cells. *Molecular Vision* 20, 921–928.
- Yalcin, T.E., Ilbasimis-Tamer, S., Takka, S., 2018. Development and characterization of gemcitabine hydrochloride loaded lipid polymer hybrid nanoparticles (LPHNs) using central composite design. *International Journal of Pharmaceutics* 548, 255–262. <https://doi.org/10.1016/j.ijpharm.2018.06.063>
- Yan, J., Wang, Y., Zhang, X., Liu, S., Tian, C., Wang, H., 2016. Targeted nanomedicine for prostate cancer therapy: docetaxel and curcumin co-encapsulated lipid-polymer hybrid nanoparticles for the enhanced anti-tumor activity in vitro and in vivo. *Drug Delivery* 23, 1757–1762. <https://doi.org/10.3109/10717544.2015.1069423>
- Yang, X.Z., Dou, S., Wang, Y.C., Long, H.Y., Xiong, M.H., Mao, C.Q., Yao, Y.D., Wang, J., 2012. Single-step assembly of cationic lipid-polymer hybrid nanoparticles for systemic delivery of siRNA. *ACS Nano* 6, 4955–4965. <https://doi.org/10.1021/nn300500u>
- Yao, J., Sapkota, A., Konno, H., Obara, H., Sugawara, M., Takei, M., 2016. Noninvasive online measurement of particle size and concentration in liquid-particle mixture by estimating equivalent circuit of electrical double layer. *Particulate Science and Technology* 34, 517–525. <https://doi.org/10.1080/02726351.2015.1089345>
- Yu, H., Wang, Q., Wu, W., Zeng, W., Feng, Y., 2021. Therapeutic Effects of Melatonin on Ocular Diseases: Knowledge Map and Perspective. *Frontiers in Pharmacology* 12, 1–9. <https://doi.org/10.3389/fphar.2021.721869>
- Zhang, J., Hu, J., Chan, H.F., Skibba, M., Liang, G., Chen, M., 2016. iRGD decorated lipid-polymer hybrid nanoparticles for targeted co-delivery of doxorubicin and sorafenib to enhance anti-hepatocellular carcinoma efficacy. *Nanomedicine: Nanotechnology, Biology, and Medicine* 12, 1303–1311. <https://doi.org/10.1016/j.nano.2016.01.017>
- Zhang, L., Chan, J.M., Gu, F.X., Rhee, J.W., Wang, A.Z., Radovic-Moreno, A.F., Alexis, F., Langer, R., Farokhzad, O.C., 2008. Self-assembled lipid-polymer hybrid nanoparticles: A robust drug delivery platform. *ACS Nano* 2, 1696–1702. <https://doi.org/10.1021/nn800275r>
- Zhang, L., Zhang, L., 2010. Lipid-Polymer Hybrid Nanoparticles: Synthesis, Characterization and Applications. *Nano Life* 01, 163–173. <https://doi.org/10.1142/s179398441000016x>
- Zhao, X., Li, F., Li, Y., Wang, H., Ren, H., Chen, J., Nie, G., Hao, J., 2015. Co-delivery of HIF1 α siRNA and gemcitabine via biocompatible lipid-polymer hybrid nanoparticles for effective treatment of pancreatic cancer. *Biomaterials* 46, 13–25.
- Zheng, Y., Yu, B., Weecharangsan, W., Piao, L., Darby, M., Mao, Y., Koynova, R., Yang, X., Li, H., Xu, S., Lee, L.J., Sugimoto, Y., Brueggemeier, R.W., Lee, R.J., 2010. Transferrin-conjugated lipid-coated PLGA nanoparticles for targeted delivery of aromatase inhibitor 7 α -APTADD to breast cancer cells. *International Journal of Pharmaceutics* 390, 234–241. <https://doi.org/10.1016/j.ijpharm.2010.02.008>

Zhong, Q., Chinta, D.M.D., Pamujula, S., Wang, H., Yao, X., Mandal, T.K., Luftig, R.B., 2010. Optimization of DNA delivery by three classes of hybrid nanoparticle/DNA complexes. *Journal of Nanobiotechnology* 8, 1-10. <https://doi.org/10.1186/1477-3155-8-6>

**CHAPTER IV: *mPEG-PLGA Nanoparticles Labelled with
Loaded or Conjugated Rhodamine-B
for Potential Nose-to-Brain Delivery***



Article

mPEG-PLGA Nanoparticles Labelled with Loaded or Conjugated Rhodamine-B for Potential Nose-to-Brain Delivery

Emanuela Fabiola Craparo¹, Teresa Musumeci^{2,*}, Angela Bonaccorso², Rosalia Pellitteri³, Alessia Romeo^{2,4}, Irina Naletova^{5,6}, Lorena Maria Cucci⁷, Gennara Cavallaro¹ and Cristina Satriano^{5,7}

¹ Department of Biological, Chemical and Pharmaceutical Science and Technologies (STEBICEF), 90123 Palermo, Italy; emanuela.craparo@unipa.it (E.F.C.); gennara.cavallaro@unipa.it (G.C.)

² Department of Drug and Health Sciences, University of Catania, 95125 Catania, Italy; abonaccorso@unict.it (A.B.); alessia.romeo@virgilio.it (A.R.)

³ Institute for Biomedical Research and Innovation, National Research Council, 95126 Catania, Italy; rosalia.pellitteri@cnr.it

⁴ PhD in Neuroscience, Department of Biomedical and Biotechnological Sciences, School of Medicine, University of Catania, 95125 Catania, Italy

⁵ Inter-University Consortium for Research on the Chemistry of Metal Ions in Biological Systems, University of Bari, 70126 Bari, Italy; irina.naletova@ic.cnr.it (I.N.); cristina.satriano@unict.it (C.S.)

⁶ Institute of Crystallography, Research National Council, 95126 Catania, Italy

⁷ Department of Chemical Science, University of Catania, 95125 Catania, Italy; lorena.cucci@unict.it

* Correspondence: teresa.musumeci@unict.it; Tel.: +39-095-738-4021

Abstract: Nowadays, neurodegenerative diseases represent a great challenge from both the therapeutic and diagnostic points of view. Indeed, several physiological barriers of the body, including the blood brain barrier (BBB), nasal, dermal, and intestinal barriers, interpose between the development of new drugs and their effective administration to reach the target organ or target cells at therapeutic concentrations. Currently, the nose-to-brain delivery with nanoformulations specifically designed for intranasal administration is a strategy widely investigated with the goal to reach the brain while bypassing the BBB. To produce nanosystems suitable to study both *in vitro* and/or *in vivo* cells trafficking for potential nose-to-brain delivery route, we prepared and characterized two types of fluorescent poly(ethylene glycol)-methyl-ether-block-poly(lactide-co-glycolide) (PLGA-PEG) nanoparticles (PNPs), i.e., Rhodamine B (RhB) dye loaded- and grafted- PNPs, respectively. The latter were produced by blending into the PLGA-PEG matrix a RhB-labeled polyaspartamide/poly(lactide) graft copolymer to ensure a stable fluorescence during the time of analysis. Photon correlation spectroscopy (PCS), UV-visible (UV-vis) spectroscopies, differential scanning calorimetry (DSC), atomic force microscopy (AFM) were used to characterize the RhB-loaded and RhB-grafted PNPs. To assess their potential use for brain targeting, cytotoxicity tests were carried out on olfactory ensheathing cells (OECs) and neuron-like differentiated PC12 cells. Both PNP types showed mean sizes suitable for nose-to-brain delivery (<200 nm, PDI < 0.3) and were not cytotoxic toward OECs in the concentration range tested, while a reduction in the viability on PC12 cells was found when higher concentrations of nanomedicines were used. Both the RhB-labelled NPs are suitable drug carrier models for exploring cellular trafficking in nose-to-brain delivery for short-time or long-term studies.

Keywords: fluorescent dye; olfactory ensheathing cells; PC12 cell line; co-polymers

1. Introduction

The intranasal (IN) drug administration route represents an intriguing strategy for obtaining the rapid delivery of the drugs to the central nervous systems (CNS), by allowing the drugs to reach the brain directly. Such a route of administration overcomes the well-known limits presented by blood brain barrier (BBB) [1,2]. First pioneering studies on the IN administration strategy for bypassing the BBB were carried out by William Frey II in 1989. Since then, with the aim of achieving direct access into the brain, innovative devices have been developed and marketed (Optinose®, Bi-Directional™ technology), to drive drugs to the olfactory region in the upper site of the nose. It is also well-known that several pathways can be involved for drugs administrated through IN route [3-5].

Despite there being several studies on the use of free drugs through nose-to-brain delivery, it has been demonstrated that most molecules do not have suitable properties to reach therapeutic doses in the brain. Such reduced bioavailability can be due to the low instilled volumes that can be given intranasally, and/or to the local physiological mechanisms that reduce the drug's access to the target site, such as the mucociliary clearance (which does not allow long residence time in the nose), or enzymatic degradation, besides temporary local disfunction (allergies, influenzae) altering the physiological function.

According to these premises, nanomedicine may offer new solutions to overcome these drawbacks of traditional administration routes to the CNS. Indeed, micro- and nano- emulsions, lipidic and polymeric NPs are widely investigated drug-delivery systems to load drugs commonly used for neurological disorders [6]. Specifically, the most studied materials to obtain polymer-based NPs for nose-to-brain delivery are chitosan and its derivatives, poly-lactide (PLA), poly-lactide-co-glycolide (PLGA), and their PEGylated derivatives [7,8].

In vitro and in vivo investigations are fundamental to understanding the potential of NPs for nanomedical application [9]. The difficulty in having an easy and effective labeling method to track nanomedicine represents the bottleneck for the developments of these formulations. Generally, fluorescent molecules were used to define well the intracellular trafficking and biodistribution fates of nanocarriers after IN administration. Encapsulation of dye into nanosystems is a widely used strategy to label them, allowing the in vivo and in vitro fate of the systems. Several advantages are associated loading the dye into the NPs: the dye signal is retained for more time due to its protection into nanocarriers; the nanocarrier can be used to encapsulate other substances or to functionalize the surface with target moiety. Referring to literature different hypothesis were disseminated, and it is a challenge the selection of most suitable dye (in term of physic-chemical properties) related to nanosystems that should be correlated also to the specific technique. A fluorescent molecule is adopted to the specific analysis, the related question is: is it possible to use it to detect NPs? And what method is it appropriately? For example, the 1-1'-dioctadecyl-3,3,3',3'-tetramethylindotricarbocyanine iodide (DiR), a lipophilic dye, is suitable for in vivo biodistribution using Fluorescence Molecular Tomography system; it was loaded into PLGA NPs in a recent investigation [10,11]. Other dye extensively used is Rhodamine B (RhB) as fluorescent for in vitro and/or in vivo studies in nanomedicine field [12-15]. After the identification of a suitable dye, the researcher defines the type of fluorescent NPs that should be prepared: dye can be covalently attached to a polymer, which is

then blended with other material to obtain nano-formulations, or it can be encapsulated into NPs as a free moiety. Both approaches are widely used, with respective advantage and disadvantages for tracking NPs.

In this work, we have developed nanomedicines suitable for nose-to-brain delivery, increasing the efficiency of the system in terms of bioavailability and capability of translocation in the brain, PLGA-PEG was chosen as raw material to prepare NPs. PLGA-PEG is a promising raw material to prepare nanomedicine [8] and it is classified as a mucus-penetrating polymer, owing to the presence of the PEG portion, in fact, mucoadhesive properties could be increased with this type of material due to its penetrating action [16]. RhB was chosen as fluorescent dye, and to produce fluorescent NPs, RhB was entrapped by following two different methods, as free or after conjugation to a polyaspartamide/poly(lactide-co-glycolide) graft copolymer [12]. We obtained, respectively, RhB-loaded PLGA-PEG NPs (thereafter named loaded-PNP) or amphiphilic copolymer bearing RhB moieties blended with PLGA-PEG (thereafter named grafted-PNP), which were properly purified and characterized. Firstly, we selected the suitable purification methods for loaded-PNPs through physicochemical and technological characterizations. Release-profile studies were carried out to prove the entrapment of RhB in PNPs for all experiments.

The two selected nanomedicine were compared in the respects of mean size, polydispersity index (PDI) and zeta potential (ZP) through photon correlation spectroscopy (PCS). Differential scanning calorimetry (DSC) for thermometric evaluation and atomic force microscopy were performed to evaluate mean size of studied NPs in terms of core structure. NMR was used to give information about the conformation of PEG on PNPs surface.

Cytotoxicity evaluation through MTT assays of both systems was performed on olfactory ensheathing cells (OECs) and neuronal PC12 cells to assess their potential use for nose-to-brain delivery.

2. Materials and Methods

2.1 Materials

Poly(ethylene glycol) methyl ether-block-poly(lactide-co-glycolide) (mPEG-*b*-PLGA, PEG average Mn 5000, PLGA Mn 55,000), polyoxyethylene sorbitan monooleate (Tween® 80) and RhB were purchased from Sigma Aldrich (Milan, Italy). All other chemical reagents used solvents and deionized water were of analytical grade. Ultrapure water was used throughout this study.

2.2 Synthesis of PHEA-*g*-RhB-*g*-PLA (Fluo-P)

α,β -Poly(N-2-hydroxyethyl)-D,L-aspartamide (PHEA), PHEA-*g*-RhB and PHEA-*g*-RhB-*g*-PLA were properly synthesized by following procedures already reported in literature [12,17,18].

¹H-NMR spectra were registered by a Bruker Avance II-300 spectrometer, working at 300 MHz (Bruker, Milan, Italy).

Both PHEA and PHEA-*g*-RhB ¹H-NMR spectra in D₂O were superimposed with those reported in previously published papers, and the derivatization degree with RhB (DD_{RhB}), resulted about 0.55 ± 0.05 mol% [18].

PHEA-*g*-RhB-*g*-PLA ¹H-NMR (300 MHz, [D₇]DMF, 25 °C, TMS): δ 1.15 (m, 12H_{RhB} -CH₂CH₂-); δ 1.3 and δ 1.7 (2d, 3H_{PLA} -[OCOCH(CH₃)]₁₉₄-); δ 2.8 (m, 2H_{PHEA} -COCHCH₂CONH-); δ 3.3 (t, 2H_{PHEA} -NHCH₂CH₂O-); δ 3.59 (t, 2H_{PHEA} -

NHCH₂CH₂O-); δ 4.2–4.5 and δ 5.1–5.5 (m, ¹H_{PLA}-[OCOCH(CH₃)]₁₉₄-), and δ 4.8 (m, ¹H_{PHEA}-NHCH(CO)CH₂-); δ 7.0–8.0 (m, ¹⁰H_{RhB} H-Ar). The degree of derivatization in PLA (DD_{PLA}), determined from the ¹H-NMR spectrum, as reported elsewhere, was equal to 4.1 ± 0.46 mol% [18].

The weight-average molecular weight (\bar{M}_w) of PHEA, PHEA-g-RhB and PHEA- RhB-PLA graft copolymers used in this study, were calculated from SEC chromatograms, resulting respectively 53.6 kDa ($\bar{M}_w/\bar{M}_n = 1.2$), 52.5 Da ($\bar{M}_w/\bar{M}_n = 1.6$), and 209.0 kDa ($\bar{M}_w/\bar{M}_n = 1.50$).

2.3 Preparation of Fluorescent Nanoparticles

2.3.1 Rhodamine-B Loaded PLGA-PEG Nanoparticles (Loaded-PNP)

RhB loaded PLGA-PEG NPs were prepared by the “nanoprecipitation method” with modification as previously reported by Bonaccorso et al., [19].

PLGA-PEG (12 mg/mL) was dissolved in the organic phase (acetone). The aqueous phase (water/ethanol 1:1 *v/v*) was composed of Tween 80® (0.1 *w/v*). RhB was added to aqueous phase at 0.005% *w/v* prior precipitation process. The organic phase was added dropwise under constant stirring at room temperature into the aqueous phase (volume ratio 1:2) until a milky suspension had formed. The organic solvent was removed under vacuum (Büchi R 111), (38–40 °C and 450–500 bar).

2.3.2 PLGA-PEG and PHEA-g-RhB-g-PLA Blended Nanoparticles (Grafted-PNP)

This sample was obtained by dissolving in the organic phase PLGA-PEG and PHEA- g-RhB-g-PLA graft copolymer 5% *w/w* on the PLGA-PEG weight, and by following the procedure described above for loaded-PNPs.

An unlabeled sample (without RhB and PHEA-g-RhB-g-PLA) was also prepared as control (PNP).

2.4 Purification Procedures to Remove Unloaded RhB from Loaded-PNP

A purification process was used for loaded-PNP. Dialysis and centrifugation were investigated to eliminate any residual of surfactant and/or unloaded fluorescent molecules. The NPs suspensions were studied in terms of mean size, PDI and surface charge, before and after the purification phases, to evaluate variations due to the purification processes.

For centrifugation process we used Thermo-scientific SL 16R Centrifuge (Thermo Scientific Inc., Waltham, MA, USA) at 12,000 rpm for 1 h at 8 °C. The obtained supernatants were collected for HPLC analysis, pellet was resuspended in water and characterized through PCS analysis.

For dialysis process we used membranes (Mwco 3000 Da, diameter 11.5 mm; Spectra/Por®) previously hydrated. The colloidal suspensions inserted in dialysis membranes were immersed in 500 mL of distilled water. The frequencies of water changes per hour in dialysis (sample PNPs and loaded-PNP) were 3/3 L/h (3 L in 3 h). At the end of the procedure the samples were collected and characterized through PCS analysis.

Further centrifugation process was carried out for collected dialyzed samples to evaluate the encapsulation efficiency (EE%) and RhB release profile. For this aim the dialyzed samples were centrifuged at 12,000 rpm for 1 h at 8 °C, the obtained supernatant and pellet were analysed by UV.

2.5 Entrapment Efficiency of RhB into Loaded-PNP

The amount of free RhB in the loaded-PNPs was calculated to determine the EE%. The pellet obtained by ultra-centrifuged sample was dissolved in acetone. The amount of RhB in the supernatant was determined spectrophotometrically using a spectrophotometer (UV-VIS 1601 spectrophotometer, Shimadzu Italia, Milan, Italy) at a wavelength of 547 nm.

The calibration curve for the quantitative evaluation of RhB in acetone was linear in the following range: 12.70–0.72 µg/mL ($R^2 = 0.9663$). The amount of RhB in the supernatant was determined. The calibration curve for the quantitative evaluation of RhB in H₂O/EtOH was linear in the following range: from 8.16 to 0.16 µg/mL at RhB λ max 547 ($R^2 = 0.9663$). The EE% was calculated using the following Equation (1):

$$\%EE = \frac{w_i - w_{\text{pellet}}}{w_i} \times 100 \quad (1)$$

where W_i is the amount of RhB added during preparation and W_{pellet} is the amount of RhB determined in the pellet after dissolution in acetone.

2.6 Yield of Purification Process

In order to determine the most efficient purification methods we investigated the purification yield for both studied procedures. Purification efficiency was expressed as the percentage amount of dialyzed RhB compared with the unencapsulated amount.

In the case of dialyzed samples, a further centrifugation step was required.

The concentration of RhB in the obtained supernatants was measured by UV Spectroscopy. The percentage of purification was calculated using the following Equation (2):

$$\text{Purification efficacy}(\%) = \frac{\mu\text{gRhB supernatant}}{\mu\text{gRhB tot} - \mu\text{gRhB encapsulated}} \times 100 \quad (2)$$

Each experiment was performed in triplicate and the results represent the mean \pm standard deviation (SD).

2.7 Particle Size Distribution and Zeta Potential Measurements

Nanocarriers' mean size, polydispersity index (PDI) and ZP were determined by PCS (Zetasizer Nano S90; Malvern Instruments, Malvern, UK). The experiments were carried out at a detection angle of 90°, at 25 °C with a 4 mW laser operating at 633 nm as light source.

Each value was measured in triplicate. The results are shown as the mean \pm SD.

2.8 In Vitro Release Profile of RhB from Loaded-PNPs

The amount of RhB released from loaded-PNPs was measured on the resuspended pellet obtained after centrifugation of the samples, the supernatants were analysed through UV and 1 mL of phosphate-buffered saline (PBS) (pH 7.4) was used to resuspend the pellets. Cellulose membrane dialysis tubing (MWCO 3.5 kDa, Flat width 18 mm, diameter 11.5 mm; Spectra/Por® Dialysis Membrane, Waltham, MA, USA) containing the nanosuspensions were incubated in 20 mL of PBS at pH 7.4) and were maintained under magnetic stirring at 37 °C, up to 72 h. Release medium (1 mL) was took out at different time points (0, 1, 5, 24, 48, 72) and replaced with the same volume

of fresh medium, to maintain the sink condition. To determine the RhB concentration in the collected samples UV analysis was used, the wavelength was 553 nm. Each formulation was analysed in triplicate.

Calibration curves for the quantitative evaluation of the probe were linear in the following ranges: (i) 6.00–0.17 $\mu\text{g/mL}$ of RhB ($R^2 = 0.997$) for analyses in PBS pH 7.4. This data was also used for in vitro release experiments.

2.9 Atomic Force Microscopy (AFM)

AFM imaging was performed on adlayers prepared by drop casting at room temperature on freshly cleaved muscovite mica (Ted Pella, Inc., Redding, CA, USA). Briefly, a 10 μL volume of the concentrated dispersion of NPs was deposited on the mica substrates and, after 5 min, the mica surface was washed with 1 mL of milli-Q water, dried under a gentle nitrogen stream and imaged. A Cypher AFM instrument (Asylum Research, Oxford Instruments, Santa Barbara, CA, USA) equipped with a scanner at an XY scan range of 30/40 μm (closed/open loop) was operated, in AC-mode, in air. Tetrahedral tips made of silicon and mounted on rectangular cantilevers (30 μm) were purchased from Olympus (AT240TS, Oxford Instruments, Santa Barbara, CA, USA). Images, with the surfaces from 1 to 10 μm^2 , were scanned and the sizes of particles were measured using a free tool in the MFP-3DTM offline section analysis software.

2.10 Differential Scanning Calorimetry (DSC)

Differential scanning calorimetry studies were carried out with a Mettler Toledo DSC 1 STARe system equipped with a Poly-Science temperature controller (PolyScience, Columbus, OH, USA). The sensitivity was automatically chosen as the maximum possible through the calorimetric system, and the reference was an empty pan (signal time constant 18 s; digital resolution of the measurement signal < 0.04 μW , calorimetric resolution 0.12 and sensitivity 11 both determined through the TAWN test; the sampling rate 50 values/second). Calibration was carried out using indium as described in the procedure of the DSC 1 Mettler TA STARe instrument. Raw materials, RhB, PNP_a, loaded- and grafted-PNP_a were sealed in an aluminum pan and submitted to DSC analysis to determinate the thermotropic parameters of samples. Each sample was submitted to heating and cooling cycles in the temperature range 10–200 $^{\circ}\text{C}$ at a scanning rate of 5 $^{\circ}\text{C}/\text{min}$ (heating) and at a scanning rate of 10 $^{\circ}\text{C}/\text{min}$ (cooling). Transition temperature was calculated from peak areas with the Mettler STARe Evaluation software system (version 16.20).

2.11 Spectroscopic Quantification of RhB Dye Loading in the PNPs

To quantify the amount RhB immobilized by the two different approaches, the molar extinction coefficient (ϵ) of RhB in ultrapure MilliQ water was determined, as shown in Supplementary Figure S1. A calibration curve was obtained by using five different dilutions, in the concentration range from 3.11×10^{-6} M to 5.18×10^{-6} M, of a stock 2.08×10^{-3} M solution prepared by dissolving 1 $\times 10^{-3}$ g of RhB in 1 mL of Milli-Q water. The linear regression of the maximum absorbance values recorded at the wavelength of 552 nm ($R^2 = 0.99823$) resulted in the ϵ value of 4.5×10^4 $\text{M}^{-1} \text{cm}^{-1}$.

The NPs purified either by dialysis or ultracentrifugation, were characterized by UV-vis spectroscopy on a Perkin Elmer UV-vis spectrometer (Lambda 2S) using quartz cuvettes with an optical path length of 1 cm, for the suspensions, and 0.1 cm, for the pellets. The spectra were recorded by diluting the suspensions, in MilliQ water, 45 and 3 times, respectively for the loaded-PNP and the grafted-PNP. Whereas the pellets derived by centrifugation or samples obtained by dialysis were diluted 100 and 8 times, respectively for the loaded-PNP and the grafted-PNP, respectively.

2.12 Determination of Surface PEG Density and PEG Chains Conformation on Nanoparticle Surface

The amount of PEG exposed on the nanoparticle surface, expressed as surface PEG density, was determined on the freeze-dried samples by following an already reported ^1H NMR method [20,21].

First, PEG dispersions in D_2O (range of concentrations: 10^{-5} – 10^{-3} M), containing ethylenediamine (EDA) ($1\ \mu\text{L}/\text{mL}$) as internal standard, were analysed to set up a calibration by using the PEG integral values at δ 3.6 ppm ($y = 8314.9x$, $R_2 = 0.9993$). Each sample of NPs was dispersed in D_2O ($12.5\ \text{mg}/\text{mL}$), the internal standard was added, and from the integral value of PEG found in the acquired spectrum, the amount of PEG was calculated by using the calibration curve.

By proper calculations and considering that the PEG chains exposed on the surface were full length of 5 kDa PEG, the number of PEG molecules per $100\ \text{nm}^2$ of NPs surface area was determined by using the following Equation (3) and expressed as the surface PEG density [Γ] parameter:

$$[\Gamma] = \left[\frac{M_{\text{PEG}} \times 6.02 \times 10^{23}}{\frac{W_{\text{NP}}}{d_{\text{NP}}} \cdot \frac{4}{3} \pi (D/2)^3} / 4\pi (D/2)^2 \right] \times 100 \quad (3)$$

where M_{PEG} is the total PEG content, W_{NP} is the total mass of NPs, d_{NP} is the density of nanoparticle (here we assume the density of NPs is equal to the density of polymer, $1.34\ \text{g}/\text{mL}$ for PLGA 50:50), D is the particle diameter as measured by the dynamic light scattering.

Then, the surface area occupied by a single PEG chain could be calculated, considering that a single PEG chain occupies an area at the interface given by a sphere of diameter ξ , as elsewhere reported [21], following Equation (4):

$$\xi\ (\text{nm}) = 0.076 \sqrt{m_{\text{PEG}}} \quad (4)$$

where m_{PEG} is the PEG Mw.

For PEG chains of 5 kDa ξ was found to be 5.4 nm and occupies an area that is $22.7\ \text{nm}^2$. Therefore, considering a NPs surface area of $100\ \text{nm}^2$, [Γ^*], the number of unconstrained PEG molecules need to cover it was found to be 4.4.

2.13 Cellular Experiments

2.13.1 Cell Culture Maintenance

RPMI1640 medium, streptomycin, L-glutamine, fetal bovine serum (FBS) and horse serum (HS) were provided by Sigma-Aldrich (St. Louis, MO, USA). NGF was obtained from Invitrogen Laboratories (Paisley, UK). Rat pheochromocytoma (PC12 line) cells were cultivated in complete medium, i.e., RPMI1640 supplemented with 10% HS, 5% FBS, 2 mM L-glutamine, 50 U/mL penicillin, and 50 $\mu\text{g}/\text{mL}$ streptomycin. The cell culture was grown in tissue-culture treated Corning® flasks (Sigma-Aldrich, St. Louis, MO, USA) in humidified atmosphere (5% CO_2) at $37\ ^\circ\text{C}$ (Heraeus Hera Cell 150C incubator).

2.13.2 Differentiation of PC12 Cells

Differentiation of PC12 cells were performed, as described in the literature [22], with some modifications. PC12 cells were plated onto 48-well tissue culture plates coated with 0.01% poly-lysine according to the manufacturer-recommended procedure. Cells were plated at a density 3×10^4 cells/well in complete medium and after 20 h of plating, the medium was replaced with RPMI1640 medium supplemented with 50 ng/mL NGF, 0.5% of HS, 0.25% of FBS, 2mM L-glutamine, 50 U/mL penicillin,

and 50 µg/mL streptomycin. At day 2, 4, and 6 a concentrated stock of NGF was added for a final concentration of 50 ng/mL.

2.13.3 Cytotoxicity Assays

3-(4,5-dimethylthiazol-2-yl)-2,5-diphenyltetrazolium bromide was purchased from Sigma-Aldrich (St. Louis, MO, USA). The effect of NPs on viability of differentiated PC12 cells was tested by incubation with the compounds, namely PNP, loaded-PNPs at the RhB concentrations of 2.1×10^{-3} and grafted-PNP at the RhB concentration of 1.1×10^{-3} M (concentrations for each), by diluting the samples with final polymer concentrations equal to 1.5 mg/mL, 3 mg/mL, 15 mg/mL from the purified pellets. The viable cells were quantified by the reaction with 3-(4,5-dimethylthiazol-2-yl)-2,5-diphenyltetrazolium bromide. After 90 min, the reaction was stopped by adding DMSO, and absorbance was measured at 570 nm (Varioskan® Flash Spectral Scanning Multimode Readers, Thermo Scientific, Waltham, MA, USA). Results were expressed as percentage of viable cells over the concentration of each compound. The experiments were repeated in triplicate and results expressed as mean \pm SEM.

2.13.4 ROS Assays

To analyze the intracellular ROS production, differentiated PC12 cells were treated with NPs for 24 h and then stained for 15 min with 2',7'-Dichlorofluorescein (DCF) and Hoechst33342. Fluorescence of the samples was analyzed by fluorescent plate reader (Varioskan® Flash Spectral Scanning Multimode Readers, Thermo Scientific, Waltham, MA, USA). Results are represented as the increase in DCF, normalized with live-cell fluorescent staining of DNA Hoechst33342, with respect to controls and are means \pm SEM for three wells for each treatment.

2.13.5 Laser Scanning Confocal Microscopy Imaging

An Olympus FV1000 confocal laser scanning microscope (LSM), equipped with diode laser (405 nm, 50 mW) and gas lasers (multiline Argon: 457 nm, 488 nm, 515 nm, total 30 mW; HeNe(G): 543 nm, 1 mW and HeNe(R): 633 nm, 1 mW) was utilized to execute confocal microscopy studies. Images were collected with oil immersion objective (60xO PLAPO), in sequential mode, randomly all through the area of the well. The detector gain was fixed at a constant value. The image analysis was carried out by means of Huygens Essential software (by Scientific Volume Imaging B.V., Hilversum, The Netherlands).

To perform the experiments of cellular uptake, PC12 cells were plated in poly-lysine precoated glass bottom dishes (WillCo-dish®, Willco Wells, B.V., Amsterdam, The Netherlands) with 12 mm of glass diameter at a density of 1×10^4 cells/well in complete medium, then differentiated according to the protocol described above. Thereafter, cells were treated for 2 h, at 37 °C into the incubator, under humidified atmosphere of air/CO₂ (95:5) with RhB (4 µM) or PNP (3 mg/mL), either bare or RhB-functionalized nanoparticles.

Afterwards, cells were stained with nuclear dye Hoechst33342 (1 µg/mL) and fixed with high purity 2% paraformaldehyde in PBS, pH = 7.3.

2.14 *In Vitro* Tests on OEC

2.14.1 Animals

Experiments were carried out on 2-day-old mouse pups (P2), provided by Envigo RMS s.r.l. (Udine, Italy). Animals were kept in a controlled environment (23 ± 1 °C, 50 ± 5 % humidity) with a 12 h light/dark cycle with food and water available

ad libitum. Experiments were carried out in compliance with the Italian law on animal care no. 116/1992 and in accordance with the European Community Council Directive (86/609/EEC) and were approved by the Ethical Committee at the University of Catania (Italy). Efforts were made to minimize the number of animals used.

2.14.2 Cell Cultures

OECs were isolated from pup's olfactory bulbs as previously described by Pellitteri et al., [23]. Briefly, bulbs were removed from decapitated pups and dissected out in cold (+4 °C) Leibowitz L-15 medium. Then, the pellets were digested in Medium Essential Medium-H containing collagenase and trypsin. Trypsinization was stopped with Dulbecco's Modified Eagle's medium (DMEM) supplemented with 10% Fetal Bovine Serum (FBS). Cells were resuspended and plated in flasks, fed with fresh complete medium DMEM/FBS, 2 mM L-glutamine and antibiotics. To reduce the number of dividing fibroblasts, cytosine arabinoside (10^{-5} M), an antimetabolic agent, was added 24 h after initial plating. Subsequently, an additional step transferring from one flask to a new one, to reduce contaminating cells, was carried out. Purified OECs were plated both on 25 cm² flasks and cultured in DMEM/FBS at 37 °C.

2.14.3 MTT Bioassay

When cells were confluent, they were detached by trypsin and re-plated in multiwell 24-well plates. After 24 h the NPs (PNP, loaded-PNP, grafted-PNP) were added in OEC cultures at different concentrations (0.1, 0.5, 1.0 e 5.0 mg/mL) and incubated at 37 °C in DMEM/FBS medium 24 h, for cell viability test. Some OECs were grown without the presence of PNPs, and they were considered as controls. The OEC morphology in all conditions was monitored and the images were captured by phase-contrast microscopy (Zeiss, Oberkochen, Germany) using a 20x lens.

After 24 h that the NPs placed inside OEC cultures, cellular viability was evaluated by the 3-[4,5-dimethylthiazol-2-yl]-2,5-diphenyl] tetrazolium bromide (MTT, Sigma, Milan, Italy) reduction assay, a quantitative colorimetric method was utilized to evaluate cellular cytotoxicity: MTT was added to each multiwell and placed for 2 h in a CO₂ incubator. We removed DMEM/FBS and added MTT solvent (acid-isopropanol/SDS), the cells were shaken for 15 min. A multiKan reader at 570 nm was used to measure the absorbance [23]. The collected data were expressed as the percentage MTT reduction in comparison with control cells. Differences between OECs grown in presence or not of NPs were assessed using one-way analysis of variance (one-way ANOVA) followed by post hoc Holm-Sidak test.

2.15 Statistical Analysis

Statistical analysis was performed using Prism 6 (GraphPad Software 6.01, Inc., La Jolla, CA, USA).

For the statistical analysis, we used a one-way analysis of variance (ANOVA) followed by Tukey's multiple comparisons test for the analysis of NPs mean size and PDI. Significance was defined as $p < 0.05$.

3. Results and Discussion

In this paper, we have produced RhB labelled PEG-PLGA NPs as potential nanostructured carriers to study the nose-to-brain pathway as an administration route for drugs. In particular, the nanoprecipitation method was followed to obtain NPs; two different strategies to load the fluorescent dye have been exploited, i.e., the physical

entrapment of the free RhB into the PEG-PLGA matrix, or the blending of PEG-PLGA with a copolymer carrying RhB covalently linked on the polymeric backbone [12,18]. Being different entrapment strategies, two different nanocarriers were obtained, respectively named loaded-PNPs when the free dye was entrapped and grafted-PNPs when the dye was entrapped into the nanoparticle matrix after conjugation with a graft copolymer.

3.1 Preparation and Evaluation of Physical-Chemical Properties of the Loaded-PNPs

In the case of loaded-PNPs, being the dye physically entrapped into PEG-PLGA matrix, a relevant question to solve was the determination of RhB release profile from the nanosystems in physiological conditions to prove that the fluorescence determined during the in vitro and in vivo experiments was due to the cargo and not to the dye released during the experiment. Thus, first step was to purify the nanoformulations to remove the excess of the surfactant and the unloaded RhB; for this purpose, we investigated two purification processes: dialysis and centrifugation. Physicochemical characterization and purification yield were performed through PCS and UV analysis to select the most suitable method (Table 1). Nanoprecipitation allowed to obtain NPs based on PLGA-PEG with a core constituted by the PLGA portion, the while PEG portion forms a hydrophilic corona, resulting in a core/corona structure. The PEG portion forms a flexible layer on the surface of the NPs, this thick layer is referred generally to as the “mushroom or brush pattern” as reported widely in literature [8,24]. Nanoprecipitation is usually selected due to its straightforwardness and user-friendliness with standard laboratory equipment. With this method, it is possible to obtain samples in small volumes, reducing the amount of starting raw materials.

Table 1. Chemico-physical properties and yield of purification of loaded-PNPs purified through centrifugation and dialysis procedures.

Type and Purification Processes Steps		Z-ave (nm) ± S.D. ^b	PDI ± S.D. ^b	ZP ± S.D. ^b	%EE ^c	%Yield of purification Respect to the Unloaded RhB
Before purification process		344.5 ± 9.9	0.098 ± 0.035	-1.4 ± 0.1	80.190 ±	
After purification process	Dialysis	143.6 ± 2.2	0.135 ± 0.018	-20.2 ± 0.9	8.234	3.857 ± 1.241
	A.C. ^a 1 step	145.9 ± 0.4	0.117 ± 0.005	-23.4 ± 0.9		34.148 ± 1.293 ^d
	A.C. ^a final step	190.2 ± 4.1	0.198 ± 0.024	-27.7 ± 0.3		40.754 ± 2.113 ^d

^a A.C. – after centrifugation; ^b S.D. – standard deviation; ^c E.E. – encapsulation efficiency; ^d total sum of the three centrifuge steps.

The decrease of solubility of the polymer and/or the molecule that should be loaded in the solvent/water mixture is the first step to obtain particles, resulting in the formation of small aggregates at critical concentrations of super-saturation, allowing the realization of a homogeneous system. The growth of the aggregates occurs until they reach the state of colloidal stability. The probability of obtaining monodisperse particles depends on different factors; one is the uniform growth of the nuclei. It is important to strictly control these critical processes to avoid independent precipitation of the polymer and the molecule. In fact, this phenomenon should occur, we could obtain poor molecule loading and a dispersion that contains multiple species, such as polymeric particles without molecule, molecule-loaded polymeric particles, and molecule crystals. In this study, the nanosystem obtained before the purification process

showed a mean size ~ 350.00 nm, representing the hydrodynamic diameter due to the extension of PEG chains as brush conformation (schematic representation in Figure 1a). Centrifugation decreased this parameter, due to the reduction of the hydrodynamic diameter represented by mushroom conformation (Figure 1b), owing to the subjected force. This phenomenon was also showed in dialysis process and in this case, it was due to the residual amount of RhB on the surface that influenced the conformation of PEG chains, as illustrated in the scheme of Figure 1c, the hypothesis was the formation of “pockets” that hold RhB on the surface.

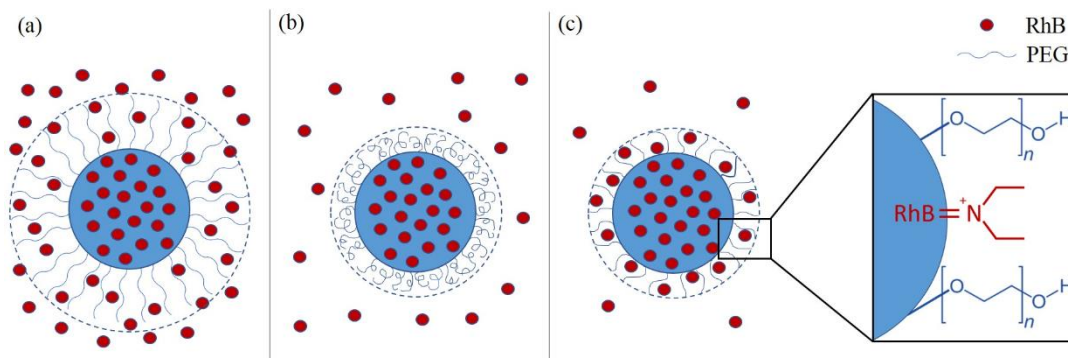


Figure 1. Scheme of possible conformation of loaded-PNPs before (a) and after purification processes with centrifugation (b) and dialysis (c).

The two purification processes allowed us to obtain monodisperse nanosystems, with an increase in the absolute values of ZP (from -1.4 to -23.4 mV). The variation of ZP values was related to surfactant remotion, and the difference for the nanosystems obtained by the two different purification processes was due to a residual amount of RhB that was not completely removed, in the case of dialysis, as confirmed by the yield-purification data (Table 1).

In-vitro release studies (Figure 2) confirmed our previous hypothesis, in fact centrifugated samples did not show RhB release until 72 h, while dialyzed samples showed 1% of RhB released during the experiment.

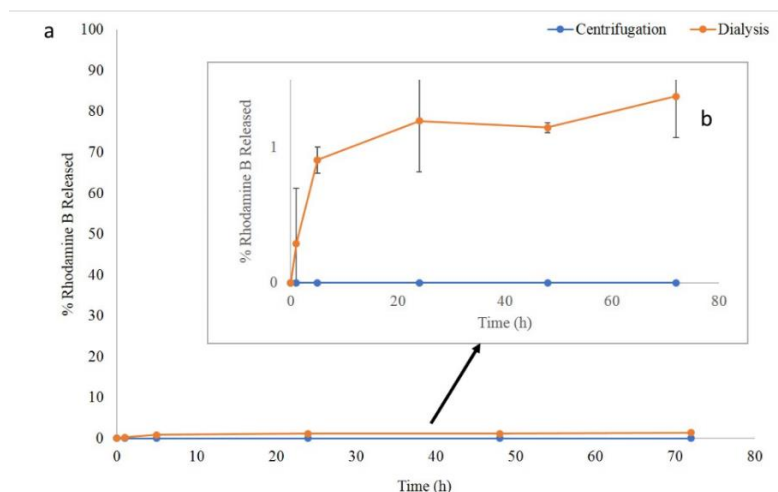


Figure 2. (a) Release profile of RhB from loaded-PNPs obtained from two different purification process, at 37 °C for 72 h; (b) Magnification of the 1% release profile.

The low percentage (1%) of RhB released was probably due to the diffusion of RhB from the “pockets” and could be probably attributed to a conformational change of PEG tails.

As previously demonstrated by Suna et al., the salt concentration of the release medium may weaken the hydrogen binding between PEG chains and water molecules. Consequently, PEG tails could stretch causing the collapse of “pockets” structures, resulting in the release of the dye that was previously retained [24,25].

Therefore, the centrifugation seems to be the most suitable purification process for loaded-PNPs to obtain NPs with RhB entrapped in the PLGA core (almost the 60 wt% of the theoretical), which limited the diffusion processes to 72 h.

3.2 Preparation of Grafted-PNP

To obtain fluorescent PLGA-PEG NPs with the probe stably incorporated inside them a graft copolymer containing covalently linked RhB was blended into the NPs matrix. In particular, the labelled graft copolymer was obtained starting from α,β -Poly(*N*- 2-hydroxyethyl)-D,L-aspartamide (PHEA) derivative, by functionalization with proper amount of RhB and polylactic acid (PLA), obtained the fluorescent PHEA-*g*-RhB-*g*-PLA graft copolymer [12,18,20]. Both these features had a very specific function: RhB made the polymer fluorescent, while PLA made it hydrophobic, ensuring the formation of insoluble nanostructures in aqueous media. It was already reported in the literature the great potential of the PHEA-*g*-RhB-*g*-PLA graft copolymer itself as starting material to produce several drug delivery systems (micro- and nano-structures) for active targeting and theranostic applications [12,18,20]. The chemical structure of PHEA-*g*-RhB-*g*-PLA graft copolymer was depicted in Figure 3. Chemical and enzymatic stability of fluorescent dye covalently linked to the copolymer backbone by ester linkage was demonstrated until 4 days of incubation [20].

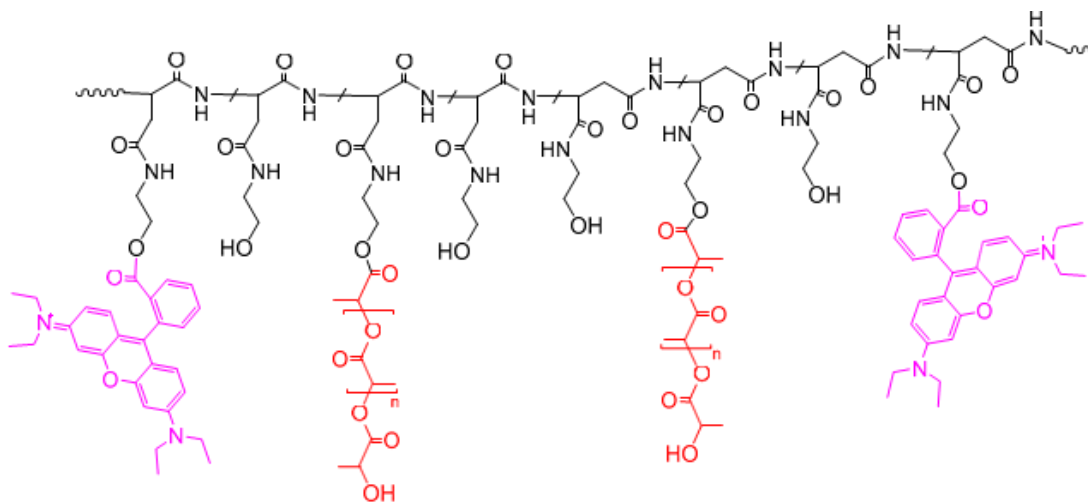


Figure 3. The chemical structure of PHEA-*g*-RhB-*g*-PLA graft copolymer (Fluo-P) ($n = 194$).

3.3 Quantitative Evaluation of RhB Dye in the Loaded-PNPs and Grafted-PNP

To determine the amount of RhB entrapped into either loaded- or grafted-PNP after purification, and to confirm that centrifugation was the process more appropriate to recover both samples, both PEG-PLGA NPs labelled with RhB by physical incorporation (loaded-PNP) or by covalent conjugation (grafted-PNP), were characterized by UV-visible spectroscopy, by using the unlabelled PEG-PLGA

nanoparticles (PNP) as control sample, using the two types of purification methods. The spectra of loaded-PNPs and grafted-PNPs are displayed in Figure 4.

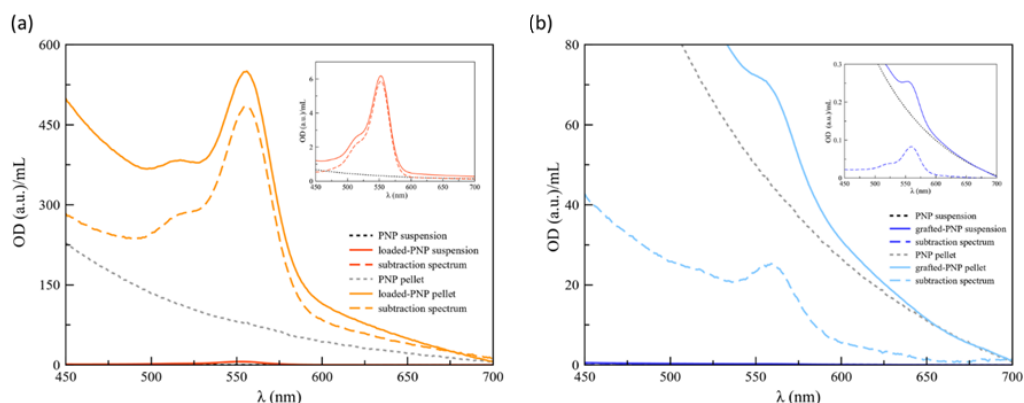


Figure 4. UV-vis optical density (OD) spectra of: (a) PNP (dotted black line) and loaded-PNPs (solid red line) suspensions, obtained after the dialysis process, compared with PNP (dotted grey line) and loaded-PNPs pellets obtained after the centrifugation steps; (b) PNP (dotted black line) and grafted-PNP (solid light blue line) suspensions, compared to PNP (dotted grey line) and grafted-PNP pellets. In the insets the magnified region for the suspensions. Dashed lines refer to the spectra obtained by the subtraction of the dye labeled PNP spectra with that of unlabeled PNPs. Spectra were recorded by diluting the suspensions, in MilliQ water, 45 and 3 times, respectively for loaded-PNPs and grafted-PNP. Whereas, the pellets were diluted 100 and 8 times, for the loaded-PNPs and grafted-PNPs, respectively.

The difference spectra (dashed lines) were shown to remove the background effect from the PEG-PLGA nanosystems, including scattering from the NPs dispersion, as particularly evident for grafted-PNP samples (Figure 4). As to the PNP suspensions obtained after the dialysis process, the RhB characteristic absorbance peak was found at 552 and 560 nm for dialyzed loaded-PNPs (Figure 4A) and for the grafted-PNP (Figure 4B), respectively. Such a red shift ($\Delta\lambda = 8$ nm) confirmed the actual covalent interaction between PNP and dye for the grafted-PNP, with a limitation of freedom of rotational movement of the RhB molecules at the interface [26]. Based on the maximum of absorbance, the estimated RhB concentration was 2.6×10^{-4} M for the loaded-PNPs and 3.7×10^{-6} M for the grafted-PNP.

As to the PNP dispersions purified by centrifugation, the loaded-PNPs showed a red-shift of the RhB absorbance peak of about 3 nm ($\lambda_{\text{max}} = 555$ nm) (Figure 4B), most likely due to the reorientation of the “disordered” layer of dye molecule physisorbed on the particle surface, as an effect of the concentration procedure [27]. As to the grafted-PNPs, the particle dispersion continued to maintain the absorbance maximum of the dye at 560 nm, as expected for a stable chemisorbed layer of molecules surrounding the nanoparticle surface. The calculated concentration of RhB, based on the maximum of absorbance values were 2.1×10^{-3} M and 1.1×10^{-4} M, respectively for loaded-PNPs and grafted-PNP pellets.

Therefore, based on our results, centrifugation seems to be the more suitable process for the purification of both loaded- and grafted-PNPs, and for this reason particles used for further characterization were obtained by centrifugation method.

3.4 Loaded-PNPs and Grafted-PNPs: Physical Evaluations

In Figure 5, the physicochemical properties of the unloaded, loaded- and grafted-PNPs are depicted. The grafted-PNPs did not show significant differences in terms

of mean size (<200.0 nm) and PDI (<0.2) from the loaded-PNPs, while the unloaded-PNPs showed a significantly higher mean size. Both labelled PNPs also presented negative ZP values, with an increase in absolute value respective to the given PNP. The small decrease in terms of mean size, in the case of loaded-PNPs and grafted-PNPs with respect to unloaded ones, is probably due to the presence of RhB that helped to form a different matrix organization.

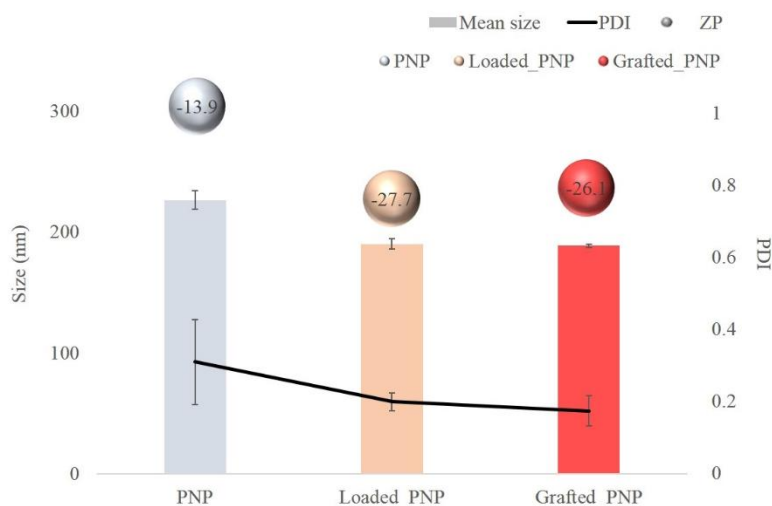


Figure 5. Comparative values in term of mean size (nm), PDI and ZP values (mV) of bare PNP; loaded-PNPs and grafted-PNPs.

In Supplementary Figure S2 reported thermograms of raw materials and investigated PNP. Loaded-PNPs (yellow curve) and grafted-PNPs (brown curve) showed an endothermic peak at ~ 50 °C due to the typical endothermic peak of PCL polymer that occurred at about 57 °C.

AFM analyses displayed a general size increase for the labelled NPs, compared with the other PNPs, especially with grafted-PNPs (Figure 6). Such a data further proved the effective functionalization via both physisorption and chemisorption of PNPs with RhB, even if a reduced size of particles was shown respect to that estimated by dynamic light scattering (Figure 5). This fact was related to a collapse of the layer surrounding the nanoparticle surface, most likely due to the de-wetting process required for the AFM sample preparation. DLS, instead, measured the hydrodynamic size of the particle, which depends on both the particle “core” and the dye and solvation shell on the nanoparticle surface.

3.5. Surface PEG Density

The physicochemical properties, such as mean size, are fundamental aspects of ensuring the nose-to-brain drug delivery of colloidal systems. However, other surface properties could improve this process, such as the PEGylation degree. To evaluate the effective amount of PEG moieties on the surface of nanoparticle samples, a ^1H NMR study was carried out [20]. A calibration curve was carried out with PEG solutions in D_2O , in concentrations ranging between 10^{-5} and 10^{-3} M, by measuring the signal at 3.6 ppm and by using ethylenediamine (EDA) as internal standard.

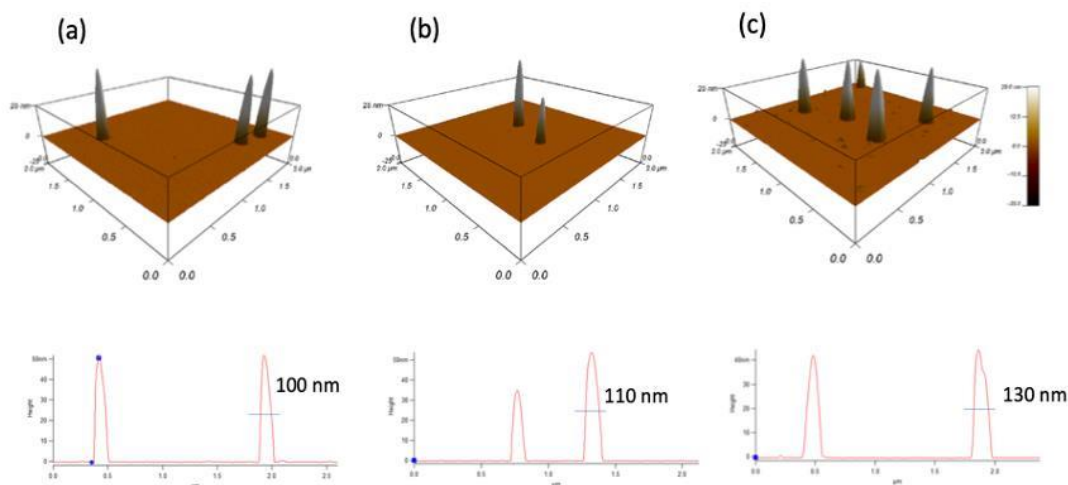


Figure 6. AFM 3D topography images, recorded in AC mode in air, for a PNP (a), a loaded-PNP (b) and a grafted-PNP (c) with the corresponding line-section curves.

By comparing the integrals of the PEG peaks in the spectra of nanoparticle sample dispersions in D₂O to the calibration curve, the quantity of PEG on the NPs surface was found. The data, reported in Table 2, showed that no significant differences in the nanoparticle surface PEGylation were found to depend on the chemical composition and RhB presence and/or entrapment method.

Table 2. Amount of PEG moieties on the NP surface, surface PEG density [Γ]. Number of PEG per 100 nm² and ratios of PEG density to full surface coverage [Γ/Γ^*] of PNP, loaded-PNPs and grafted-PNPs. Sample PEG amount on NP surface (mmol/100 mg) [Γ] (PEG chains/100 nm²).

Sample	PEG amount on NP surface (mmol/100 mg)	[Γ] (PEG chains/100 nm ²)	Γ / Γ^*
<i>PNP</i>	$2,79 \times 10^{-4}$	13.7	3.1
<i>Loaded-PNP</i>	$3,99 \times 10^{-4}$	8.4	1.9
<i>Grafted-PNP</i>	$4,86 \times 10^{-4}$	17.4	4.0

Surface PEG density [Γ] (number of PEG per 100 nm²), calculated as described in the experimental part and reported in the Table 2, demonstrated a high surface PEG density of all obtained samples.

To assess the surface PEG density and PEG chains' conformation on the NP surface, the number of unconstrained PEG molecules that occupy 100 nm² of particle surface area ξ , was calculated and expressed as [Γ^*]. Considering the Mw of PEG, it resulted to be 4.4 [21] [Γ/Γ^*] is an index to measure the PEG density on the nanoparticle surface: values < 1 indicates low PEG density where PEG molecules are in a mushroom-like conformation; whereas values >1 indicate high PEG density where PEG molecules are in a brush-like conformation. For all samples, [Γ/Γ^*] resulted to be higher than 1, indicating a high surface PEG density in all NPs, where PEG molecules were in a brush-like conformation. The PEGylation surface density of the NPs obtained

by incorporating the P-Fluo graft copolymer seems to be quite similar to that of the systems obtained without RhB, while the use of free RhB seems to reduce PEG exposure (more leaning towards mushroom hypothesis due to the purification process), although, in all cases, this PEGylation was high enough to allow only the brush like conformation on the surface, with long, thin bristles of PEG extending from the NP surface when the sample was hydrated.

3.6 Biological Studies

3.6.1 Cytotoxicity Study on OECs

The image 7A shows the OEC density grown with different NPs (PNP, loaded-PNP and grafted-PNP) at different concentrations (0.1, 0.5, 0.1 and 0.5 mg/mL). In Figure 7A are depicted cell viability percentages of the different nanosystems and in Figure 7B we showed the qualitative analysis by phase-contrast microscopy of representative fields of OECs. Our results demonstrated that PNPs were not cytotoxic toward OEC, as evidenced by no variation in cells' viability, the differences between the type of PNPs were not significant for all concentrations tested (Figure 7). In this experiment, OECs were chosen because they represent a special glial population of the olfactory system that accompanies the unmyelinated olfactory axons of receptor neurons. Our previous investigations focused on the possible uptake of the different NPs into OECs to realize a drug carrier for intranasal administration used for nose-to-brain delivery. NPs could be switched with neuronal cells to reach the brain via an anterograde axonal pathway; this hypothesis should be deeply investigated [9].

3.6.2 Cytotoxicity Effect on a Differentiated Pheochromocytoma Cell Line (d-PC12)

Dose-response effect on cell-growth and -death levels were performed to compare the cytotoxic activity of labelled NPs on a differentiated rat pheochromocytoma cell line (d-PC12).

Neural differentiation of PC12 has been widely used in neuroscience both in neurobiological and neurotoxicological studies as a neuronal cell model [28]. Following treatment with nerve growth factor (NGF) PC12 cells exhibit a typical phenotype of neuronal cells, sending out neurites and acquiring several features typical of sympathetic neurons. To address this, PC12 cells were treated with NGF over the course of one week to allow for neuronal differentiation [29]. Figure 8 shows the effect of 50 ng/mL NGF on PC12 cells and as expected, NGF activated the cells differentiation, forming a complex neuronal network.

To gain information on the biocompatibility of labelled of PNPs, loaded-PNPs and grafted-PNPs, d-PC12 cells were treated with them at different concentrations (15, 3, 1.5 mg/mL) for 24 h. Cell-viability data are reported in Figure 9. Figure 9 also shows that the unlabeled NPs' addition to the culture medium significantly decreased the number of cells at all studied concentrations, 15, 3 and 1.5 mg/mL ($86 \pm 4\%$, $81 \pm 3\%$ and $72 \pm 3\%$ of untreated control). It is important to note, both loaded-PNPs and grafted-PNPs did not show any significant difference at concentration 1.5 mg/mL, compared with the untreated control $93 \pm 5\%$ and $76 \pm 15\%$, respectively. At 3 and 15 mg/mL, both labelled PNPs induced a concentration-dependent decrease of PC12 cell viability, up to $66 \pm 15\%$, $61 \pm 6\%$ for 3 mg/mL, and $52 \pm 4\%$, $41 \pm 3\%$ for 1.5 mg/mL, respectively. We tested very high concentrations of NPs to simulate a potential accumulation of them in neuronal cells after more of one administration.

To understand if the toxicity of the studied PNPs depended on RhB's presence,

we examined RhB at the different concentration (2, 4, 20 μ M). It is important to note, that RhB at all tested concentrations did not decrease cell viability after 24 h of treatment (data not shown).

It has been reported that PC12 is a cell line that has been widely used as an in vitro model for investigating the neuronal oxygen sensor mechanism [30].

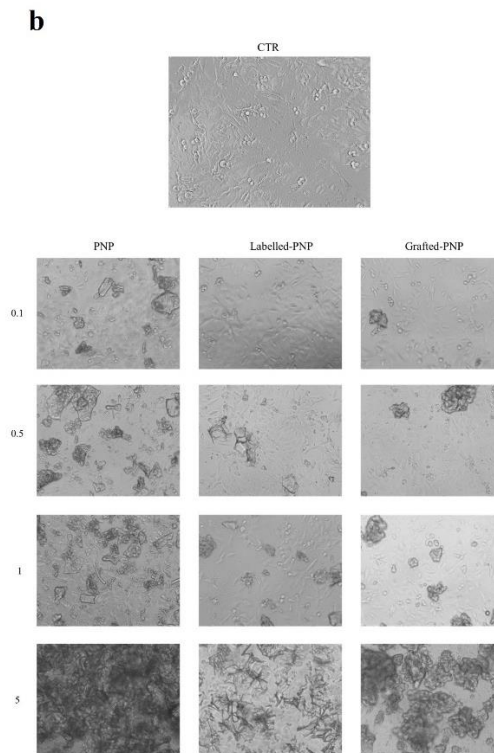
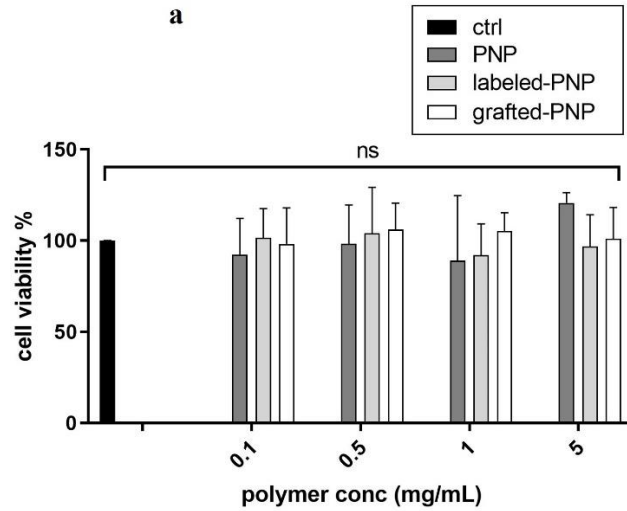


Figure 7. (a) Cell viability after exposure for 24 h of normal olfactory ensheathing cells (OECs) to PNPs, loaded-PNPs and grafted-PNPs at different concentrations, ns means not significant statistically **(b)** Qualitative analysis by phase-contrast microscopy of representative fields of OECs, both as control and loaded to PNP, loaded-PNP and grafted-PNP at different concentrations (0.1, 0.5, 0.1 and 0.5 mg/mL).

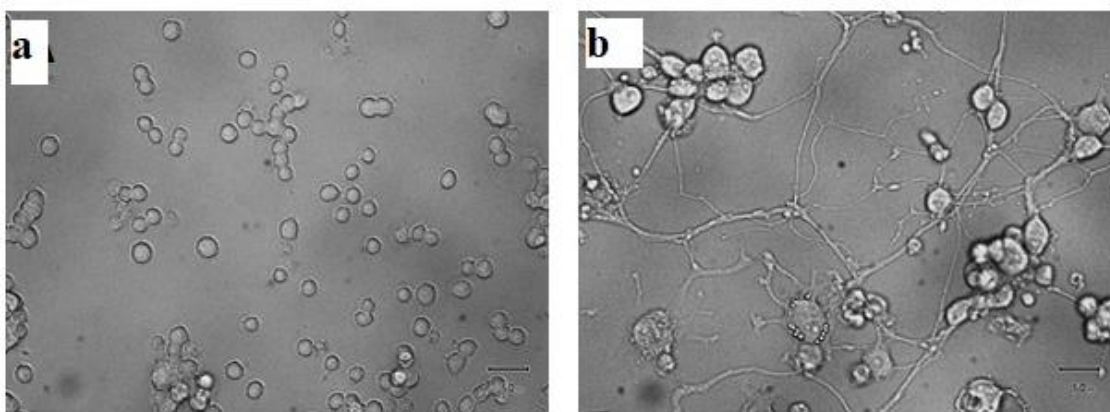


Figure 8. NGF-dependent neuronal phenotype differentiation of PC12 cells. Representative photomicrographs obtained by microscopy of PC12 cells untreated (a) or treated with 50 ng/mL NGF (b) for 72 h. Scale bar = 50 μ m.

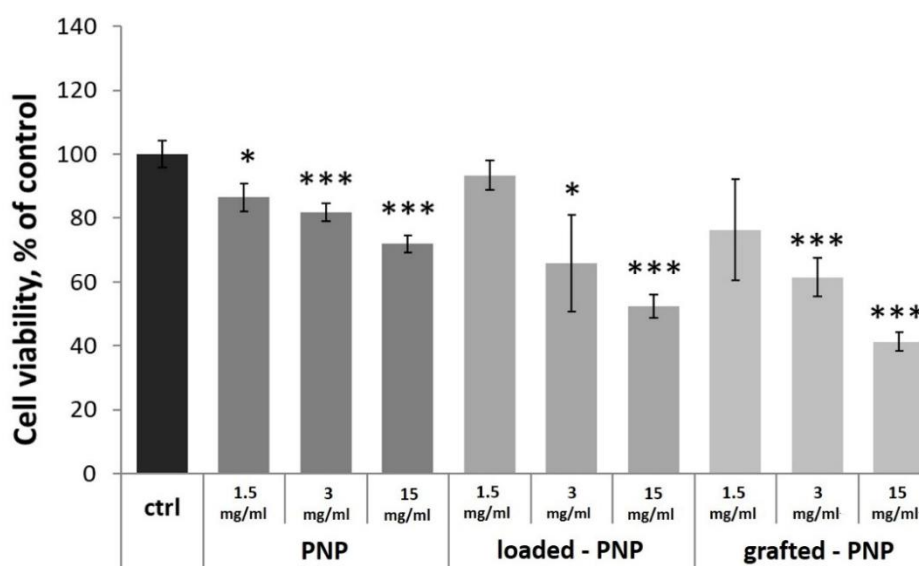


Figure 9. Dose-response experiment on d-PC12 cells. Cells were incubated for 24 h with PNPs. Results are presented as mean \pm SD and normalized with respect to the control untreated cells. (* $p < 0.05$; *** $p < 0.001$ versus control untreated cells, one-way ANOVA).

Here, intracellular ROS production was studied by using an oxidation-sensitive fluorescent probe dye (DCF), run to verify the damaging effects of NPs in the chosen neuron cell model. To quantify the level of intracellular ROS, such as H_2O_2 , $\cdot OH$ - and $ONOO^-$, we controlled DCF fluorescence, that, afterward, was normalized with Hoechst33342 nuclear stain to quantify the cell number for every well. Normal d-PC12 cells exhibited weak green fluorescence in the control group and the unloaded PNP group (data not shown). Results, shown in Figure 10, clearly demonstrated that loaded-PNPs and grafted-PNPs injured d-PC12 cells, depict enhanced green fluorescence, implying ROS accumulation in the injured cells. Especially, after the treatment with 3 and 1.5 mg/mL (polymer concentration in PNPs) of RhB-functionalized NPs, the DCF

fluorescence intensity was increased after 24 h treatment up to $133 \pm 16\%$ and $165 \pm 28\%$ for loaded-PNPs and $136 \pm 17\%$ and $155 \pm 11\%$ for grafted-PNPs. It is important to note that incubation with RhB did not show a damaging effect for the cells (data not shown).

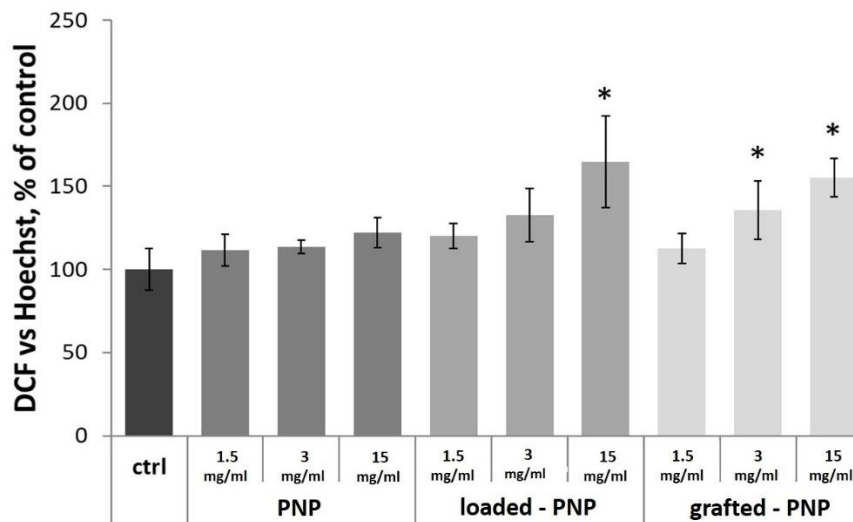


Figure 10. Detection of total ROS production in d-PC12 cells using DCF. Cells were treated 24 h with NPs and then analyzed by a Varioscan multimode microplate reader. Results are represented as the increase in DCF, normalized with live-cell fluorescent staining of DNA Hoechst33342, with respect to untreated control cells. Results are presented as mean \pm SD. (* $p < 0.05$ versus PEG-PLGA NP-3, one-way ANOVA).

It has been shown that RhB, due to the positive charges in its structure, is able to bind to certain DNA sequences, potentially causing genotoxicity. DNA damage stimulates ROS production in cell cultures [31,32]. ROS accumulation in cells treated with loaded- and grafted-PNPs at the highest concentrations could be attributed to a more effective internalization of the dye when delivered into the NPs [33].

Laser scanning confocal microscopy (LSM) analyses were carried out to image the actual internalization of loaded- and grafted-PNPs by the d-PC12 cells (Figure 11). Untreated cells (Figure 11a) and cells treated for 2 h with RhB (Figure 11b) or bare PNPs (Figure 11c) were added into the study as negative and positive controls, respectively.

A similar diffuse red emission was clearly visible in the cell cytoplasm for both cells treated with the fluorescent dye alone and those treated with RhB-loaded PNPs (Figure 11d). On the other hand, the cells treated with RhB-grafted PNPs (Figure 11e) exhibited a speckled, but still evident, red fluorescence, which was not observed in the cells untreated nor in those treated with bare PNPs.

The internalization of the labelled PNPs with the fluorescent dye RhB was quantified in d-PC12 cells exposed to 15, 3 and 1.5 mg/mL dilutions of each nanoparticle sample (Figure 12). It is known that RhB crosses biological membranes and can be used in microfluidic and microscopic applications [34]. In accordance with our results (Figures 4 and 5) and literature data, we analyzed d-PC12-treated cells for RhB intracellular fluorescence with an absorption peak centered at 554 nm, and an emission peak at 576 nm [35].

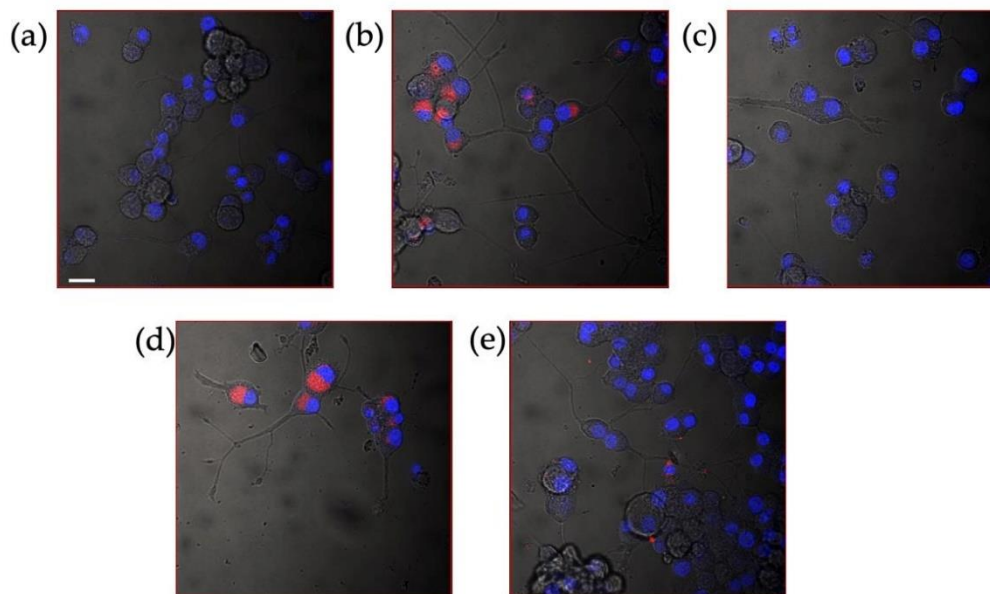


Figure 11. LSM-merged micrographs of bright field (in grey) and fluorescence (blue: Hoechst33342 nuclear staining, $\lambda_{ex}/\lambda_{em} = 405/425\text{--}450\text{ nm}$; red: Rhodamine B, $\lambda_{ex}/\lambda_{em} = 543/550\text{--}600\text{ nm}$) of *d*-PC12 cells untreated (negative control, (a) and after 2 h of treatment with: 4 μM RhB (positive control, (b), 3 mg/mL bare PNP (positive control, (c), 3 mg/mL RhB loaded-PNP (d), 3 mg/mL RhB grafted-PNP (e). Scale bar 20 μm .

As expected, control- and PNP-treated cells did not show any emission in red spectra. Figure 11 demonstrated that after the 24 h of incubation with both loaded- and grafted-PNPs increased the intracellular levels of fluorescence at 576 nm.

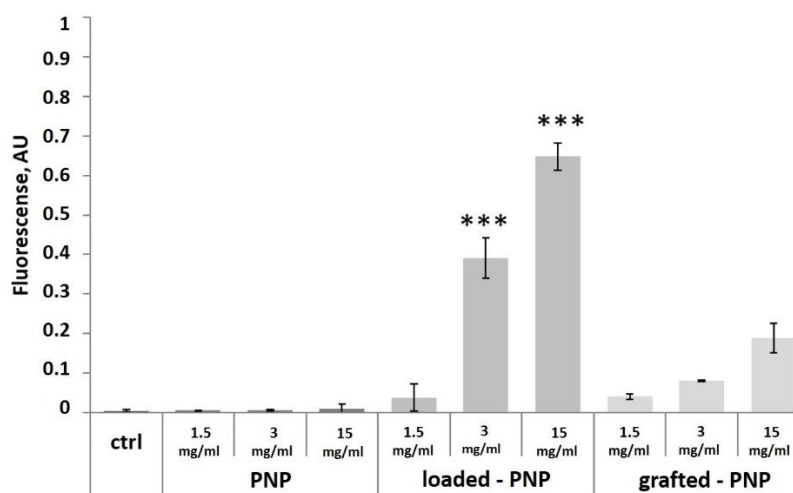


Figure 12. Detection of intracellular RhdB emission in *d*-PC12 cells. Cells were treated 24 h with NPs or RhB (data not shown) and then analyzed by a Varioscan multimode microplate reader. Results are represented as the increase in fluorescence, normalized with live-cell fluorescent staining of DNA Hoechst33342, with respect to untreated control cells. Results are presented as mean \pm SD. (***) $p < 0.001$ versus grafted-PNP, one-way ANOVA).

Important to underline that emission was significantly higher for loaded-PNPs

than for grafted-PNPs at all tested concentrations, because each type of formulation incorporated different amounts of dye. Our results suggested that both nanosystems are efficient for in vitro/in vivo investigations.

4. Conclusions

In this work, we have produced Rhodamine (RhB)-labelled NPs for in vitro/in vivo fluorescence imaging studies, a potentially useful carrier to investigate the nose-to-brain delivery administration route of drugs. The studied NPs were obtained by the nanoprecipitation method and by following two different strategies to entrap RhB into the PEG-PLGA nanoparticles (PNPs), i.e., the physical entrapment of free dye into the particles (loaded-PNPs) or the use of a graft copolymer, where RhB was covalently linked on the polymeric backbone (grafted-PNPs). The latter grafted polymer was obtained by covalent binding of the RhB on a polyaspartamide/polylactide graft copolymer backbone. The involvement of RhB in a covalent linkage was confirmed by UV-vis characterization studies on the polymer matrix, which showed a slightly shifted UV-vis peak compared to the loaded-PNPs matrix [20]. The obtained systems were characterized by PCS analysis showed suitable size for nose-to-brain delivery (<200 nm), homogeneous particle populations with PDI < 0.3, a negative surface charge (23.4 mV) and high PEGylation density with brush-like conformation in all investigated systems. The most appropriate purification process was centrifugation, which allowed removal of approximately 40% of the unencapsulated dye and allowed us to obtain a zero-dye release profile up to 72 h for loaded-PNPs. On the other hand, the labeling method of the grafted-PNPs, i.e., by the entrapment of RhB stably linked on the PHEA-g-RhB-g-PLA backbone, ensured the stability of the fluorescent dye inside the matrix, avoiding any diffusion process. Cell-viability tests on OEC cells showed the absence of cytotoxicity at all tested concentrations. Dose-dependent toxicity was observed in vitro studies on d-PC12 cells and was higher for grafted-PNPs than for loaded-PNPs. Although cytotoxicity studies revealed that loaded-PNPs showed lower cytotoxicity compared with grafted-PNPs, the level of ROS production was rather comparable between both investigated systems. Moreover, by in vitro studies we have demonstrated that both PNPs are internalized from cells as the endocellular fluorescence increases, as a function of the concentration of PNPs in the incubation medium. In conclusion, both RhB labelled nanocarriers described in this paper proved to be useful for potential in vitro/in vivo imaging after intranasal administration.

Supplementary Materials: The following are available online at <https://www.mdpi.com/article/10.3390/pharmaceutics13091508/s1>, Figure S1: UV-vis calibration curve for RhB in Milli-Q water determined at the wavelength of the maximum of absorbance ($\lambda = 552$ nm). Figure S2: DSC thermograms of PLGA-PEG (red curve), PHEA-g-RhB-g-PLA (black curve), RhB (blue curve) as raw materials, unlabeled PNPs (green

curve), loaded-PNPs (yellow curve) and grafted-PNPs (brown curve).

Author Contributions: Conceptualization, T.M.; Data curation, A.B., A.R. and L.M.C.; Formal analysis, A.R. and L.M.C.; Funding acquisition, T.M.; Investigation, E.F.C., A.B., R.P., I.N. and C.S.; Methodology, E.F.C., T.M. and C.S.; Project administration, E.F.C., T.M. and C.S.; Software, C.S.; Writing—original draft, E.F.C. and T.M.; Writing—review and editing, G.C. and C.S. All authors have read and agreed to the published version of the manuscript.

Funding: This research was funded by Ricerca di Ateneo 2020–2022, Piano di incentivi per la ricerca (PIA.CE.RI.) 2020–2022, Linea di intervento 1 CHANCE and 2 (Projects: 3N-ORACLE and GRABIO).

A. R. has been supported by the International Ph.D. program in Neuroscience, University of Catania, Italy. C.S. acknowledges funding by the Italian Ministry of University and Research (MUR) (PRIN call, project code: 2017WBZFHL).

Institutional Review Board Statement: The study was conducted according to the guidelines of the Italian law on animal care no. 116/1992 and in accordance with the European Community Council Directive (86/609/EEC) and were approved by the Ethical Committee at the University of Catania (Italy).

Informed Consent Statement: Not applicable.

Data Availability Statement: The data presented in this study are available on request from the corresponding author through email: teresa.musumeci@unict.it.

Conflicts of Interest: The authors declare no conflict of interest.

References

1. Illum, L. Transport of Drugs from the Nasal Cavity to the Central Nervous System. *Eur. J. Pharm. Sci.* **2000**, *11*, 1–18. [[CrossRef](#)]
2. Musumeci, T.; Bonaccorso, A.; Puglisi, G. Epilepsy Disease and Nose-to-Brain Delivery of Polymeric Nanoparticles: An Overview. *Pharmaceutics* **2019**, *11*, 118. [[CrossRef](#)] [[PubMed](#)]
3. Agrawal, M.; Saraf, S.; Saraf, S.; Antimisiaris, S.G. Nose-to-Brain Drug Delivery: An Update on Clinical Challenges and Progress towards Approval of Anti-Alzheimer Drugs. *J. Control. Release* **2018**, *281*, 139–177. [[CrossRef](#)] [[PubMed](#)]
4. Badhan, R.K.S.; Kaur, M.; Lungare, S.; Obuobi, S. Improving Brain Drug Targeting through Exploitation of the Nose-to-Brain Route: A Physiological and Pharmacokinetic Perspective. *Curr. Drug Deliv.* **2014**, *11*, 458–471. [[CrossRef](#)]
5. Dhuria, S.V.; Hanson, L.R.; Frey, W.H. Intranasal Delivery to the Central Nervous System: Mechanisms and Experimental Considerations. *J. Pharm. Sci.* **2010**, *99*, 1654–1673. [[CrossRef](#)] [[PubMed](#)]
6. Ul Islam, S.; Shehzad, A.; Bilal Ahmed, M.; Lee, Y.S. Intranasal Delivery of Nanoformulations: A Potential Way of Treatment for Neurological Disorders. *Molecules* **2020**, *25*, 1929. [[CrossRef](#)] [[PubMed](#)]
7. Tosi, G.A.; Musumeci, T.B.; Ruozi, B.A.; Carbone, C.B.; Belletti, D.A.; Pignatello, R.B.; Vandelli, M.A.A.; Puglisi, G.B. The “Fate” of Polymeric and Lipid Nanoparticles for Brain Delivery and Targeting: Strategies and Mechanism of Blood-Brain Barrier Crossing and Trafficking into the Central Nervous System. *J. Drug Deliv. Sci. Technol.*

- 2016, 32, 66–76. [[CrossRef](#)]
8. Lakkireddy, H.R.; Bazile, D. Building the Design, Translation and Development Principles of Polymeric Nanomedicines Using the Case of Clinically Advanced Poly(Lactide(Glycolide))-Poly(Ethylene Glycol) Nanotechnology as a Model: An Industrial Viewpoint. *Adv. Drug Deliv. Rev.* **2016**, *107*, 289–332. [[CrossRef](#)]
 9. Musumeci, T.; Pellitteri, R.; Spatuzza, M.; Puglisi, G. Nose-to-Brain Delivery: Evaluation of Polymeric Nanoparticles on Olfactory Ensheathing Cells Uptake. *J. Pharm. Sci.* **2014**, *103*, 628–635. [[CrossRef](#)]
 10. Dal Magro, R.; Ornaghi, F.; Cambianica, I.; Beretta, S.; Re, F.; Musicanti, C.; Rigolio, R.; Donzelli, E.; Canta, A.; Ballarini, E.; et al. ApoE-Modified Solid Lipid Nanoparticles: A Feasible Strategy to Cross the Blood-Brain Barrier. *J. Control. Release* **2017**, *249*, 103–110. [[CrossRef](#)]
 11. Musumeci, T.; Serapide, M.; Pellitteri, R.; Dalpiaz, A.; Ferraro, L.; Dal Magro, R.; Bonaccorso, A.; Carbone, C.; Veiga, F.; Sancini, G.; et al. Oxcarbazepine Free or Loaded PLGA Nanoparticles as Effective Intranasal Approach to Control Epileptic Seizures in Rodents. *Eur. J. Pharm. Biopharm.* **2018**, *133*, 309–320. [[CrossRef](#)]
 12. Craparo, E.F.; Porsio, B.; Mauro, N.; Giammona, G.; Cavallaro, G. Polyaspartamide-Polylactide Graft Copolymers with Tunable Properties for the Realization of Fluorescent Nanoparticles for Imaging. *Macromol. Rapid Commun.* **2015**, *36*, 1409–1415. [[CrossRef](#)]
 13. Bonaccorso, A.; Musumeci, T.; Serapide, M.F.; Pellitteri, R.; Uchegbu, I.F.; Puglisi, G. Nose to Brain Delivery in Rats: Effect of Surface Charge of Rhodamine B Labeled Nanocarriers on Brain Subregion Localization. *Colloids Surf. B Biointerfaces* **2017**, *154*, 297–306. [[CrossRef](#)]
 14. Zhu, Y.H.; Wang, J.L.; Zhang, H.B.; Khan, M.I.; Du, X.J.; Wang, J. Incorporation of a Rhodamine B Conjugated Polymer for Nanoparticle Trafficking Both: In Vitro and in Vivo. *Biomater. Sci.* **2019**, *7*, 1933–1939. [[CrossRef](#)]
 15. Li, J.; Liu, D.; Tan, G.; Zhao, Z.; Yang, X.; Pan, W. A Comparative Study on the Efficiency of Chitosan-N-Acetylcysteine, Chitosan Oligosaccharides or Carboxymethyl Chitosan Surface Modified Nanostructured Lipid Carrier for Ophthalmic Delivery of Curcumin. *Carbohydr. Polym.* **2016**, *146*, 435–444. [[CrossRef](#)] [[PubMed](#)]
 16. Netsomboon, K.; Bernkop-Schnürch, A. Mucoadhesive vs. Mucopenetrating Particulate Drug Delivery. *Eur. J. Pharm. Biopharm.* **2016**, *98*, 76–89. [[CrossRef](#)]
 17. Mendichi, R.; Giammona, G.; Cavallaro, G.; Giacometti Schieron, A. Molecular Characterization of α,β -Poly[(N-Hydroxyethyl)-DL-Aspartamide] by Light Scattering and Viscometry Studies. *Polymer* **2000**, *41*, 8649–8657. [[CrossRef](#)]
 18. Craparo, E.F.; Licciardi, M.; Conigliaro, A.; Palumbo, F.S.; Giammona, G.; Alessandro, R.; de Leo, G.; Cavallaro, G. Hepatocyte- Targeted Fluorescent Nanoparticles Based on a Polyaspartamide for Potential Theranostic Applications. *Polymer* **2015**, *70*, 257–270. [[CrossRef](#)]
 19. Bonaccorso, A.; Musumeci, T.; Carbone, C.; Vicari, L.; Lauro, M.R.; Puglisi, G. Revisiting the Role of Sucrose in PLGA-PEG Nanocarrier for Potential Intranasal

- Delivery. *Pharm. Dev. Technol.* **2017**, *23*, 265–274. [[CrossRef](#)] [[PubMed](#)]
20. Craparo, E.F.; Porsio, B.; Sardo, C.; Giammona, G.; Cavallaro, G. Pegylated Polyaspartamide-Polylactide-Based Nanoparticles Penetrating Cystic Fibrosis Artificial Mucus. *Biomacromolecules* **2016**, *17*, 767–777. [[CrossRef](#)] [[PubMed](#)]
 21. Xu, Q.; Boylan, N.J.; Cai, S.; Miao, B.; Patel, H.; Hanes, J. Scalable Method to Produce Biodegradable Nanoparticles That Rapidly Penetrate Human Mucus. *J. Control. Release* **2013**, *170*, 279–286. [[CrossRef](#)] [[PubMed](#)]
 22. Das, K.P.; Freudenrich, T.M.; Mundy, W.R. Assessment of PC12 Cell Differentiation and Neurite Growth: A Comparison of Morphological and Neurochemical Measures. *Neurotoxicol. Teratol.* **2004**, *26*, 397–406. [[CrossRef](#)] [[PubMed](#)]
 23. Pellitteri, R.; Catania, M.V.; Bonaccorso, C.M.; Ranno, E.; Dell'Albani, P.; Zaccheo, D. Viability of Olfactory Ensheathing Cells after Hypoxia and Serum Deprivation: Implication for Therapeutic Transplantation. *J. Neurosci. Res.* **2014**, *92*, 1757–1766. [[CrossRef](#)]
 24. Rabanel, J.M.; Hildgen, P.; Banquy, X. Assessment of PEG on Polymeric Particles Surface, a Key Step in Drug Carrier Translation. *J. Control. Release* **2014**, *185*, 71–87. [[CrossRef](#)]
 25. Sun, M.; Deng, J.; Tang, Z.; Wu, J.; Li, D.; Chen, H.; Gao, C. A Correlation Study of Protein Adsorption and Cell Behaviors on Substrates with Different Densities of PEG Chains. *Colloids Surf. B Biointerfaces* **2014**, *122*, 134–142. [[CrossRef](#)]
 26. Mallah, H.A.; Naoufal, D.M.; Safa, A.I.; El Jamal, M.M. Study of the Discoloration Rate of Rhodamine B as a Function of the Operating Parameters at Pt and BDD Electrodes. *Port. Electrochim. Acta* **2013**, *31*, 185–193. [[CrossRef](#)]
 27. Avnir, D.; Levy, D.; Reisfeld, R. The Nature of the Silica Cage as Reflected by Spectral Changes and Enhanced Photostability of Trapped Rhodamine 6G. *J. Phys. Chem.* **1984**, *88*, 5956–5959. [[CrossRef](#)]
 28. Teng, K.K.; Angelastro, J.M.; Cunningham, M.E.; Lloyd, G.A. Chapter 21 – Cultured PC12 Cells: A Model for Neuronal Function, Differentiation, and Survival. In *Cell Biology: A Laboratory Handbook*, 3rd ed.; Academic Press: Cambridge, MA, USA, 2006; Volume 1, pp. 171–176.
 29. Sierra-Fonseca, J.A.; Najera, O.; Martinez-Jurado, J.; Walker, E.M.; Varela-Ramirez, A.; Khan, A.M.; Miranda, M.; Lamango, N.S.; Roychowdhury, S. Nerve Growth Factor Induces Neurite Outgrowth of PC12 Cells by Promoting G β γ -Microtubule Interaction. *BMC Neurosci.* **2014**, *15*, 132. [[CrossRef](#)]
 30. Wu, Y.; Shang, Y.; Sun, S.G.; Liu, R.G.; Yang, W.Q. Protective Effect of Erythropoietin against 1-Methyl-4-Phenylpyridinium- Induced Neurodegeneration in PC12 Cells. *Neurosci. Bull.* **2007**, *23*, 156–164. [[CrossRef](#)]
 31. Islam, M.M.; Chakraborty, M.; Pandya, P.; al Masum, A.; Gupta, N.; Mukhopadhyay, S. Binding of DNA with Rhodamine B: Spectroscopic and Molecular Modeling Studies. *Dye. Pigment.* **2013**, *99*, 412–422. [[CrossRef](#)]
 32. Kang, M.A.; So, E.Y.; Simons, A.L.; Spitz, D.R.; Ouchi, T. DNA Damage Induces Reactive Oxygen Species Generation through the H2AX-Nox1/Rac1 Pathway. *Cell Death Dis.* **2012**, *3*, 1–8. [[CrossRef](#)] [[PubMed](#)]

33. Donini, M.; Gaglio, S.C.; Laudanna, C.; Perduca, M.; Dusi, S. Oxyresveratrol-Loaded PLGA Nanoparticles Inhibit Oxygen Free Radical Production by Human Monocytes: Role in Nanoparticle Biocompatibility. *Molecules* **2021**, *26*, 4351. [[CrossRef](#)]
34. Reungpatthanaphong, P.; Dechsupa, S.; Meesungnoen, J.; Loetchutinat, C.; Mankhetkorn, S. Rhodamine B as a Mitochondrial Probe for Measurement and Monitoring of Mitochondrial Membrane Potential in Drug-Sensitive and -Resistant Cells. *J. Biochem. Biophys. Methods* **2003**, *57*, 1–16. [[CrossRef](#)]
35. Bartasun, P.; Cies'lin'ski, H.; Bujacz, A.; Wierzbicka-Wos', A.; Kur, J. A Study on the Interaction of Rhodamine B with Methylthioadenosine Phosphorylase Protein Sourced from an Antarctic Soil Metagenomic Library. *PLoS ONE* **2013**, *8*, e55697. [[CrossRef](#)] [[PubMed](#)]

**CHAPTER V: *Fluorescent Nanosystems for Drug Tracking
and Theranostics: Recent Applications in the Ocular Field***



Review

Fluorescent Nanosystems for Drug Tracking and Theranostics: Recent Applications in the Ocular Field

Elide Zingale ^{1,†}, Alessia Romeo ^{1,†}, Salvatore Rizzo ¹, Cinzia Cimino ¹, Angela Bonaccorso ^{1,2}, Claudia Carbone ^{1,2}, Teresa Musumeci ^{1,2} and Rosario Pignatello ^{1,2,*}

¹ Department of Pharmaceutical and Health Sciences, University of Catania, 95124 Catania, Italy; elide.zingale@gmail.com (E.Z.); alessia.romeo@phd.unict.it (A.R.); salvo_rizzo@outlook.it (S.R.); cinzia.cimino@phd.unict.it (C.C.); angela.bonaccorso@unict.it (A.B.); ccarbone@unict.it (C.C.); teresa.musumeci@unict.it (T.M.)

² NANO-i—Research Center for Ocular Nanotechnology, University of Catania, 95124 Catania, Italy

* Correspondence: rosario.pignatello@unict.it

† These authors contributed equally to this work.

Abstract: The greatest challenge associated with topical drug delivery for the treatment of diseases affecting the posterior segment of the eye is to overcome the poor bioavailability of the carried molecules. Nanomedicine offers the possibility to overcome obstacles related to physiological mechanisms and ocular barriers by exploiting different ocular routes. Functionalization of nanosystems by fluorescent probes could be a useful strategy to understand the pathway taken by nanocarriers into the ocular globe and to improve the desired targeting accuracy. The application of fluorescence to decorate nanocarrier surfaces or the encapsulation of fluorophore molecules makes the nanosystems a light probe useful in the landscape of diagnostics and theranostics. In this review, a state of the art on ocular routes of administration is reported, with a focus on pathways undertaken after topical application. Numerous studies are reported in the first section, confirming that the use of fluorescent within nanoparticles is already spread for tracking and biodistribution studies. The first section presents fluorescent molecules used for tracking nanosystems' cellular internalization and permeation of ocular tissues; discussions on the classification of nanosystems according to their nature (lipid-based, polymer-based, metallic-based and protein-based) follows. The following sections are dedicated to diagnostic and theranostic uses, respectively, which represent an innovation in the ocular field obtained by combining dual goals in a single administration system. For its great potential, this application of fluorescent nanoparticles would experience a great development in the near future. Finally, a brief overview is dedicated to the use of fluorescent markers in clinical trials and the market in the ocular field.

Keywords: nanotechnology; fluorescence; ocular delivery; probes; diagnostics; PKs

1. Introduction

In recent years, vision-related problems have acquired a greater relevance due to the ageing of the world's population, which leads to an increase in visual problems, such as cataracts, glaucoma, age-related macular degeneration and diabetic retinopathy, occurring more frequently among over-60s [1,2]. Many visual diseases are associated with neurodegenerative disorders [3,4]. Young people over the age of 18 also suffer from visual problems, which increase especially with the growing use of electronic devices [5]. The rising number of people with vision impairment leads to a greater interest in dedicated care and treatments. This situation increases the costs in the global economy destined for the care of these disorders [6]. In addition, ocular

therapy is a serious challenge because of the difficulty in targeting a drug to the appropriate ocular tissues.

In this landscape, technological research is actively involved, with the aim of developing innovative systems for targeted drug delivery [7]. The eye is a very complex structure, both anatomically and physiologically, and the treatment of pathologies affecting this organ is therefore not simple [8–10]. This is related to the various aspects that limit the transportation of drugs to the target site: anatomical barriers, physiological processes, mechanisms and metabolic aspects [11,12]. Reaching the target becomes more complicated if therapy is addressed to the posterior segment of the eye [13–16]. For this purpose, the major administration route remains intravitreal injection, which is invasive and produces undesirable effects such as pain and discomfort, inducing patient noncompliance [17,18]. The preferred route of administration would undoubtedly be the topical one, but conventionally it is used to treat diseases of the anterior eye. In fact, it is estimated that only a very small percentage of the drug instilled in the eye surface reaches the anterior chamber (around 5%) and even less in the posterior segment [19–21].

Nanotechnology represents a field of recent interest to overcome these issues. One potential strategy for improving drug delivery to the different eye tissues uses nanocarriers with specific size and surface properties, designed to ensure successful achievement of the drug to the target tissue, as well as the potential for a controlled release of the loaded drug, reducing the frequency of treatment and improving the retention time on the corneal surface [22–24]. Currently, the most widely studied nanosystems are used in the treatment of anterior eye diseases such as cataracts [25], glaucoma [26], dry eye syndrome [27], keratitis [28], conjunctivitis [29] and uveitis [30], but also posterior eye diseases such as retinitis [31], macular degeneration [32], endophthalmitis [33] and ocular tumors [34]. Suitable drug nanocarriers possess a mean size in the nanometric range (around 200 nm) and are classified according to their structural composition and the materials used, which must be biodegradable and biocompatible [35,36]. Many reviews focus on the development of nanosystems designed for ocular delivery, but none on the ophthalmic use of fluorescent nanocarriers. It is not certain that after their administration, the drug effectively reaches the target site; therefore, during its design, tracking studies are necessary to demonstrate its distribution and positioning.

One possible strategy is to follow the nanosystem movements using a fluorescent probe. Fluorescence is a simple and non-invasive way to track the drug through the eye tissues, and it is also widely used in diagnostics to visualize diseased tissues, lesions and pathological markers. The development of personalized medicine and the need for early intervention in the diagnosis and treatment of specific diseases have promoted the birth and development of a new discipline: theranostics [37]. It can be defined as the combination of diagnostics with a specific therapeutic treatment. In vitro diagnostics and prognostics, in vivo molecular imaging, molecular therapeutics, image-guided therapy, biosensors, nanobiosensors and bioelectronics, system biology and translational medicine and point-of-care are some recent application examples.

This review deals with the use of fluorescent probes in the last 5 years applied to nanomedicine in the ophthalmic field. The aim is to illustrate state-of-the-art fluorescent nanosystems divided according to their application: fluorescent nanosystems for biodistribution studies to clarify the best performing nanoparticle design and delivery strategies able to address specific ocular diseases, for diagnostics

and finally, for the emerging field of theranostics. PubMed database was used to perform an advanced search. The time frame included the range from January 2017 to February 2022. The keywords used were “fluorescence”, “nanoparticles”, “ocular” and “delivery”, “theranostics”, “diagnostics”. Articles were limited to “Free full text” and “Full text” articles in the English language published in journals with an impactor factor not less than 4. The same process was repeated on ScienceDirect database. Reference lists of articles were also reviewed for additional citations.

General Aspect of the Human Eye

The eyeball consists of three chambers: anterior, posterior (containing the aqueous humor) and the vitreous chamber (containing the vitreous body). The wall is composed of three tunics [8,38]. The first, called external, is composed anteriorly of the cornea and for the remaining part of the sclera. The middle tunic (uvea) is richly vascularized and pigmented and includes the iris, the ciliary body and the choroid. Finally, the internal or nervous tunic is represented by the retina [39]. The sclera is anteriorly lined by the conjunctiva. Its function is to maintain the shape of the bulb and to provide attachment to the tendons of the striated muscles of the eye [40]. The cornea is a transparent lamina without vessels (necessary conditions for the passage of light). A cross-section of the corneal tissues is shown in Figure 1. Under the cornea, there is the iris, a sphincter of pigmented smooth muscle that regulates pupillary caliber. Trophism in this district is provided by the aqueous humor [41]. The ciliary body is an ocular anatomical structure responsible for both the production of aqueous humor and the control of accommodation. The ciliary body is located immediately posterior to the iris and anterior to the choroid. Posterior to the iris and in front of the vitreous body is where the crystalline is situated, which transmits and focuses light onto the retina. It consists of a single layer of epithelial cells that, during fetal development, migrate laterally toward the equator of the lens where it inverts, elongates, synthesizes large amounts of specific proteins and finally, degrades organelles so as to increase transparency [20]. From a physiological perspective, there are two reflexes involved in vision: lens accommodation (regulates convexity) and pupillary reflex (regulates pupil caliber). The accommodation allows the focal point to fall always at the level of the retina, allowing both short- and long-distance vision. Furthermore, the pupillary reflex regulates the intensity of incoming light. Finally, the transduction of light impulses at the retinal level into visual images is mediated by photoreceptors which generate nerve stimuli that reach the contralateral posterior cortex through the optic nerve [42–44]. The delivery of a drug into the eye tissues is related to two different routes of administration, which are divided into invasive and non-invasive routes. A list of these routes is shown in Table 1.

Table 1. Conventional route of ocular delivery: benefits and limits.

Administration Route	Benefits	Limits	Ocular Anterior/Posterior Target	References
Oral	Non-invasive. Increased compliance.	Difficult achievement of the anterior and posterior tracts of the eye. Possible degradation by digestive fluids. Possible low absorption and bioavailability. Hepatic first-pass metabolism. Presence of anatomical barriers (blood-aqueous barrier and the blood-retinal barrier).	Potentially both	[45-48]
Systemic (Intravenous and intramuscular)	Avoided first-pass metabolism.	Difficult achievement of the anterior or posterior segment of the eye. Lower compliance. Presence of anatomical barriers (blood-aqueous barrier and the blood-retinal barrier). Sterility of the final form	Potentially both	[48,49]
Parenteral (Intravitreal, subretinal, suprachoroidal, subconjunctival, intracameral, intrascleral, and intrastromal)	Deposit of the therapeutic agent in the eye, in some cases directly at the site of action. Increased local concentration of the drug. Reduced required dose and avoided off-target actions. Bypassing of ocular epithelium and other barriers, resulting in increased bioavailability.	Administration performed by specialized personnel. Invasive technique. Short-term complications, including retinal damage, endophthalmitis, haemorrhage, intraocular inflammation, and increased Intraocular Pressure (IOP). Sterility of the final form	Posterior	[50-55]
Topical	Over 90% of the ophthalmic product on the market.	Rapid precorneal elimination of the drug due to eyelid reflex, tear drainage, dilution by tears, and systemic absorption from the conjunctival sac. Misapplication of the product to the ocular surface. Presence of corneal epithelial barrier. Narrow barriers at the front and back of the eye (limit and regulate fluid and solute uptake). Complex kinetic processes of absorption, distribution and elimination, influenced by physiology, the physicochemical properties of the drug (lipophilicity, charge, size and shape of the molecule) and the formulation (pH, buffer, tonicity, viscosity, possible presence of preservatives and stabilizers). Allowed permeation of small lipophilic molecules through the cornea and of larger or hydrophilic compounds through the conjunctiva and the sclera. Achievement of the anterior segment for only 1% of the administered dose segment, and an even smaller percentage to the posterior segment. Sterility of the final form	Both	[56-64]

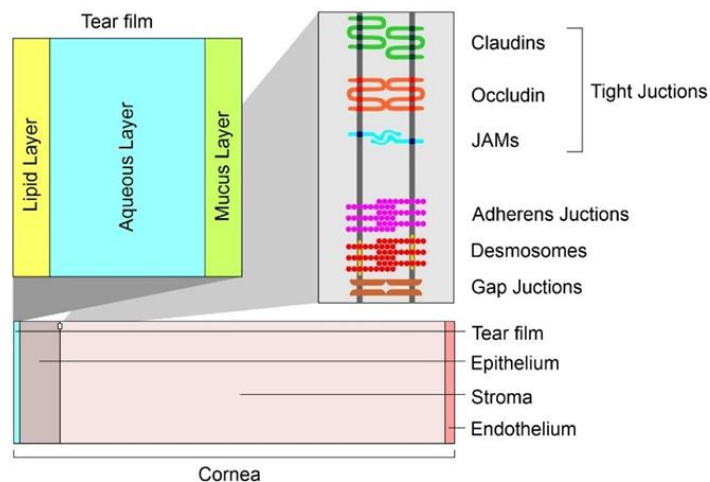


Figure 1. Cross-section of corneal tissues: barriers to drug penetration after topical instillation.

The corneal epithelium and endothelium (lipophilic in nature) consist of cells connected by tight junctions that limit the passage of large molecules (Figure 1). The hydrophilic stroma consists of tightly packed collagen. The epithelium, however, provides the greatest resistance to diffusion. The paracellular pathway through the intercellular pores is allowed for small ionic and hydrophilic molecules of size <350 Da, whereas the transcellular pathway allows the passage of larger lipophilic molecules. The variations in lipophilicity of the corneal layers allowed the realization of a parabolic relationship between corneal permeability and diffusion coefficient. pH is another important factor in corneal permeability [38]. Many studies that have examined permeability across conjunctiva, tenon and sclera have shown that the conjunctiva is more permeable to hydrophilic molecules than the cornea. The greater surface area (in humans, about 17 times bigger than the cornea) and the presence of larger pore sizes promote increased permeability compared to the cornea. However, mucus and the presence of lymphatics and vasculature increases systemic leakage [24,38]. In ocular topical administration, reaching the posterior portion is size-dependent [65]. Nanocarriers with a diameter of 20–200 nm are suitable for retinal-targeted delivery. Small nanoparticles (20 nm) are able to cross the sclera and are rapidly eliminated due to periocular circulation. The larger ones (200 nm) do not cross the sclera or the sclera-choroid-retinal pigment epithelium (RPE) and remain in the periocular site releasing their contents even for long periods. Even in the case of intravitreal administration, the kinetics are size-dependent. Nanocarriers with a diameter of 2 μm remain in the vitreous cavity or migrate into the trabeculae. Those with a diameter of less than 200 nm reach the retina [66]. In order to discuss the application of nanosystems in the ocular field, an emergent role is represented by fluorescent nanosystems. The tailor ability of design, architecture and photophysical properties has attracted the attention of many research groups, resulting in numerous reports related to novel nanosensors to analyze a great variety of biological analytes.

2. Fluorescent Probes in Ocular Applications

Before focusing on the published experimental studies, in this section, a brief discussion on fluorescence and on the molecules applied in the ocular field is given. Absorption of a photon from a fluorescent chemical species causes a transition to an excited state of the same multiplicity (spin) as the fundamental state (S₀). In solution, S_n states (with n > 1) rapidly relax to S₁ through nonradiative processes. Ultimately, relaxation from S₁ to S₀ causes the emission of a photon with an energy lower than the absorbed photon. The fluorescence quantum yield (ϕ), one of the most important parameters, provides the efficiency of the fluorescence process; it is defined as the ratio between the number of photons emitted to those absorbed.

$$\phi = \frac{\text{Number of photons emitted}}{\text{Number of photons absorbed}}$$

In Figure 2, we reproduce a brief history of the discovery of the fluorescence phenomenon. This discovery enabled the development of fluorescent probes that achieve single-molecule sensitivity. The figure shows that the first observation of a fluorescence phenomenon was described in 1560 by Bernardino de Sahagun; the same experiment was repeated by Nicolas Monardes in 1565. The fluorescence of the infusion known as lignum nephriticum was observed. This phenomenon was caused by the fluorescence of the oxidation product of one of the flavonoids present in those woods: matlaline. In the middle of the nineteenth century, George Gabriel Stokes coined the term fluorescence, derived from fluorite. The knowledge of atomic structure needed to understand and describe the nature of the phenomenon was not acquired until the beginning of the 20th century. By providing detailed information, this technique has enormous advantages over classical microscopy techniques [67]. In fact, literature is plentiful of studies dealing with the design of new fluorescent probes such as (bio)sensors to detect (even with the naked eye) enzymes, metals, biomaterials and others. Since 1945, the ability of analytes to promote the opening of rhodamine spirolactams has been exploited to design probes that detect metal ions and biological targets [68,69]. The pH sensitivity of fluorescein can be used to detect changes in a specific environment. By controlling the balance of ring-opening and ring-closing, following the interaction with specific targets, it can be used to detect metal ions from industrial and commercial specimens [70]. Curcumin is also widely used as a fluorescent probe for different applications, from producing drug carriers to the realization of specific sensors for ions and biomolecules [71,72].

The following section delineates the family of fluorescent probes reported in reviewed studies, while Table 2 gathers the probes that are used in the experimental papers cited in this review.

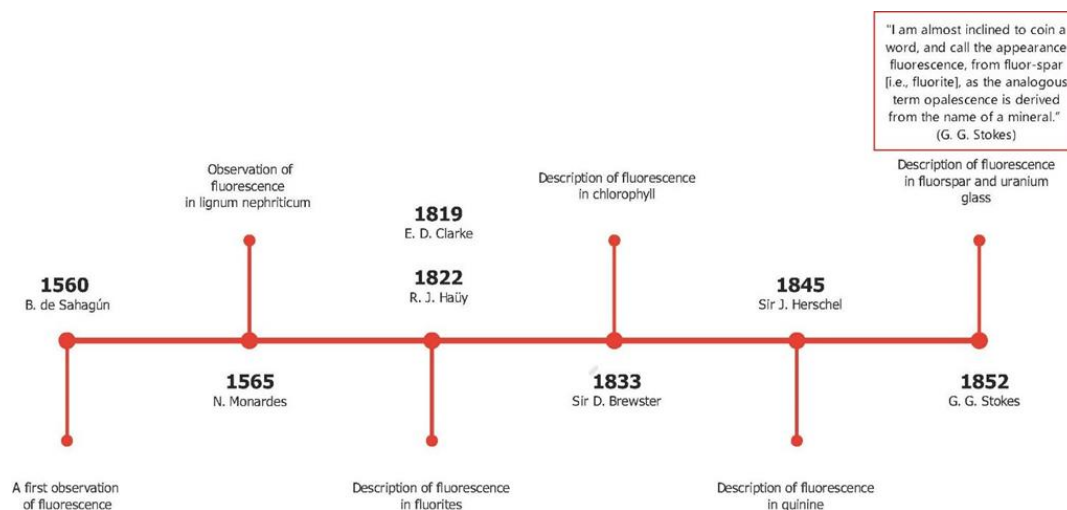
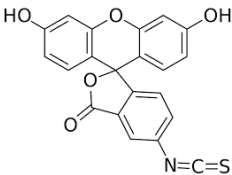
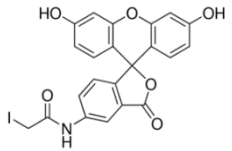
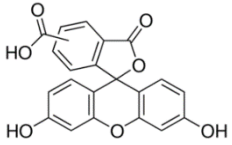
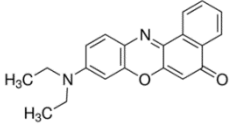
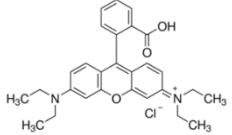
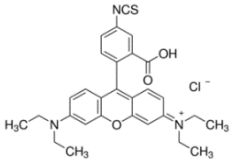
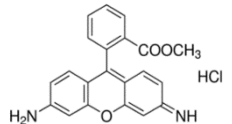
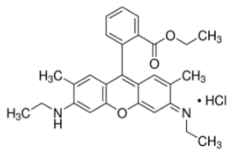
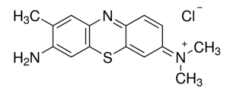


Figure 2. Timeline of the fluorescence discovery.

Table 2. Physico-chemical properties of the main fluorescent probes used in ocular bioimaging.

Probe	Chemical Structure	Molar Mass (g mol ⁻¹)	Solubility in Water	Excitation (nm)	Fluorescence (nm)
Coumarin-6		350.43	Insoluble	488–666	502–649
Curcumin		368.38	Insoluble	300–470	571
Cyanine 5-phosphoramidite		944.21	Insoluble	649	666
1,1'-di-octadecyl-3,3,3',3'-tetramethylindocarbocyanine perchlorate		933.87	Low	550	565–588
Fluorescein		332.31	Insoluble	465–490	494
Fluorescein sodium salt		376.27	Soluble	460	512
5-aminofluorescein		347.32	Soluble	450–490	500–550

Fluorescein-5- isothiocyanate		389.38	Insoluble	495	519
5- (iodoacetamido) fluorescein		515.25	Insoluble	492	518
5(6)-carboxy- fluorescein		376.32	Low	495	520
Nile Red		318.37	Insoluble	543-633	550-700
Rhodamine B		479.01	Soluble	488-530	600-633
Rhodamine B isothiocyanate		536.08	Insoluble	553	563-650
Rhodamine 123		380.82	Low	488	515-575
Rhodamine 6G		479.01	Soluble	480	530
Toluidine Blue O		305.83	Soluble	595	626

2.1 The Coumarins Family

Coumarins have a conjugated double ring system. In the industry, coumarins find application as cosmetic ingredients, perfumers, food additives and in synthetic pharmaceuticals. In nature, coumarins are found in a wide variety of plants: tonka bean (*Dipteryx odorata*), sweet wood (*Galium odoratum*), vanilla grass (*Anthoxanthum odoratum*) and sweet grass (*Hierochloe odorata*) [73]. Among the different synthetic derivatives, Coumarin-6 (C6) exhibits acid-base properties. In the study of Duong et al., a membrane with C6 demonstrated to exhibit colorimetric and ratiometric fluorescence

properties with a dynamic pH range between 4.5 and 7.5 (the study uses blue Nile in parallel) [74].

2.2 Fluorescein Family

Fluorescein is a xanthene dye with yellowish-green fluorescence. It was first synthesized in 1871 by von Bayer via Friedel's acylation/cyclodegradation reaction using resorcinol and phthalic anhydride [75]. It has a rigid tricyclic-coplanar structure with two aryl groups fused to a pyran ring. It has two distinct structures, an open fluorescent ring in the carboxylic acid form and a closed non-fluorescent ring in the spirocyclic lactone form. The open-closed equilibrium in the structure of fluorescein makes it sensitive to the pH of the medium [76]. Among the amine derivatives of fluorescein, those with one or two NH_2 groups in the phthalic residue are of particular interest. The corresponding (di)anions do not show intense fluorescence unless the amine groups are involved in new covalent bonds. In alcohols, the quantum yield, ϕ , is quite low. In dimethylsulfoxide (DMSO), acetone and other hydrogen bond donor solvents, ϕ values approach dianionic values [77]. Its sodium salt form finds wide use in angiography [78,79] and glioma studies [80]. Fluorescein 5(6)-isothiocyanate has been used for fluorescence labeling of bacteria, exosomes, proteins (immunofluorescence) and H Protein for gel chromatography. The 5-(iodoacetamido)-fluorescein is used for the synthesis of fluorescently labeled organelles, proteins, peptides and enzymes. Finally, the 5(6)-carboxyfluorescein, a fluorescent polyanionic probe, was used to measure changes in intracellular pH and to highlight processes such as dendrimer aggregation and absorption [81].

2.3 Rhodamine Family

These compounds were discovered in 1887. In the 4–10 pH range, their fluorescence spectra are unaffected by changes. The typical chemical structure of rhodamines involves three benzene rings, whose spirocyclic/open-ring conversion results in their off/on fluorescence [82]. In nonpolar solvents, they exist as spironolactone forms with very low ϕ due to disruption of p-conjugation of the xanthene core. In polar solutions, the lactone form undergoes charge separation to form a zwitterion [68]. In open-loop forms, rhodamine dyes exist as ammonium cations that can be driven into mitochondria via MMP (Matrix MetalloProteinase). A famous example is rhodamine 123, which forms the basis of the Mito-Tracker dye [83]. Lastly, the rhodamine 6G is a rhodamine analog useful in Pgp (P-glycoprotein) efflux assays, and it has been used to characterize the kinetics of MRP1 (multidrug resistance protein 1)-mediated efflux. An *in vivo* study of rhodamine B-labeled polymeric nanoparticles was conducted by Bonaccorso et al. to evaluate the distribution in brain areas after intranasal administration of the formulation [84].

2.4 Cyanine Family

Cyanine dyes are among the most widely used families of fluorophores. Cyanine 5 (Cy5) has five carbon atoms in the bridge. It becomes reversibly photocommutable between a bright and dark state in the presence of a primary thiol [85]. Cy5 excited by visible light undergoes thiolation with a thiol anion and transforms into a non-fluorescent thiolated Cy5. The thiolated Cy5 returns to the light-emitting dethiolated form simply by UV irradiation [86]. The photophysical properties of organic dyes with rotatable bonds are strongly governed by their internal rotation in

the excited state since rotation can greatly affect molecular conformation and bond conjugation [87]. In the biological field, it finds use in comparative genomic hybridization, transcriptomics in proteomics, and RNA localization [88]. Moreover, DiI is a cyanine-derived dialkyl carbon sensitive to the polarity of the environment. It is weakly fluorescent in water but highly fluorescent in nonpolar solvents. It is commonly used as a lipophilic marker for fluorescence microscopy in the biological field. DiI molecules penetrate in cell membranes with the 2 long alkyl chains (12 carbons) immersed in the bilayer and the rings parallel to the bilayer surface. The dye emits characteristic bright red fluorescence when its alkyl chains are incorporated into membranes making it particularly useful for tracking in the biological membrane [89]. In the study by Musumeci et al. the 1-1'-dioctadecyl-3,3,3',3'-tetramethylindotricarbocyanine iodide dye was used to label polymeric nanoparticles and study their cerebral delivery after intranasal administration [90].

2.5 Nile Red

Nile red is a hydrophobic dye of recent interest in the identification of microplastics [91]. It is widely used in biophysical studies focusing on proteins, lipids and live-cell analysis. Depending on the environment, Nile Red shows different absorption and fluorescence spectra. In particular, in organic solvents or nonpolar environments, it shows strong fluorescence that changes depending on the environment, presenting shifts toward blue emission in nonpolar environments [92].

2.6 Curcumin

Curcumin is the main natural polyphenol found in the rhizome of *Curcuma longa* (turmeric) and in others *Curcuma* spp. Its countless benefits in the treatment of inflammatory states, metabolic syndrome, pain and inflammatory-degenerative conditions of the eyes are related to its antioxidant and anti-inflammatory effects [93]. Theoretical studies have predicted that its wide absorption band (410 and 430 nm) is due to the π - π^* transition, while the maximum absorption between 389 and 419 nm is related to the keto and enol form, respectively [67].

2.7 Toluidine Blue O

Toluidine blue (TB) is a thiazine-based metachromatic dye. It has a high affinity for acidic tissue components. This characteristic allows colorimetric identification of DNA- and RNA-rich tissues [94]. In the ocular field, Navahi et al. performed a study on the use of TB in the diagnosis of ocular surface squamous neoplasm (OSSN) [95]. In the Su et al. study, in vivo antibacterial efficacy of TB-mediated photodynamic therapy on bacterial keratitis by *Staphylococcus aureus* in a rabbit was demonstrated. This provides a new option for the clinical treatment of bacterial keratitis [96].

3. Fluorescent Nanosystems in Ocular Application

The following section is focused on recently investigated fluorescent nanomaterials and nanosystems for ocular applications. The reviewed works have been divided according to the use of such fluorescent nanosystems. Most studies concern the use of probes to assess nanosystems distribution within the ocular tissues. Among the most investigated fluorescent nanosystems, there are lipid-based nanocarriers – such as nanostructured lipid carriers (NLCs) and solid lipid nanoparticles (SLNs), polymeric nanoparticles and nanocapsules, hybrid nanoparticles, cubosomes, emulsomes, nanoemulsions, niosomes, liposomes, films, nanomicelles and hydrogels. Fluorescence is introduced through the

methods commonly used to prepare nanosystems [97,98]. The fluorescent nanosystems are essentially divided into (i) probe-loaded, in which the dye or probe is encapsulated into the system mostly during the formulation processes, and (ii) labeled/grafted, in which the probe is covalently bound to the surface of the nanosystem (often linked to some matrix component, such as polymers or lipids), always forming an adduct (Figure 3).

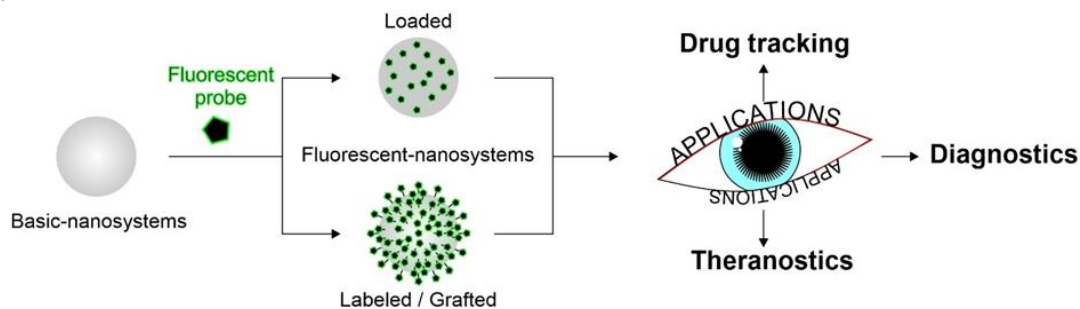


Figure 3. Schematic structure of fluorescent nanosystems for ocular applications.

3.1 Biodistribution

As above cited, the tissues that compose the eye are many and with different properties. The difficulty for a nanosystem to reach the target tissue is high; thus, the profile of drug delivery is not always predictable. When the target is located in deeper ocular tissues, it is even more difficult to predict the ideal pathways followed by the carriers in vivo and through the ocular barriers. Tracking the drug after topical administration is important for several factors. Firstly, it allows for assessment of the effective achievement of the target site in order to accomplish the desired therapeutic action. Another factor to consider is the non-productive distribution of the drug in non-desired tissues, which could lead to the possible occurrence of side effects in addition to reducing the effective drug concentration. Furthermore, studying the pathways followed by the nanosystems is necessary to avoid issues related to barriers, tight junctions and physiological phenomena (tear flow and blinking), which could impair the routes. Size, surface charge and morphology of the nanocarriers have a great influence on their biodistribution, clearance and cellular uptake [99–102]. Before performing biodistribution studies, it is important to characterize the system and to proceed with in vitro and in vivo assays. For instance, mean size measurement, zeta potential, mucoadhesion studies and morphological analyses are, of course, also required to make the system as conformable as possible to a correct drug release. Tracking of nanosystems can be carried out in two ways, invasive and non-invasive; bioimaging using fluorescent molecules is a non-invasive method [103,104]. Among the most important characteristics that the nanosystem should have are small size, necessary to enter cells for allowing bioimaging, high sensitivity for effective detection, fast response, compatibility, absence of toxicity, good dispersibility in the biological environment and highly selective detection in the tissues. In Figure 4, a summary is gathered of the fluorescent probes used in the studied nanosystems discussed in Sections 3.1–3.3.

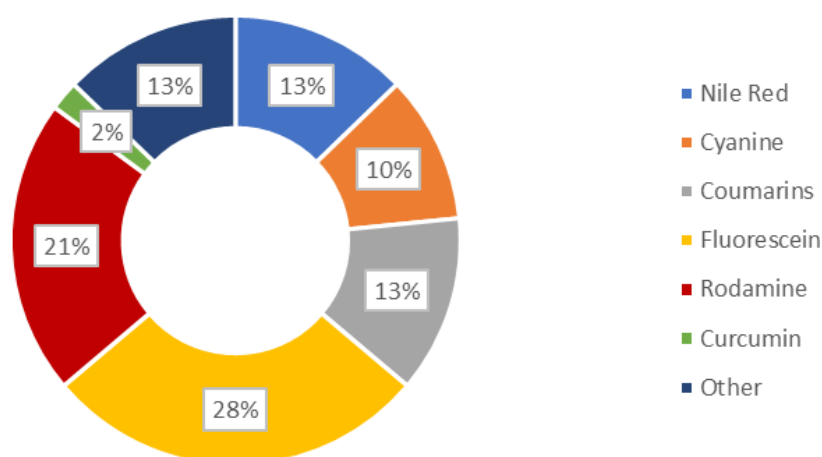


Figure 4. Graphical analysis of the fluorescent probes discussed in this review.

3.1.1 Fluorescent Lipid-Based Nanosystems

Lipid systems are of great interest for drug delivery in ocular tissues; their biocompatible and biodegradable composition makes them technologically safe, while their lipidic nature and structural characteristics allow them to pass through the corneal layers and achieve an efficient drug dosage even in the deepest tissues of the eye. The distribution of these systems occurs mainly in lipophilic layers, with minimal involvement of the stroma, since it has hydrophilic nature, and the lipid systems are difficult to distribute there. This was confirmed in the work of Namprem et al., in which confocal scanning microfluorometer (CSMF) analysis confirmed poor penetration of NLC labeled with Nile Red in hydrophilic compartments such as the stroma compared to corneal layers [105]. Due to eye barriers and obstacles to ocular administration, understanding the path taken by the designed nanosystem is necessary, especially if it is targeted to the back of the eye. The main route through which lipid systems reach the deeper tissues is the transcorneal one. There is growing evidence that successful drug delivery by functionalized nanocarriers depends largely on their efficient intra/paracellular transport, a process that is not fully understood yet. Therefore, the development of new imaging and diagnostic techniques is very important, particularly in a complex biological system such as the eye. Due to its lipophilic nature, one of the most used dyes for the preparation of fluorescent-lipid nanosystems is Nile Red (NR) Cubosomes labeled with Nile Red were prepared in the work of El Gendy et al. to assess the role of nine different lipids as penetration enhancers. The type of lipid used in the preparation plays an important role in tissue distribution. Among the prepared lipid systems, fluorescence analysis showed that the combination of oleic acid, Captex® 8000 and Capmul® MCM improved the penetration of the systems into the mucosa by increasing diffusivity due to both surfactant properties and the ability to disrupt the organization of the lipid bilayer [106]. Once again, Nile Red was used in the work of Kapadia et al. in order to visualize drug-loaded emulsomes. For the physico-chemical characterization and subsequent analyses, the nanosystems were loaded with triamcinolone acetonide, while for the studies of precorneal retention and ocular distribution, the fluorescent dye was loaded instead of the drug. The study revealed that after topical administration, the pathways taken to reach the back of the eye were basically three: corneal (via the iris and aqueous humor), conjunctival and systemic. The drug may diffuse through the sclera by lateral diffusion, followed by penetration of Bruch's membrane and retinal

pigment epithelium (RPE). To a lesser extent, the drug may be absorbed into the systemic circulation either through the conjunctival vessels and the nasolacrimal duct, and gain systemic access to the retinal vessel [107]. Another lipophilic DiI dye (1,1-dioctadecyl-3,3,3 tetramethyl indocarbocyanine perchlorate) was used to label lipid nanocapsules (LNCs) fluorescently. An important finding was made in the study by Eldesouky et al., where, despite the lipophilic nature of the dye, better penetration was achieved by encapsulation in lipid systems compared to simple dispersion. Fluorescence analysis showed that, without the use of lipid nanocarriers, the dye is unable to cross the hydrophobic corneal layer [108]. Mucoadhesion plays a key role in the enhancement of bioavailability. Efforts are made to design systems that have the ability to improve retention on the ocular surface. In this respect, the use of chitosan to improve the delivery of drugs into the eye tissues for its properties as a mucoadhesive agent, controlled drug release and permeation enhancer is interesting [24]. It is used in conjugation with a drug, such as in the study of Dubashynskaya et al., to improve the intravitreal delivery of dexamethasone [109]. In the major cases, it was used as a coating of nanocarriers to promote intraocular penetration, as reported by which designed modified NLCs with three different types of chitosan: chitosan acetyl-L-cysteine (CS-NAC), chitosan oligosaccharides (COS) and carboxymethyl chitosan (CMCS). The distribution profile was evaluated by loading the hydrophobic dye C6 into the NLCs. It was revealed through CLSM analysis that only NLCs modified with COS and CS-NAC were able to pass the cornea through the opening of tight junctions between epithelial cells [110]. Rhodamine-labeled NLCs were used to assess the corneal retention of such lipid nanocarriers, modified with a complex containing boronic acid, which is able to bind with high affinity the sialic acids of mucin. The NLCs were loaded with dexamethasone and designed for the treatment of dry eye syndrome. Fluorescence marking revealed the increased retention time due to the mucoadhesive property of the nanosystem, which also proved to be a potential not irritant treatment for dry eye syndrome [111]. Another key factor that improves retention time on the ocular surface is the positive charge of nanosystems interacting with the negative charges of mucin. The addition of octa-arginine (R8) to the nanoemulsions prepared by Liu et al. imparted a positive charge to the system with the aim of increasing eye retention. Once again, C6 was used to label lipid emulsions of disulfiram. In particular, the permeation of these systems under the influence of particle size and the presence of R8 was investigated and revealed that the addition of R8 and a size of ~50 nm improved the ocular delivery performance of nanosystems. In addition, the study showed that C6 passed through the corneal epithelium mainly by paracellular pathways, but there was also a fluorescent signal in the cytoplasm, indicating a transport also by transcellular pathways [112]. The internalization of lipid nanoparticles occurs mainly through an endocytosis mechanism. This is in fact the route taken by the mRNA-based solid lipid nanoparticles prepared by Gómez-Aguado et al. The SLN were developed in order to produce IL-10 to treat corneal inflammation and was loaded with Nile Red to assess cellular uptake in corneal epithelial cells (HCE-2 cells). This platform could also be used as a theranostic model as GFP (green fluorescent protein) is produced inside the cells, so the intensity of the fluorescence is indicative of the amount of protein produced. Since GFP, once produced, remains at the intracellular level, instillation on the ocular surface of mice of the samples permitted the identification of the corneal layers where transfection occurred. All the prepared mRNA-based SLN formulations showed higher fluorescence intensity than naked mRNA, demonstrating the enhancement of their

targeting ability [113]. Fluorescein is one of the most widely used fluorescent dyes for drug tracking and visualization of ocular damage following treatment. In Section 4, some clinical trials using fluorescein as a fluorescent in the study will be proposed. Fluorescein was used by Jounaki et al. for tracking vancomycin loaded NLCs. The aim of the work is the idea that NLCs for topical use could be a valid substitute of intravitreal injection in the treatment of bacterial endophthalmitis caused especially by *Staphylococcus*. Both drug-loaded and fluorescein-loaded NLCs (0.2 mg/mL) were prepared by cold homogenization technique and were used to evaluate precorneal retention with an inverted fluorescent microscope. The increased fluorescence found in the corneal epithelium demonstrated that dye-loaded, stearylamine-coated NLCs were retained more in the ocular surface. Indeed, the cationic lipid stearylamine is trapped in the mucin layer and retained due to the interaction between the fillers, facilitating the penetration and delivery of the drug to the intraocular tissues [101]. In the work of Kakkar et al., fluorescein was also used in concentrations almost like the previous work (0.25 mg/mL) to track hybrid nanoparticles. Solid lipid nanoparticles were prepared and then coated with PEG in order to encapsulate the antimycotic fluconazole. Analysis to assess the penetration into the ocular internal layers revealed that fluorescence was observed in the vitreous humor, retina, sclera and choroid after instillation of a single drop of Fluconazole-SLNs into the rat eye. In addition, the ex vivo study showed that the system exhibited a 164.64% higher flux through the porcine cornea when compared to the commercial drops ZoconVR [114]. In addition to coating the nanosystems, fluorescein was used to label them binding it covalently to the material of the nanosystem. In the work of Puglia et al. [66] an adduct is prepared between fluorescein and stearic acid named ODAF (N-(30,60-dihydroxy-3-oxospiro[isobenzofuran-1(3H),90-[9H]xanthen]-5-yl]-octadecanamide). In this case, the dye was grafted (and not loaded) and the conjugation of the lipid with the dye leads to a fluorescent probe. Solvent-diffusion technique was used to prepare SLNs of about 120 nm. The in vivo distribution from 1 h to 16 h was evaluated in rabbits and the results showed that, after ocular instillation, ODAF SLNs were mostly located in the cornea (up to 2 h), whereas over a longer time (from the second hour to the eighth hour) the fluorescent signal gradually extended toward the back of the eye, confirming the ability of controlled delivery by the lipid nanosystems [66].

Considering that the influence of blinking and tearing on ocular drug absorption was rarely evaluated in studies, Pretor et al. evaluated absorption of two lipid-based formulations, a liposome and a SLN, in presence of these two physiological conditions. The SLNs were also labeled with a fluorescent phospholipid, thus constituting another example of a grafted nanosystem. From the study, using C6 as the fluorescent compound, it is evaluated that liposomes are shown to provide a greater absorption, despite the influence of blinking (shear stress of 0.1 Pa.) and tear flow. This interesting study was carried out by coupling the use of microfluidics with channels and cultured HCE-T cells as well as the use of a fluorescent dye to simulate the physiological mechanisms; it could be useful to add this kind of assay to the basic characterization of the nanosystem addressed to ocular targets [115]. In the rhodamine family, Rhodamine B is widely available and low-cost. The following two studies promote the use of this molecule for tracking nanosystems. The first is focused on the preparation of lipid systems (niosomes vesicles) and Eudragit nanoparticles for the treatment of eye fungal infections. Encapsulation of fluconazole within these systems resulted in being a good way to increase the bioavailability of the drug compared to free drugs. The systems obtained

were innovative in terms of formulation as there is a triple step: the drug was first complexed using β -cyclodextrin, then encapsulated into niosomes, and the niosomes were finally incorporated into an in-situ gelling system made by Poloxamer, HPMC and chitosan. Niosomes were labeled with Rhodamine B and then were compared to labeled polymeric nanoparticles. The fluorescent signal of CLSM analysis increased in intensity when the NPs were incorporated into the hydrogel, whereas the signal of the pure dye was limited to the superficial epithelial layers, suggesting effective permeation of the nanosystems into the inner tissues [116]. Rhodamine B was also used to study the transport of curcumin as a model drug in multilamellar liposomes. These were coated with sodium alginate grafted acrylic acid conjugated with riboflavin. These multi-dye vesicles (rhodamine and curcumin), prepared using the lipid film hydration technique, have proven to be excellent carriers for drug delivery to the retina. The study evaluated both the encapsulation efficiency of the two dyes and their in vitro release. The release test in pH 7.4 medium demonstrated time-dependent release, which was faster for rhodamine than for curcumin. An extended-release profile was obtained using fluorescence, red for rhodamine and green for curcumin, showing greater entrance into the cell at 12 h than at 3 h, and greater endocytosis for smaller, more spherical particles [117].

3.1.2 Polymer-Based Nanocarriers

Topical delivery of polymeric nanosystems is useful to improve corneal penetration and prolong the therapeutic response of several drugs. Nanocarriers need to be evaluated to find clinical application; specifically, their distribution in biological environment should be examined in order to understand the most appropriate strategy to address specific ocular pathologies. Plausible routes of topically instilled drug delivery for the treatment of ocular diseases involving the posterior segment include several pathways, including corneal, non-corneal and uveal routes. Successful nanocarrier development, therefore, involves fluorescent labeling useful for investigating mechanisms and biodistribution profiles of the designed systems. Polymeric nanostructures to be used as imaging diagnostic agents include various kinds of systems, such as nanoparticles, niosomes, film and nanomicelles and in-situ gel. The review of Swetledge et al. offers a detailed discussion on the biodistribution of polymer nanoparticles in major ocular tissues [118]. To improve retention time on the ocular surface, release profile and mucoadhesion performance, nanocarriers are often coated with polymers. Poly-lactide (PLA), polyglycolide (PGA), poly-lactide-co-glycolide (PLGA) and chitosan, Eudragit[®], but also different copolymers such as PLGA-PEG, poly-(3-hydroxybutyrate-co-3-hydroxyvalerate) (PHBV) constituted by hydroxybutyrate (HB) and hydroxyvalerate (HV) and chitosan modified copolymer are some of these. Among them, many polysaccharides are used as a useful coating for nanocarriers. Some of these, including chitosan, alginate sodium, hyaluronate sodium and cellulose derivatives, are approved for ophthalmic use by the FDA and are already present in the composition of ophthalmic products on the market [119]. Depending on the type of polymer, the most suitable fluorescent probe should be chosen. A study conducted by Zhukova et al. focused on understanding the interactions between probes, polymeric nanoparticles and the biological environment. Four dyes with different degrees of hydrophobicity were encapsulated (C6, rhodamine 123, DiI) or covalently bound to the polymer (amine Cyanin 5.5, Cy5.5) in order to label PLGA nanoparticles. To increase the accuracy of the interpretation of in vivo biodistribution data, dual-labeled nanoparticles were administered, using C6 as the encapsulated label and Cy5.5

as the grafted label. Neuroimaging results showed that the signal of the nanoparticles bounded with Cy5.5 was detected in retinal vessels, whereas the signal of the encapsulated C6 was found outside of blood vessels and in tissue background. The extra vasal distribution of C6 could falsify the data interpretation, leading to erroneous assumptions that the nanoparticles could efficiently cross the blood-retinal barrier. Assessing the affinity of the dye to the polymer and the lipophilic structures could be useful in scaling up these issues. Although C6 has not proved to be an ideal label, it aided in explaining the phenomenon whereby drugs are delivered to tissues through encapsulation in nanocarriers without involving any nanoparticle penetration [120]. Similar results were obtained by Zhang et al. tracking in vivo the distribution of PLGA-NPs in the retinal blood circulation after intravenous injection. NPs were labeled with lipophilic perchlorate carbocyanins (DiI) or hydrophilic rhodamine 123 (Rho123). DiI fluorescent signal was detected for a long time (>90 min) in retinal vessels, in contrast with Rho123 whose fluorescence was short (>15 min), due to diffusion from particles and elimination from the blood circulation. To avoid artefacts, dual-labeled nanoparticles were also injected intravenously in rats. Colocalization of fluorescent markers was performed by conjugating the polymer with Cy5.5 and loading the systems with probes (DiI/Rho 123). Cy5.5 signal was detected for both cargoes in retinal vessels for more than 90 min; however, colocalization was observed only for lipophilic DiI dye, which was more closely related to the hydrophobic polymer matrix. These findings further confirm that the affinity of the dye for the polymer and cell membranes played a key role in biodistribution kinetics [121]. The hydrophilic properties of rhodamine B make it a suitable fluorescent candidate for polymers of a hydrophilic nature such as chitosan, whose mucoadhesive qualities have been exploited by X et al. for the design of topical films for the treatment of glaucoma. Corneal permeation studies demonstrated the mucoadhesive efficacy of polymeric films in transporting rhodamine B molecules through the cornea with a high permeation rate [122]. A water-insoluble derivative of the rhodamine family is rhodamine B isothiocyanate, which has affinity for hydrophobic polymers. This dye was used as a label for nanoparticles consisting of hydrophobic PHBV polymer to obtain information regarding the depth and rate of penetration after topical administration. Confocal analysis showed improved penetration deepness of encapsulated marker compared to the free one, used as a control [123]. Recently, hydrophobic C6 was doubly used as a model drug and a fluorescent marker to track surface-modified PLGA-NPs with chitosan, glycol chitosan and polysorbate 80 in retinal tissues. Tracking of NPs after topical instillation was performed by fluorescence microscopy, revealing intense staining throughout the whole eyeball, anterior segment including cornea and conjunctiva, lens, iris/ciliary body and retina, with a peak at 30 min after administration and the disappearance of the signal after 60 min. Ocular tissue autofluorescence was distinct around the outer segments of the photoreceptor. Based on the average size of the NPs (<200 nm), the specific pathway of the NPs to the retina did not exclude any of the plausible routes of delivery to the posterior segment (corneal, noncorneal or uveal pathways) [124]. C6 was also used to label polymeric nanomicelles designed for the topical treatment of fungal keratitis. The nanomicelles consisted of a chitosan oligosaccharide-vitamin E copolymer conjugated to phenylboronic acid (PBA-CS-VE) to enhance corneal retention. C6 delivery through a monolayer of HCE-T cells and 3D cell spheroids demonstrated strong corneal penetration ability. Several characteristics of the polymer were able to influence nanomicelle uptake, but the key role in the process of cellular

endocytosis was attributed to the high-affinity interaction between the PBA portion and sialic acid on the surface of the cell membrane [125].

Another study using C6 as a fluorescent probe was reported by Sai et al., aiming to evaluate the corneal transportation of an in-situ gelling system based on mixed micelles.

This formulation designed for curcumin was composed of micelles, consisting of 1,2-distearoyl- sn-glycero-3-phosphoethanolamine-N-[methoxy(polyethyleneglycol)-2000] (PEG-DSPE) and poly(oxyethylene) esters of 12-hydroxystearic acid (Solutol HS 15), incorporated in a gellan gum gel. Incubation of human corneal epithelial cells (HCEC) with the fluorescently labeled systems showed time-dependent and improved absorption for the encapsulated dye, compared to free C6. Transcorneal penetration was investigated in vivo by CLSM and results suggested that curcumin was able to penetrate more effectively when incorporated into the gelled systems, probably due to the increased retention time conferred by the gellan gum, which was five-fold higher than the mixed micelles alone [126]. A pilot study with C6 was performed to evaluate the feasibility of the approach in assessing the biodistribution of PLGA-PEG nanoparticles suspended in hydrogels. The preliminary study showed an important limitation due to the high green autofluorescence of the examined ocular tissues. To deal with the drawbacks highlighted by the pilot study, PLGA nanoparticles in the full study were labeled with Cy-5, a far-red fluorophore that did not overlap with the natural autofluorescence of the ocular tissues. Results from the full study showed that topical application allowed the nanoparticles to be distributed into the outer ocular tissues (cornea, episcleral tissue and sclera) and the choroid was the only internal tissue to show a slight increased fluorescence, probably attributed to the permeation of [118]. Another dye recently used as a model drug to label mucoadhesive films with a hydrophilic nature based on chitosan and poly(2-ethyl-2-oxazoline) is fluorescein sodium. To avoid precipitation of complexes between the negatively charged dye and the positively charged chitosan backbones, concentrations less than 0.1 mg/mL were used. Films tested by ex vivo (bovine cornea) and in vivo (chinchilla rabbits) studies showed excellent corneal adhesion (up to 50 min) [127]. From this review of recently published papers, it emerged that, to ascertain the applicability of nanosystems to biodistribution studies, it was necessary to (i) take in account the degree of affinity and interference between probe, polymeric carriers and cell membranes, and (ii) accurately interpret the data by selecting an effective labeling method upstream. The most reliable way to track the pathways of the systems remains the conjugation of the fluorescent dye to the polymeric core. Therefore, colocalization by double labeling may be the most appropriate technique to minimize errors in the interpretation of fluorescence signals. Currently, there is no unique approach to fluorescent polymer nanosystems that can be used for all types of labeling systems and probes.

3.1.3 Metallic-Based and Inorganic-Based Nanosystems

Inorganic nanodevices became of great interest in ocular delivery due to their unique properties such as low cost, easy preparation methods, small size, tunable porosity, high surface-volume and robust stability. Fluorescent labeling has been applied to these delivery systems to assess their ability to cross ocular barriers and provide therapeutic efficacy [128]. Corneal barrier functions were investigated by Mun et al. using two types of silica nanoparticles (thiolate and PEGylated) fluorescently labeled with 5-(iodoacetamido)-fluorescein (5-IAF). Permeation studies were performed in vitro on intact or β -cyclodextrin pretreated bovine corneas. To provide experimental

parameters close to in vivo conditions and to avoid artifacts such as the potential risk of corneal swelling when using Franz diffusion cells, the “whole-eye” method was used. 5-IAF-loaded thiolate silica nanoparticles, PEG-grafted silica nanoparticles (5-IAF-PEG), sodium fluorescein and fluorescein isothiocyanate dextran solutions were tested. It resulted that fluorescein salt (376 Da) did not uniformly penetrate the cornea; however, the dye was detected in the stroma. Larger molecules such as FITC-dextran (400 Da) and 5-IAF-PEG formed a layer on the corneal surface with no permeation of the epithelial membrane. β -cyclodextrin pre-treatment disrupted the integrity of the cornea by providing homogeneous permeation of the low-molecular-weight dye, although it did not improve the penetration of larger molecules. Concerning NPs, no permeation was reported regardless of surface modification, particle size and pre-treatment with β -cyclodextrin, thus suggesting that the tight junctions of the corneal epithelium acted as the main barrier to permeation. The absence of penetration and confinement on the corneal surface was observed for thiolated NPs because of the formation of disulfide bonds between the NPs thiol groups and the cysteine domains of the mucus glycoprotein layer. The interaction between mucin and -SH thiol groups remained a limiting permeation factor even after the removal of the epithelial layer. NPs PEGylation was able to mask thiol groups, allowing passage into the stroma [129]. Baran-Rachwalska et al. designed a novel platform consisting of hybrid silicon-lipid nanoparticles, aiming to deliver siRNA to the cornea by topical administration. A fluorescent oligonucleotide duplex, siRNA transfection indicator (siGLO), was employed as a tracking probe to assess in vitro cellular uptake on a human corneal epithelial cell line (HCE-S) and in vivo corneal penetration on wild-type mice. Red fluorescence of the oligonucleotide marker allowed detection of nanoparticles in all layers of the cornea 3 h after instillation, in contrast to the control siGLO. The tracking of biodegradable nanosystems in corneal tissues was confirmed by the reduction of protein expression in the corneal epithelium, making them ideal candidates for therapeutic oligonucleotide delivery [130]. Biodegradable mesoporous silica nanoparticles (MSNs) loaded with carboplatin were designed by Qu et al. for the treatment of retinoblastoma. Carboplatin, being an anticancer drug, causes severe side effects; therefore, it is necessary to focus the action strictly on the target site. For this purpose, MSNs were surface modified by conjugation with an ideal target, epithelial cell adhesion molecule (EpCAM), in order to increase specificity as well as therapeutic efficacy. To assess the targeting efficacy of the designed systems, the authors evaluated the cellular uptake of untargeted and targeted MSNs in retinoblastoma Y79 tumor cells. Rhodamine B and LysoTracker Green were used as fluorescent probes to track cellular and subcellular uptake of the vectors. Increased cellular uptake for targeted MSNs was attributed to EpCAM-specific receptor-mediated cellular internalization. Lysosomal localization of MSNs confirmed that the nanosystems followed the endocytosis pathway for drug delivery [131]. A hexa-histidine with metal ions nanosystem was designed to deliver Avastin in the treatment of corneal neovascularization (CNV). Pre-corneal retention time and ability to cross ocular barriers were studied on a rat CNV model induced by alkaline burns by FITC labeling the systems. Avastin encapsulated in the vectors showed a longer precorneal adhesion time compared to the free drug. These innovative systems have emerged as a promising platform for ocular topical delivery of protein drugs [132]. An interesting zirconium-porphyrin metal-organic framework (NPMOF) has been designed for drug tracking and delivery. The bright fluorescence self-emitted by the metal-organic framework qualifies the carriers to be applied for imaging. NPMOF was used as a skeleton for the delivery of methylprednisolone, a very efficacious corticosteroid in the treatment of retinal degenerative diseases. Adult zebrafish with photoreceptor degeneration induced by high-intensity light exposure were used to test in vivo distribution and therapeutic efficacy. Red fluorescence signals were detected in choroid, retina, photoreceptors and retinal pigment epithelium for up

to 7 days. Recovery of visual function by rapid regeneration of photoreceptors and proliferation of Müller's glia and retinal regeneration were reached after a single intravitreal injection. NPMOF vectors represent a novel delivery system for the treatment of diseases affecting the posterior eye segment [133].

3.1.4 Protein-Based Nanosystems

Protein-based nanosystems have attracted considerable interest in recent years and are designed for drug delivery, diagnostics and bioimaging. These highly bio-compatible systems, which have been extensively studied in the biomedical field, owe their properties to the protein they are composed of. Among the proteins used in their preparation, there are antibodies, enzymes, animal and plant proteins, collagen, plasma proteins, gelatin and proteins derived from virus capsids [134]. Fluorescent proteins are usually used to monitor protein-protein interactions, protein localization and gene expression. However, without any carrier, the fluorescent efficiency of a single protein is relatively low. The use of fluorescent protein-labeled nanomaterials improves loading due to increased surface area and allows the development of fluorescent nanosystems useful in bioimaging and biosensing. In the study carried out by Yang et al., nanoparticles were prepared from regenerated silk fibroin. This protein, which is the most abundant in silk, is considered to have high biocompatibility and degradability properties. In the biomedical field, it has been used for drug delivery in small nanosystems, biological drug delivery, gene therapy, wound healing and bone regeneration. The formulation is targeted for intravitreal injection with the aim of increasing the bioavailability of the drug in the retina. Fluorescein isothiocyanate labeled bovine serum albumin (FITC-BSA) has been encapsulated as a model drug. In vitro cytotoxicity studies were conducted on ARPE-19 cells, showing that these nanosystems were very compatible. In addition, in vivo comparison of the biodistribution in posterior ocular tissues in rabbits revealed increased retention in the retina due to encapsulation in the nanosystem rather than with a solution of model drug [135,136]. Albumin is widely used in the preparation of ocular nanosystems [137]. In a recent study, bovine serum albumin nanoparticles loaded with apatinib were prepared for the treatment of diabetic retinopathy. In contrast to the previous study, in this disease, invasive administration has to be avoided, so topical administration is the ultimate goal. The nanoparticles were coated with hyaluronic acid (HA) to increase mucoadhesion. The biodistribution study in retinal tissue was carried out by preparing fluorescent nanosystems with 1,1'-dioctadecyl-3,3,3',3'-tetramethylindodicarbocyanine, 4-chlorobenzenesulfonate salt (DiD) solution in ethanol (0.5 mg/mL), which was added during the formulation phase. Through the comparative in vivo biodistribution study, it was shown that HA-coated nanoparticles demonstrate higher fluorescence in retinal tissue compared to uncoated nanoparticles, thus representing a viable alternative to intravitreal injection, maintaining comparable perfusion and bioavailability [138]. Another study involved the preparation of nanoparticles using pseudo-proteins for the potential treatment of ophthalmic diseases. Ten types of nanoparticles obtained by precipitation of pseudo-proteins were prepared, then they were loaded, and some of them were also pegylated; finally, they were labeled with a fluorescent probe, fluorescein diacetate (FDA) or rhodamine 6G (Rh6G), to assess ocular penetration. Corneal fluorescence was obtained as expected, while surprising results were the reaching of tissues such as the sclera and retina. Thus, they proved to be a promising delivery system for topical use in chronic eye diseases [139].

3.2 Diagnostics

Labeling nanoparticles with fluorescent probes was demonstrated to be a useful approach to improve the effectiveness of some diagnostic tests aimed to detect ocular pathologies. In fact, some eye diseases require a prompt diagnosis in order to contain possible damages related to the ongoing pathways involved. Age-related macular degeneration (AMD) is the main cause of vision loss for over-65-year-olds [37]; this pathology has often been analyzed to improve diagnostic techniques since it has several predisposing factors, and early detection is crucial to avoid degeneration toward blindness [140]. AMD has an unclear etiology, although oxidative stress is considered one of the main risk factors [141]; as a matter of fact, clinical studies demonstrated the importance of supplementation with antioxidants in order to slow down the progression of AMD [142,143]. Physiological antioxidant patterns involve metallothioneins (MT), low molecular mass proteins characterized by the presence of cysteine sulfur ligands, which are able to scavenge free radicals, thus protecting cells and tissues. The retina is particularly subject to oxidative stress due to visible and UV light exposure; moreover, age progression involves a reduction of MT expression, predisposing to AMD [144]. For this reason, bioimaging these proteins in ocular tissues could be an important tool useful to highlight the tendency to develop AMD. For this purpose, fluorescent gold nanoclusters involving Cu and Zn and bioconjugated with specific primary antibodies were developed by Cruz-Alonso and coworkers [145]. Laser ablation (LA)-inductively coupled plasma (ICP)-mass spectrometry (MS) technique was used to identify $^{63}\text{Cu}^+$ and $^{64}\text{Zn}^+$ in the retina of post-mortem donors since MT bind both Cu and Zn [146]. This method showed results comparable with conventional immunohistochemistry for MT proteins, with amplification of signals related to the presence of nanoclusters, which allowed the obtainment of higher resolution bioimages. An *in vivo* model of human “wet” AMD is laser-induced choroidal neovascularization (mouse LCNV) mouse, in which the inflammatory biomarker vascular cell adhesion molecule-1 (VCAM-1) is highly expressed. Gold nanoparticles functionalized with anti-sense DNA complementary to VCAM-1 mRNA were developed by Uddin et al., who aimed to detect this molecule, thus assessing the occurrence of oxidative stress [147]. The fluorescence *in-situ* hybridization (FISH) technique was used to perform photothermal-optical coherence tomography (PT-OCT) involving a fluorescent probe (Alexafluor-647) bonded to 3' end of anti-sense DNA in order to highlight its interaction with the target mRNA. The conjugation of anti-sense DNA to gold nanoparticles proved to protect from the degradation performed by DNase while enhancing the uptake, probably through endocytosis, as suggested by transmission electron microscopic (TEM) images of retinal cells; moreover, it was verified that no inference in the fluorescence was produced due to low pH, which is characteristic of inflamed tissues. Compared to the control group, *in vivo* systemic injection in mice confirmed the enhancement in the fluorescent signal for anti-sense DNA coupled with nanoparticles, which mostly depended on VCAM-1 mRNA hybridization, thus demonstrating the potentiality of the developed platform as a tool to obtain direct images of endogenous mRNA in a tissue. In some cases, this pathology requires transplantation of photoreceptor precursors (PRPs) in the subretinal space, which was successfully performed, guaranteeing a certain vision restoration [148]. For a certain period, monitoring of the efficiency of the transplantations needs to be performed. As confirmed by Chemla and coworkers [149], gold nanoparticles could be transplanted together with photoreceptor precursors cells labeled with a fluorescent probe (Alexa 594) in order to ameliorate the efficiency of

computed tomography (CT) and optical coherence tomography (OCT) in assessing the success of the transplant. The nanoparticles were firstly characterized in order to assess their safety, thus demonstrating no toxicity toward the transplanted cells and no occurrence of inflammation in the retina and vitreous. Furthermore, this platform demonstrated to enhance X-ray signal detected by CT and related to cell survival without interference from the particles secreted from the cells [150]; moreover, they were also able to increase optical signal for OCT by up to 1.4-fold and track cells migration toward layers deeper than the injection site. These results confirm the efficiency of such a platform in the monitoring of transplantation but also suggest a potential use for ameliorating existent molecular imaging in cell therapy and diagnostic. Another important diagnostic test is fundus fluorescein angiography (FFA), which allows highlighting vascular leakages in retinal and choroidal pathologies [151]. This clinical tool is useful to diagnose several ocular diseases: age-related macular degeneration, which is characterized by hemorrhaging and exudation in the retina [140]; diabetic retinopathy, which involves retinal damages related to microvascular modification which are clinically not revealable in the early stages [152]; diabetic macular edema, whose pathophysiology implicates modifications of choroidal and retinal vasculature due to BRB impairment [153]. Furthermore, the aforementioned diseases are characterized by alterations of ocular vessels, and share the consequent compromission of visual activity, if not quickly detected and treated. Fluorescein sodium (FS) is injected intravenously to perform this analysis, diffusing in the blood vessels, thus allowing us to observe them through a confocal scanning laser ophthalmoscopy system. Despite it being considered relatively safe, nausea and vomiting frequently occur, while severe effects such as anaphylaxis are rare. The main drawbacks are the diffusion of FS into normal tissues and cellular absorption, with long retention, which were overcome using nanoparticles. Cai et al. coworkers developed a high molecular weight polyethyleneimine (PEI) nanoparticles which demonstrated to successfully couple fluorescein [151]; moreover, in vitro studies showed good cytocompatibility, no significant difference in apoptosis rates considering various concentration tested, no genotoxicity, and no morphological changes or significant difference in endothelial tube formation. Cellular uptake assays, carried on with different concentrations of free FS and FS-NP, confirmed similar rapid uptake by cells, with a concentration-dependent and time-dependent fluorescence of main retinal vessels and microvessels. Furthermore, free FS was longer retained in cells when compared to FS-NP, as highlighted by in vivo fluorescence studies, suggesting a potential decrease in FS toxicity. These results confirm the potentiality of this platform as a diagnostic tool to detect retinal vessels; moreover, PEI enhances fluorescein metabolism, thus reducing its toxicity. Other polymeric nanoparticles developed as a potential diagnostic tool are composed of copolymerized glycerol mono methacrylate (GMMA), glycidyl methacrylate (GME) and ethylene glycol dimethacrylate (EGDMA), which were functionalized with Vancomycin, Polymyxin B or Amphotericin B, in order to detect the presence of Gram-positive bacteria, Gram-negative bacteria and fungi through a specific bond with the respective antibiotic or antimycotic [154]. The occurrence of such bonds was differently highlighted using fluorescent Vancomycin, and probes such as fluorescein isothiocyanate (FITC) and Calcofluor White. Tests conducted on various microbiological strains showed a proportional increase in the fluorescence signal with the increase in the number of organisms involved; moreover, the presence of functionalized polymers favored the microorganism bonding. Besides the

biocompatibility of this platform, another advantage of this platform is the possibility to be shaped as a contact lens requiring only a 30-min exposure to efficiently detect the occurrence of infection, thus demonstrating to be a promising approach for an easy diagnosis of corneal infections.

3.3 Nanotheranostics

The recent development of systems that integrate the treatment of diseases with their diagnostics is referred to as theranostics. When the system is in a nanoscale range, it is called nanotheranostics. Figure 5 shows prototypes of nanosystems suitable for theranostic purposes.

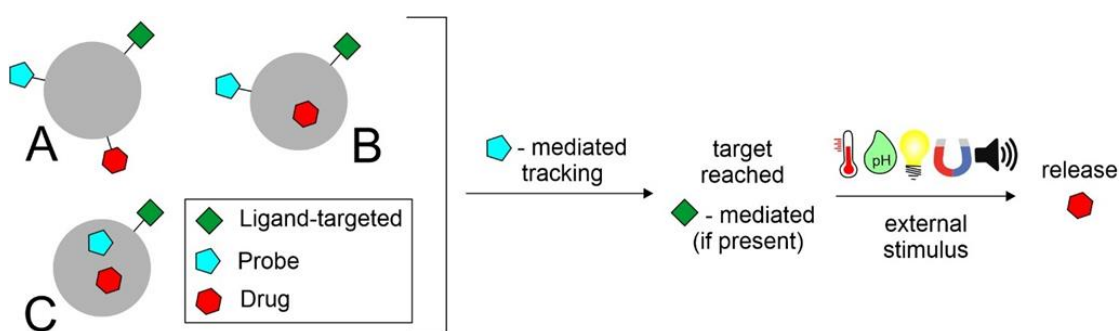


Figure 5. Prototypes of theranostic nanosystems and their mechanism of action. In figure: (A) labeling of both probe and drug; (B) loading of drug and labeling of probe; (C) co-loading of drug and probe.

The development of these applications has given researchers a new way of diagnosing and treating diseases such as cancer, diabetic retinopathy and age-related macular degeneration [37,155]. Among the major chronic eye diseases, diabetic retinopathy is the most prevalent. Angiogenesis in the posterior eye segment is the main cause of retinal impairment. Clinical management consists of pathological diagnosis and intravitreal injections of vascular endothelial growth factor (VEGF) inhibitors to suppress neovascularization. The development of innovative nanotheranostic systems is emerging to overcome these critical problems with less invasive methods to diagnose and treat ocular angiogenesis synergistically. Silicon nanoparticles conjugated to the peptide Cyclo-(Arg-Gly-Asp-d-Tyr-Cys) (c-(RGDyC)) (SiNP-RGD) were designed by Tang et al. with the dual action of imaging and treating ocular neovascularization. The effective anti-angiogenic capability of these biocompatible theranostic nanoprobe was based on the combination of a specific detection by labeling endothelial cells and angiogenic blood vessels and a selective inhibition of neovascularization [156]. Metal NPs are receiving a lot of attention as carriers for the delivery of biomolecules, among which silver NPs (AgNPs) have found numerous applications. Stati et al. designed curcumin stabilized AgNPs using a green and cost-effective method to exploit the promising characteristics of this polyphenol in the *in vivo* treatment of human pterygo. Curcumin is a molecule suitable for theranostic application, as widely reported in the work of Shabbir et al. [157]. Pterygo is a progressive eye disease that could culminate in an irreversible impairment of visual function. Available treatments require invasive surgical procedures, such as excision, which often leads to a worsening of the clinical picture. Spectroscopic techniques revealed a strong plasmonic resonance between the silver nuclei and the curcumin molecule, demonstrating the presence of the polyphenol

on the surface of AgNPs. The biological efficacy of the formulation was tested in vitro on human keratinocytes derived from pterygium explants, showing decreased cell viability in treated samples compared to controls. Although no studies have been conducted to track the fate of NPs, the fluorescent emission of the samples could be exploited for bioimaging applications [158]. Fluorescent silicon nanoparticles modified with Vancomycin were designed by Zhang et al. for the simultaneous non-invasive diagnosis and treatment of keratitis induced by Gram-positive bacteria. These nanotheranostic agents have demonstrated, in combination with strong antimicrobial activity against *Staphylococcus aureus*, a rapid (<10 min) imaging capability both in vitro and in vivo. The rapidity with which bacterial keratitis was diagnosed at an early stage suggests that these devices may be useful in preventing the progress of the disease, which could impair visual function if not treated [159]. Oliveira et al. designed hybrid theranostic systems consisting of a lipid matrix of 1,2-dipalmitoyl-sn-glycero-3-phosphatidylcholine (DPPC), coated with Pluronic® F127, covalently bound with the fluorescent probe 5(6)-carboxyfluorescein and loaded with the photosensitizing agent verteporfin. Preliminary studies on a glioblastoma cell line (T98G) were conducted to evaluate the potential application as theranostic nanodevices. The fluorescence of the systems revealed on the cancer cell membrane and the 98% reduction in cell viability of T98G cells encouraged further investigation of such multifunctional platforms for the treatment and diagnosis of ophthalmic diseases [160]. Photothermal therapy has been making inroads into the eye sector for a couple of years now. Heat therapy refers to the use of heat as a therapeutic tool to treat diseases such as tumors. In the recent work of Li et al., an approach to treat choroidal melanoma using nanocomposites was designed. Nanosystems were synthesized based on hydrogel, which is itself based on rare-earth nanoparticles. These platforms emit fluorescence in an NIR-II region. Characterized by their tiny size of less than 5 nm, they are targeted for the treatment and simultaneous bioimaging of choroidal melanoma. They have been incorporated into biodegradable hydrogels based on PNIPAM dual response, which could release the drug in a controlled manner by responding to heat and glutathione in the tumor microenvironment. The nanocomposites were then further decorated with indocyanine green (ICS) and folic acid (FA) to enhance therapeutically and to target specificity and the possibility of achieving photothermal therapy [161]. A lot of studies showed the potential of therapeutic contact lenses in the management of eye disease [162]. Infectious endophthalmitis is a growing concern that causes irreversible damage to intraocular tissue and the optic nerve. The work of Huang et al. focuses on the design of contact lenses consisting of hybrid hydrogels based on quaternized chitosan composite (HTCC), silver nanoparticles and graphene oxide (GO). Fungal keratitis infection often leads to the formation of a biofilm, which is particularly difficult to be penetrated by antifungal agents, especially through eye drops. In addition, the bioavailability of a drug such as Voriconazole is very limited. The function of these nanoparticles is not only to deliver Voriconazole in the treatment of fungal keratitis, but also to act as an antimicrobial agent due to its properties. In fact, the materials used, such as quaternized chitosan, have inherent antimicrobial capabilities. The dual functionality makes this system a useful theranostic approach for the treatment of eye infections [163]. The study by Jin et al. reports a therapeutic nanoplatform based on UiO-66-NH₂ to combine photodynamic therapy (PDT) and targeting lipopolysaccharides (LPS) through polypeptide modification (YVLWKRKFCFI-NH₂). The fluorescent used was Toluidine blue (TB), which acted as a photosensitiser (PS) and

was loaded into UiO-66-NH₂ nanoparticles (NPs). The dye acts both as a tracer and as a therapeutic agent through photodynamics. The release of the fluorescent is pH-dependent. The study proved beneficial against *Pseudomonas aeruginosa* and *Staphylococcus epidermidis*, and the in vivo model showed positive results in the treatment of endophthalmitis [164].

4. Fluorescent Status for Ocular Therapies in Clinical Trials and Market

Scientific progress in the field of ocular nanomedicine is constantly advancing, many nanoformulations for the treatment of ophthalmic diseases have been clinically investigated, and some have already been introduced to the market. A list of nanomedicines for eye diseases in clinical trials and approved by the Food and Drug Administration (FDA) is discussed in the review provided by Khiev et al. [165].

Novel nanosystems on the market included NorFLO, a dietary supplement based on a patented curcuma-phospholipid formula (iphytoone®). Phospholipids enhanced the targeted distribution of curcumin in the eye, and the efficacy of the formulation has been demonstrated in over 40 studies in processes triggered or sustained by chronic inflammation, found to be the cause of many eye diseases. Prolidofta is another supplement marketed as an ocular spray to counteract inflammatory processes affecting the palpebral component and restore any functional and structural changes. This spray consists of small vesicles (50–500 nm) made up of a double layer of phospholipids surrounding an aqueous core for the delivery of vitamins A and E. OMK1-LF is an ophthalmic liposomal solution based on citicolin, an endogenous molecule that restores the damage caused by glaucoma in the cell membranes and hyaluronic acid, which acts to hydrate, protect and lubricate the tear film. TriMix is an eye drop with cross-linked Hyaluronic Acid, Trehalose and Stearylamine Liposome indicated to counteract dryness and eye irritation.

Regarding imaging in surgery, near-infrared fluorescence (NIRF) with the dye indocyanine green has been widely used. Indocyanine green (ICG) is a clinically approved NIRF dye in ophthalmology for imaging retinal blood vessels; an overview of surgical applications using indocyanine green fluorescence imaging has been proposed by Alander et al. [166]. Based on clinicaltrials.gov, a website database of clinical trials conducted around the world (as accessed on 1 April 2022), since 2010 fluorescence imaging has been used in clinical trials to assess the integrity or damage of ocular surfaces after administration of novel nanosystems. Green dye fluorescein was used in 13 clinical trials for the evaluation of nanosystems with different ocular indications, from dry eye to autoimmune Sjögren's syndrome. The role of the dye and details of the studies are given in Table 3.

Table 3. Use of Fluorescein dye in clinical trials of drug delivery systems for eye diseases.

Role of Molecule in the Study	Name and Type of Formulation Tested	Name of the Study	Pathologies	Status	Identified Number of the Study
Evaluate corneal and conjunctival damage	LAMELLEYE Liposomal suspension	Lamelleye vs. Comparator for the Treatment of Dry Eye Disease	Dry Eye Syndromes	Completed	NCT03052140
Evaluate tear break up time and corneal damage	AQUORAL LIPO (liposomal solution) in contact lens	Efficacy of "Aquoral Lipo" Artificial Tears in Contact Lens Wearers With Discomfort	Contact Lens Complication	New study (March, 2022) not yet recruiting	NCT05290727
Evaluate corneal and conjunctival damage	LAMELLEYE Liposomal suspension	LAMELLEYE for the Treatment of Dry Eye Symptoms in pSS Patients	Primary Sjögren Syndrome	Unknown	NCT03140111
Evaluate corneal damage	LIPOSIC AND TEARS NATURALE FORTE (liposomal suspension)	Comparison of the Effects of Two Tear Substitutes in Patients with Dry Eye Syndrome	Dry eye	Completed	NCT03211351
Evaluate ocular surface damage	TEARS AGAIN (liposomal spray)	Dry Eye Treatment with Artificial Tears	Dry eye	Completed	NCT02420834
Evaluate the absence of anterior chamber cells	(Dexamethasone Cyclodextrin Nanoparticle Ophthalmic Suspension 1.5%)	OCS-01 in Treating Inflammation and Pain in Post-cataract Patients (SKYGGN)	inflammation and pain following cataract surgery	Completed	NCT04130802
Evaluate corneal damage	Intravenous Administration of Secukinumab (AIN457) or Canakinumab (ACZ885) solution	The Effects of a Single Intravenous Administration of Secukinumab (AIN457) or Canakinumab (ACZ885) in Dry Eye Patients	Dry eye	Completed	NCT01250171
Evaluate corneal and conjunctival damages	Tanfanercept (HL036) Topical Ophthalmic Solution	A Study to Assess the Efficacy and Safety of Tanfanercept (HL036) Ophthalmic Solution in Participants With Dry Eye (VELO-3)	Dry eye	Recruiting, Phase III	NCT05109702
Evaluate conjunctival damage	HL036 0.10 percent (%) ophthalmic solution as topical ophthalmic drops	A Study to Assess Efficacy of HL036 in Subjects With Dry Eyes (VELO-1)	Dry eye	Completed, Phase II	NCT03334539
Evaluate changes in inferior cornea	NCX 4251 (fluticasone propionate nanocrystal)	Study Evaluating the Safety and Efficacy of NCX 4251 Ophthalmic Suspension for the Treatment of Blepharitis	Blepharitis	Completed	NCT04675242
Evaluate Tear Film Break-up Time	SYSTANE® Complete Nanoemulsion ocular lubricant (Propylene glycol-based eye drops)	Study of Efficacy and Tolerability of SYSTANE Complete in Patients with Dry Eye Disease	Dry eye	Completed	NCT03492541
Evaluate corneal damage	TJO-087 Cyclosporine ophthalmic Nanoemulsion (0.08%)	Evaluating the Efficacy and Safety of TJO-087 in Moderate to Severe Dry Eye Disease Patients	Dry eye	Recruiting	NCT05245604
Evaluate corneal damage	OCU300 Brimonidine Tartrate Nanoemulsion	Study of Brimonidine Tartrate Nanoemulsion Eye Drops in Patients With Ocular Graft-vs-Host Disease	Ocular Graft Versus Host Disease	Completed	NCT03591874

Fluorescence for the development and clinical investigation of innovative ocular nanosystems seems to be a promising strategy to increase the number of formulations able to reach market commercialization. In Table 4, few products with fluorescein approved by the FDA are reported.

Table 4. FDA-approved products with fluorescein.

Name	Active Ingredients	Company	Description	NDA
Altafluor Benox	Benoxinate Hydrochloride; Fluorescein Sodium (0.4%; 0.25%)	Altaire Pharms Inc. (Aquibogue, NY, USA)	Solution/Drops; Ophthalmic	208582
Fluorescein Sodium And Benoxinate Hydrochloride	Benoxinate Hydrochloride; Fluorescein Sodium (0.4%; 0.3%)	Bausch Lomb (Dublin, Ireland)	Solution/Drops; Ophthalmic	211039

5.Challenges and Future Perspectives

The growing number of people who have blindness and visual impairment indicates a continuous increase in the need for care and treatment. Given this evidence, urgent action is required to address this largely preventable global problem and provide adequate eye care services. There are still many gaps in the literature regarding optimal design and traffic pathways within the eye. In particular, further research is needed to unravel the transport mechanisms across certain barriers in the eye. Moreover, rapid clearance remains a challenge for nanosystems as they need to release their payload before being eliminated from the eye. Many studies focus on assessing the distribution in various tissues once the formulation has been instilled into the eye [106–132,134,137–139]. Unfortunately, few studies focus on assessing how mechanisms including blinking, tear drainage and ocular metabolism may interact with nanosystems [66,115]. Among other things, a very important aspect is the evaluation of the toxicity and the actual applicability of these systems. In fact, many of them are quite complex, and the applicability, especially in the theranostic field, is not entirely easy. The evaluation has to be as precise as possible because many eye studies use rodent models; this is highly questionable, especially in the quantification of distribution and kinetic properties of nanoparticles in the eye, as there are many significant differences between the rodent and human eye. Therefore, the most impactful future studies on this topic will come from larger animal models with eyes that are physiologically and anatomically more similar to ours.

The increasing use of fluorescent probes in the realization of biosensors for colorimetric and radiometric identification of specific targets is a great step forward since the fluorescence represents a non-invasive diagnostic method. This has important benefits in early diagnosis through self-medication screening based on membranes or other platforms containing the appropriate fluorescent probe. These tools are also applicable in epidemics through the realization of specific self-tests based on ELISA or other strategies able to identify the etiological agent selectively. A large and growing field is the use of these probes as part of theranostic photo switch structures, able to change their structure after light stimulus, releasing the therapeutic agent and activating or switching off the fluorescence of the probe. Thus, fluorescence allows accurate and quantitative identification (under certain conditions even by the naked eye as also through in vitro tests) of the drug release process. Therefore, the use of fluorescent probes is finding increasing use in experimental and advanced ocular chemotherapy using photo-activated systems.

6.Conclusions

The eye has a complex anatomical structure, representing the main difficulty for drugs to achieve this target. Nanomedicine has made it possible to overcome several difficulties

related to the administration of this almost isolated compartment. The study of the pathways followed by the nanosystems makes it possible to assess the effective achievement of the target site and to consider any non-productive distribution in undesirable tissues with the possible onset of side effects. The biodistribution study also allows the correlation between the chemico-physical parameters of the nanosystems (e.g., ZP, size, morphology, mucoadhesive properties, etc.) and the paths followed by them. This investigation is also aimed at evaluating and developing strategies to bypass physiological barriers of the eye, including tight junctions, tearing and blinking, that could compromise targeting effectiveness. The development of bioimaging mediated by fluorescent probes has improved the efficiency of some diagnostic tests for eye diseases. It is known that early (or rather preventive) diagnosis is a necessity to limit the damage, especially in the long term, caused by specific diseases. The involvement of fluorescent nanoparticles as diagnostics demonstrated to be suitable for detecting the occurrence of pathological pathways, ameliorating techniques already employed in ocular diagnostic, thus providing better results through equipment of common use (OCT, CT, FFA, etc.). This is where the important contribution of fluorescent probes to nanotheranostic approaches becomes relevant since, in these systems, diagnostic and therapy coexist. Tracking the nanoparticles makes it possible to highlight the effective achievement of the target, thus following the release of the therapeutic agent through an external stimulus (e.g., ultrasounds, magnetic fields, light, etc.). In conclusion, as highlighted in this review, the potential applications of fluorescence in the ocular field have been demonstrated as a useful strategy for translating nanoformulations into marketable drug candidates. In addition, to the best of our knowledge, there are no reviews focused on this topic, so this work aims to raise awareness and summarize the use of fluorescents in the ocular field.

Author Contributions: Conceptualization, R.P.; data curation, C.C. (Cinzia Cimino), S.R., A.R. and E.Z.; writing – original draft preparation, C.C. (Cinzia Cimino), A.R. and E.Z.; writing – review and editing, A.B., C.C. (Claudia Carbone), T.M. and R.P.; visualization C.C. (Cinzia Cimino) and E.Z.; funding, T.M.; supervision, R.P.; project administration, R.P. All authors have read and agreed to the published version of the manuscript.

Funding: The work was partially financed under the 3N-ORACLE project (University of Catania, PIACERI – Linea 2 funding program 2020–2022).

Institutional Review Board Statement: Not applicable.

Informed Consent Statement: Not applicable.

Data Availability Statement: Not applicable.

Acknowledgments: C.C. (Cinzia Cimino) was supported by the PhD program in Biotechnology, XXXVI cycle, University of Catania; A.R. was supported by the International PhD program in Neurosciences, XXXV cycle, University of Catania and E.Z. was supported by the International PhD program in Neurosciences, XXXVII cycle, University of Catania. A.B. is a researcher at the University of Catania within the EU-funded PON REACT project (Azione IV.4 – “Dottorati e contratti di ricerca su tematiche dell’innovazione”, nuovo Asse IV del PON Ricerca e Innovazione 2014–2020 “Istruzione e ricerca per il recupero – REACT – EU”; Progetto “Approcci terapeutici innovativi per il targeting cerebrale di farmaci e materiale genico”, CUP E65F21002640005).

Conflicts of Interest: The authors declare no conflict of interest.

References

1. Flaxman, S.R.; Bourne, R.R.A.; Resnikoff, S.; Ackland, P.; Braithwaite, T.; Cicinelli, M.V.; Das, A.; Jonas, J.B.; Keeffe, J.; Kempen, J.; et al. Global causes of blindness and distance vision impairment 1990–2020: A systematic review and meta-analysis. *Lancet Glob. Health* **2017**, *5*, e1221–e1234. [[CrossRef](#)]
2. Marques, A.P.; Ramke, J.; Cairns, J.; Butt, T.; Zhang, J.H.; Muirhead, D.; Jones, I.; Tong, B.A.M.A.; Swenor, B.K.; Faal, H.; et al. Global economic productivity losses from vision impairment and blindness. *EClinicalMedicine* **2021**, *35*, 100852. [[CrossRef](#)]
3. Nagarajan, N.; Assi, L.; Varadaraj, V.; Motaghi, M.; Sun, Y.; Couser, E.; Ehrlich, J.R.; Whitson, H.; Swenor, B.K. Vision impairment and cognitive decline among older adults: A systematic review. *BMJ Open* **2022**, *12*, e047929. [[CrossRef](#)] [[PubMed](#)]
4. Lorenzo-Veiga, B.; Alvarez-Lorenzo, C.; Loftsson, T.; Sigurdsson, H.H. Age-related ocular conditions: Current treatments and role of cyclodextrin-based nanotherapies. *Int. J. Pharm.* **2021**, *603*, 120707. [[CrossRef](#)] [[PubMed](#)]
5. Pacheco, E.; Lips, M.; Yoong, P. Transition 2.0: Digital technologies, higher education, and vision impairment. *Internet High. Educ.* **2018**, *37*, 1–10. [[CrossRef](#)]
6. Bourne, R.R.A.; Steinmetz, J.D.; Saylan, M.; Mersha, A.M.; Weldemariam, A.H.; Wondmeneh, T.G.; Sreeramareddy, C.T.; Pinheiro, M.; Yaseri, M.; Yu, C.; et al. Causes of blindness and vision impairment in 2020 and trends over 30 years, and prevalence of avoidable blindness in relation to VISION 2020: The Right to Sight: An analysis for the Global Burden of Disease Study. *Lancet Glob. Health* **2021**, *9*, e144–e160. [[CrossRef](#)]
7. Lyu, Q.; Peng, L.; Hong, X.; Fan, T.; Li, J.; Cui, Y.; Zhang, H.; Zhao, J. Smart nano-micro platforms for ophthalmological applications: The state-of-the-art and future perspectives. *Biomaterials* **2021**, *270*, 120682. [[CrossRef](#)] [[PubMed](#)]
8. Kels, B.D.; Grzybowski, A.; Grant-Kels, J.M. Human ocular anatomy. *Clin. Dermatol.* **2015**, *33*, 140–146. [[CrossRef](#)]
9. Jonas, J.B.; Ohno-Matsui, K.; Panda-Jonas, S. Myopia: Anatomic changes and consequences for its etiology. *Asia-Pac. J. Ophthalmol.* **2019**, *8*, 355–359. [[CrossRef](#)] [[PubMed](#)]
10. Lindfield, D.; Das-Bhaumik, R. Emergency department management of penetrating eye injuries. *Int. Emerg. Nurs.* **2009**, *17*, 155–160. [[CrossRef](#)] [[PubMed](#)]
11. Maulvi, F.A.; Shetty, K.H.; Desai, D.T.; Shah, D.O.; Willcox, M.D.P. Recent advances in ophthalmic preparations: Ocular barriers, dosage forms and routes of administration. *Int. J. Pharm.* **2021**, *608*, 121105. [[CrossRef](#)] [[PubMed](#)]
12. Suri, R.; Beg, S.; Kohli, K. Target strategies for drug delivery bypassing ocular barriers. *J. Drug Deliv. Sci. Technol.* **2020**, *55*, 101389. [[CrossRef](#)]
13. Varela-Fernández, R.; Díaz-Tomé, V.; Luaces-Rodríguez, A.; Conde-Penedo, A.; García-Otero, X.; Luzardo-álvarez, A.; Fernández-Ferreiro, A.; Otero-Espinar, F.J. Drug delivery to the posterior segment of the eye: Biopharmaceutic and pharmacokinetic considerations. *Pharmaceutics* **2020**, *12*, 269. [[CrossRef](#)]
14. Madni, A.; Rahem, M.A.; Tahir, N.; Sarfraz, M.; Jabar, A.; Rehman, M.; Kashif, P.M.; Badshah, S.F.; Khan, K.U.; Santos, H.A. Non-invasive strategies for targeting the posterior segment of eye. *Int. J. Pharm.* **2017**, *530*, 326–345. [[CrossRef](#)] [[PubMed](#)]
15. Bansal, P.; Garg, S.; Sharma, Y.; Venkatesh, P. Posterior Segment Drug Delivery Devices: Current and Novel Therapies in Development. *J. Ocul. Pharmacol. Ther.* **2016**, *32*, 135–144. [[CrossRef](#)] [[PubMed](#)]
16. Kamaledin, M.A. Nano-ophthalmology: Applications and considerations. *Nanomed. Nanotechnol. Biol. Med.* **2017**, *13*, 1459–1472. [[CrossRef](#)]
17. Yorston, D. Intravitreal injection technique. *Community Eye Health J.* **2014**, *27*, 47. [[CrossRef](#)]
18. Seah, I.; Zhao, X.; Lin, Q.; Liu, Z.; Su, S.Z.Z.; Yuen, Y.S.; Hunziker, W.; Lingam, G.; Loh, X.J.; Su, X. Use of biomaterials for sustained delivery of anti-VEGF to treat retinal

- diseases. *Eye* **2020**, *34*, 1341–1356. [[CrossRef](#)] [[PubMed](#)]
19. Jumelle, C.; Gholizadeh, S.; Annabi, N.; Dana, R. Advances and limitations of drug delivery systems formulated as eye drops. *J. Control. Release* **2020**, *321*, 1–22. [[CrossRef](#)] [[PubMed](#)]
 20. Shiels, A.; Hejtmancik, J.F. Biology of Inherited Cataracts and Opportunities for Treatment. *Annu. Rev. Vis. Sci.* **2019**, *5*, 123–149. [[CrossRef](#)]
 21. Al-Ghananeem, A.M.; Crooks, P.A. Phase I and phase II ocular metabolic activities and the role of metabolism in ophthalmic prodrug and codrug design and delivery. *Molecules* **2007**, *12*, 373–388. [[CrossRef](#)]
 22. Tang, Z.; Fan, X.; Chen, Y.; Gu, P. Ocular Nanomedicine. *Adv. Sci.* **2022**, *2003699*, 1–36. [[CrossRef](#)] [[PubMed](#)]
 23. Leonardi, A.; Bucolo, C.; Drago, F.; Salomone, S.; Pignatello, R. Cationic solid lipid nanoparticles enhance ocular hypotensive effect of melatonin in rabbit. *Int. J. Pharm.* **2015**, *478*, 180–186. [[CrossRef](#)] [[PubMed](#)]
 24. Burhan, A.M.; Klahan, B.; Cummins, W.; Andrés-Guerrero, V.; Byrne, M.E.; O’reilly, N.J.; Chauhan, A.; Fitzhenry, L.; Hughes, H. Posterior segment ophthalmic drug delivery: Role of muco-adhesion with a special focus on chitosan. *Pharmaceutics* **2021**, *13*, 1685. [[CrossRef](#)] [[PubMed](#)]
 25. Gautam, D.; Pedler, M.G.; Nair, D.P.; Petrash, J.M. Nanogel-facilitated in-situ delivery of a cataract inhibitor. *Biomolecules* **2021**, *11*, 1150. [[CrossRef](#)]
 26. Gagandeep, G.T.; Malik, B.; Rath, G.; Goyal, A.K. Development and characterization of nano-fiber patch for the treatment of glaucoma. *Eur. J. Pharm. Sci.* **2014**, *53*, 10–16. [[CrossRef](#)] [[PubMed](#)]
 27. Ghosh, A.K.; Thapa, R.; Hariani, H.N.; Volyanyuk, M.; Ogle, S.D.; Orloff, K.A.; Ankireddy, S.; Lai, K.; Žiniauskaitė, A.; Stubbs, E.B.; et al. Poly(Lactic-co-glycolic acid) nanoparticles encapsulating the prenylated flavonoid, xanthohumol, protect corneal epithelial cells from dry eye disease-associated oxidative stress. *Pharmaceutics* **2021**, *13*, 1362. [[CrossRef](#)] [[PubMed](#)]
 28. Shi, L.; Li, Z.; Liang, Z.; Zhang, J.; Liu, R.; Chu, D.; Han, L.; Zhu, L.; Shen, J.; Li, J. A dual-functional chitosan derivative platform for fungal keratitis. *Carbohydr. Polym.* **2022**, *275*, 118762. [[CrossRef](#)]
 29. Liu, Y.C.; Lin, M.T.Y.; Ng, A.H.C.; Wong, T.T.; Mehta, J.S. Nanotechnology for the treatment of allergic conjunctival diseases. *Pharmaceutics* **2020**, *13*, 351. [[CrossRef](#)]
 30. Nirbhavane, P.; Sharma, G.; Singh, B.; Begum, G.; Jones, M.C.; Rauz, S.; Vincent, R.; Denniston, A.K.; Hill, L.J.; Katare, O.P. Triamcinolone acetate loaded-cationic nano-lipoidal formulation for uveitis: Evidences of improved biopharmaceutical performance and anti-inflammatory activity. *Colloids Surfaces B Biointerfaces* **2020**, *190*, 110902. [[CrossRef](#)]
 31. Du, S.; Wang, H.; Jiang, F.; Wang, Y. Diabetic Retinopathy Analysis – Effects of Nanoparticle-Based Triamcinolone. *J. Nanosci. Nanotechnol.* **2020**, *20*, 6111–6115. [[CrossRef](#)] [[PubMed](#)]
 32. Suri, R.; Neupane, Y.R.; Mehra, N.; Nematullah, M.; Khan, F.; Alam, O.; Iqbal, A.; Jain, G.K.; Kohli, K. Sirolimus loaded chitosan functionalized poly (lactic-co-glycolic acid) (PLGA) nanoparticles for potential treatment of age-related macular degeneration. *Int. J. Biol. Macromol.* **2021**, *191*, 548–559. [[CrossRef](#)] [[PubMed](#)]
 33. Youssef, A.; Dudhipala, N.; Majumdar, S. Ciprofloxacin Loaded Nanostructured Lipid Carriers Incorporated into In-Situ Gels to Improve Management of Bacterial Endophthalmitis. *Pharmaceutics* **2020**, *12*, 572. [[CrossRef](#)] [[PubMed](#)]
 34. Tabatabaei, S.N.; Derbali, R.M.; Yang, C.; Superstein, R.; Hamel, P.; Chain, J.L.; Hardy, P. Co-delivery of miR-181a and melphalan by lipid nanoparticles for treatment of seeded retinoblastoma. *J. Control. Release* **2019**, *298*, 177–185. [[CrossRef](#)] [[PubMed](#)]
 35. Allyn, M.M.; Luo, R.H.; Hellwarth, E.B.; Swindle-Reilly, K.E. Considerations for Polymers Used in Ocular Drug Delivery. *Front. Med.* **2022**, *8*, 1–25. [[CrossRef](#)]

36. Toropainen, E.; Fraser-Miller, S.J.; Novakovic, D.; Del Amo, E.M.; Vellonen, K.S.; Ruponen, M.; Viitala, T.; Korhonen, O.; Auriola, S.; Hellinen, L.; et al. Biopharmaceutics of topical ophthalmic suspensions: Importance of viscosity and particle size in ocular absorption of indomethacin. *Pharmaceutics* **2021**, *13*, 452. [[CrossRef](#)]
37. Divya, K.; Yashwant, V.P.; Kevin, B.S. Theranostic Applications of Nanomaterials for Ophthalmic Applications. *Int. J. Sci. Adv.* **2021**, *2*, 354–364. [[CrossRef](#)]
38. Awwad, S.; Mohamed Ahmed, A.H.A.; Sharma, G.; Heng, J.S.; Khaw, P.T.; Brocchini, S.; Lockwood, A. Principles of pharmacology in the eye. *Br. J. Pharmacol.* **2017**, *174*, 4205–4223. [[CrossRef](#)]
39. Dosmar, E.; Walsh, J.; Doyel, M.; Bussett, K.; Oladipupo, A.; Amer, S.; Goebel, K. Targeting Ocular Drug Delivery: An Examination of Local Anatomy and Current Approaches. *Bioengineering* **2022**, *9*, 41. [[CrossRef](#)]
40. Atta, G.; Tempfer, H.; Kaser-Eichberger, A.; Traweger, A.; Heindl, L.M.; Schroedl, F. Is the human sclera a tendon-like tissue? A structural and functional comparison. *Ann. Anat.* **2022**, *240*, 151858. [[CrossRef](#)]
41. Lopes, B.T.; Bao, F.; Wang, J.; Liu, X.; Wang, L.; Abass, A.; Eliasy, A.; Elsheikh, A. Review of in-vivo characterisation of corneal biomechanics. *Med. Nov. Technol. Devices* **2021**, *11*, 100073. [[CrossRef](#)]
42. Zénon, A. Eye pupil signals information gain. *Proc. R. Soc. B Biol. Sci.* **2019**, *286*, 20191593. [[CrossRef](#)] [[PubMed](#)]
43. Domkin, D.; Forsman, M.; Richter, H.O. Effect of ciliary-muscle contraction force on trapezius muscle activity during computer mouse work. *Eur. J. Appl. Physiol.* **2019**, *119*, 389–397. [[CrossRef](#)] [[PubMed](#)]
44. Chow, L.S.; Paley, M.N.J. Recent advances on optic nerve magnetic resonance imaging and post-processing. *Magn. Reson. Imaging* **2021**, *79*, 76–84. [[CrossRef](#)]
45. Kaur, I.P.; Smitha, R.; Aggarwal, D.; Kapil, M. Acetazolamide: Future perspective in topical glaucoma therapeutics. *Int. J. Pharm.* **2002**, *248*, 1–14. [[CrossRef](#)]
46. Nielsen, L.H.; Keller, S.S.; Boisen, A. Microfabricated devices for oral drug delivery. *Lab Chip* **2018**, *18*, 2348–2358. [[CrossRef](#)]
47. Underhill, G.H.; Khetani, S.R. Advances in engineered human liver platforms for drug metabolism studies. *Drug Metab. Dispos.* **2018**, *46*, 1626–1637. [[CrossRef](#)]
48. Pitkänen, L.; Ranta, V.P.; Moilanen, H.; Urtti, A. Permeability of retinal pigment epithelium: Effects of permeant molecular weight and lipophilicity. *Investig. Ophthalmol. Vis. Sci.* **2005**, *46*, 641–646. [[CrossRef](#)]
49. Reinholz, J.; Landfester, K.; Mailänder, V. The challenges of oral drug delivery via nanocarriers. *Drug Deliv.* **2018**, *25*, 1694–1705. [[CrossRef](#)]
50. Kim, Y.C.; Chiang, B.; Wu, X.; Prausnitz, M.R. Ocular delivery of macromolecules. *J. Control. Release* **2014**, *190*, 172–181. [[CrossRef](#)]
51. Urtti, A. Challenges and obstacles of ocular pharmacokinetics and drug delivery. *Adv. Drug Deliv. Rev.* **2006**, *58*, 1131–1135. [[CrossRef](#)] [[PubMed](#)]
52. Falavarjani, K.G.; Nguyen, Q.D. Adverse events and complications associated with intravitreal injection of anti-VEGF agents: A review of literature. *Eye* **2013**, *27*, 787–794. [[CrossRef](#)] [[PubMed](#)]
53. Ibrahim, S.S. The Role of Surface Active Agents in Ophthalmic Drug Delivery: A Comprehensive Review. *J. Pharm. Sci.* **2019**, *108*, 1923–1933. [[CrossRef](#)]
54. Liebmann, J.M.; Barton, K.; Weinreb, R.N.; Eichenbaum, D.A.; Gupta, P.K.; McCabe, C.M.; Wolfe, J.D.; Ahmed, I.; Sheybani, A.; Craven, E.R. Evolving Guidelines for Intracameral Injection. *J. Glaucoma* **2020**, *29*, 1–7. [[CrossRef](#)] [[PubMed](#)]
55. Takahashi, K.; Morizane, Y.; Hisatomi, T.; Tachibana, T.; Kimura, S.; Hosokawa, M.M.; Shiode, Y.; Hirano, M.; Doi, S.; Toshima, S.; et al. The influence of subretinal injection pressure on the microstructure of the monkey retina. *PLoS ONE* **2018**, *13*, e0209996. [[CrossRef](#)] [[PubMed](#)]
56. Sebbag, L.; Moody, L.M.; Mochel, J.P. Albumin levels in tear film modulate the

- bioavailability of medically-relevant topical drugs. *Front. Pharmacol.* **2020**, *10*, 1–9. [[CrossRef](#)] [[PubMed](#)]
57. Järvinen, K.; Järvinen, T.; Urtti, A. Ocular absorption following topical delivery. *Adv. Drug Deliv. Rev.* **1995**, *16*, 3–19. [[CrossRef](#)]
 58. Patere, S.; Newman, B.; Wang, Y.; Choi, S.; Vora, S.; Ma, A.W.K.; Jay, M.; Lu, X. Influence of Manufacturing Process Variables on the Properties of Ophthalmic Ointments of Tobramycin. *Pharm. Res.* **2018**, *35*, 1–6. [[CrossRef](#)]
 59. Lazcano-Gomez, G.; Castillejos, A.; Kahook, M.; Jimenez-Roman, J.; Gonzalez-Salinas, R. Videographic assessment of glaucoma drop instillation. *J. Curr. Glaucoma Pract.* **2015**, *9*, 47–50. [[CrossRef](#)]
 60. Taneja, M.; Chappidi, K.; Harsha Ch, S.N.S.; Richhariya, A.; Mohamed, A.; Rathi, V.M. Innovative bulls eye drop applicator for self-instillation of eye drops. *Contact Lens Anterior Eye* **2020**, *43*, 256–260. [[CrossRef](#)]
 61. Davies, I.; Williams, A.M.; Muir, K.W. Aids for eye drop administration. *Surv. Ophthalmol.* **2017**, *62*, 332–345. [[CrossRef](#)]
 62. Hornof, M.; Toropainen, E.; Urtti, A. Cell culture models of the ocular barriers. *Eur. J. Pharm. Biopharm.* **2005**, *60*, 207–225. [[CrossRef](#)] [[PubMed](#)]
 63. Juretić, M.; Cetina-Čizmek, B.; Filipović-Grićić, J.; Hafner, A.; Lovrić, J.; Pepić, I. Biopharmaceutical evaluation of surface active ophthalmic excipients using in vitro and ex vivo corneal models. *Eur. J. Pharm. Sci.* **2018**, *120*, 133–141. [[CrossRef](#)] [[PubMed](#)]
 64. Li, Q.; Weng, J.; Wong, S.N.; Thomas Lee, W.Y.; Chow, S.F. Nanoparticulate Drug Delivery to the Retina. *Mol. Pharm.* **2021**, *18*, 506–521. [[CrossRef](#)] [[PubMed](#)]
 65. Karki, R.; Meena, M.; Prakash, T.; Rajeswari, T.; Goli, D.; Kumar, S. Reduction in drop size of ophthalmic topical drop preparations and the impact of treatment. *J. Adv. Pharm. Technol. Res.* **2011**, *2*, 192. [[CrossRef](#)]
 66. Puglia, C.; Santonocito, D.; Romeo, G.; Intagliata, S.; Romano, G.L.; Strettoi, E.; Novelli, E.; Ostacolo, C.; Campiglia, P.; Sommella, E.M.; et al. Lipid nanoparticles traverse non-corneal path to reach the posterior eye segment: In vivo evidence. *Molecules* **2021**, *26*, 4673. [[CrossRef](#)]
 67. Bechnak, L.; El Kurdi, R.; Patra, D. Fluorescence Sensing of Nucleic Acid by Curcumin Encapsulated Poly(Ethylene Oxide)-Block-Poly(Propylene Oxide)-Block-Poly(Ethylene Oxide) Based Nanocapsules. *J. Fluoresc.* **2020**, *30*, 547–556. [[CrossRef](#)] [[PubMed](#)]
 68. Beija, M.; Afonso, C.A.M.; Martinho, J.M.G. Synthesis and applications of rhodamine derivatives as fluorescent probes. *Chem. Soc. Rev.* **2009**, *38*, 2410–2433. [[CrossRef](#)] [[PubMed](#)]
 69. Han, Z.X.; Zhang, X.B.; Li, Z.; Gong, Y.J.; Wu, X.Y.; Jin, Z.; He, C.M.; Jian, L.X.; Zhang, J.; Shen, G.L.; et al. Efficient fluorescence resonance energy transfer-based ratiometric fluorescent cellular imaging probe for Zn²⁺ using a rhodamine spirolactam as a trigger. *Anal. Chem.* **2010**, *82*, 3108–3113. [[CrossRef](#)] [[PubMed](#)]
 70. Keerthana, S.; Sam, B.; George, L.; Sudhakar, Y.N.; Varghese, A. Fluorescein Based Fluorescence Sensors for the Selective Sensing of Various Analytes. *J. Fluoresc.* **2021**, *31*, 1251–1276. [[CrossRef](#)]
 71. El Khoury, E.; Patra, D. Length of hydrocarbon chain influences location of curcumin in liposomes: Curcumin as a molecular probe to study ethanol induced interdigitation of liposomes. *J. Photochem. Photobiol. B Biol.* **2016**, *158*, 49–54. [[CrossRef](#)] [[PubMed](#)]
 72. Khorasani, M.Y.; Langari, H.; Sany, S.B.T.; Rezayi, M.; Sahebkar, A. The role of curcumin and its derivatives in sensory applications. *Mater. Sci. Eng. C* **2019**, *103*, 109792. [[CrossRef](#)] [[PubMed](#)]
 73. Carneiro, A.; Matos, M.J.; Uriarte, E.; Santana, L. Trending topics on coumarin and its derivatives in 2020. *Molecules* **2021**, *26*, 501. [[CrossRef](#)] [[PubMed](#)]
 74. Duong, H.D.; Shin, Y.; Rhee, J. II Development of novel optical pH sensors based on coumarin 6 and nile blue A encapsulated in resin particles and specific support materials. *Mater. Sci. Eng. C* **2020**, *107*, 110323. [[CrossRef](#)] [[PubMed](#)]
 75. Grimm, J.B.; Lavis, L.D. Synthesis of rhodamines from fluoresceins using pd-catalyzed

- c-n cross-coupling. *Org. Lett.* **2011**, *13*, 6354–6357. [[CrossRef](#)] [[PubMed](#)]
76. Rajasekar, M. Recent development in fluorescein derivatives. *J. Mol. Struct.* **2021**, *1224*, 129085. [[CrossRef](#)]
 77. McHedlov-Petrosyan, N.O.; Cheipesh, T.A.; Roshal, A.D.; Shekhovtsov, S.V.; Moskaeva, E.G.; Omelchenko, I.V. Aminofluoresceins Versus Fluorescein: Peculiarity of Fluorescence. *J. Phys. Chem. A* **2019**, *123*, 8860–8870. [[CrossRef](#)]
 78. Zhao, X.; Belykh, E.; Cavallo, C.; Valli, D.; Gandhi, S.; Preul, M.C.; Vajkoczy, P.; Lawton, M.T.; Nakaji, P. Application of Fluorescein Fluorescence in Vascular Neurosurgery. *Front. Surg.* **2019**, *6*, 52. [[CrossRef](#)]
 79. Küçükürük, B.; Korkmaz, T.S.; Nemayire, K.; Özlen, F.; Kafadar, A.M.; Akar, Z.; Kaynar, M.Y.; Sanus, G.Z. Intraoperative Fluorescein Sodium Videoangiography in Intracranial Aneurysm Surgery. *World Neurosurg.* **2021**, *147*, e444–e452. [[CrossRef](#)]
 80. Bömers, J.P.; Danielsen, M.E.; Schulz, M.K.; Halle, B.; Kristensen, B.W.; Sørensen, M.D.; Poulsen, F.R.; Pedersen, C.B. Sodium fluorescein shows high surgeon-reported usability in glioblastoma surgery. *Surgeon* **2020**, *18*, 344–348. [[CrossRef](#)]
 81. Voronin, D.V.; Kozlova, A.A.; Verkhovskii, R.A.; Ermakov, A.V.; Makarkin, M.A.; Inozemtseva, O.A.; Bratashov, D.N. Detection of rare objects by flow cytometry: Imaging, cell sorting, and deep learning approaches. *Int. J. Mol. Sci.* **2020**, *21*, 2323. [[CrossRef](#)] [[PubMed](#)]
 82. Wang, L.; Du, W.; Hu, Z.; Uvdal, K.; Li, L.; Huang, W. Hybrid Rhodamine Fluorophores in the Visible/NIR Region for Biological Imaging. *Angew. Chem.-Int. Ed.* **2019**, *58*, 14026–14043. [[CrossRef](#)] [[PubMed](#)]
 83. Marnett, L.J. Synthesis of 5- and 6-Carboxy-X-rhodamines. *Org. Lett.* **2008**, *10*, 4799–4801.
 84. Bonaccorso, A.; Musumeci, T.; Serapide, M.F.; Pellitteri, R.; Uchegbu, I.F.; Puglisi, G. Nose to brain delivery in rats: Effect of surface charge of rhodamine B labeled nanocarriers on brain subregion localization. *Colloids Surf. B Biointerfaces* **2017**, *154*, 297–306. [[CrossRef](#)] [[PubMed](#)]
 85. Dempsey, G.T.; Bates, M.; Kowtoniuk, W.E.; Liu, D.R.; Tsien, R.Y.; Zhuang, X. Photoswitching mechanism of cyanine dyes. *J. Am. Chem. Soc.* **2009**, *131*, 18192–18193. [[CrossRef](#)]
 86. Lim, E.; Kwon, J.; Park, J.; Heo, J.; Kim, S.K. Selective thiolation and photoswitching mechanism of Cy5 studied by time-dependent density functional theory. *Phys. Chem. Chem. Phys.* **2020**, *22*, 14125–14129. [[CrossRef](#)]
 87. Bae, S.; Lim, E.; Hwang, D.; Huh, H.; Kim, S.K. Torsion-dependent fluorescence switching of amyloid-binding dye NIAD-4. *Chem. Phys. Lett.* **2015**, *633*, 109–113. [[CrossRef](#)]
 88. Blower, M.D.; Feric, E.; Weis, K.; Heald, R. Genome-wide analysis demonstrates conserved localization of messenger RNAs to mitotic microtubules. *J. Cell Biol.* **2007**, *179*, 1365–1373. [[CrossRef](#)]
 89. Martos, A.; Berger, M.; Kranz, W.; Spanopoulou, A.; Menzen, T.; Friess, W.; Wuchner, K.; Hawe, A. Novel High-Throughput Assay for Polysorbate Quantification in Biopharmaceutical Products by Using the Fluorescent Dye DiI. *J. Pharm. Sci.* **2020**, *109*, 646–655. [[CrossRef](#)] [[PubMed](#)]
 90. Musumeci, T.; Serapide, M.F.; Pellitteri, R.; Dalpiaz, A.; Ferraro, L.; Dal Magro, R.; Bonaccorso, A.; Carbone, C.; Veiga, F.; Sancini, G.; et al. Oxcarbazepine free or loaded PLGA nanoparticles as effective intranasal approach to control epileptic seizures in rodents. *Eur. J. Pharm. Biopharm.* **2018**, *133*, 309–320. [[CrossRef](#)]
 91. Capolungo, C.; Genovese, D.; Montalti, M.; Rampazzo, E.; Zaccheroni, N.; Prodi, L. Photoluminescence-Based Techniques for the Detection of Micro- and Nanoplastics. *Chem.-A Eur. J.* **2021**, *27*, 17529–17541. [[CrossRef](#)]
 92. Sancataldo, G.; Avellone, G.; Vetri, V. Nile Red lifetime reveals microplastic identity. *Environ. Sci. Process. Impacts* **2020**, *22*, 2266–2275. [[CrossRef](#)]
 93. Hewlings, S.J.; Kalman, D.S. Curcumin: A review of its effects on human health. *Foods* **2017**, *6*, 92. [[CrossRef](#)] [[PubMed](#)]

94. Sridharan, G.; Shankar, A.A. Toluidine blue: A review of its chemistry and clinical utility. *J. Oral Maxillofac. Pathol.* **2012**, *16*, 251–255. [[CrossRef](#)] [[PubMed](#)]
95. Aliakbar Navahi, R.; Hosseini, S.B.; Kanavi, M.R.; Rakhshani, N.; Aghaei, H.; Kheiri, B. Comparison of toluidine blue 1% staining patterns in cytopathologically confirmed ocular surface squamous neoplasias and in non-neoplastic lesions. *Ocul. Surf.* **2019**, *17*, 578–583. [[CrossRef](#)]
96. Su, G.; Wei, Z.; Wang, L.; Shen, J.; Baudouin, C.; Labbé, A.; Liang, Q. Evaluation of toluidine blue-mediated photodynamic therapy for experimental bacterial keratitis in rabbits. *Transl. Vis. Sci. Technol.* **2020**, *9*, 1–10. [[CrossRef](#)] [[PubMed](#)]
97. Craparo, E.F.; Musumeci, T.; Bonaccorso, A.; Pellitteri, R.; Romeo, A.; Naletova, I.; Cucci, L.M.; Cavallaro, G.; Satriano, C. Mpeg-plga nanoparticles labeled with loaded or conjugated rhodamine-b for potential nose-to-brain delivery. *Pharmaceutics* **2021**, *13*, 1508. [[CrossRef](#)]
98. Turcsányi, Á.; Ungor, D.; Csapó, E. Fluorescent labeling of hyaluronic acid-chitosan nanocarriers by protein-stabilized gold nanoclusters. *Crystals* **2020**, *10*, 1113. [[CrossRef](#)]
99. Romero, G.B.; Keck, C.M.; Müller, R.H.; Bou-Chacra, N.A. Development of cationic nanocrystals for ocular delivery. *Eur. J. Pharm. Biopharm.* **2016**, *107*, 215–222. [[CrossRef](#)]
100. Pignatello, R.; Corsaro, R.; Santonocito, D. Chapter A Method for Efficient Loading of Ciprofloxacin Hydrochloride in Cationic Solid Lipid Nanoparticles. *Nanomaterials* **2018**, *8*, 304. [[CrossRef](#)]
101. Jounaki, K.; Makhmalzadeh, B.S.; Feghhi, M.; Heidarian, A. Topical ocular delivery of vancomycin loaded cationic lipid nanocarriers as a promising and non-invasive alternative approach to intravitreal injection for enhanced bacterial endophthalmitis management. *Eur. J. Pharm. Sci.* **2021**, *167*, 105991. [[CrossRef](#)] [[PubMed](#)]
102. Vaishya, R.D.; Khurana, V.; Patel, S.; Mitra, A.K. Controlled ocular drug delivery with nanomicelles. *Wiley Interdiscip. Rev. Nanomed. Nanobiotechnology* **2014**, *6*, 422–437. [[CrossRef](#)] [[PubMed](#)]
103. Zhang, W.H.; Hu, X.X.; Zhang, X.B. Dye-doped fluorescent silica nanoparticles for live cell and in vivo bioimaging. *Nanomaterials* **2016**, *6*, 81. [[CrossRef](#)]
104. Siddique, S.; Chow, J.C.L. Application of nanomaterials in biomedical imaging and cancer therapy. *Nanomaterials* **2020**, *10*, 1700. [[CrossRef](#)] [[PubMed](#)]
105. Niamprem, P.; Srinivas, S.P.; Tiyafoonchai, W. Penetration of Nile red-loaded nanostructured lipid carriers (NLCs) across the porcine cornea. *Colloids Surf. B Biointerfaces* **2019**, *176*, 371–378. [[CrossRef](#)] [[PubMed](#)]
106. El-Gendy, M.A.; Mansour, M.; El-Assal, M.I.A.; Ishak, R.A.H.; Mortada, N.D. Delineating penetration enhancer-enriched liquid crystalline nanostructures as novel platforms for improved ophthalmic delivery. *Int. J. Pharm.* **2020**, *582*, 119313. [[CrossRef](#)]
107. Kapadia, R.; Parikh, K.; Jain, M.; Sawant, K. Topical instillation of triamcinolone acetone-loaded emulsomes for posterior ocular delivery: Statistical optimization and in vitro-in vivo studies. *Drug Deliv. Transl. Res.* **2021**, *11*, 984–999. [[CrossRef](#)] [[PubMed](#)]
108. Eldesouky, L.M.; El-Moslemany, R.M.; Ramadan, A.A.; Morsi, M.H.; Khalafallah, N.M. Cyclosporine lipid nanocapsules as thermoresponsive gel for dry eye management: Promising corneal mucoadhesion, biodistribution and preclinical efficacy in rabbits. *Pharmaceutics* **2021**, *13*, 360. [[CrossRef](#)] [[PubMed](#)]
109. Dubashynskaya, N.V.; Bokaty, A.N.; Golovkin, A.S.; Kudryavtsev, I.V.; Serebryakova, M.K.; Trulioff, A.S.; Dubrovskii, Y.A.; Skorik, Y.A. Synthesis and characterization of novel succinyl chitosan-dexamethasone conjugates for potential intravitreal dexamethasone delivery. *Int. J. Mol. Sci.* **2021**, *22*, 10960. [[CrossRef](#)] [[PubMed](#)]
110. Li, J.; Tan, G.; Cheng, B.; Liu, D.; Pan, W. Transport mechanism of chitosan-N-acetylcysteine, chitosan oligosaccharides or carboxymethyl chitosan decorated coumarin-6 loaded nanostructured lipid carriers across the rabbit ocular. *Eur. J. Pharm. Biopharm.* **2017**, *120*, 89–97. [[CrossRef](#)] [[PubMed](#)]

111. Tan, G.; Li, J.; Song, Y.; Yu, Y.; Liu, D.; Pan, W. Phenylboronic acid-tethered chondroitin sulfate-based mucoadhesive nanostructured lipid carriers for the treatment of dry eye syndrome. *Acta Biomater.* **2019**, *99*, 350–362. [[CrossRef](#)] [[PubMed](#)]
112. Liu, C.; Lan, Q.; He, W.; Nie, C.; Zhang, C.; Xu, T.; Jiang, T.; Wang, S. Octa-arginine modified lipid emulsions as a potential ocular delivery system for disulfiram: A study of the corneal permeation, transcorneal mechanism and anti-cataract effect. *Colloids Surf. B Biointerfaces* **2017**, *160*, 305–314. [[CrossRef](#)] [[PubMed](#)]
113. Gómez-Aguado, I.; Rodríguez-Castejón, J.; Beraza-Millor, M.; Vicente-Pascual, M.; Rodríguez-Gascón, A.; Garelli, S.; Battaglia, L.; Del Pozo-Rodríguez, A.; Solinís, M.Á. Mrna-based nanomedicinal products to address corneal inflammation by interleukin-10 supplementation. *Pharmaceutics* **2021**, *13*, 1472. [[CrossRef](#)] [[PubMed](#)]
114. Kakkar, S.; Singh, M.; Mohan Karuppayil, S.; Raut, J.S.; Giansanti, F.; Papucci, L.; Schiavone, N.; Nag, T.C.; Gao, N.; Yu, F.S.X.; et al. Lipo-PEG nano-ocular formulation successfully encapsulates hydrophilic fluconazole and traverses corneal and non-corneal path to reach posterior eye segment. *J. Drug Target.* **2021**, *29*, 631–650. [[CrossRef](#)]
115. Pretor, S.; Bartels, J.; Lorenz, T.; Dahl, K.; Finke, J.H.; Peterat, G.; Krull, R.; Dietzel, A.; Bu, S.; Behrends, S.; et al. Cellular Uptake of Coumarin-6 under Microfluidic Conditions into HCE-T Cells from Nanoscale Formulations. *Mol. Pharm.* **2015**, *12*, 34–45. [[CrossRef](#)] [[PubMed](#)]
116. Elmotasem, H.; Awad, G.E.A. A stepwise optimization strategy to formulate in situ gelling formulations comprising fluconazole- hydroxypropyl-beta-cyclodextrin complex loaded niosomal vesicles and Eudragit nanoparticles for enhanced antifungal activity and prolonged ocular delivery. *Asian J. Pharm. Sci.* **2020**, *15*, 617–636. [[CrossRef](#)] [[PubMed](#)]
117. Anishiya chella daisy, E.R.; Rajendran, N.K.; Jeyaraj, M.; Ramu, A.; Rajan, M. Retinal photoreceptors targeting SA-g-AA coated multilamellar liposomes carrier system for cytotoxicity and cellular uptake evaluation. *J. Liposome Res.* **2021**, *31*, 203–216. [[CrossRef](#)]
118. Swetledge, S.; Carter, R.; Stout, R.; Astete, C.E.; Jung, J.P.; Sabliov, C.M. Stability and ocular biodistribution of topically administered PLGA nanoparticles. *Sci. Rep.* **2021**, *11*, 1–11. [[CrossRef](#)]
119. Dubashynskaya, N.; Poshina, D.; Raik, S.; Urtti, A.; Skorik, Y.A. Polysaccharides in ocular drug delivery. *Pharmaceutics* **2020**, *12*, 22. [[CrossRef](#)]
120. Zhukova, V.; Osipova, N.; Semyonkin, A.; Malinovskaya, J.; Melnikov, P.; Valikhov, M.; Porozov, Y.; Solovev, Y.; Kuliaev, P.; Zhang, E.; et al. Fluorescently labeled plga nanoparticles for visualization in vitro and in vivo: The importance of dye properties. *Pharmaceutics* **2021**, *13*, 1145. [[CrossRef](#)]
121. Zhang, E.; Zhukova, V.; Semyonkin, A.; Osipova, N.; Malinovskaya, Y.; Maksimenko, O.; Chernikov, V.; Sokolov, M.; Grigartzik, L.; Sabel, B.A.; et al. Release kinetics of fluorescent dyes from PLGA nanoparticles in retinal blood vessels: In vivo monitoring and ex vivo localization. *Eur. J. Pharm. Biopharm.* **2020**, *150*, 131–142. [[CrossRef](#)] [[PubMed](#)]
122. Li, B.; Wang, J.; Gui, Q.; Yang, H. Drug-loaded chitosan film prepared via facile solution casting and air-drying of plain water-based chitosan solution for ocular drug delivery. *Bioact. Mater.* **2020**, *5*, 577–583. [[CrossRef](#)] [[PubMed](#)]
123. Álvarez-Álvarez, L.; Barral, L.; Bouza, R.; Farrag, Y.; Otero-Espinar, F.; Feijóo-Bandín, S.; Lago, F. Hydrocortisone loaded poly-(3-hydroxybutyrate-co-3-hydroxyvalerate) nanoparticles for topical ophthalmic administration: Preparation, characterization and evaluation of ophthalmic toxicity. *Int. J. Pharm.* **2019**, *568*, 118519. [[CrossRef](#)] [[PubMed](#)]
124. Tahara, K.; Karasawa, K.; Onodera, R.; Takeuchi, H. Feasibility of drug delivery to the eye's posterior segment by topical instillation of PLGA nanoparticles. *Asian J. Pharm. Sci.* **2017**, *12*, 394–399. [[CrossRef](#)] [[PubMed](#)]
125. Sun, X.; Sheng, Y.; Li, K.; Sai, S.; Feng, J.; Li, Y.; Zhang, J.; Han, J.; Tian, B. Mucoadhesive phenylboronic acid conjugated chitosan oligosaccharide-vitamin E copolymer for topical ocular delivery of voriconazole: Synthesis, in vitro/vivo evaluation, and mechanism.

- Acta Biomater.* **2022**, *138*, 193–207. [[CrossRef](#)]
126. Sai, N.; Dong, X.; Huang, P.; You, L.; Yang, C.; Liu, Y.; Wang, W.; Wu, H.; Yu, Y.; Du, Y.; et al. A novel gel-forming solution based on PEG-DSPE/Solutol HS 15 mixed micelles and gellan gum for ophthalmic delivery of curcumin. *Molecules* **2020**, *25*, 81. [[CrossRef](#)]
 127. Abilova, G.K.; Kaldybekov, D.B.; Ozhmukhametova, E.K.; Saimova, A.Z.; Kazybayeva, D.S.; Irmukhametova, G.S.; Khutoryanskiy, V.V. Chitosan/poly(2-ethyl-2-oxazoline) films for ocular drug delivery: Formulation, miscibility, in vitro and in vivo studies. *Eur. Polym. J.* **2019**, *116*, 311–320. [[CrossRef](#)]
 128. Chi, H.; Gu, Y.; Xu, T.; Cao, F. Multifunctional organic–inorganic hybrid nanoparticles and nanosheets based on chitosan derivative and layered double hydroxide: Cellular uptake mechanism and application for topical ocular drug delivery. *Int. J. Nanomedicine* **2017**, *12*, 1607–1620. [[CrossRef](#)]
 129. Mun, E.A.; Morrison, P.W.J.; Williams, A.C.; Khutoryanskiy, V.V. On the barrier properties of the cornea: A microscopy study of the penetration of fluorescently labeled nanoparticles, polymers, and sodium fluorescein. *Mol. Pharm.* **2014**, *11*, 3556–3564. [[CrossRef](#)]
 130. Baran-Rachwalska, P.; Torabi-Pour, N.; Sutera, F.M.; Ahmed, M.; Thomas, K.; Nesbit, M.A.; Welsh, M.; Moore, C.B.T.; Saffie-Siebert, S.R. Topical siRNA delivery to the cornea and anterior eye by hybrid silicon-lipid nanoparticles. *J. Control. Release* **2020**, *326*, 192–202. [[CrossRef](#)]
 131. Qu, W.; Meng, B.; Yu, Y.; Wang, S. EpCAM antibody-conjugated mesoporous silica nanoparticles to enhance the anticancer efficacy of carboplatin in retinoblastoma. *Mater. Sci. Eng. C* **2017**, *76*, 646–651. [[CrossRef](#)] [[PubMed](#)]
 132. Xu, H.; Tang, B.; Huang, W.; Luo, S.; Zhang, T.; Yuan, J.; Zheng, Q.; Zan, X. Deliver protein across bio-barriers via hexa-histidine metal assemblies for therapy: A case in corneal neovascularization model. *Mater. Today Bio* **2021**, *12*, 100143. [[CrossRef](#)] [[PubMed](#)]
 133. Wang, Y.; Liu, W.; Yuan, B.; Yin, X.; Li, Y.; Li, Z.; Cui, J.; Yuan, X.; Li, Y. The application of methylprednisolone nanoscale zirconium- porphyrin metal-organic framework (MPS-NPMOF) in the treatment of photoreceptor degeneration. *Int. J. Nanomedicine* **2019**, *14*, 9763–9776. [[CrossRef](#)] [[PubMed](#)]
 134. Ding, S.; Zhang, N.; Lyu, Z.; Zhu, W.; Chang, Y.C.; Hu, X.; Du, D.; Lin, Y. Protein-based nanomaterials and nanosystems for biomedical applications: A review. *Mater. Today* **2021**, *43*, 166–184. [[CrossRef](#)]
 135. Nguyen, T.P.; Nguyen, Q.V.; Nguyen, V.H.; Le, T.H.; Huynh, V.Q.N.; Vo, D.V.N.; Trinh, Q.T.; Kim, S.Y.; Van Le, Q. Silk fibroin-based biomaterials for biomedical applications: A review. *Polymers* **2019**, *11*, 1933. [[CrossRef](#)]
 136. Yang, P.; Dong, Y.; Huang, D.; Zhu, C.; Liu, H.; Pan, X.; Wu, C. Silk fibroin nanoparticles for enhanced bio-macromolecule delivery to the retina. *Pharm. Dev. Technol.* **2019**, *24*, 575–583. [[CrossRef](#)]
 137. Tiwari, R.; Sethiya, N.K.; Gulbake, A.S.; Mehra, N.K.; Murty, U.S.N.; Gulbake, A. A review on albumin as a biomaterial for ocular drug delivery. *Int. J. Biol. Macromol.* **2021**, *191*, 591–599. [[CrossRef](#)]
 138. Radwan, S.E.S.; El-Kamel, A.; Zaki, E.I.; Burgalassi, S.; Zucchetti, E.; El-Moslemany, R.M. Hyaluronic-coated albumin nanoparticles for the non-invasive delivery of apatinib in diabetic retinopathy. *Int. J. Nanomed.* **2021**, *16*, 4481–4494. [[CrossRef](#)]
 139. Zhang, W.; Kantaria, T.; Zhang, Y.; Kantaria, T.; Kobauri, S.; Tugushi, D.; Brücher, V.; Katsarava, R.; Eter, N.; Heiduschka, P. Biodegradable Nanoparticles Based on Pseudo-Proteins Show Promise as Carriers for Ophthalmic Drug Delivery. *J. Ocul. Pharmacol. Ther.* **2020**, *36*, 421–432. [[CrossRef](#)]
 140. Thomas, C.J.; Mirza, R.G.; Gill, M.K. Age-Related Macular Degeneration. *Med. Clin. North Am.* **2021**, *105*, 473–491. [[CrossRef](#)]
 141. Hanus, J.; Anderson, C.; Wang, S. RPE necroptosis in response to oxidative stress and in AMD. *Ageing Res. Rev.* **2015**, *24*, 286–298. [[CrossRef](#)] [[PubMed](#)]

142. Hammond, B.R.; Johnson, M.A. The age-related eye disease study (AREDS). *Nutr. Rev.* **2002**, *60*, 283–288. [[CrossRef](#)] [[PubMed](#)]
143. Gregori, N.Z.; Goldhardt, R. Nutritional Supplements for Age-Related Macular Degeneration. *Curr. Ophthalmol. Rep.* **2015**, *3*, 34–39. [[CrossRef](#)] [[PubMed](#)]
144. Álvarez-Barrios, A.; Álvarez, L.; García, M.; Artime, E.; Pereiro, R.; González-Iglesias, H. Antioxidant defenses in the human eye: A focus on metallothioneins. *Antioxidants* **2021**, *10*, 89. [[CrossRef](#)] [[PubMed](#)]
145. Cruz-Alonso, M.; Fernandez, B.; Álvarez, L.; González-Iglesias, H.; Traub, H.; Jakubowski, N.; Pereiro, R. Bioimaging of metallothioneins in ocular tissue sections by laser ablation-ICP-MS using bioconjugated gold nanoclusters as specific tags. *Microchim. Acta* **2018**, *185*, 1–9. [[CrossRef](#)]
146. Osredkar, J. Copper and Zinc, Biological Role and Significance of Copper/Zinc Imbalance. *J. Clin. Toxicol.* **2011**, *3*, 1–18. [[CrossRef](#)]
147. Uddin, M.I.; Kilburn, T.C.; Yang, R.; McCollum, G.W.; Wright, D.W.; Penn, J.S. Targeted imaging of VCAM-1 mRNA in a mouse model of laser-induced choroidal neovascularization using antisense hairpin-DNA-functionalized gold-nanoparticles. *Mol. Pharm.* **2018**, *15*, 5514–5520. [[CrossRef](#)]
148. Pearson, R.A.; Barber, A.C.; Rizzi, M. Restoration of vision after transplantation of photoreceptors. *Nature* **2012**, *485*, 99–103. [[CrossRef](#)]
149. Chemla, Y.; Betzer, O.; Markus, A.; Farah, N.; Motiei, M.; Popovtzer, R.; Mandel, Y. Gold nanoparticles for multimodal high-resolution imaging of transplanted cells for retinal replacement therapy. *Nanomedicine* **2019**, *14*, 1857–1871. [[CrossRef](#)]
150. Meir, R.; Shamalov, K.; Betzer, O.; Motiei, M.; Horovitz-Fried, M.; Yehuda, R.; Popovtzer, A.; Popovtzer, R.; Cohen, C.J. Nanomedicine for Cancer Immunotherapy: Tracking Cancer-Specific T-Cells in Vivo with Gold Nanoparticles and CT Imaging. *ACS Nano* **2015**, *9*, 6363–6372. [[CrossRef](#)] [[PubMed](#)]
151. Cai, W.; Chen, M.; Fan, J.; Jin, H.; Yu, D.; Qiang, S.; Peng, C.; Yu, J. Fluorescein sodium loaded by polyethyleneimine for fundus fluorescein angiography improves adhesion. *Nanomedicine* **2019**, *14*, 2595–2611. [[CrossRef](#)] [[PubMed](#)]
152. Safi, H.; Safi, S.; Hafezi-Moghadam, A.; Ahmadi, H. Early detection of diabetic retinopathy. *Surv. Ophthalmol.* **2018**, *63*, 601–608. [[CrossRef](#)]
153. Wang, X.; Li, S.; Li, W.; Hua, Y.; Wu, Q. Choroidal Variations in Diabetic Macular Edema: Fluorescein Angiography and Optical Coherence Tomography. *Curr. Eye Res.* **2018**, *43*, 102–108. [[CrossRef](#)] [[PubMed](#)]
154. Shivshetty, N.; Swift, T.; Pinnock, A.; Pownall, D.; Neil, S.M.; Douglas, I.; Garg, P.; Rimmer, S. Evaluation of ligand modified poly (N-Isopropyl acrylamide) hydrogel for etiological diagnosis of corneal infection. *Exp. Eye Res.* **2022**, *214*, 108881. [[CrossRef](#)] [[PubMed](#)]
155. Ladju, R.B.; Ulhaq, Z.S.; Soraya, G.V. Nanotheranostics: A powerful next-generation solution to tackle hepatocellular carcinoma. *World J. Gastroenterol.* **2022**, *28*, 176–187. [[CrossRef](#)] [[PubMed](#)]
156. Tang, M.; Ji, X.; Xu, H.; Zhang, L.; Jiang, A.; Song, B.; Su, Y.; He, Y. Photostable and Biocompatible Fluorescent Silicon Nanoparticles-Based Theranostic Probes for Simultaneous Imaging and Treatment of Ocular Neovascularization. *Anal. Chem.* **2018**, *90*, 8188–8195. [[CrossRef](#)] [[PubMed](#)]
157. Shabbir, U.; Rubab, M.; Tyagi, A.; Oh, D.H. Curcumin and its derivatives as theranostic agents in Alzheimer's disease: The implication of nanotechnology. *Int. J. Mol. Sci.* **2021**, *22*, 196. [[CrossRef](#)] [[PubMed](#)]
158. Stati, G.; Rossi, F.; Trakoolwilaiwan, T.; Tung, L.D.; Mourdikoudis, S.; Thanh, N.T.K.; Di Pietro, R. Development and Characterization of Curcumin-Silver Nanoparticles as a Promising Formulation to Test on Human Pterygium-Derived Keratinocytes. *Molecules* **2022**, *27*, 282. [[CrossRef](#)] [[PubMed](#)]
159. Zhang, L.; Ji, X.; Su, Y.; Zhai, X.; Xu, H.; Song, B.; Jiang, A.; Guo, D.; He, Y. Fluorescent silicon

- nanoparticles-based nanotheranostic agents for rapid diagnosis and treatment of bacteria-induced keratitis. *Nano Res.* **2021**, *14*, 52–58. [[CrossRef](#)]
160. de Oliveira, D.C.S.; de Freitas, C.F.; Calori, I.R.; Goncalves, R.S.; Cardinali, C.A.E.F.; Malacarne, L.C.; Ravanelli, M.I.; de Oliveira, H.P.M.; Tedesco, A.C.; Caetano, W.; et al. Theranostic verteporfin-loaded lipid-polymer liposome for photodynamic applications. *J. Photochem. Photobiol. B Biol.* **2020**, *212*, 112039. [[CrossRef](#)]
161. Li, L.; Zeng, Z.; Chen, Z.; Gao, R.; Pan, L.; Deng, J.; Ye, X.; Zhang, J.; Zhang, S.; Mei, C.; et al. Microenvironment-triggered degradable hydrogel for imaging diagnosis and combined treatment of intraocular choroidal melanoma. *ACS Nano* **2020**, *14*, 15403–15416. [[CrossRef](#)] [[PubMed](#)]
162. Maulvi, F.A.; Desai, D.T.; Shetty, K.H.; Shah, D.O.; Willcox, M.D.P. Advances and challenges in the nanoparticles-laden contact lenses for ocular drug delivery. *Int. J. Pharm.* **2021**, *608*, 121090. [[CrossRef](#)] [[PubMed](#)]
163. Huang, J.F.; Zhong, J.; Chen, G.P.; Lin, Z.T.; Deng, Y.; Liu, Y.L.; Cao, P.Y.; Wang, B.; Wei, Y.; Wu, T.; et al. A Hydrogel-Based Hybrid Theranostic Contact Lens for Fungal Keratitis. *ACS Nano* **2016**, *10*, 6464–6473. [[CrossRef](#)] [[PubMed](#)]
164. Jin, Y.; Wang, Y.; Yang, J.; Zhang, H.; Yang, Y.W.; Chen, W.; Jiang, W.; Qu, J.; Guo, Y.; Wang, B. An Integrated Theranostic Nanomaterial for Targeted Photodynamic Therapy of Infectious Endophthalmitis. *Cell Reports Phys. Sci.* **2020**, *1*, 100173. [[CrossRef](#)]
165. Khiev, D.; Mohamed, Z.A.; Vichare, R.; Paulson, R.; Bhatia, S.; Mohapatra, S.; Lobo, G.P.; Valapala, M.; Kerur, N.; Passaglia, C.L.; et al. Emerging nano-formulations and nanomedicines applications for ocular drug delivery. *Nanomaterials* **2021**, *11*, 173. [[CrossRef](#)]
166. Alander, J.T.; Kaartinen, I.; Laakso, A.; Tommi, P.; Spillmann, T.; Tuchin, V.V.; Venermo, M.; Petri, V. A Review of Indocyanine Green Fluorescent Imaging in Surgery. *Int. J. Biomed. Imaging* **2012**, *2012*, 7. [[CrossRef](#)] [[PubMed](#)]

CHAPTER VI: *Multilevel statistical optimization: ion pair complexes with flunarizine dihydrochloride encapsulated in nanostructured lipid carriers for potential ocular delivery*

(Manuscript in progress)

Introduction

As discussed in chapter I CCBs have been widely used in the treatment as neuroprotective agents in the treatments of neurodegenerative diseases. Another peculiarity of these class of drugs is their hypotensive properties, inhibiting the intracellular Ca^{2+} influx resulting in relaxation of the vascular muscles with consequent vasodilation and increase in blood flow.

The combination of hypotensive and neuroprotective effects makes these drugs ideal candidates for the treatment of glaucoma [1]. It has been demonstrated that topical administration of diltiazem, verapamil, nifedipine, phenylamine and flunarizine resulted in a reduction in IOP in rabbits, primates and humans [2][3][4].

Flunarizine dihydrochloride ((E)-1-[Bis(4-fluorophenyl)methyl]-4-cinnamyl-piperazine dihydrochloride, (FLN)) is considered a broad-spectrum non-selective CCB. The multiple mechanisms of action exerted by this molecule contribute, each in a different way, to reducing IOP [5][6]. A study by Noguchi et al showed that, after intravenous administration, FLN was the only CCB to act selectively on retinal blood vessels, causing no cardiovascular side effects [7]. FLN is an ionized salt characterized by poor permeability. Over the years, several strategies have been undertaken to modify the solubility and thus the permeability of this molecule, such as inclusion in cyclodextrins and incorporation into solid dispersions, organogel systems and lipid nanoemulsions [8][9][10][11]. Among the approaches used to modify physico-chemical properties, such as solubility of an ionizable hydrophilic drug, hydrophobic ion-pairing (HIP) has proven to be a very useful strategy. HIP technique involves pairing by electrostatic interaction between the ionized drug and an oppositely charged counterion [12][13][14]. This strategy has been widely exploited to enhance drug encapsulation in lipid delivery

systems due to the increased lipophilicity of the complex, which facilitated incorporation into the carriers [15][16][17]. In a study conducted by Li et al., HIP method was applied to modify the permeability of pyranzepine dihydrochloride by complexing with organic acids as counterions [18].

In our study, we chose to investigate three organic acids, a monocarboxylic acid (sorbic acid, SA), a dicarboxylic acid (oxalic acid, OA) and a tricarboxylic acid (citric acid, CA). To ensure a successful complexation, it is necessary to observe the ionization degree of both components of ion-pair. In fact, the pH of the complexation medium has a critical influence on the yield of the process. Another parameter of fundamental importance, to be considered in the formation of ionic complex, is the stoichiometry between the two species. The most used molar ratios between drug and counterion (D:C) vary between 1:0.5 and 1:8 [18][19][20][21][22]. Based on the complexation yields reported in the above studies, 1:1, 1:2 and 1:4 were chosen as molar ratios to be investigated. Ion-pair complexes can be formed before or during encapsulation, in the first case it is called a "preformed" complex and in the second case an "in situ" complex [23]. Following the first method, a combined strategy was proposed in the following study, with the concomitant development of ion-pair in combination with NLC to improve the incorporation of FLN into lipid carrier systems.

A preliminary study was performed to evaluate the solubility of FLN and to select the most suitable medium for complexation. The design and optimization of the ion-pair complex and the empty NLCs were performed by DoE. The optimal condition for HIP strategy were explored using a FFD set up with two factors on 3-levels. Specifically, the effect of two independent variables including (A) the type of organic acid (SA, OA and CA) and (B) the molar ratios D:C (1:1, 1:2 and 1:4) were studied on the output response,

i.e., the percentage binding efficiency (BE%) for the prepared complexes which was evaluated by spectrophotometric analysis.

HIP complexes were prepared according to previously reported methods with slight modifications [21][18]. The proposed technique consisted of simple mixing of aqueous solutions containing FLN and the ion-pairing agent. Briefly, FLN and ion-pairing agents were dissolved in phosphate buffer at pH 3 (50 μ M) separately, then the ion-pairing solution was added slowly to the drug solution. The two stock solutions were mixed at the different molar ratios and left on constant stirring (100 rpm) for 3 hours.

The formation of HIP complexes was evaluated using a spectrophotometer to track the presence of spectral changes. Solid-state complexes were characterized by differential scanning calorimetry (DSC) and Fourier-Transform Infrared Spectroscopy (FT-IR).

The blank NLC formulation was optimized by applying a D-optimal design consisting of three independent variables as the concentration of gelucire[®] 44/14, concentration of mygliol[®] 812 and the ratio of two surfactants in mixture (tween[®] 80 and solutol[®] HS15). D-optimal design experiments were carried out in 15 runs. For each run the effect of the factors was studied on particle size, PDI and ZP of the formulations, selected as dependent variables. The empty NLC was prepared using an adapted melt-emulsification combined with a low-energy injection technique, without the application of ultrasound or high-pressure homogenization, which require specific high-cost equipment [31].

Once both components (HIP and NLC) were optimized, the lipid nanocarriers were loaded with the complexed drug and the formulation was subjected to characterization studies to evaluate the physico-chemical properties.

Preliminary results

PB at pH 3 was the solvent in which FLN showed the highest solubility (97.63%). The good drug dissolution could be attributed to the acidic pH, where FLN ($pK_a = 7.6$) results in an ionized form. In addition, the acidic pH would promote ionization of the carboxyl groups of organic acids. Ion-pairing agents have a $pK_a < 5$ due to the carboxylic functional group, which completely ionizes at pH 3. Therefore, the acidic environment could promote the electrostatic interaction between the protonated amine (FLN) and the carboxylate ion (of the ion-pairing agents) with opposite charge. So, PB at pH 3 was selected as the reaction medium to dissolve FLN and organic acids.

The influence of investigated factors on BE% illustrated in Figure 1 suggested that the HIP complex able to provide the highest binding yield (100%) consisted of SA counterion to the same amount of drug (1:1 molar ratio).

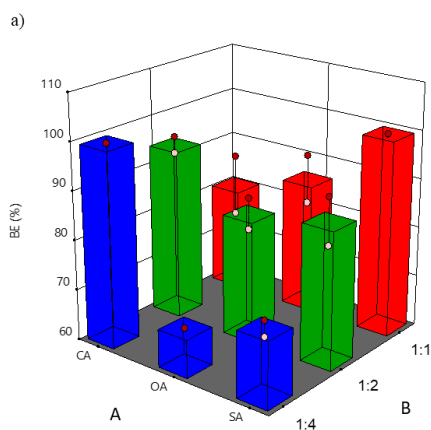


Figure 1. 3D Response surface plot illustrating influence of organic acid type (A) and molar ratio (D:C) (B) on Binding Efficiency (%).

To validate the model used, the proposed complex was prepared and characterized. Predicted error equal to 0.4 % demonstrated a strong correlation between the observed (99.55 %) and predicted (99.98 %) BE%, confirming the reliability of the model.

Absorption spectra of HIP complexes were compared with that of pure FLN. UV scanning of FLN₁SA₁ complex showed a red shift of the characteristic peak to λ 258 nm. The bathochromic shift could be the result of salt formation between oppositely charged ionic groups [24][25]. The absorption curve of the ionic complex exhibited a less inclined ascending segment compared to that seen in pure FLN, resulting in a broader band. The shoulder formed in the 270-300 nm region of the absorption band could be attributed to constructive interference between drug and counterion [26][27].

Thermograms of the HIP complexes (Figure 2) showed the absence of a T_m consistent with the amorphous nature of the complexes, and the presence of events attributable to glass transitions. It has been widely reported that a common property of these chemical entities is low crystallinity. Amorphization therefore could indicate the result of an occurred interaction between ionic species [28].

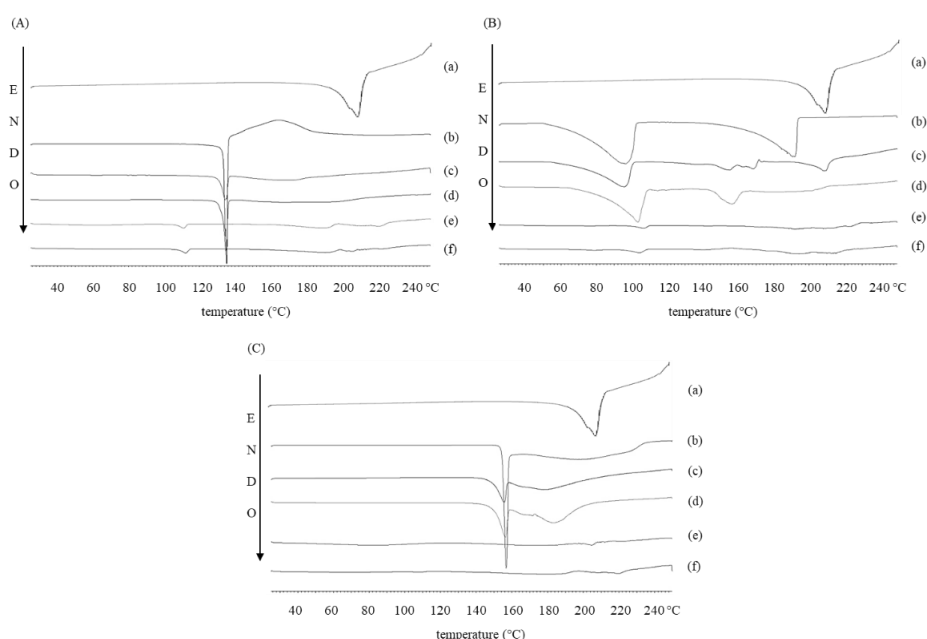


Figure 2. DSC curves of (A) FLN (a), sorbic acid (b), physical mixture FLN+SA₁ (c), physical mixture FLN+SA₂ (d), FLN-SA₁ (e) and FLN-SA₂ ion-pair complex (f); (B) FLN (a), oxalic acid (b), physical mixture FLN+OA₁ (c), physical mixture FLN+OA₂ (d), FLN-OA₁ (e) and FLN-OA₂ ion-pair complex (f); (C) FLN (a), citric acid (b), physical mixture FLN+CA₁ (c), physical mixture FLN+CA₂ (d), FLN-CA₁ (e) and FLN-CA₂ ion-pair complex (f).

As regard FT-IR analysis (Figure 3) a new absorption band between 1507 and 1548 cm^{-1} was observed in the spectrum of each complex, indicating the modification of the FLN amine group. The detection of the new peak suggested a successful complexation process through the ionic interaction occurring between amine group (FLN) and the carboxylic group (counterions) [29][30].

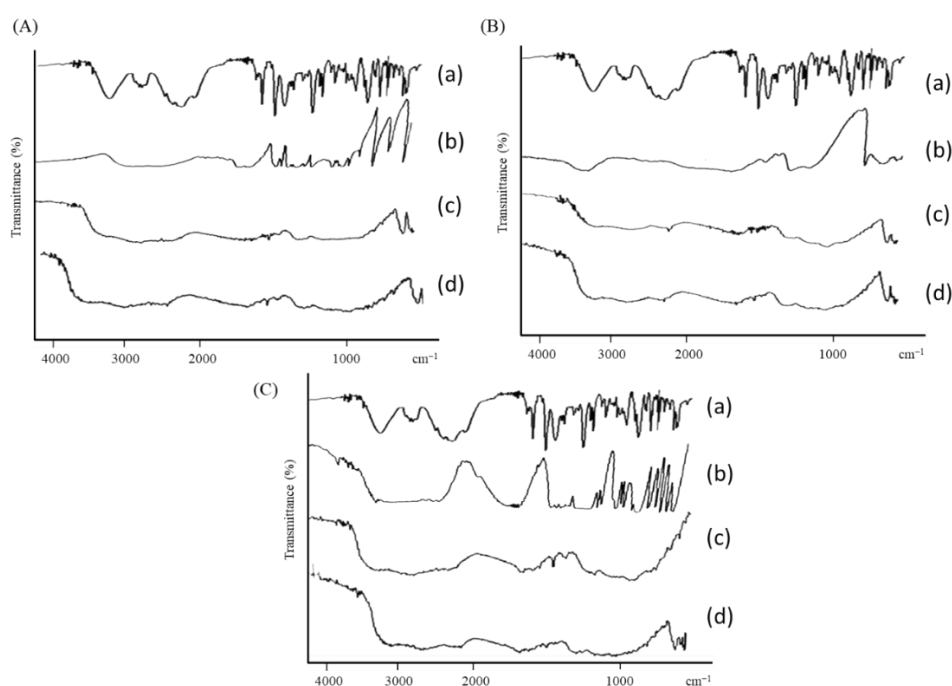


Figure 3. FT-IR spectra of (A) FLN (a), sorbic acid (b), FLN-SA1 (c) and FLN-SA2 ion-pair complex (d); (B) FLN (a), oxalic acid (b), FLN-OA1 (c) and FLN-OA2 ion-pair complex (d); (C) FLN (a), citric acid (b), FLN-CA1 (c) and FLN-CA2 ion-pair complex (d).

After determining the influence that factors exerted on the output responses, the formulation was optimized, prepared and experimentally validated. Predicted error (%) was calculated for all responses except for ZP, which was discarded from this consideration. Although the measured ZP (1.50 ± 0.651 mV) deviated greatly from the predicted ZP (0.546), the system maintained neutral surface charge values as required. The estimated errors for particle size showed a good correlation between the theoretical

value (100.05) and the one experimentally determined (88.99 ± 12.23); a nearly overlapping correlation was observed in the case of polydispersity index (PDI), with an error < 4%. The prediction ability of the model was thus validated.

The formation of electrostatic interactions between the two components provides a useful approach to enhance the permeability of FLN and reverse the highly hydrophilic nature of the dichlorhydrate salt, in order to facilitate encapsulation in a matrix of lipid nature. Further technological investigations are currently ongoing to evaluate the encapsulation efficiency and release profiles of complexed drug-loaded NLCs.

References

- [1] R.F. Wang, D.J. Gagliuso, S.M. Podos, Effect of flunarizine, a calcium channel blocker, on intraocular pressure and aqueous humor dynamics in monkeys, *J Glaucoma*. 17 (2008) 73–78. <https://doi.org/10.1097/IJG.0b013e318133a845>.
- [2] J. Santafé, M.J. Martínez De Ibarreta, J. Segarra, J. Melena, A long-lasting hypotensive effect of topical diltiazem on the intraocular pressure in conscious rabbits, *Naunyn Schmiedebergs Arch Pharmacol*. 355 (1997) 645–650. <https://doi.org/10.1007/PL00004996>.
- [3] E.K.A. Siegner S. W., Netland P.A., Schroeder A., Effect of Calcium Channel Blockers Alone and in Combination With Antiglaucoma Medications on Intraocular Pressure in the Primate Eye, *J Glaucoma*. (2000).
- [4] M.B. Abelson, C. Mitchell Gilbert, L.M. Smith, Sustained reduction of intraocular pressure in humans with the calcium channel blocker verapamil, *Am J Ophthalmol*. 105 (1988) 155–159. [https://doi.org/10.1016/0002-9394\(88\)90179-1](https://doi.org/10.1016/0002-9394(88)90179-1).
- [5] N.N. Osborne, J.P.M. Wood, A. Cupido, J. Melena, G. Chidlow, Topical flunarizine reduces IOP and protects the retina against ischemia-excitotoxicity, *Invest Ophthalmol Vis Sci*. 43 (2002) 1456–1464.
- [6] G. Campana, C. Bucolo, G. Murari, S. Spampinato, Ocular hypotensive action of topical flunarizine in the rabbit: Role of σ_1 recognition sites, *Journal of Pharmacology and Experimental Therapeutics*. 303 (2002) 1086–1094. <https://doi.org/10.1124/jpet.102.040584>.

- [7] M. Noguchi, A. Mori, K. Sakamoto, T. Nakahara, K. Ishii, Vasodilator effects of flunarizine on retinal blood vessels in anesthetized rats, *Biol Pharm Bull.* 32 (2009) 2068–2071. <https://doi.org/10.1248/bpb.32.2068>.
- [8] S.K. Upadhyay, S.M. Ali, Molecular recognition of flunarizine dihydrochloride and β -cyclodextrin inclusion complex by NMR and computational approaches, *Chem Cent J.* 12 (2018) 1–9. <https://doi.org/10.1186/s13065-018-0395-4>.
- [9] M. Dai, L. Bai, H. Zhang, Q. Ma, R. Luo, F. Lei, Q. Fei, N. He, A novel flunarizine hydrochloride-loaded organogel for intraocular drug delivery in situ: Design, physicochemical characteristics and inspection, *Int J Pharm.* 576 (2020) 119027. <https://doi.org/10.1016/j.ijpharm.2020.119027>.
- [10] M. J. Newton, K. Harjot, Fabrication, Characterization, In vitro Evaluation of Solid Lipid Nanoemulsion of Flunarizine dihydrochloride for Nasal Delivery, *Antiinflamm Antiallergy Agents Med Chem.* 15 (2017) 204–220. <https://doi.org/10.2174/1871523015666161216141812>.
- [11] M.T. Marín, M.V. Margarit, G.E. Salcedo, Characterization and solubility study of solid dispersions of flunarizine and polyvinylpyrrolidone, *Farmaco.* 57 (2002) 723–727. [https://doi.org/10.1016/S0014-827X\(02\)01262-4](https://doi.org/10.1016/S0014-827X(02)01262-4).
- [12] M. Gallarate, L. Battaglia, E. Peira, M. Trotta, Peptide-loaded solid lipid nanoparticles prepared through coacervation technique, *International Journal of Chemical Engineering.* 2011 (2011). <https://doi.org/10.1155/2011/132435>.
- [13] S. Arpicco, L. Battaglia, P. Brusa, R. Cavalli, D. Chirio, F. Dosio, M. Gallarate, P. Milla, E. Peira, F. Rocco, S. Sapino, B. Stella, E. Ugazio, M. Ceruti, Recent studies on the delivery of hydrophilic drugs in nanoparticulate systems, *J Drug Deliv Sci Technol.* 32 (2016) 298–312. <https://doi.org/10.1016/j.jddst.2015.09.004>.
- [14] S. Morel, E. Ugazio, R. Cavalli, M.R. Gasco, Thymopentin in solid lipid nanoparticles, *Int J Pharm.* 132 (1996) 259–261. [https://doi.org/10.1016/0378-5173\(95\)04388-8](https://doi.org/10.1016/0378-5173(95)04388-8).
- [15] R. Cavalli, S. Morel, M.R. Gasco, P. Chetoni, m. F. Saettone, Preparation and evaluation in vitro of colloidal lipospheres containing pilocarpine as ion pair, *Int J Pharm.* 117 (1995) 243–246. [https://doi.org/10.1016/0378-5173\(94\)00339-7](https://doi.org/10.1016/0378-5173(94)00339-7).

- [16] R. Cavalli, M.R. Gasco, P. Chetoni, S. Burgalassi, M.F. Saettone, Solid lipid nanoparticles (SLN) as ocular delivery system for tobramycin, *Int J Pharm.* 238 (2002) 241–245. [https://doi.org/10.1016/S0378-5173\(02\)00080-7](https://doi.org/10.1016/S0378-5173(02)00080-7).
- [17] M.S. Oliveira, G.C.A. Goulart, L.A.M. Ferreira, G. Carneiro, Hydrophobic ion pairing as a strategy to improve drug encapsulation into lipid nanocarriers for the cancer treatment, *Expert Opin Drug Deliv.* 14 (2017) 983–995. <https://doi.org/10.1080/17425247.2017.1266329>.
- [18] Y. Li, Y. Zhang, P. Li, G. Mi, J. Tu, L. Sun, T.J. Webster, Y. Shen, Ion-paired pirenzepine-loaded micelles as an ophthalmic delivery system for the treatment of myopia, *Nanomedicine.* 13 (2017) 2079–2089. <https://doi.org/10.1016/j.nano.2017.05.001>.
- [19] R.D. Vaishya, A. Mandal, M. Gokulgandhi, S. Patel, A.K. Mitra, Reversible hydrophobic ion-pairing complex strategy to minimize acylation of octreotide during long-term delivery from PLGA microparticles, *Int J Pharm.* 489 (2015) 237–245. <https://doi.org/10.1016/j.ijpharm.2015.04.075>.
- [20] I. Lozoya-Agullo, M. Planelles, M. Merino-Sanjuán, M. Bermejo, B. Sarmento, I. González-Álvarez, M. González-Álvarez, Ion-pair approach coupled with nanoparticle formation to increase bioavailability of a low permeability charged drug, *Int J Pharm.* 557 (2019) 36–42. <https://doi.org/10.1016/j.ijpharm.2018.12.038>.
- [21] J. Liu, Y. Xu, Z. Liu, H. Ren, Z. Meng, K. Liu, Z. Liu, J. Yong, Y. Wang, X. Li, A modified hydrophobic ion-pairing complex strategy for long-term peptide delivery with high drug encapsulation and reduced burst release from PLGA microspheres, *European Journal of Pharmaceutics and Biopharmaceutics.* 144 (2019) 217–229. <https://doi.org/10.1016/j.ejpb.2019.09.022>.
- [22] B.D. Asuman Bozkır, Design and Evaluation of Hydrophobic Ion-Pairing Complexation of Lysozyme with Sodium Dodecyl Sulfate for Improved Encapsulation of Hydrophilic Peptides/Proteins by Lipid-Polymer Hybrid Nanoparticles, *J Nanomed Nanotechnol.* 06 (2015) 1–5. <https://doi.org/10.4172/2157-7439.1000259>.
- [23] K.D. Ristoph, R.K. Prud'homme, Hydrophobic ion pairing: Encapsulating small molecules, peptides, and proteins into nanocarriers, *Nanoscale Adv.* 1 (2019) 4207–4237. <https://doi.org/10.1039/c9na00308h>.

- [24] S.T. Muntaha, M.N. Khan, Study of changes in conductivity and spectral behaviour before and after micelle formation in the dye-surfactant system, *J Mol Liq.* 197 (2014) 191–196. <https://doi.org/10.1016/j.molliq.2014.05.008>.
- [25] A. Shah, M. Zaheer, R. Qureshi, Z. Akhter, M. Faizan Nazar, Voltammetric and spectroscopic investigations of 4-nitrophenylferrocene interacting with DNA, *Spectrochim Acta A Mol Biomol Spectrosc.* 75 (2010) 1082–1087. <https://doi.org/10.1016/j.saa.2009.12.061>.
- [26] B. Gohain, S. Sarma, R.K. Dutta, Protonated dye-surfactant ion pair formation between neutral red and anionic surfactants in aqueous submicellar solutions, *J Mol Liq.* 142 (2008) 130–135. <https://doi.org/10.1016/j.molliq.2008.05.015>.
- [27] A.M. Khan, S. Bashir, A. Shah, M.F. Nazar, H.M.A. Rahman, S.S. Shah, A.Y. Khan, A.R. Khan, F. Shah, Spectroscopically probing the effects of Holmium(III) based complex counterion on the dye-cationic surfactant interactions, *Colloids Surf A Physicochem Eng Asp.* 539 (2018) 407–415. <https://doi.org/10.1016/j.colsurfa.2017.12.023>.
- [28] K.D. Ristroph, R.K. Prud'homme, Hydrophobic ion pairing: Encapsulating small molecules, peptides, and proteins into nanocarriers, *Nanoscale Adv.* 1 (2019) 4207–4237. <https://doi.org/10.1039/c9na00308h>.
- [29] N.M. Pinkerton, A. Grandeury, A. Fisch, J. Brozio, B.U. Riebesehl, R.K. Prud'Homme, Formation of stable nanocarriers by in Situ ion pairing during block-copolymer-directed rapid precipitation, *Mol Pharm.* 10 (2013) 319–328. <https://doi.org/10.1021/mp300452g>.
- [30] R. Ariadi Lusiana, D. Siswanta, Preparation of Citric Acid Crosslinked Chitosan/Poly(Vinyl Alcohol) Blend Membranes for Creatinine Transport, 2016.
- [31] A.C. Ortiz, O. Yañez, E. Salas-Huenuleo, J.O. Morales, Development of a nanostructured lipid carrier (NLC) by a low-energy method, comparison of release kinetics and molecular dynamics simulation, *Pharmaceutics.* 13 (2021). <https://doi.org/10.3390/pharmaceutics130405>

**CHAPTER VII: *Electrospun nanofibers for melatonin ocular
delivery***

(Manuscript in progress)

Introduction

This research project was carried out during the international mobility period at the University Pharmacy Department of Pharmacy Administration in Semmelweis University under the supervision of Prof. Romàna Zelkó. Part of the period was funded by an Erasmus+ Mobility Network grant.

Given the interesting results by delivering melatonin in paper II, in this work we designed nanofiber-based inserts for ocular delivery of this molecule. To date to the best of our knowledge, no nanofiber-based device has been investigated to improve ocular bioavailability of MEL. Electrospinning is a top-down, efficient, easy and versatile process that has gained much attention in the last decade for the fabrication of nanofibers [1]. This technique allows obtaining polymeric nanofibers with diameters in the nanometric range from polymeric solutions and melts. Among the commonly used polymers for electrospun nanofibers PLA, PLGA, PVA and PVP. The interesting mechanical, chemical and electrical properties of polymers are useful to obtain resorbable devices with flexible, porous structures and a high surface-to-volume ratio [2,3]. All of them are FDA-approved for use in formulations intended for ocular application [4].

PVA is a hydrophilic semi-crystalline polymer that possesses properties of high mechanical strength and excellent electroconductivity. The hydroxyl groups on the side chains of PVA allow the polymer to self-crosslink in aqueous solutions to form soft, flexible but at the same time resistant hydrogels. Due to these unique properties and the recognized biodegradability and biocompatibility, PVA hydrogels have been widely used to produce nanofibers by electrospinning [5]. PLA polymer is synthesized from renewable sources and possesses attractive manufacturing properties [6]. Its high mechanical strength, low cost and electrospinnability make it an excellent polymer to

produce nanofibers [7]. The hydrophobic nature of PLA results in slow erosion in a physiological environment, and this feature has been exploited to produce nanocomposite fibers with prolonged and sustained drug release profiles [8]. The enormous advantages of biodegradable polymers combined with those of electrospun nanofibers make nanofiber-based inserts promising ocular drug delivery systems. The positioning of the scaffolds in the conjunctival sac bypasses the precorneal barriers (rapid tear fluid turnover and nasolacrimal drainage) typically associated with topical instillation of eye drops [9].

The purpose of this current study was to explore for the first time the ocular delivery of MEL via nanofibers prepared by electrospinning technique. Hydrophobic PLA and hydrophilic PVA polymers were selected to develop electrospun nanofibers. Both nanosystems were loaded with different concentrations of MEL (0.1, 0.3 and 0.5% wt). Tween[®] 80 as permeation enhancer was investigated for all nanofibers to observe variations in the final properties of the nanosystems compared to the ones obtained without the addition of permeation enhancer.

To produce PLA nanofibers, the electrospinning process was performed at 7% wt PLA polymer concentration, using binary solvent system (Chl:DMF in a 6:1 molar ratio) to solubilize the hydrophobic polymer. Voltages were varied from 10 to 15 kV; the flow rates were investigated from 0.2 to 0.5 $\mu\text{L}/\text{sec}$ and the collector was fixed as 20 cm. The appropriate flow rate for electrospinning the drug blended PLA polymer solutions was set at 0.5 $\mu\text{L}/\text{sec}$ and the voltage was adjusted ~ 11 kV. As regard PVA-based nanofibers polymer concentration of 12% wt was used. To improve the solubility in distilled water and to disrupt the strong intra- and interchain bonding of PVA polymer, the PVA solutions were stirred on a magnetic plate and heated to about 80 °C. When a clear gel was obtained the polymeric solution was electrospun at a flow rate 0.1 $\mu\text{L}/\text{sec}$, the applied

voltage was 15-20 kV and the fixed distance between the needle and the collector was 12.5 cm. The jet coming out from the needle took the typical Taylor cone shape at a voltage of ~16-17 kV.

The structural characterization of formulated fibrous inserts was in the focus of this work. DSC and FT-IR were performed to characterize the solid-state samples. The morphology of the composite nanofibers was investigated by scanning electron microscope (SEM). The dissolution test was performed by modifying a previously described technique based on the basket method reported by the Pharmacopoeia (Ph.Hg. VIII) [12]. The in vitro release behavior of MEL-loaded nanofibers with and without Tween[®] 80 was evaluated in PBS at pH 7.4 (37 °C). An in-line probe was immersed in the beaker and to monitor the MEL release at a λ max of 278 nm. The swelling degree (%SD) of the produced nanofibers was also determined in aqueous medium (pH 5.5 and 7.4) within 24 h using a gravimetric method at room temperature.

Preliminary results

In this study, the electrospinning technique was successfully used to produce MEL-loaded nanofibers. SEM studies confirmed the nanofibrous structure (Figure 1).

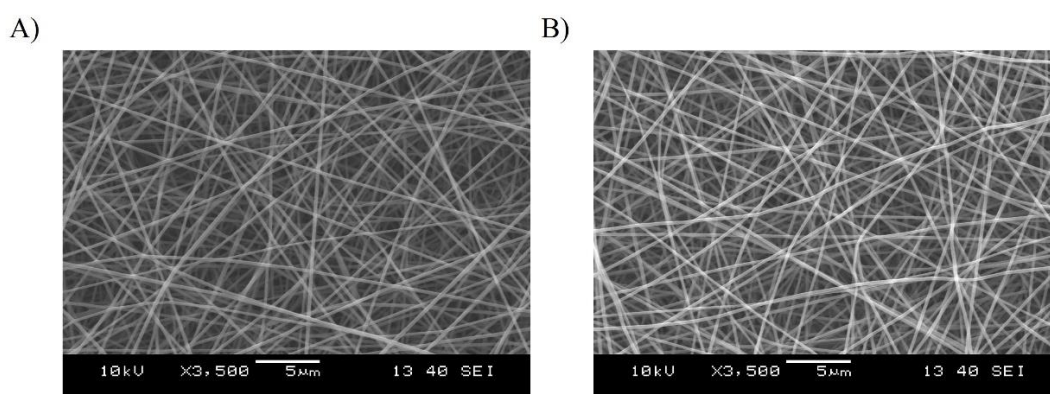


Figure 1. SEM image of empty PVA-based (A) and PLA-based (B) nanofibers.

Thermal characterization of the samples confirmed that the crystalline neat MEL was in the amorphous form into the scaffolds. FT-IR analysis was performed on pure components, physical mixtures (PhM) and electrospun nanofibers to assess potential molecular interactions and to confirm the chemical composition of the composite nanofibers. The FT-IR spectrum of pure substances showed the characteristic absorption bands. Concerning the spectrum of PhM between MEL and PVA presented the high-frequency regions of the spectrum like the MEL scan, with narrow peaks attributable to N-H stretching and CH₂ alkyl groups. The low-frequency region was similar to pure PVA polymer, with identifying bands for C=O and C-O stretching. Similar results were observed for PhM containing the PLA polymer. No difference was observed for all PVA nanofibers scans (empty, loaded with different concentrations of MEL and with or without Tween[®] 80). In detail, the spectra showed no peak attributable to MEL, but rather similarities with the spectrum of neat polymer. Similar results were also obtained for PLA fibers. The higher intensity that was observed for C=O and C-O stretches in both types of nanofibers could suggest the formation of hydrogen bonds that probably occurred during the polymer dissolution phase [10]. It has been demonstrated that polymer solubility in polar solvents is dominated by interactions such as hydrogen bonds [11]. The results of FT-IR analysis proved that PVA and PLA nanofibers were successfully fabricated.

Regarding the in vitro release study, the two nanofibers showed different release profiles according to their nature. The PVA-based nanofibers released the entire melatonin load within 20 minutes; the release profiles of the fibers produced with or without Tween[®] 80 showed overlapping curves. In contrast, nanofibers composed of PLA exhibit slower drug release, and the curves of scaffolds prepared with and without Tween[®] 80 showed substantial differences. The nanofibers containing Tween[®] 80

released the full amount of encapsulated melatonin within 4, 5, and 6 hours for drug concentrations of 0.1, 0.3, and 0.5 % wt, respectively. In contrast, nanofibers produced in the absence of Tween[®] showed sustained release; after 12 hours percentages of melatonin between 40 and 55 % were released from the scaffolds. The faster release from PVA nanofibers could be explained by the interaction of the hydrophilic polymer with the water molecules in the release medium. The interaction of the hydroxyl groups of PVA in contact with the water molecules results in the dissolution of the fibers and therefore a fast amount of drug could be released. Conversely, hydrophobic PLA has a weak interaction with water molecules, resulting in a slower release profile [13]. The significant difference in the release profiles of PLA fibers with or without Tween[®] could presumably be attributed to the porosity of the nanofibers prepared with the addition of the surfactant. In fact, Tween[®] 80 could result in the formation of fibers with a more open structure that speeds up melatonin release compared with fibers obtained without the surfactant [14].

An interesting finding was that the addition of Tween[®] 80 in PLA-based nanofibers provided an increase in swelling around 20-fold, suggesting an improvement in the elastic behaviour of nanofibrous inserts and confirming the reason of faster drug diffusion.

These data were presented at a preliminary stage, further technological investigation is currently in progress to characterize the ocular inserts in order to validate their use for potential ocular application.

References

- [1] S. Meraz-Dávila, C.E. Pérez-García, A.A. Feregrino-Perez, Challenges and advantages of electrospun nanofibers in agriculture: A review, *Mater Res Express*. 8 (2021). <https://doi.org/10.1088/2053-1591/abee55>.
- [2] T. Subbiah, G.S. Bhat, R.W. Tock, S. Parameswaran, S.S. Ramkumar, Electrospinning of nanofibers, *J Appl Polym Sci*. 96 (2005) 557–569. <https://doi.org/10.1002/app.21481>.
- [3] T. Wu, M. Ding, C. Shi, Y. Qiao, P. Wang, R. Qiao, X. Wang, J. Zhong, Resorbable polymer electrospun nanofibers: History, shapes and application for tissue engineering, *Chinese Chemical Letters*. 31 (2020) 617–625. <https://doi.org/10.1016/j.ccllet.2019.07.033>.
- [4] R.S. Bhattarai, A. Das, R.M. Alzhrani, D. Kang, S.B. Bhaduri, S.H.S. Boddu, Comparison of electrospun and solvent cast polylactic acid (PLA)/poly(vinyl alcohol) (PVA) inserts as potential ocular drug delivery vehicles, *Materials Science and Engineering C*. 77 (2017) 895–903. <https://doi.org/10.1016/j.msec.2017.03.305>.
- [5] W. Song, X. Yu, D.C. Markel, T. Shi, W. Ren, Coaxial PCL/PVA electrospun nanofibers: Osseointegration enhancer and controlled drug release device, *Biofabrication*. 5 (2013). <https://doi.org/10.1088/1758-5082/5/3/035006>.
- [6] N.E. Duygulu, F. Ciftci, C.B. Ustundag, Electrospun drug blended poly(lactic acid) (PLA) nanofibers and their antimicrobial activities, *Journal of Polymer Research*. 27 (2020) 12–16. <https://doi.org/10.1007/s10965-020-02215-0>.
- [7] K.J.P. Pavezi, A. Rocha, E.G. Bonafé, A.F. Martins, Electrospinning-electrospraying of poly(acid lactic) solutions in binary chloroform/formic acid and chloroform/acetic acid mixtures, *J Mol Liq*. 320 (2020) 114448. <https://doi.org/10.1016/j.molliq.2020.114448>.
- [8] M. Mohiti-Asli, S. Saha, S. v. Murphy, H. Gracz, B. Pourdeyhimi, A. Atala, E.G. Lobo, Ibuprofen loaded PLA nanofibrous scaffolds increase proliferation of human skin cells in vitro and promote healing of full thickness incision wounds in vivo, *J Biomed Mater Res B Appl Biomater*. 105 (2017) 327–339. <https://doi.org/10.1002/jbm.b.33520>.
- [9] S. Mirzaeei, S. Taghe, K. Asare-Addo, A. Nokhodchi, Polyvinyl Alcohol/Chitosan Single-Layered and Polyvinyl Alcohol/Chitosan/Eudragit RL100

Multi-layered Electrospun Nanofibers as an Ocular Matrix for the Controlled Release of Ofloxacin: an In Vitro and In Vivo Evaluation, *AAPS PharmSciTech.* 22 (2021). <https://doi.org/10.1208/s12249-021-02051-5>.

[10] T. Wang, Y. Li, S. Geng, C. Zhou, X. Jia, F. Yang, L. Zhang, X. Ren, H. Yang, Preparation of flexible reduced graphene oxide/poly(vinyl alcohol) film with superior microwave absorption properties, *RSC Adv.* 5 (2015) 88958–88964. <https://doi.org/10.1039/c5ra16158d>.

[11] M.X. Du, Y.F. Yuan, J.M. Zhang, C.Y. Liu, Hydrogen-Bonding Interactions in Polymer-Organic Solvent Mixtures, *Macromolecules.* (2022). <https://doi.org/10.1021/acs.macromol.2c00799>.

[12] A. Kazsoki, S.M. Omer, Z. Kovacs, Formulation of Levocetirizine-Loaded Core – Shell Type Nanofibrous Orally Dissolving Webs as a Potential Alternative for Immediate Release Dosage Forms, (2022).

[13] B.P. Panda, M.X. Wei, N.K.H. Shivashekaregowda, S. Patnaik, Design, Fabrication and Characterization of PVA/PLGA Electrospun Nanofibers Carriers for Improvement of Drug Delivery of Gliclazide in Type-2 Diabetes, *Proc West Mark Ed Assoc Conf.* (2020) 14. <https://doi.org/10.3390/iecp2020-08689>.

[14] P. Shao, Y. Liu, C. Ritzoulis, B. Niu, Preparation of zein nanofibers with cinnamaldehyde encapsulated in surfactants at critical micelle concentration for active food packaging, *Food Packag Shelf Life.* 22 (2019) 100385. <https://doi.org/10.1016/j.fpsl.2019.100385>.

CHAPTER VIII: *General Discussion*

Neurodegenerative ocular diseases afflict millions of people worldwide affecting vision function and eye health. The prevalence of these disorders increases exponentially with age, and the aging population is increasing. Therefore, neurodegenerative diseases are expected to have an increasing impact on quality of life. Currently available diagnostic and therapeutic methods can rarely detect pathologies at an early stage or restore vision loss. Few drugs have been approved for the management of such conditions and are generally limited to symptomatic action (Weng et al., 2017).

Often the effectiveness of therapeutic treatment is not achieved because of poor bioavailability of drugs in ocular tissues due to the presence of the dynamic and static barriers of the eye.

Nanomedicine offers numerous advantages to overcome these obstacles, such as the ability to control and tune the physico-chemical properties of delivery devices to achieve formulations with a desired target profile. Sustained and controlled drug release profiles, prolonged retention times on the corneal surface, and improved penetration of the anatomical and physiological barriers of the eye are all advantageous features that can be controlled by choosing the constituents of nanocarriers matrices (Meng et al., 2019).

In accordance with these considerations, we focused attention in studying and influencing of chemistry and hydrophobicity surface of nanocarriers. Physico-chemical properties are critical determinants of the biological identity of nanocarriers because they influence pharmacokinetic steps. Indeed, by modulating the technological properties of nanosystems, it has been possible to predict their fate after *in vivo* administration (Zhao et al., 2019).

Polymers such as PLGA, PLA and PLGA-PEG have been chosen for the preparation of nanocarriers because of their recognized biocompatibility, biodegradability, adjustable

mechanical and physical properties that result in devices with controllable erosion times and mucopenetrating properties to improve tissue penetration and thus ocular delivery.

Positively charged lipids like CTAB and DDAB were chosen to impart mucoadhesive properties to the nanosystems in order to prolong contact time with the ocular surface mucosa and improve drug bioavailability. Gelucire[®] 44/14 solid lipid was selected for its absorption enhancing properties to improve corneal permeation and to ensure sustained drug release. Its combination with Miglyol[®] 812 liquid lipid was used to increase the loading efficiency of the devices and to modulate drug release kinetics.

These surface modifications would improve interaction with biological tissues and thus enhance ocular delivery. Our work highlights the importance of starting material selection and in-depth cross-technological analyses to obtain delivery systems for specific applications.

In **Paper I**, polymeric NPs were intended for intravitreal delivery. So, the goal was to impart anionic surface characteristics to the NPs to facilitate penetration of the intravitreal network to the retina (Sakurai et al., 2001). PLGA and PLA polymers selected produced NPs with strongly negative ZP values (between -23.8 and -39.0 mV), desirable for formulations intended for intravitreal injection.

To ensure safe ocular administration, with no contaminants, trace surfactants and solvents, nanovectors must be purified. Purification allows to obtain formulations with uniform size and shape. This step is difficult and time-consuming because each nanocarrier has different physico-chemical characteristics. So, there are no reproducible techniques depending on the nature of the carrier, and the research for the most suitable method can take long time and vast consumption of raw materials. The first step to achieving the most suitable purification method provides that the physico-chemical

properties of the carriers remain unchanged before and after purification processes. Among the usual techniques for purifying nanosystems are centrifugation, filtration and dialysis (Kokorina et al., 2019). From purification studies conducted in Paper I, it was found that the ZP values of NPs were affected depending on the purification technique employed. In this study, dialysis at different frequencies of water exchange (0.5 and 1 L/h) and centrifugation were investigated as purification methods. The results showed that for the purification of these polymeric systems, centrifugation was the least suitable technique, while dialysis with different frequencies of water exchange ensured the maintenance of mean particle size but showed a strong influence on ZP values. The different nature of polymers has shown variations in purification efficacy, encapsulation efficiency and release profiles. Therefore, to obtain nanodevices suitable for a desired route of administration a rational technological assessment is the basis for therapeutic success and differs for each type of starting material.

For example, in **Paper II**, the eye drops were designed for topical instillation. So, the hybrid NPs were coated with cationic lipids to enhance electrostatic interaction with the anionic ocular mucosa. The polymer matrix consisting of PLGA-PEG polymer was chosen to take advantage of the mucopenetrating properties of the polymer, so as to synergistically combine mucoadhesive and mucopenetrating action to promote the passage of precorneal and corneal barriers. Purification of the nanocarriers by centrifugation had a significant impact on the surface charge of the nanosystems, going from neutral to positive values. The folding of the PEG chains from brush to mushroom conformation allowed the positively charged lipid heads to emerge on the surface and confer superior mucoadhesive properties compared with NPs consisting of PLGA-PEG polymer alone, as demonstrated by the mucin particles method.

In **Paper III**, NPs developed for nose-brain delivery were prepared with the mucopenetrating PLGA-PEG polymer. Here, nanocarrier purification was a relevant process in order to remove traces of unencapsulated fluorescent probe that could create misinterpretation in *in vitro/in vivo* cell tracking. In this case, however, the centrifugation technique provided a better purification yield (34-40%) than dialysis (<4%). Regarding the mean size, both purification methods resulted in a reduction in the hydrodynamic radius of NPs. The reason of this decrease can be attributed to the conformation of the PEG chains. Before the purification processes these were extended in a brush conformation; purification by centrifugation would have folded the PEG chains into the mushroom conformation, reducing by almost half the mean size compared with the unpurified samples. Dialysis also resulted in a reduction in the hydrodynamic radius, but in this case the change in the conformation of the PEG chains could be attributed to the presence of the dye on the NP surface, which, by forcing the PEG tails in "pocket" shaped folds, was retained in the NP. This hypothesis was further confirmed by the poor dye purification efficiency obtained by the dialysis method and the results of the release studies. The release profiles of the dialyzed samples showed a percentage of released dye, probably caused by the collapse of the "pockets" due to the salt concentration of the release medium.

In recent years, the statistical QbD approach has been a powerful design tool useful for implementing rational development of new formulations to obtain desired attributes through a robust manufacturing process (Kumar and Vishal Gupta, 2015).

In this thesis work, the design of nanomedicines was carried out through different approaches. The nanosystems studied in papers I, III, and VI had been previously investigated and validated by the research group's know-how; therefore, the OVAT

approach allowed a desired target profile to be achieved without considerable loss of time and money. In papers II and V, the formulations were newly designed; therefore, experimental trials to achieve the QTTP would have required a significant economic and time investment. Based on these evaluations, to provide desired performance to the developed formulations while ensuring robust reproducibility, the multivariate DoE approach methodology was employed to investigate the nanosystems studied in paper II and V. DoE has been a useful tool to achieve desirable characteristics such as size, surface charge, mucopenetrating and mucoadhesive properties. Fine-tuning these properties could be helpful to predict the probable pathway that systems might take to cross ocular barriers *in vivo*.

Despite this, to assess the effective achievement of the drug at the target site, it should be necessary to track the targeting of nanomedicine to ensure that the predicted pathways are not compromised. To this end, tracking nanosystems *in vitro* and *in vivo* could be useful both to quantify and assess drug release as well as to monitor biodistribution, accumulation at the target site and in healthy organs and tissues. Bioimaging can be performed in an invasive or noninvasive way. In the first case following administration of the nanosystems, blood or tissue samples are taken at several time points. In the second case magnetic and optical properties are induced to the nanomaterials, which are used as effective diagnostic agents for various types of noninvasive imaging. Notable among these are magnetic resonance imaging, computed tomography, positron emission tomography, single photon emission computed tomography, optical, photoacoustic, and ultrasound imaging. The advantages of optical imaging in terms of simplicity, performance, cost, and time have made it the most popular imaging technique for *in vivo*

tracking of nanosystems (Kunjachan et al., 2013). Therefore, our interest focused on the use of fluorescent dyes in ocular field (**Paper IV**).

Fluorescent probes are used in optical imaging to generate contrast to label nanomaterials and collect pharmacokinetic information by in vitro and in vivo studies.

Labeling of nanosystems can be done in three ways: by encapsulating the probe within the nanosystem, by grafting the fluorophore on the surface of the nanomaterial via covalent bonding, or by double labeling by combining these two techniques (Zhukova et al., 2021). To fully understand which labeling technique was most effective in **Paper III**, the Rhodamine B probe was encapsulated in the polymer matrix or covalently bonded to the backbone of PLGA-PEG polymer. Although in both cases the NPs were internalized by the cells, proving to be useful tools for exploring cell trafficking, the most stable labeling method for possible applications in biodistribution studies was achieved by grafting the dye on the polymer, in agreement with previous studies (Craparo et al., 2016).

When a source of excitation such as ultraviolet radiation impacts a fluorescent molecule exciting its atoms, it re-emits the received electromagnetic radiation in the visible range and fluoresces at a specific wavelength. Some ocular tissues are characterized by natural green autofluorescence (Swetledge et al., 2021). Therefore, when fluorescent probes falling in the green band (500-550 nm) are used for tracking nanomaterials in these tissues, a preliminary study is important to assess the existence of overlaps that can possibly be bypassed by opting for a fluorophore that absorbs at a distant wavelength. The choice of probe to be used is crucial and should be appropriate for the type of system being tracked. Dyes with low affinity to the nanomaterial could leak from them and falsify the results (Zhukova et al., 2021).

CHAPTER IX: Conclusions

Given the increase in visual impairment in the global population, a major challenge for researchers is directed toward the development of new ocular delivery systems to improve the diagnosis and management of these difficult-to-treat chronic diseases affecting the posterior segment of the eye.

Based on these issues, we decided to explore the use of nanomedicine to overcome obstacles related to physiological and anatomical mechanisms and to provide targeted and sustained drug delivery to intraocular tissues.

Nanometer-sized carriers could represent an improved delivery strategy for reusing drugs that administered with conventional therapies showed poor therapeutic efficacy. The ability to increase the stability of carrier compounds, protecting them from the degradation they would undergo in the biological environment and providing sustained, prolonged, and targeted deliveries into target tissues, could be the breakthrough to open new horizons for drug therapies in the treatment and prevention of chronic neurodegenerative disorders.

The multivariate DoE approach methodology proved to be a very powerful tool that allowed us to achieve the desired goals with minimal effort and by reducing the number of experiments and hence the cost of investment, in terms of resources, time, equipment, and reagents.

The use of fluorescent probes has provided an important contribution to the feasibility of biodistribution studies. Certainly, the basis of successful optical imaging is *(i)* the selection of the most suitable fluorophore (in terms of chemical/physical properties) for labeling the nanomaterial, *(ii)* the conduction of preliminary studies to ascertain the absence of overlap to the auto-fluorescence of the studied tissues, and *(iii)* the choice of labeling technique (encapsulation/grafting) most favorable for the aimed purpose.

In conclusion, the pre-commercial production phase is of fundamental importance. Intelligent selection of starting materials, rational design using statistical and multivariate tools, thoroughly and cross-executed technological analyses, and suitable fluorescent labeling of the developed nanodevices cover critical requirements to be able to guarantee obtaining robust, effective and successful therapeutic formulations.

CHAPTER IX: *References*

- Abdelkader, H., G. Alany, R., 2012. Controlled and Continuous Release Ocular Drug Delivery Systems: Pros and Cons. *Curr. Drug Deliv.* 9, 421–430. <https://doi.org/10.2174/156720112801323125>
- Ahmad, I., Pandit, J., Sultana, Y., Mishra, A.K., Hazari, P.P., Aqil, M., 2019. Optimization by design of etoposide loaded solid lipid nanoparticles for ocular delivery: Characterization, pharmacokinetic and deposition study. *Mater. Sci. Eng. C* 100, 959–970. <https://doi.org/10.1016/j.msec.2019.03.060>
- Ain, N., Anas, A., Fen, Y.W., Yusof, N.A., Alia, N., Omar, S., 2020. Cetyltrimethylammonium Bromide / Hydroxylated Graphene Quantum Dots Thin Film for Potential. *Materials (Basel)*. 13, 16.
- Alam, M.A., Subhan, N., Hossain, H., Hossain, M., Reza, H.M., Rahman, M.M., Ullah, M.O., 2016. Hydroxycinnamic acid derivatives: A potential class of natural compounds for the management of lipid metabolism and obesity. *Nutr. Metab.* 13, 1–13. <https://doi.org/10.1186/s12986-016-0080-3>
- Alara, O.R., Abdurahman, N.H., Ukaegbu, C.I., 2021. Extraction of phenolic compounds: A review. *Curr. Res. Food Sci.* 4, 200–214. <https://doi.org/10.1016/j.crfs.2021.03.011>
- Alkozi, H.A., Navarro, G., Franco, R., Pintor, J., 2020. Melatonin and the control of intraocular pressure. *Prog. Retin. Eye Res.* 75, 100798. <https://doi.org/10.1016/j.preteyeres.2019.100798>
- Allyn, M.M., Luo, R.H., Hellwarth, E.B., Swindle-Reilly, K.E., 2022. Considerations for Polymers Used in Ocular Drug Delivery. *Front. Med.* 8, 1–25. <https://doi.org/10.3389/fmed.2021.787644>
- Almeida, H., Amaral, M., Lobao, P., Frigerio, C., Sousa Lobo, J., 2015. Nanoparticles in

- Ocular Drug Delivery Systems for Topical Administration: Promises and Challenges. *Curr. Pharm. Des.* 21, 5212–5224.
<https://doi.org/10.2174/1381612821666150923095155>
- Amadio, M., Pascale, A., Cupri, S., Pignatello, R., Osera, C., Agata, V.D., Grazia, A., Amico, D., Marco, G., Ruozi, B., Govoni, S., Drago, F., Bucolo, C., 2016. Nanosystems based on siRNA silencing HuR expression counteract diabetic retinopathy in rat. *Pharmacol. Res.* 111, 713–720.
<https://doi.org/10.1016/j.phrs.2016.07.042>
- Ambati, J., Canakis, C.S., Miller, J.W., Gragoudas, E.S., Edwards, A., Weissgold, D.J., Kim, I., Delori, F.C., Adamis, A.P., 2000. Diffusion of high molecular weight compounds through sclera. *Investig. Ophthalmol. Vis. Sci.* 41, 1181–1185.
- Andreadis, I.I., Karavasili, C., Thomas, A., Komnenou, A., Tzimtzimis, M., Tzetzis, D., Andreadis, D., Bouropoulos, N., Fatouros, D.G., 2022. In Situ Gelling Electrospun Ocular Films Sustain the Intraocular Pressure-Lowering Effect of Timolol Maleate: In Vitro, Ex Vivo, and Pharmacodynamic Assessment. *Mol. Pharm.* 19, 274–286.
<https://doi.org/10.1021/acs.molpharmaceut.1c00766>
- Arora, D., Khurana, B., Narang, R.K., Nanda, S., 2016. Quality by Design (QbD) Approach for Optimization and Development of Nano Drug Delivery Systems. *Trends Drug Deliv.* 3, 23–32.
- Aryal, S., Hu, C.M.J., Zhang, L., 2010. Combinatorial drug conjugation enables nanoparticle dual-drug delivery. *Small* 6, 1442–1448.
<https://doi.org/10.1002/sml.201000631>
- Attama, A.A., Reichl, S., Müller-Goymann, C.C., 2009. Sustained release and permeation of timolol from surface-modified solid lipid nanoparticles through bioengineered

- human cornea. *Curr. Eye Res.* 34, 698–705.
<https://doi.org/10.1080/02713680903017500>
- Azimi, B., Nourpanah, P., Rabiee, M., Arbab, S., 2014. Poly (lactide-co-glycolide) fiber: An overview. *J. Eng. Fiber. Fabr.* 9, 47–66.
<https://doi.org/10.1177/155892501400900107>
- Bachu, R.D., Chowdhury, P., Al-Saedi, Z.H.F., Karla, P.K., Boddu, S.H.S., 2018. Ocular drug delivery barriers—role of nanocarriers in the treatment of anterior segment ocular diseases. *Pharmaceutics* 10, 1–31.
<https://doi.org/10.3390/pharmaceutics10010028>
- Baig, M.S., Owida, H., Njoroge, W., Siddiqui, A. ur R., Yang, Y., 2020. Development and evaluation of cationic nanostructured lipid carriers for ophthalmic drug delivery of besifloxacin. *J. Drug Deliv. Sci. Technol.* 55, 101496.
<https://doi.org/10.1016/j.jddst.2019.101496>
- Balguri, S.P., Adelli, G.R., Majumdar, S., 2016. Topical ophthalmic lipid nanoparticle formulations (SLN, NLC) of indomethacin for delivery to the posterior segment ocular tissues. *Eur. J. Pharm. Biopharm.* 109, 224–235.
<https://doi.org/10.1016/j.ejpb.2016.10.015>
- Bancila, M., Copin, J.C., Daali, Y., Schatlo, B., Gasche, Y., Bijlenga, P., 2011. Two structurally different T-type Ca²⁺ channel inhibitors, mibefradil and pimoziide, protect CA1 neurons from delayed death after global ischemia in rats. *Fundam. Clin. Pharmacol.* 25, 469–478. <https://doi.org/10.1111/j.1472-8206.2010.00879.x>
- Barber, A.J., Baccouche, B., 2017. Neurodegeneration in diabetic retinopathy: Potential for novel therapies. *Vision Res.* 139, 82–92.
<https://doi.org/10.1016/j.visres.2017.06.014>

- Barot, M., Gokulgandhi, M.R., Mitra, A.K., 2011. Mitochondrial dysfunction in retinal diseases. *Curr. Eye Res.* 36, 1069–1077. <https://doi.org/10.3109/02713683.2011.607536>
- Basarkar, A., Devineni, D., Palaniappan, R., Singh, J., 2007. Preparation, characterization, cytotoxicity and transfection efficiency of poly(dl-lactide-co-glycolide) and poly(dl-lactic acid) cationic nanoparticles for controlled delivery of plasmid DNA. *Int. J. Pharm.* 343, 247–254. <https://doi.org/10.1016/j.ijpharm.2007.05.023>
- Battaglia, L., Serpe, L., Foglietta, F., Muntoni, E., Gallarate, M., Del Pozo Rodriguez, A., Solinis, M.A., 2016. Application of lipid nanoparticles to ocular drug delivery. *Expert Opin. Drug Deliv.* 13, 1743–1757. <https://doi.org/10.1080/17425247.2016.1201059>
- Bhardwaj, N., Kundu, S.C., 2010. Electrospinning: A fascinating fiber fabrication technique. *Biotechnol. Adv.* 28, 325–347. <https://doi.org/10.1016/j.biotechadv.2010.01.004>
- Bhatt, P., Fnu, G., Bhatia, D., Shahid, A., Sutariya, V., 2020. Nanodelivery of Resveratrol-Loaded PLGA Nanoparticles for Age-Related Macular Degeneration. *AAPS PharmSciTech* 21, 1–9. <https://doi.org/10.1208/s12249-020-01836-4>
- Bilbao-Malavé, V., González-Zamora, J., de la Puente, M., Recalde, S., Fernandez-Robredo, P., Hernandez, M., Layana, A.G., de Viteri, M.S., 2021. Mitochondrial dysfunction and endoplasmic reticulum stress in age related macular degeneration, role in pathophysiology, and possible new therapeutic strategies. *Antioxidants* 10. <https://doi.org/10.3390/antiox10081170>
- Bíró, T., Aigner, Z., 2019. Current approaches to use cyclodextrins and mucoadhesive

- polymers in ocular drug delivery-a mini-review. *Sci. Pharm.* 87.
<https://doi.org/10.3390/scipharm87030015>
- Bohr, A., Wang, Y., Harmankaya, N., Water, J.J., Baldursdottir, S., Almdal, K., Beck-Broichsitter, M., 2017. Molecular weight-dependent degradation and drug release of surface-eroding poly(ethylene carbonate). *Eur. J. Pharm. Biopharm.* 115, 140–148.
<https://doi.org/10.1016/j.ejpb.2017.02.011>
- Bonaccorso, A., Gigliobianco, M.R., Pellitteri, R., Santonocito, D., Carbone, C., Di Martino, P., Puglisi, G., Musumeci, T., 2020. Optimization of curcumin nanocrystals as promising strategy for nose-to-brain delivery application. *Pharmaceutics* 12.
<https://doi.org/10.3390/pharmaceutics12050476>
- Bonaccorso, A., Pepe, V., Zappulla, C., Cimino, C., Pricoco, A., Puglisi, G., Giuliano, F., Pignatello, R., Carbone, C., 2021a. Sorafenib repurposing for ophthalmic delivery by lipid nanoparticles: A preliminary study. *Pharmaceutics* 13, 1–16.
<https://doi.org/10.3390/pharmaceutics13111956>
- Bonaccorso, A., Russo, G., Pappalardo, F., Carbone, C., Puglisi, G., Pignatello, R., Musumeci, T., 2021b. Quality by design tools reducing the gap from bench to bedside for nanomedicine. *Eur. J. Pharm. Biopharm.* 169, 144–155.
<https://doi.org/10.1016/j.ejpb.2021.10.005>
- Bonaccorso, A., Russo, N., Romeo, A., Carbone, C., Grimaudo, M.A., Alvarez-Lorenzo, C., Randazzo, C., Musumeci, T., Caggia, C., 2021c. Coating *Lacticaseibacillus rhamnosus* GG in Alginate Systems: an Emerging Strategy Towards Improved Viability in Orange Juice. *AAPS PharmSciTech* 22. <https://doi.org/10.1208/s12249-021-01996-x>
- Bougaki, M., Searles, R.J., Kida, K., Yu, J. De, Buys, E.S., Ichinose, F., 2010. NOS3

- protects against systemic inflammation and myocardial dysfunction in murine polymicrobial sepsis. *Shock* 34, 281–290. <https://doi.org/10.1097/SHK.0b013e3181cdc327.NOS3>
- Braakman, S.T., Moore, J.E., Ethier, C.R., Overby, D.R., 2016. Transport across Schlemm's canal endothelium and the blood-aqueous barrier. *Exp. Eye Res.* 146, 17–21. <https://doi.org/10.1016/j.exer.2015.11.026>
- Breig, S.J.M., Luti, K.J.K., 2021. Response surface methodology: A review on its applications and challenges in microbial cultures. *Mater. Today Proc.* 42, 2277–2284. <https://doi.org/10.1016/j.matpr.2020.12.316>
- Brini, M., Cali, T., Ottolini, D., Carafoli, E., 2014. Neuronal calcium signaling: Function and dysfunction. *Cell. Mol. Life Sci.* 71, 2787–2814. <https://doi.org/10.1007/s00018-013-1550-7>
- Bristow, E.A., Griffiths, P.G., Andrews, R.M., Johnson, M.A., Turnbull, D.M., 2002. The distribution of mitochondrial activity in relation to optic nerve structure. *Arch. Ophthalmol.* 120, 791–796. <https://doi.org/10.1001/archopht.120.6.791>
- Bucolo, C., Drago, F., 2004. Effects of neurosteroids on ischemia-reperfusion injury in the rat retina: Role of σ 1 recognition sites. *Eur. J. Pharmacol.* 498, 111–114. <https://doi.org/10.1016/j.ejphar.2004.06.067>
- Bunevicius, A., Iervasi, G., Bunevicius, R., 2015. Neuroprotective actions of thyroid hormones and low-T3 syndrome as a biomarker in acute cerebrovascular disorders. *Expert Rev. Neurother.* 15, 315–326. <https://doi.org/10.1586/14737175.2015.1013465>
- Burkersroda, F. Von, Schedl, L., Göpferich, A., 2002. Why degradable polymers undergo surface erosion or bulk erosion. *Biomaterials* 23, 4221–4231.

[https://doi.org/10.1016/S0142-9612\(02\)00170-9](https://doi.org/10.1016/S0142-9612(02)00170-9)

Calì, T., Ottolini, D., Brini, M., 2012. Mitochondrial Ca²⁺ and neurodegeneration. *Cell Calcium* 52, 73–85. <https://doi.org/10.1016/j.ceca.2012.04.015>

Carbone, C., Manno, D., Serra, A., Musumeci, T., Pepe, V., Tisserand, C., Puglisi, G., 2016. Innovative hybrid vs polymeric nanocapsules: The influence of the cationic lipid coating on the “4S.” *Colloids Surfaces B Biointerfaces* 141, 450–457. <https://doi.org/10.1016/j.colsurfb.2016.02.002>

Carracedo-Rodríguez, G., Martínez-Águila, A., Rodríguez-Pomar, C., Bodas-Romero, J., Sanchez-Naves, J., Pintor, J., 2020. Effect of nutritional supplement based on melatonin on the intraocular pressure in normotensive subjects. *Int. Ophthalmol.* 40, 419–422. <https://doi.org/10.1007/s10792-019-01199-1>

Cavalli, R., Morel, S., Gasco, M.R., Chetoni, P., Saettone, m. F., 1995. Preparation and evaluation in vitro of colloidal lipospheres containing pilocarpine as ion pair. *Int. J. Pharm.* 117, 243–246. [https://doi.org/10.1016/0378-5173\(94\)00339-7](https://doi.org/10.1016/0378-5173(94)00339-7)

Cecilia, O.M., Jose Alberto, C.G., Jose, N.P., Ernesto German, C.M., Ana Karen, L.C., Luis Miguel, R.P., Ricardo Raul, R.R., Adolfo Daniel, R.C., 2019. Oxidative Stress as the Main Target in Diabetic Retinopathy Pathophysiology. *J. Diabetes Res.* 2019. <https://doi.org/10.1155/2019/8562408>

Céspedes Rubio, Á.E., Pérez-Alvarez, M.J., Chala, C.L., Wandosell, F., 2018. Sex steroid hormones as neuroprotective elements in ischemia models. *J. Endocrinol.* 237, R65–R81. <https://doi.org/10.1530/JOE-18-0129>

Chan, A., Leung, L.S., Blumenkranz, M.S., 2011. Critical appraisal of the clinical utility of the dexamethasone intravitreal implant (Ozurdex®) for the treatment of macular edema related to branch retinal vein occlusion or central retinal vein occlusion. *Clin.*

- Ophthalmol. 5, 1043–1049. <https://doi.org/10.2147/OPHTH.S13775>
- Chan, J.M., Rhee, J.W., Drum, C.L., Bronson, R.T., Golomb, G., Langer, R., Farokhzad, O.C., 2011. In vivo prevention of arterial restenosis with paclitaxel-encapsulated targeted lipid-polymeric nanoparticles. *Proc. Natl. Acad. Sci. U. S. A.* 108, 19347–19352. <https://doi.org/10.1073/pnas.1115945108>
- Chen, H.-W., Rainey, R.N., Balatoni, C.E., Dawson, D.W., Troke, J.J., Wasiak, S., Hong, J.S., McBride, H.M., Koehler, C.M., Teitell, M.A., French, S.W., 2006. Mammalian Polynucleotide Phosphorylase Is an Intermembrane Space RNase That Maintains Mitochondrial Homeostasis. *Mol. Cell. Biol.* 26, 8475–8487. <https://doi.org/10.1128/mcb.01002-06>
- Chen, H., Jin, Y., Sun, L., Li, X., Nan, K., Liu, H., Zheng, Q., Wang, B., 2018. Recent Developments in Ophthalmic Drug Delivery Systems for Therapy of Both Anterior and Posterior Segment Diseases. *Colloids Interface Sci. Commun.* 24, 54–61. <https://doi.org/10.1016/j.colcom.2018.03.008>
- Chen, P., Chen, H., Zang, X., Chen, M., Jiang, H., Han, S., Wu, X., 2013. Expression of efflux transporters in human ocular tissues. *Drug Metab. Dispos.* 41, 1934–1948. <https://doi.org/10.1124/dmd.113.052704>
- Cheng, C.Y., Su, S.Y., Tang, N.Y., Ho, T.Y., Chiang, S.Y., Hsieh, C.L., 2008. Ferulic acid provides neuroprotection against oxidative stress-related apoptosis after cerebral ischemia/reperfusion injury by inhibiting ICAM-1 mRNA expression in rats. *Brain Res.* 1209, 136–150. <https://doi.org/10.1016/j.brainres.2008.02.090>
- Cheow, W.S., Hadinoto, K., 2011. Factors affecting drug encapsulation and stability of lipid-polymer hybrid nanoparticles. *Colloids Surfaces B Biointerfaces* 85, 214–220. <https://doi.org/10.1016/j.colsurfb.2011.02.033>

- Chern, C.M., Liao, J.F., Wang, Y.H., Shen, Y.C., 2012. Melatonin ameliorates neural function by promoting endogenous neurogenesis through the MT2 melatonin receptor in ischemic-stroke mice. *Free Radic. Biol. Med.* 52, 1634–1647. <https://doi.org/10.1016/j.freeradbiomed.2012.01.030>
- Chetoni, P., Burgalassi, S., Monti, D., Tampucci, S., Tullio, V., Cuffini, A.M., Muntoni, E., Spagnolo, R., Zara, G.P., Cavalli, R., 2016. Solid lipid nanoparticles as promising tool for intraocular tobramycin delivery: Pharmacokinetic studies on rabbits. *Eur. J. Pharm. Biopharm.* 109, 214–223. <https://doi.org/10.1016/j.ejpb.2016.10.006>
- Chrysostomou, V., Rezania, F., Trounce, I.A., Crowston, J.G., 2013. Oxidative stress and mitochondrial dysfunction in glaucoma. *Curr. Opin. Pharmacol.* 13, 12–15. <https://doi.org/10.1016/j.coph.2012.09.008>
- Cipolat, S., Rudka, T., Hartmann, D., Costa, V., Serneels, L., Craessaerts, K., Metzger, K., Frezza, C., Annaert, W., D’Adamio, L., Derks, C., Dejaegere, T., Pellegrini, L., D’Hooge, R., Scorrano, L., De Strooper, B., 2006. Mitochondrial Rhomboid PARL Regulates Cytochrome c Release during Apoptosis via OPA1-Dependent Cristae Remodeling. *Cell* 126, 163–175. <https://doi.org/10.1016/j.cell.2006.06.021>
- Cipolla-Neto, J., Amaral, F.G., Soares, J.M., Gallo, C.C., Furtado, A., Cavaco, J.E., Gonçalves, I., Santos, C.R.A., Quintela, T., 2022. The Crosstalk between Melatonin and Sex Steroid Hormones. *Neuroendocrinology* 112, 115–129. <https://doi.org/10.1159/000516148>
- Costa, V.P., Harris, A., Anderson, D., Stodtmeister, R., Cremasco, F., Kergoat, H., Lovasik, J., Stalmans, I., Zeitz, O., Lanzl, I., Gugleta, K., Schmetterer, L., 2014. Ocular perfusion pressure in glaucoma. *Acta Ophthalmol.* 92, 252–266. <https://doi.org/10.1111/aos.12298>

- Craparo, E.F., Porsio, B., Sardo, C., Giammona, G., Cavallaro, G., 2016. Pegylated Polyaspartamide-Polylactide-Based Nanoparticles Penetrating Cystic Fibrosis Artificial Mucus. *Biomacromolecules* 17, 767–777. <https://doi.org/10.1021/acs.biomac.5b01480>
- Da Fonseca Antunes, A.B., De Geest, B.G., Vervaet, C., Remon, J.P., 2013. Gelucire 44/14 based immediate release formulations for poorly water-soluble drugs. *Drug Dev. Ind. Pharm.* 39, 791–798. <https://doi.org/10.3109/03639045.2012.709251>
- Date, A.A., Srivastava, D., Nagarsenker, M.S., Mulherkar, R., Panicker, L., Aswal, V., Hassan, P.A., Steiniger, F., Thamm, J., Fahr, A., 2011. Lecithin-based novel cationic nanocarriers (LeciPlex) I: Fabrication, characterization and evaluation. *Nanomedicine* 6, 1309–1325. <https://doi.org/10.2217/nmm.11.38>
- Dave, V., Tak, K., Sohgaura, A., Gupta, A., Sadhu, V., Reddy, K.R., 2019. Lipid-polymer hybrid nanoparticles: Synthesis strategies and biomedical applications. *J. Microbiol. Methods* 160, 130–142. <https://doi.org/10.1016/j.mimet.2019.03.017>
- De Angelis, M.M., Owen, L.A., Morrison, M.A., Morgan, D.J., Li, M., Shakoor, A., Vitale, A., Iyengar, S., Stambolian, D., Kim, I.K., Farrer, L.A., 2017. Genetics of age-related macular degeneration (AMD). *Hum. Mol. Genet.* 26, R45–R50. <https://doi.org/10.1093/hmg/ddx228>
- De Merlis, C.C., Schoneker, D.R., 2003. Review of the oral toxicity of polyvinyl alcohol (PVA). *Food Chem. Toxicol.* 41, 319–326. [https://doi.org/10.1016/S0278-6915\(02\)00258-2](https://doi.org/10.1016/S0278-6915(02)00258-2)
- De Vrieze, S., Van Camp, T., Nelvig, A., Hagström, B., Westbroek, P., De Clerck, K., 2009. The effect of temperature and humidity on electrospinning. *J. Mater. Sci.* 44, 1357–1362. <https://doi.org/10.1007/s10853-008-3010-6>

- Deepak, A., Goyal, A.K., Rath, G., 2018. Nanofiber in transmucosal drug delivery. *J. Drug Deliv. Sci. Technol.* 43, 379–387. <https://doi.org/10.1016/j.jddst.2017.11.008>
- Di Prima, G., Licciardi, M., Carfi Pavia, F., Lo Monte, A.I., Cavallaro, G., Giammona, G., 2019. Microfibrillar polymeric ocular inserts for triamcinolone acetonide delivery. *Int. J. Pharm.* 567, 118459. <https://doi.org/10.1016/j.ijpharm.2019.118459>
- Diaz-Coranguez, M., Ramos, C., Antonetti, D.A., 2017. The inner Blood-Retinal Barrier: Cellular Basis and Development. *Vision Res.* 176, 139–148. <https://doi.org/10.1016/j.visres.2017.05.009>.The
- Djebli, N., Khier, S., Griguer, F., Coutant, A.L., Tavernier, A., Fabre, G., Leriche, C., Fabre, D., 2017. Ocular Drug Distribution After Topical Administration: Population Pharmacokinetic Model in Rabbits. *Eur. J. Drug Metab. Pharmacokinet.* 42, 59–68. <https://doi.org/10.1007/s13318-016-0319-4>
- Duan, R., Li, C., Wang, F., Yangi, J.C., 2017. Polymer–lipid hybrid nanoparticles-based paclitaxel and etoposide combinations for the synergistic anticancer efficacy in osteosarcoma. *Colloids Surfaces B Biointerfaces* 159, 880–887. <https://doi.org/10.1016/j.colsurfb.2017.08.042>
- Duarte, A.I., Santos, P., Oliveira, C.R., Santos, M.S., Rego, A.C., 2008. Insulin neuroprotection against oxidative stress is mediated by Akt and GSK-3 β signaling pathways and changes in protein expression. *Biochim. Biophys. Acta - Mol. Cell Res.* 1783, 994–1002. <https://doi.org/10.1016/j.bbamcr.2008.02.016>
- Duchen, M.R., 2012. Mitochondria, calcium-dependent neuronal death and neurodegenerative disease. *Pflugers Arch. Eur. J. Physiol.* 464, 111–121. <https://doi.org/10.1007/s00424-012-1112-0>
- Duvvuri, S., Janoria, K.G., Pal, D., Mitra, A.K., 2007. Controlled delivery of ganciclovir

- to the retina with drug-loaded poly(D,L-lactide-co-glycolide) (PLGA) microspheres dispersed in PLGA-PEG-PLGA gel: A novel intravitreal delivery system for the treatment of cytomegalovirus retinitis. *J. Ocul. Pharmacol. Ther.* 23, 264–274. <https://doi.org/10.1089/jop.2006.132>
- Edsman, K., Carlfors, J., Petersson, R., 1998. Rheological evaluation of poloxamer as an in situ gel for ophthalmic use. *Eur. J. Pharm. Sci.* 6, 105–112. [https://doi.org/10.1016/S0928-0987\(97\)00075-4](https://doi.org/10.1016/S0928-0987(97)00075-4)
- Edward, D.P., Lam, T.T., Shahinfar, S., Li, J., Tso, M.O.M., 1991. Amelioration of Light-Induced Retinal Degeneration by a Calcium Overload Blocker: Flunarizine. *Arch. Ophthalmol.* 109, 554–562. <https://doi.org/10.1001/archopht.1991.01080040122042>
- Edwards, A., Prausnitz, M.R., 2001. Predicted permeability of the cornea to topical drugs. *Pharm. Res.* 18, 1497–1508. <https://doi.org/10.1023/A:1013061926851>
- El-Salamouni, N.S., Farid, R.M., El-Kamel, A.H., El-Gamal, S.S., 2018. Nanostructured lipid carriers for intraocular brimonidine localisation: development, in-vitro and in-vivo evaluation, *Journal of Microencapsulation*. Taylor & Francis. <https://doi.org/10.1080/02652048.2018.1425753>
- EMA, 2009. Pharmaceutical Development Q8 (R2). ICH Harmon. Tripart. Guidel. 6, 32–38. <https://doi.org/10.1016/j.comtox.2018.04.001>
- Eschweiler, G.W., Bähr, M., 1993. Flunarizine enhances rat retinal ganglion cell survival after axotomy. *J. Neurol. Sci.* 116, 34–40. [https://doi.org/10.1016/0022-510X\(93\)90086-E](https://doi.org/10.1016/0022-510X(93)90086-E)
- Espana, E.M., Birk, D.E., 2020. Composition, structure and function of the corneal stroma. *Exp. Eye Res.* 198, 108137. <https://doi.org/10.1016/j.exer.2020.108137>

- Fangueiro, Joana F., Andreani, T., Egea, M.A., Garcia, M.L., Souto, S.B., Silva, A.M., Souto, E.B., 2014. Design of cationic lipid nanoparticles for ocular delivery: Development, characterization and cytotoxicity. *Int. J. Pharm.* 461, 64–73. <https://doi.org/10.1016/j.ijpharm.2013.11.025>
- Fangueiro, Joana F, Andreani, T., Fernandes, L., Garcia, M.L., Egea, M.A., Silva, A.M., Souto, E.B., 2014. Physicochemical characterization of epigallocatechin gallate lipid nanoparticles (EGCG-LNs) for ocular instillation. *Colloids Surfaces B Biointerfaces* 123, 452–460. <https://doi.org/10.1016/j.colsurfb.2014.09.042>
- Fangueiro, J.F., Calpena, A.C., Clares, B., Andreani, T., Egea, M.A., Veiga, F.J., Garcia, M.L., Silva, A.M., Souto, E.B., 2016. Biopharmaceutical evaluation of epigallocatechin gallate-loaded cationic lipid nanoparticles (EGCG-LNs): In vivo, in vitro and ex vivo studies. *Int. J. Pharm.* 502, 161–169. <https://doi.org/10.1016/j.ijpharm.2016.02.039>
- Fanne, R.A., Nassar, T., Heyman, S.N., Hijazi, N., Higazi, A.A.R., 2011. Insulin and glucagon share the same mechanism of neuroprotection in diabetic rats: Role of glutamate. *Am. J. Physiol. - Regul. Integr. Comp. Physiol.* 301, 668–673. <https://doi.org/10.1152/ajpregu.00058.2011>
- Ferreira de Melo, I.M., Martins Ferreira, C.G., Lima da Silva Souza, E.H., Almeida, L.L., Bezerra de Sá, F., Cavalcanti Lapa Neto, C.J., Paz de Castro, M.V., Teixeira, V.W., Coelho Teixeira, Á.A., 2020. Melatonin regulates the expression of inflammatory cytokines, VEGF and apoptosis in diabetic retinopathy in rats. *Chem. Biol. Interact.* 327, 109183. <https://doi.org/10.1016/j.cbi.2020.109183>
- Ferrington, D.A., Fisher, C.R., Kowluru, R.A., 2020. Mitochondrial Defects Drive Degenerative Retinal Diseases. *Trends Mol. Med.* 26, 105–118.

<https://doi.org/10.1016/j.molmed.2019.10.008>

- Fialho, S.L., Da Silva Cunha, A., 2005. Manufacturing techniques of biodegradable implants intended for intraocular application. *Drug Deliv. J. Deliv. Target. Ther. Agents* 12, 109–116. <https://doi.org/10.1080/10717540590921432>
- Fritsche, L.G., Loenhardt, T., Janssen, A., Fisher, S.A., Rivera, A., Keilhauer, C.N., Weber, B.H.F., 2008. Age-related macular degeneration is associated with an unstable ARMS2 (LOC387715) mRNA. *Nat. Genet.* 40, 892–896. <https://doi.org/10.1038/ng.170>
- Gaaz, T.S., Sulong, A.B., Akhtar, M.N., Kadhum, A.A.H., Mohamad, A.B., Al-Amiery, A.A., McPhee, D.J., 2015. Properties and applications of polyvinyl alcohol, halloysite nanotubes and their nanocomposites. *Molecules* 20, 22833–22847. <https://doi.org/10.3390/molecules201219884>
- Galindo, R., Sánchez-López, E., Gómara, M.J., Espina, M., Ettcheto, M., Cano, A., Haro, I., Camins, A., García, M.L., 2022. Development of Peptide Targeted PLGA-PEGylated Nanoparticles Loading Licochalcone-A for Ocular Inflammation. *Pharmaceutics* 14. <https://doi.org/10.3390/pharmaceutics14020285>
- Gan, L., Wang, J., Zhao, Y., Chen, D., Zhu, C., Liu, J., Gan, Y., 2013. Hyaluronan-modified core-shell liponanoparticles targeting CD44-positive retinal pigment epithelium cells via intravitreal injection. *Biomaterials* 34, 5978–5987. <https://doi.org/10.1016/j.biomaterials.2013.04.035>
- Gelb, M.B., Punia, A., Sellers, S., Kadakia, P., Ormes, J.D., Khawaja, N.N., Wylie, J., Lamm, M.S., 2022. Effect of drug incorporation and polymer properties on the characteristics of electrospun nanofibers for drug delivery. *J. Drug Deliv. Sci. Technol.* 68, 103112. <https://doi.org/10.1016/j.jddst.2022.103112>

- Ghate, D., Edelhauser, H.F., 2006. Ocular drug delivery systems. *Expert Opin. Drug Deliv.* 3, 275–278. <https://doi.org/10.1079/9781780644479.0160>
- Giannavola, C., Bucolo, C., Maltese, A., Paolino, D., Vandelli, M.A., Puglisi, G., Lee, V.H.L., Fresta, M., 2003. Influence of preparation conditions on acyclovir-loaded poly-d,l-lactic acid nanospheres and effect of PEG coating on ocular drug bioavailability. *Pharm. Res.* 20, 584–590. <https://doi.org/10.1023/A:1023290514575>
- Gonzalez-Pizarro, R., Parrotta, G., Vera, R., Sánchez-López, E., Galindo, R., Kjeldsen, F., Badia, J., Baldoma, L., Espina, M., García, M.L., 2019. Ocular penetration of fluorometholone-loaded PEG-PLGA nanoparticles functionalized with cell-penetrating peptides. *Nanomedicine* 14, 3089–3104. <https://doi.org/10.2217/nnm-2019-0201>
- Goto, S., Kawakatsu, M., Izumi, S. ichi, Urata, Y., Kageyama, K., Ihara, Y., Koji, T., Kondo, T., 2009. Glutathione S-transferase π localizes in mitochondria and protects against oxidative stress. *Free Radic. Biol. Med.* 46, 1392–1403. <https://doi.org/10.1016/j.freeradbiomed.2009.02.025>
- Goyal, R., Macri, L.K., Kaplan, H.M., Kohn, J., 2016. Nanoparticles and nanofibers for topical drug delivery. *J. Control. Release* 240, 77–92. <https://doi.org/10.1016/j.jconrel.2015.10.049>
- Gubin, D., Neroev, V., Malishevskaya, T., Cornelissen, G., Astakhov, S.Y., Kolomeichuk, S., Yuzhakova, N., Kabitskaya, Y., Weinert, D., 2021. Melatonin mitigates disrupted circadian rhythms, lowers intraocular pressure, and improves retinal ganglion cells function in glaucoma. *J. Pineal Res.* 70, 1–16. <https://doi.org/10.1111/jpi.12730>

- Gunasekaran, T., Haile, T., Nigusse, T., Dhanaraju, M.D., 2014. Nanotechnology: An effective tool for enhancing bioavailability and bioactivity of phytomedicine. *Asian Pac. J. Trop. Biomed.* 4, S1–S7. <https://doi.org/10.12980/APJTB.4.2014C980>
- Gupta, V., Gupta, V.B., Chitranshi, N., Gangoda, S., Vander Wall, R., Abbasi, M., Golzan, M., Dheer, Y., Shah, T., Avolio, A., Chung, R., Martins, R., Graham, S., 2016. One protein, multiple pathologies: multifaceted involvement of amyloid β in neurodegenerative disorders of the brain and retina. *Cell. Mol. Life Sci.* 73, 4279–4297. <https://doi.org/10.1007/s00018-016-2295-x>
- Hadinoto, K., Sundaresan, A., Cheow, W.S., 2013. Lipid-polymer hybrid nanoparticles as a new generation therapeutic delivery platform: A review. *Eur. J. Pharm. Biopharm.* 85, 427–443. <https://doi.org/10.1016/j.ejpb.2013.07.002>
- Haider, A., Haider, S., Kang, I.K., 2018. A comprehensive review summarizing the effect of electrospinning parameters and potential applications of nanofibers in biomedical and biotechnology. *Arab. J. Chem.* 11, 1165–1188. <https://doi.org/10.1016/j.arabjc.2015.11.015>
- Hassan, D.H., Abdelmonem, R., Abdellatif, M.M., 2018. Formulation and characterization of carvedilol leciplex for glaucoma treatment: In-vitro, ex-vivo and in-vivo study. *Pharmaceutics* 10. <https://doi.org/10.3390/pharmaceutics10040197>
- Hekmati, A.H., Rashidi, A., Ghazisaeidi, R., Drean, J.Y., 2013. Effect of needle length, electrospinning distance, and solution concentration on morphological properties of polyamide-6 electrospun nanowebs. *Text. Res. J.* 83, 1452–1466. <https://doi.org/10.1177/0040517512471746>
- Herrero-Vanrell, R., Molina-Martinez, I.T., 2007. PLA and PLGA microparticles for intravitreal drug delivery: An overview. *J. Drug Deliv. Sci. Technol.* 17, 11–17.

[https://doi.org/10.1016/S1773-2247\(07\)50002-X](https://doi.org/10.1016/S1773-2247(07)50002-X)

Hiral J Shah, J.N.S., 2014. Nanoparticulate Transscleral Ocular Drug Delivery. *J. Biomol.*

Res. Ther. 03. <https://doi.org/10.4172/2167-7956.1000116>

Hosoya, K.I., Tomi, M., Tachikawa, M., 2011. Strategies for therapy of retinal diseases using systemic drug delivery: Relevance of transporters at the bloodretinal barrier.

Expert Opin. Drug Deliv. 8, 1571–1587.

<https://doi.org/10.1517/17425247.2011.628983>

Hu, C.J., Kaushal, S., Cao, H.S.T., Aryal, S., Sartor, M., Esener, S., Bouvet, M., Zhang, L., 2010. Half-Antibody Functionalized Lipid - Polymer Hybrid Nanoparticles for Targeted Drug Delivery to Carcinoembryonic Antigen Presenting Pancreatic Cancer Cells. *Mol. Pharm.* 7, 914–920.

Hu, X., Liu, S., Zhou, G., Huang, Y., Xie, Z., Jing, X., 2014. Electrospinning of polymeric nanofibers for drug delivery applications. *J. Control. Release* 185, 12–21.

<https://doi.org/10.1016/j.jconrel.2014.04.018>

Huang, A.J.W., Tseng, S.C.G., Kenyon, K.R., 1989. Paracellular permeability of corneal and conjunctival epithelia. *Investig. Ophthalmol. Vis. Sci.* 30, 684–689.

Huang, H. -S, Schoenwald, R.D., Lach, J.L., 1983. Corneal penetration behavior of β -blocking agents II: Assessment of barrier contributions. *J. Pharm. Sci.* 72, 1272–

1279. <https://doi.org/10.1002/jps.2600721109>

Huang, Z.M., Zhang, Y.Z., Kotaki, M., Ramakrishna, S., 2003. A review on polymer nanofibers by electrospinning and their applications in nanocomposites. *Compos. Sci. Technol.* 63, 2223–2253. [https://doi.org/10.1016/S0266-3538\(03\)00178-7](https://doi.org/10.1016/S0266-3538(03)00178-7)

Ibrahim, H.M., Ismail, H.R., Lila, A.E.A., 2012. Formulation and optimization of ocular poly-d, l-lactic acid nano drug delivery system of amphotericin-b using box behnken

- design. *Int. J. Pharm. Pharm. Sci.* 4, 342–349.
- Islam, M.S., Ang, B.C., Andriyana, A., Afifi, A.M., 2019. A review on fabrication of nanofibers via electrospinning and their applications. *SN Appl. Sci.* 1, 1–16. <https://doi.org/10.1007/s42452-019-1288-4>
- Ismail, R., Sovány, T., Gácsi, A., Ambrus, R., Katona, G., Imre, N., Csóka, I., 2019. Synthesis and Statistical Optimization of Poly (Lactic-Co-Glycolic Acid) Nanoparticles Encapsulating GLP1 Analog Designed for Oral Delivery. *Pharm. Res.* 36. <https://doi.org/10.1007/s11095-019-2620-9>
- Janoria, K.G., Gunda, S., Boddu, S.H.S., Mitra, A.K., 2007. Novel approaches to retinal drug delivery. *Expert Opin. Drug Deliv.* 4, 371–388. <https://doi.org/10.1517/17425247.4.4.371>
- Janoria, K.G., Mitra, A.K., 2007. Effect of lactide/glycolide ratio on the in vitro release of ganciclovir and its lipophilic prodrug (GCV-monobutyrate) from PLGA microspheres. *Int. J. Pharm.* 338, 133–141. <https://doi.org/10.1016/j.ijpharm.2007.01.038>
- Jia, L., Qin, X.H., 2013. The effect of different surfactants on the electrospinning poly(vinyl alcohol) (PVA) nanofibers. *J. Therm. Anal. Calorim.* 112, 595–605. <https://doi.org/10.1007/s10973-012-2607-9>
- Jiang, M., Gan, L., Zhu, C., Dong, Y., Liu, J., Gan, Y., 2012. Cationic core-shell liponanoparticles for ocular gene delivery. *Biomaterials* 33, 7621–7630. <https://doi.org/10.1016/j.biomaterials.2012.06.079>
- Jiang, S., Liu, S., Feng, W., 2011. PVA hydrogel properties for biomedical application. *J. Mech. Behav. Biomed. Mater.* 4, 1228–1233. <https://doi.org/10.1016/j.jmbbm.2011.04.005>

- Jindal, V., 2015. Interconnection Between Brain and Retinal Neurodegenerations. *Mol. Neurobiol.* 51, 885–892. <https://doi.org/10.1007/s12035-014-8733-6>
- Jones, M., Mitchell, P., Wang, J.J., Sue, C., 2004. MELAS A3243G mitochondrial DNA mutation and age related maculopathy. *Am. J. Ophthalmol.* 138, 1051–1053. <https://doi.org/10.1016/j.ajo.2004.06.026>
- Jose, C., Amra, K., Bhavsar, C., Momin, M., Omri, A., 2018. Polymeric lipid hybrid nanoparticles: Properties and therapeutic applications. *Crit. Rev. Ther. Drug Carrier Syst.* 35, 555–588. <https://doi.org/10.1615/CritRevTherDrugCarrierSyst.2018024751>
- Ju, W.K., Liu, Q., Kim, K.Y., Crowston, J.G., Lindsey, J.D., Agarwal, N., Ellisman, M.H., Perkins, G.A., Weinreb, R.N., 2007. Elevated hydrostatic pressure triggers mitochondrial fission and decreases cellular ATP in differentiated RGC-5 cells. *Investig. Ophthalmol. Vis. Sci.* 48, 2145–2151. <https://doi.org/10.1167/iovs.06-0573>
- Kan, E., Alici, Ö., Kan, E.K., Ayar, A., 2017. Effects of alpha-lipoic acid on retinal ganglion cells, retinal thicknesses, and VEGF production in an experimental model of diabetes. *Int. Ophthalmol.* 37, 1269–1278. <https://doi.org/10.1007/s10792-016-0396-z>
- Kanda, A., Chen, W., Othman, M., Branham, K.E.H., Brooks, M., Khanna, R., He, S., Lyons, R., Abecasis, G.R., Swaroop, A., 2007. A variant of mitochondrial protein LOC387715/ARMS2, not HTRA1, is strongly associated with age-related macular degeneration. *Proc. Natl. Acad. Sci. U. S. A.* 104, 16227–16232. <https://doi.org/10.1073/pnas.0703933104>
- Kansara, V., Mitra, A., 2006. Evaluation of an ex vivo model implication for carrier-

- mediated retinal drug delivery. *Curr. Eye Res.* 31, 415–426.
<https://doi.org/10.1080/02713680600646890>
- Kasahara, E., Lin, L.R., Ho, Y.S., Reddy, V.N., 2005. SOD2 protects against oxidation-induced apoptosis in mouse retinal pigment epithelium: Implications for age-related macular degeneration. *Investig. Ophthalmol. Vis. Sci.* 46, 3426–3434.
<https://doi.org/10.1167/iovs.05-0344>
- Käsdorf, B.T., Arends, F., Lieleg, O., 2015. Diffusion Regulation in the Vitreous Humor. *Biophys. J.* 109, 2171–2181. <https://doi.org/10.1016/j.bpj.2015.10.002>
- Kaur, I.P., Kanwar, M., 2002. Ocular preparations: The formulation approach. *Drug Dev. Ind. Pharm.* 28, 473–493. <https://doi.org/10.1081/DDC-120003445>
- Khodaei, M., Rostamizadeh, K., Taramchi, A.H., Monirinasab, H., Fathi, M., 2021. DDAB cationic lipid-mPEG, PCL copolymer hybrid nano-carrier synthesis and application for delivery of siRNA targeting IGF-1R into breast cancer cells. *Clin. Transl. Oncol.* 23, 1167–1178. <https://doi.org/10.1007/s12094-020-02507-3>
- Kidron, H., Del Amo, E.M., Vellonen, K.S., Urtti, A., 2012. Prediction of the vitreal half-life of small molecular drug-like compounds. *Pharm. Res.* 29, 3302–3311.
<https://doi.org/10.1007/s11095-012-0822-5>
- Kim, D.H., Lee, S.E., Pyo, Y.C., Tran, P., Park, J.S., 2020. Solubility enhancement and application of cyclodextrins in local drug delivery. *J. Pharm. Investig.* 50, 17–27.
<https://doi.org/10.1007/s40005-019-00434-2>
- Kimura, H., Ogura, Y., 2001. Biodegradable Polymers for Ocular Drug Delivery. *Ophthalmologica* 215, 143–155.
- Kohno, M., Musashi, K., Ikeda, H.O., Horibe, T., Matsumoto, A., Kawakami, K., 2020. Oral administration of ferulic acid or ethyl ferulate attenuates retinal damage in

- sodium iodate-induced retinal degeneration mice. *Sci. Rep.* 10, 1–9.
<https://doi.org/10.1038/s41598-020-65673-y>
- Kokorina, A.A., Sapelkin, A. V., Sukhorukov, G.B., Goryacheva, I.Y., 2019. Luminescent carbon nanoparticles separation and purification. *Adv. Colloid Interface Sci.* 274. <https://doi.org/10.1016/j.cis.2019.102043>
- Komeima, K., Rogers, B.S., Lu, L., Campochiaro, P.A., 2006. Antioxidants reduce cone cell death in a model of retinitis pigmentosa. *Proc. Natl. Acad. Sci. U. S. A.* 103, 11300–11305. <https://doi.org/10.1073/pnas.0604056103>
- Kompella, U.B., Hartman, R.R., Patil, M.A., 2021. Extraocular, periocular, and intraocular routes for sustained drug delivery for glaucoma. *Prog. Retin. Eye Res.* 82, 100901. <https://doi.org/10.1016/j.preteyeres.2020.100901>
- Kowluru, R.A., Abbas, S.N., 2003. Diabetes-Induced Mitochondrial Dysfunction in the Retina. *Investig. Ophthalmol. Vis. Sci.* 44, 5327–5334.
<https://doi.org/10.1167/iovs.03-0353>
- Kumar, V.P., Vishal Gupta, N., 2015. A review on quality by design approach (QBD) for pharmaceuticals. *Int. J. Drug Dev. Res.* 7, 52–60.
- Kunjachan, S., Gremse, F., Theek, B., Koczera, P., Pola, R., Pechar, M., Etrych, T., Ulbrich, K., Storm, G., Kiessling, F., Lammers, T., 2013. Noninvasive optical imaging of nanomedicine biodistribution. *ACS Nano* 7, 252–262.
<https://doi.org/10.1021/nn303955n>
- Kuppermann, B.D., Patel, S.S., Boyer, D.S., Augustin, A.J., Freeman, W.R., Kerr, K.J., Guo, Q., Schneider, S., López, F.J., 2021. Phase 2 Study of the Safety and Efficacy of Brimonidine Drug Delivery System (Brimo Dds) Generation 1 in Patients With Geographic Atrophy Secondary To Age-Related Macular Degeneration. *Retina* 41,

144–155. <https://doi.org/10.1097/IAE.0000000000002789>

Kurniawansyah, I.S., Rusdiana, T., Sopyan, I., Ramoko, H., Wahab, H.A., Subarnas, A., 2020. In situ ophthalmic gel forming systems of poloxamer 407 and hydroxypropyl methyl cellulose mixtures for sustained ocular delivery of chloramphenicol: optimization study by factorial design. *Heliyon* 6. <https://doi.org/10.1016/j.heliyon.2020.e05365>

Lai, S.K., Wang, Y.Y., Hanes, J., 2009. Mucus-penetrating nanoparticles for drug and gene delivery to mucosal tissues. *Adv. Drug Deliv. Rev.* 61, 158–171. <https://doi.org/10.1016/j.addr.2008.11.002>

Lai, T.Y.Y., Liu, S., Das, S., Lam, D.S.C., 2015. Intravitreal injection-technique and safety. *Asia-Pacific J. Ophthalmol.* 4, 321–328. <https://doi.org/10.1097/APO.0000000000000146>

Lakhani, P., Patil, A., Wu, K.W., Sweeney, C., Tripathi, S., Avula, B., Taskar, P., Khan, S., Majumdar, S., 2019. Optimization, stabilization, and characterization of amphotericin B loaded nanostructured lipid carriers for ocular drug delivery. *Int. J. Pharm.* 572, 118771. <https://doi.org/10.1016/j.ijpharm.2019.118771>

Lancina, M.G., Singh, S., Kompella, U.B., Husain, S., Yang, H., 2017. Fast Dissolving Dendrimer Nanofiber Mats as Alternative to Eye Drops for More Efficient Antiglaucoma Drug Delivery. *ACS Biomater. Sci. Eng.* 3, 1861–1868. <https://doi.org/10.1021/acsbiomaterials.7b00319>

Lanier, O.L., Manfre, M.G., Bailey, C., Liu, Z., Sparks, Z., Kulkarni, S., Chauhan, A., 2021. Review of Approaches for Increasing Ophthalmic Bioavailability for Eye Drop Formulations. *AAPS PharmSciTech* 22. <https://doi.org/10.1208/s12249-021-01977-0>

- Lee, S., Van Bergen, N.J., Kong, G.Y., Chrysostomou, V., Waugh, H.S., O'Neill, E.C., Crowston, J.G., Troncone, I.A., 2011. Mitochondrial dysfunction in glaucoma and emerging bioenergetic therapies. *Exp. Eye Res.* 93, 204–212. <https://doi.org/10.1016/j.exer.2010.07.015>
- Leonardi, A., Bucolo, C., Drago, F., Salomone, S., Pignatello, R., 2015. Cationic solid lipid nanoparticles enhance ocular hypotensive effect of melatonin in rabbit. *Int. J. Pharm.* 478, 180–186. <https://doi.org/10.1016/j.ijpharm.2014.11.032>
- Li, H., Wang, Y., Feng, D., Liu, Y., Xu, M., Gao, A., Tian, F., Zhang, L., Cui, Y., Wang, Z., Chen, G., 2014. Alterations in the time course of expression of the Nox family in the brain in a rat experimental cerebral ischemia and reperfusion model: Effects of melatonin. *J. Pineal Res.* 57, 110–119. <https://doi.org/10.1111/jpi.12148>
- Li, X., Nie, S. fang, Kong, J., Li, N., Ju, C. yi, Pan, W. san, 2008. A controlled-release ocular delivery system for ibuprofen based on nanostructured lipid carriers. *Int. J. Pharm.* 363, 177–182. <https://doi.org/10.1016/j.ijpharm.2008.07.017>
- Liaw, J., Rojanasakul, Y., Robinson, J.R., 1992. The effect of drug charge type and charge density on corneal transport. *Int. J. Pharm.* 88, 111–124. [https://doi.org/10.1016/0378-5173\(92\)90308-O](https://doi.org/10.1016/0378-5173(92)90308-O)
- Liu, D., Lian, Y., Fang, Q., Liu, L., Zhang, J., Li, J., 2018. Hyaluronic-acid-modified lipid-polymer hybrid nanoparticles as an efficient ocular delivery platform for moxifloxacin hydrochloride. *Int. J. Biol. Macromol.* 116, 1026–1036. <https://doi.org/10.1016/j.ijbiomac.2018.05.113>
- Liu, R., Liu, Z., Zhang, C., Zhang, B., 2011. Gelucire44/14 as a Novel Absorption Enhancer for Drugs with Different Hydrophilicities: inVitroand inVivoImprovement on Transcorneal Permeation. *J. Pharm. Sci.* 100, 3186–3195.

<https://doi.org/10.1002/jps>

- Liu, R., Wang, S., Fang, S., Wang, J., Chen, J., Huang, X., He, X., Liu, C., 2016. Liquid Crystalline Nanoparticles as an Ophthalmic Delivery System for Tetrandrine: Development, Characterization, and In Vitro and In Vivo Evaluation. *Nanoscale Res. Lett.* 11. <https://doi.org/10.1186/s11671-016-1471-0>
- Liu, S., Jones, L., Gu, F.X., 2012. Nanomaterials for Ocular Drug Delivery. *Macromol. Biosci.* 12, 608–620. <https://doi.org/10.1002/mabi.201100419>
- Luo, Q., Zhao, J., Zhang, X., Pan, W., 2011. Nanostructured lipid carrier (NLC) coated with Chitosan Oligosaccharides and its potential use in ocular drug delivery system. *Int. J. Pharm.* 403, 185–191. <https://doi.org/10.1016/j.ijpharm.2010.10.013>
- Lynch, C., Kondiah, P.P.D., Choonara, Y.E., du Toit, L.C., Ally, N., Pillay, V., 2019. Advances in biodegradable nano-sized polymer-based ocular drug delivery. *Polymers (Basel)*. 11. <https://doi.org/10.3390/polym11081371>
- Madsen-Bouterse, S.A., Mohammad, G., Kanwar, M., Kowluru, R.A., 2010. Role of mitochondrial DNA damage in the development of diabetic retinopathy, and the metabolic memory phenomenon associated with its progression. *Antioxidants Redox Signal.* 13, 797–805. <https://doi.org/10.1089/ars.2009.2932>
- Mancini, A., Raimondo, S., Di Segni, C., Persano, M., Gadotti, G., Silvestrini, A., Festa, R., Tiano, L., Pontecorvi, A., Meucci, E., 2013. Thyroid hormones and antioxidant systems: Focus on oxidative stress in cardiovascular and pulmonary diseases. *Int. J. Mol. Sci.* 14, 23893–23909. <https://doi.org/10.3390/ijms141223893>
- Marazita, M.C., Dugour, A., Marquioni-Ramella, M.D., Figueroa, J.M., Suburo, A.M., 2016. Oxidative stress-induced premature senescence dysregulates VEGF and CFH expression in retinal pigment epithelial cells: Implications for Age-related Macular

- Degeneration. *Redox Biol.* 7, 78–87. <https://doi.org/10.1016/j.redox.2015.11.011>
- Marchesi, N., Fahmideh, F., Boschi, F., Pascale, A., Barbieri, A., 2021. Ocular Neurodegenerative Diseases : Interconnection between. *Cells* 10, 2394.
- Mariappan, N., Elks, C.M., Fink, B., Francis, J., 2009. TNF-induced mitochondrial damage: a link between mitochondrial complex I activity and left ventricular dysfunction. *Free Radic. Biol. Med.* 46, 462–470. <https://doi.org/10.1016/j.freeradbiomed.2008.10.049>
- Martinez Villadiego, K., Arias Tapia, M.J., Useche, J., Escobar Macías, D., 2022. Thermoplastic Starch (TPS)/Polylactic Acid (PLA) Blending Methodologies: A Review. *J. Polym. Environ.* 30, 75–91. <https://doi.org/10.1007/s10924-021-02207-1>
- Mashaghi, S., Jadidi, T., Koenderink, G., Mashaghi, A., 2013. Lipid nanotechnology, *International Journal of Molecular Sciences.* <https://doi.org/10.3390/ijms14024242>
- Masuda, T., Shimazawa, M., Hara, H., 2017. Retinal Diseases Associated with Oxidative Stress and the Effects of a Free Radical Scavenger (Edaravone). *Oxid. Med. Cell. Longev.* 2017. <https://doi.org/10.1155/2017/9208489>
- Maurice, D.M., Polgar, J., 1977. Diffusion across the sclera. *Exp. Eye Res.* 25, 577–582. [https://doi.org/10.1016/0014-4835\(77\)90136-1](https://doi.org/10.1016/0014-4835(77)90136-1)
- Mehrzadi, S., Hemati, K., Reiter, R.J., Hosseinzadeh, A., 2020. Mitochondrial dysfunction in age-related macular degeneration: melatonin as a potential treatment. *Expert Opin. Ther. Targets* 24, 359–378. <https://doi.org/10.1080/14728222.2020.1737015>
- Mendoza, M., Caselli, L., Salvatore, A., Montis, C., Berti, D., 2019. Nanoparticles and organized lipid assemblies: From interaction to design of hybrid soft devices. *Soft*

Matter 15, 8951–8970. <https://doi.org/10.1039/c9sm01601e>

Meng, T., Kulkarni, V., Simmers, R., Brar, V., Xu, Q., 2019. Therapeutic implications of nanomedicine for ocular drug delivery. *Drug Discov. Today* 00. <https://doi.org/10.1016/j.drudis.2019.05.006>

Mirzaeei, S., Barfar, D., 2022. Design and Development of Antibacterial/Anti-inflammatory Dual Drug-Loaded Nanofibrous Inserts for Ophthalmic Sustained Delivery of Gentamicin and Methylprednisolone: In Vitro Bioassay, Solvent, and Method Effects' Evaluation. *Adv. Pharm. Bull.* 12, 531–540. <https://doi.org/10.15171/jcvtr.2015.24>

Mirzaeei, S., Berenjian, K., Khazaei, R., 2018. Preparation of the potential ocular inserts by electrospinning method to achieve the prolong release profile of triamcinolone acetonide. *Adv. Pharm. Bull.* 8, 21–27. <https://doi.org/10.15171/apb.2018.003>

Mishima, S., Gasset, A., Klyce, S.D., 1966. Determination of tear volume and tear flow. *Investig. Ophthalmol. Vis. Sci.* 5, 264–276.

Mitchell, P., Liew, G., Gopinath, B., Wong, T.Y., 2018. Age-related macular degeneration. *Lancet* 392, 1147–1159. [https://doi.org/10.1016/S0140-6736\(18\)31550-2](https://doi.org/10.1016/S0140-6736(18)31550-2)

Mohanty, A., Uthaman, S., Park, I.K., 2020. Utilization of polymer-lipid hybrid nanoparticles for targeted anti-cancer therapy. *Molecules* 25. <https://doi.org/10.3390/molecules25194377>

Moiseev, R. V., Morrison, P.W.J., Steele, F., Khutoryanskiy, V. V., 2019. Penetration enhancers in ocular drug delivery. *Pharmaceutics* 11. <https://doi.org/10.3390/pharmaceutics11070321>

Monteiro, M.C., Coleman, M.D., Hill, E.J., Prediger, R.D., Maia, C.S.F., 2017.

- Neuroprotection in Neurodegenerative Disease: From Basic Science to Clinical Applications. *Oxid. Med. Cell. Longev.* 2017, 1–4. <https://doi.org/10.1155/2017/2949102>
- Morais, M., Coimbra, P., Pina, M.E., 2021. Comparative analysis of morphological and release profiles in ocular implants of acetazolamide prepared by electrospinning. *Pharmaceutics* 13, 1–14. <https://doi.org/10.3390/pharmaceutics13020260>
- Morita, Y., Ohtori, A., Kimura, M., Tojo, K., 1998. Intravitreal Delivery of Dexamethasone Sodium m-Sulfobenzoate from Poly(DL-Lactic Acid) Implants. *Biol. Pharm. Bull.* 21, 188–190.
- Musumeci, T., Bonaccorso, A., Carbone, C., Russo, G., Pappalardo, F., Puglisi, G., 2019. Design and optimization of PEGylated nanoparticles intended for Berberine Chloride delivery. *J. Drug Deliv. Sci. Technol.* 52, 521–530. <https://doi.org/10.1016/j.jddst.2019.05.012>
- Musumeci, T., Bucolo, C., Carbone, C., Pignatello, R., Drago, F., Puglisi, G., 2013. Polymeric nanoparticles augment the ocular hypotensive effect of melatonin in rabbits. *Int. J. Pharm.* 440, 135–140. <https://doi.org/10.1016/j.ijpharm.2012.10.014>
- Nair, K.G.S., Velmurugan, R., Sukumaran, S.K., 2020. Formulation and Optimization of Ansamycin-Loaded Polymeric Nanoparticles Using Response Surface Methodology for Bacterial Meningitis. *Bionanoscience* 10, 279–291. <https://doi.org/10.1007/s12668-019-00713-0>
- Namjoshi, S., Dabbaghi, M., Roberts, M.S., Grice, J.E., Mohammed, Y., 2020. Quality by design: Development of the quality target product profile (QTPP) for semisolid topical products. *Pharmaceutics* 12.
- <https://doi.org/10.3390/pharmaceutics12030287>

- Narvekar, P., Bhatt, P., Fnu, G., Sutariya, V., 2019. Axitinib-Loaded Poly(Lactic-Co-Glycolic Acid) Nanoparticles for Age-Related Macular Degeneration: Formulation Development and in Vitro Characterization. *Assay Drug Dev. Technol.* 17, 167–177. <https://doi.org/10.1089/adt.2019.920>
- Netsomboon, K., Bernkop-Schnürch, A., 2016. Mucoadhesive vs. mucopenetrating particulate drug delivery. *Eur. J. Pharm. Biopharm.* 98, 76–89. <https://doi.org/10.1016/j.ejpb.2015.11.003>
- Omer, S., Zelkó, R., 2021. A systematic review of drug-loaded electrospun nanofiber-based ophthalmic inserts. *Pharmaceutics* 13. <https://doi.org/10.3390/pharmaceutics13101637>
- Ortiz, A.C., Yañez, O., Salas-Huenuleo, E., Morales, J.O., 2021. Development of a nanostructured lipid carrier (NLC) by a low-energy method, comparison of release kinetics and molecular dynamics simulation. *Pharmaceutics* 13. <https://doi.org/10.3390/pharmaceutics13040531>
- Osborne, N.N., Wood, J.P.M., Cupido, A., Melena, J., Chidlow, G., 2002. Topical flunarizine reduces IOP and protects the retina against ischemia-excitotoxicity. *Investig. Ophthalmol. Vis. Sci.* 43, 1456–1464.
- Oyewumi, M.O., Wehrung, D., Sadana, P., 2016. Gelucire-stabilized nanoparticles as a potential DNA delivery system. *Pharm. Dev. Technol.* 21, 647–654. <https://doi.org/10.3109/10837450.2015.1041043>
- Pallagi, E., Ambrus, R., Szabó-Révész, P., Csóka, I., 2015. Adaptation of the quality by design concept in early pharmaceutical development of an intranasal nanosized formulation. *Int. J. Pharm.* 491, 384–392. <https://doi.org/10.1016/j.ijpharm.2015.06.018>

- Pandit, J., Sultana, Y., Aqil, M., 2021. Chitosan coated nanoparticles for efficient delivery of bevacizumab in the posterior ocular tissues via subconjunctival administration. *Carbohydr. Polym.* 267, 118217. <https://doi.org/10.1016/j.carbpol.2021.118217>
- Pannuzzo, M., Horta, B.A.C., La Rosa, C., Decuzzi, P., 2020. Predicting the Miscibility and Rigidity of Poly(lactic- co-glycolic acid)/Polyethylene Glycol Blends via Molecular Dynamics Simulations. *Macromolecules* 53, 3643–3654. <https://doi.org/10.1021/acs.macromol.0c00110>
- Paredes, S.D., Rancan, L., Kireev, R., González, A., Louzao, P., González, P., Rodríguez-Bobada, C., García, C., Vara, E., Tresguerres, J.A.F., 2015. Melatonin Counteracts at a Transcriptional Level the Inflammatory and Apoptotic Response Secondary to Ischemic Brain Injury Induced by Middle Cerebral Artery Blockade in Aging Rats. *Biores. Open Access* 4, 407–416. <https://doi.org/10.1089/biores.2015.0032>
- Park, J., Bungay, P.M., Lutz, R.J., Augsburger, J.J., Millard, R.W., Roy, A.S., Banerjee, R.K., 2005. Evaluation of coupled convective-diffusive transport of drugs administered by intravitreal injection and controlled release implant. *J. Control. Release* 105, 279–295. <https://doi.org/10.1016/j.jconrel.2005.03.010>
- Patrojanasophon, P., Tidjarat, S., Opanasopit, P., Ngawhirunpat, T., Rojanarata, T., 2020. Influence of nanofiber alignment on the release of a water-soluble drug from cellulose acetate nanofibers. *Saudi Pharm. J.* 28, 1210–1216. <https://doi.org/10.1016/j.jsps.2020.08.011>
- Peng, R., Dai, W., Li, Y., 2018. Neuroprotective effect of a physiological ratio of testosterone and estradiol on corticosterone-induced apoptosis in PC12 cells via Traf6/TAK1 pathway. *Toxicol. Vitro.* 50, 257–263. <https://doi.org/10.1016/j.tiv.2018.03.018>

- Pescosolido, N., Barbato, A., Giannotti, R., Komaiha, C., Lenarduzzi, F., 2016. Age-related changes in the kinetics of human lenses: Prevention of the cataract. *Int. J. Ophthalmol.* 9, 1506–1517. <https://doi.org/10.18240/ijo.2016.10.23>
- Peynshaert, K., Devoldere, J., De Smedt, S.C., Remaut, K., 2018. In vitro and ex vivo models to study drug delivery barriers in the posterior segment of the eye. *Adv. Drug Deliv. Rev.* 126, 44–57. <https://doi.org/10.1016/j.addr.2017.09.007>
- Pitkänen, L., Ranta, V.P., Moilanen, H., Urtili, A., 2005. Permeability of retinal pigment epithelium: Effects of permeant molecular weight and lipophilicity. *Investig. Ophthalmol. Vis. Sci.* 46, 641–646. <https://doi.org/10.1167/iovs.04-1051>
- Place, E.S., George, J.H., Williams, C.K., Stevens, M.M., 2009. Synthetic polymer scaffolds for tissue engineering. *Chem. Soc. Rev.* 38, 1139–1151. <https://doi.org/10.1039/b811392k>
- Platania, C.B.M., Dei Cas, M., Cianciolo, S., Fidilio, A., Lazzara, F., Paroni, R., Pignatello, R., Stretto, E., Ghidoni, R., Drago, F., Bucolo, C., 2019. Novel ophthalmic formulation of myriocin: implications in retinitis pigmentosa. *Drug Deliv.* 26, 237–243. <https://doi.org/10.1080/10717544.2019.1574936>
- Polat, H.K., Bozdağ Pehlivan, S., Özkul, C., Çalamak, S., Öztürk, N., AYTEKİN, E., FIRAT, A., ULUBAYRAM, K., KOCABEYOĞLU, S., İRKEÇ, M., ÇALIŞ, S., 2020. Development of besifloxacin HCl loaded nanofibrous ocular inserts for the treatment of bacterial keratitis: In vitro, ex vivo and in vivo evaluation. *Int. J. Pharm.* 585. <https://doi.org/10.1016/j.ijpharm.2020.119552>
- Popov, A., Enlow, E., Bourassa, J., Chen, H., 2016. Mucus-penetrating nanoparticles made with “mucoadhesive” poly(vinyl alcohol). *Nanomedicine Nanotechnology, Biol. Med.* 12, 1863–1871. <https://doi.org/10.1016/j.nano.2016.04.006>

- Prausnitz, M.R., 1998. Permeability of cornea, sciera, and conjunctiva: A literature analysis for drug delivery to the eye. *J. Pharm. Sci.* 87, 1479–1488. <https://doi.org/10.1021/js9802594>
- Qiu, F., Meng, T., Chen, Q., Zhou, K., Shao, Y., Matlock, G., Ma, X., Wu, W., Du, Y., Wang, X., Deng, G., Ma, J.X., Xu, Q., 2019. Fenofibrate-Loaded Biodegradable Nanoparticles for the Treatment of Experimental Diabetic Retinopathy and Neovascular Age-Related Macular Degeneration. *Mol. Pharm.* 16, 1958–1970. <https://doi.org/10.1021/acs.molpharmaceut.8b01319>
- Radwan, S.E.S., El-Moslemany, R.M., Mehanna, R.A., Thabet, E.H., Abdelfattah, E.Z.A., El-Kamel, A., 2022. Chitosan-coated bovine serum albumin nanoparticles for topical tetrandrine delivery in glaucoma: in vitro and in vivo assessment. *Drug Deliv.* 29, 1150–1163. <https://doi.org/10.1080/10717544.2022.2058648>
- Rawal, M., Singh, A., Amiji, M.M., 2019. Quality-by-Design Concepts to Improve Nanotechnology-Based Drug Development. *Pharm. Res.* 36. <https://doi.org/10.1007/s11095-019-2692-6>
- Razavi, M.S., Ebrahimnejad, P., Fatahi, Y., D’Emanuele, A., Dinarvand, R., 2022. Recent Developments of Nanostructures for the Ocular Delivery of Natural Compounds. *Front. Chem.* 10, 1–25. <https://doi.org/10.3389/fchem.2022.850757>
- Reardon, G., Kotak, S., Schwartz, G.F., 2011. Objective assessment of compliance and persistence among patients treated for glaucoma and ocular hypertension: A systematic review. *Patient Prefer. Adherence* 5, 441–463. <https://doi.org/10.2147/PPA.S23780>
- Ren, Z., Li, Yu, Zhang, R., Li, Yuanyuan, Yang, Z., Yang, H., 2017. Ferulic acid exerts neuroprotective effects against cerebral ischemia/reperfusion-induced injury via

- antioxidant and anti-apoptotic mechanisms in vitro and in vivo. *Int. J. Mol. Med.* 40, 1444–1456. <https://doi.org/10.3892/ijmm.2017.3127>
- Rivelli, G.G., Perez, A.C., Silva, P.H.R., Gomes, E.C. de L., Moreira, C.P. de S., Tamashiro, E., Valera, F.C.P., Anselmo-Lima, W.T., Pianetti, G.A., Silva-Cunha, A., 2021. Biodegradable Electrospun Nanofibers: A New Approach For Rhinosinusitis Treatment. *Eur. J. Pharm. Sci.* 163, 1–11. <https://doi.org/10.1016/j.ejps.2021.105852>
- Rodrigues de Azevedo, C., von Stosch, M., Costa, M.S., Ramos, A.M., Cardoso, M.M., Danhier, F., Pr at, V., Oliveira, R., 2017. Modeling of the burst release from PLGA micro- and nanoparticles as function of physicochemical parameters and formulation characteristics. *Int. J. Pharm.* 532, 229–240. <https://doi.org/10.1016/j.ijpharm.2017.08.118>
- Russo, L., Berardi, V., Tardani, F., La Mesa, C., Risuleo, G., 2013. Delivery of RNA and its intracellular translation into protein mediated by SDS-CTAB vesicles: Potential use in nanobiotechnology. *Biomed Res. Int.* 2013. <https://doi.org/10.1155/2013/734596>
- Sah, A.K., Suresh, P.K., Verma, V.K., 2017. PLGA nanoparticles for ocular delivery of loteprednol etabonate: a corneal penetration study. *Artif. Cells, Nanomedicine Biotechnol.* 45, 1156–1164. <https://doi.org/10.1080/21691401.2016.1203794>
- Sai, N., Dong, X., Huang, P., You, L., Yang, C., Liu, Y., Wang, W., Wu, H., Yu, Y., Du, Y., Leng, X., Yin, X., Qu, C., Ni, J., 2020. A novel gel-forming solution based on PEG-DSPE/Solutol HS 15 mixed micelles and gellan gum for ophthalmic delivery of curcumin. *Molecules* 25, 1–15. <https://doi.org/10.3390/molecules25010081>
- Sakurai, E., Ozeki, H., Kunou, N., Ogura, Y., 2001. Effect of particle size of polymeric

- nanospheres on intravitreal kinetics. *Ophthalmic Res.* 33, 31–36.
<https://doi.org/10.1159/000055638>
- Salmaso, S., Caliceti, P., 2013. Stealth Properties to Improve Therapeutic Efficacy of Drug Nanocarriers. *J. Drug Deliv.* 2013, 1–19. <https://doi.org/10.1155/2013/374252>
- Sampat, K.M., Garg, S.J., 2010. Complications of intravitreal injections. *Curr. Opin. Ophthalmol.* 21, 178–183. <https://doi.org/10.1097/ICU.0b013e328338679a>
- Sanders, E.J., Lin, W.Y., Parker, E., Harvey, S., 2010. Growth hormone expression and neuroprotective activity in a quail neural retina cell line. *Gen. Comp. Endocrinol.* 165, 111–119. <https://doi.org/10.1016/j.ygcen.2009.06.013>
- Sebbag, L., Moody, L.M., Mochel, J.P., 2020. Albumin levels in tear film modulate the bioavailability of medically-relevant topical drugs. *Front. Pharmacol.* 10, 1–9. <https://doi.org/10.3389/fphar.2019.01560>
- Senjoti, F.G., Timmins, P., Conway, B.R., Smith, A.M., 2020. Optimizing ophthalmic delivery of a poorly water soluble drug from an aqueous in situ gelling system. *Eur. J. Pharm. Biopharm.* 154, 1–7. <https://doi.org/10.1016/j.ejpb.2020.06.016>
- Shah, Sunny, Bhandari, B., Soniwala, M., Chavda, J., 2022. Lutein-Loaded Solid Lipid Nanoparticles for Ocular Delivery: Statistical Optimization and Ex Vivo Evaluation. *J. Pharm. Innov.* 17, 584–598. <https://doi.org/10.1007/s12247-021-09537-6>
- Shah, Saurabh, Famta, P., Raghuvanshi, R.S., Singh, S.B., Srivastava, S., 2022. Lipid polymer hybrid nanocarriers: Insights into synthesis aspects, characterization, release mechanisms, surface functionalization and potential implications. *Colloids Interface Sci. Commun.* 46, 100570. <https://doi.org/10.1016/j.colcom.2021.100570>
- Sharifi-Rad, M., Lankatillake, C., Dias, D.A., Docea, A.O., Mahomoodally, M.F., Lobine, D., Chazot, P.L., Kurt, B., Tumer, T.B., Moreira, A.C., Sharopov, F.,

- Martorell, M., Martins, N., Cho, W.C., Calina, D., Sharifi-Rad, J., 2020. Impact of natural compounds on neurodegenerative disorders: From preclinical to pharmacotherapeutics. *J. Clin. Med.* 9. <https://doi.org/10.3390/jcm9041061>
- Shi, J., Xu, Y., Xu, X., Zhu, X., Pridgen, E., Wu, J., Votruba, A.R., Swami, A., Zetter, B.R., Farokhzad, O.C., 2014. Hybrid lipid-polymer nanoparticles for sustained siRNA delivery and gene silencing. *Nanomedicine Nanotechnology, Biol. Med.* 10, e897–e900. <https://doi.org/10.1016/j.nano.2014.03.006>
- Shin, D.H., Lee, E., Kim, J.W., Kwon, B.S., Jung, M.K., Jee, Y.H., Kim, J., Bae, S.R., Chang, Y.P., 2004. Protective effect of growth hormone on neuronal apoptosis after hypoxia-ischemia in the neonatal rat brain. *Neurosci. Lett.* 354, 64–68. <https://doi.org/10.1016/j.neulet.2003.09.070>
- Shirley, M., 2020. Bimatoprost Implant: First Approval. *Drugs and Aging* 37, 457–462. <https://doi.org/10.1007/s40266-020-00769-8>
- Silva, B., São Braz, B., Delgado, E., Gonçalves, L., 2021. Colloidal nanosystems with mucoadhesive properties designed for ocular topical delivery. *Int. J. Pharm.* 606. <https://doi.org/10.1016/j.ijpharm.2021.120873>
- Singla, J., Bajaj, T., Goyal, A.K., Rath, G., 2019. Development of Nanofibrous Ocular Insert for Retinal Delivery of Fluocinolone Acetonide. *Curr. Eye Res.* 44, 541–550. <https://doi.org/10.1080/02713683.2018.1563196>
- So, K.S., Oh, J.E., Han, J.H., Jung, H.K., Lee, Y.S., Kim, S.H., Chun, Y.J., Kim, M.Y., 2008. Induction of apoptosis by a stilbene analog involves Bax translocation regulated by p38 MAPK and Akt. *Arch. Pharm. Res.* 31, 438–444. <https://doi.org/10.1007/s12272-001-1176-7>
- Somasundaran, S., Constable, I.J., Mellough, C.B., Carvalho, L.S., 2020. Retinal pigment

- epithelium and age-related macular degeneration: A review of major disease mechanisms. *Clin. Exp. Ophthalmol.* 48, 1043–1056. <https://doi.org/10.1111/ceo.13834>
- Song, R., Murphy, M., Li, C., Ting, K., Soo, C., Zheng, Z., 2018. Current development of biodegradable polymeric materials for biomedical applications. *Drug Des. Devel. Ther.* 12, 3117–3145. <https://doi.org/10.2147/DDDT.S165440>
- Souto, E.B., Wissing, S.A., Barbosa, C.M., Müller, R.H., 2004. Development of a controlled release formulation based on SLN and NLC for topical clotrimazole delivery. *Int. J. Pharm.* 278, 71–77. <https://doi.org/10.1016/j.ijpharm.2004.02.032>
- Subramaniam, B., Siddik, Z.H., Nagoor, N.H., 2020. Optimization of nanostructured lipid carriers: understanding the types, designs, and parameters in the process of formulations. *J. Nanoparticle Res.* 22. <https://doi.org/10.1007/s11051-020-04848-0>
- Sun, X., Sun, P., Liu, L., Jiang, P., Li, Y., 2021. Ferulic acid attenuates microglia-mediated neuroinflammation in retinal degeneration. *BMC Ophthalmol.* 21, 1–9. <https://doi.org/10.1186/s12886-020-01765-7>
- Sun, Y., Cheng, S., Lu, W., Wang, Y., Zhang, P., Yao, Q., 2019. Electrospun fibers and their application in drug controlled release, biological dressings, tissue repair, and enzyme immobilization. *RSC Adv.* 9, 25712–25729. <https://doi.org/10.1039/c9ra05012d>
- Suri, R., Neupane, Y.R., Mehra, N., Nematullah, M., Khan, F., Alam, O., Iqbal, A., Jain, G.K., Kohli, K., 2021. Sirolimus loaded chitosan functionalized poly (lactic-co-glycolic acid) (PLGA) nanoparticles for potential treatment of age-related macular degeneration. *Int. J. Biol. Macromol.* 191, 548–559. <https://doi.org/10.1016/j.ijbiomac.2021.09.069>

- Swetledge, S., Carter, R., Stout, R., Astete, C.E., Jung, J.P., Sabliov, C.M., 2021. Stability and ocular biodistribution of topically administered PLGA nanoparticles. *Sci. Rep.* 11, 1–11. <https://doi.org/10.1038/s41598-021-90792-5>
- Szwajgier, D., Borowiec, K., Pustelniak, K., 2017. The neuroprotective effects of phenolic acids: Molecular mechanism of action. *Nutrients* 9, 1–21. <https://doi.org/10.3390/nu9050477>
- Taghe, S., Mehrandish, S., Mirzaeei, S., 2022. Preparation of Azithromycin Nanofibers as Controlled Release Ophthalmic Drug Carriers Using Electrospinning Technique: In Vitro and In Vivo Characterization. *Adv. Pharm. Bull.* 12, 346–355. <https://doi.org/10.34172/apb.2022.033>
- Tamboli, V., Mishra, G.P., Mitra, A.K., 2011. Polymeric vectors for ocular gene delivery. *Ther. Deliv.* 2, 523–536. <https://doi.org/10.4155/tde.11.20>
- Tan, D.X., Manchester, L.C., Liu, X., Rosales-Corral, S.A., Acuna-Castroviejo, D., Reiter, R.J., 2013. Mitochondria and chloroplasts as the original sites of melatonin synthesis: A hypothesis related to melatonin's primary function and evolution in eukaryotes. *J. Pineal Res.* 54, 127–138. <https://doi.org/10.1111/jpi.12026>
- Tan, D.X., Manchester, L.C., Terron, M.P., Flores, L.J., Reiter, R.J., 2007. One molecule, many derivatives: A never-ending interaction of melatonin with reactive oxygen and nitrogen species? *J. Pineal Res.* 42, 28–42. <https://doi.org/10.1111/j.1600-079X.2006.00407.x>
- Tavakoli, S., Peynshaert, K., Lajunen, T., Devoldere, J., del Amo, E.M., Ruponen, M., De Smedt, S.C., Remaut, K., Urtti, A., 2020. Ocular barriers to retinal delivery of intravitreal liposomes: Impact of vitreoretinal interface. *J. Control. Release* 328, 952–961. <https://doi.org/10.1016/j.jconrel.2020.10.028>

- Tavares Luiz, M., Santos Rosa Viegas, J., Palma Abriata, J., Viegas, F., Testa Moura de Carvalho Vicentini, F., Lopes Badra Bentley, M.V., Chorilli, M., Maldonado Marchetti, J., Tapia-Blácido, D.R., 2021. Design of experiments (DoE) to develop and to optimize nanoparticles as drug delivery systems. *Eur. J. Pharm. Biopharm.* 165, 127–148. <https://doi.org/10.1016/j.ejpb.2021.05.011>
- Taylor, G., A, P.R.S.L., 1969. Electrically driven jets. *Proc. R. Soc. London. A. Math. Phys. Sci.* 313, 453–475. <https://doi.org/10.1098/rspa.1969.0205>
- Teixeira, M.C., Carbone, C., Souto, E.B., 2017. Beyond liposomes: Recent advances on lipid based nanostructures for poorly soluble/poorly permeable drug delivery. *Prog. Lipid Res.* 68, 1–11. <https://doi.org/10.1016/j.plipres.2017.07.001>
- Tian, B.C., Zhang, W.J., Xu, H.M., Hao, M.X., Liu, Y. Bin, Yang, X.G., Pan, W.S., Liu, X.H., 2013. Further investigation of nanostructured lipid carriers as an ocular delivery system: In vivo transcorneal mechanism and in vitro release study. *Colloids Surfaces B Biointerfaces* 102, 251–256. <https://doi.org/10.1016/j.colsurfb.2012.08.021>
- Toriu, N., Akaike, A., Yasuyoshi, H., Zhang, S., Kashii, S., Honda, Y., Shimazawa, M., Hara, H., 2000. Lomerizine, a Ca²⁺ channel blocker, reduces glutamate-induced neurotoxicity and ischemia/reperfusion damage in rat retina. *Exp. Eye Res.* 70, 475–484. <https://doi.org/10.1006/exer.1999.0809>
- Toro-Urrego, N., Garcia-Segura, L.M., Echeverria, V., Barreto, G.E., 2016. Testosterone protects mitochondrial function and regulates neuroglobin expression in astrocytic cells exposed to glucose deprivation. *Front. Aging Neurosci.* 8, 1–9. <https://doi.org/10.3389/fnagi.2016.00152>
- Valls, R., Vega, E., Garcia, M., Egea, M., Valls, J., 2008. Transcorneal Permeation in

- a Corneal Device of Non-Steroidal Anti-Inflammatory Drugs in Drug Delivery Systems. *Open Med. Chem. J.* 2, 66–71. <https://doi.org/10.2174/1874104500802010066>
- Varela-Fernández, R., Díaz-Tomé, V., Luaces-Rodríguez, A., Conde-Penedo, A., García-Otero, X., Luzardo-álvarez, A., Fernández-Ferreiro, A., Otero-Espinar, F.J., 2020. Drug delivery to the posterior segment of the eye: Biopharmaceutic and pharmacokinetic considerations. *Pharmaceutics* 12, 1–39. <https://doi.org/10.3390/pharmaceutics12030269>
- Vieira, R., Severino, P., Nalone, L.A., Souto, S.B., Silva, M., Lucarini, M., Durazzo, A., Santini, A., 2020. Sucupira Oil-Loaded Nanostructured Lipid Carriers (NLC): Lipid Screening, Factorial Design, Release Profile, and Cytotoxicity. *Molecules* 029, 1–22.
- Visan, A.I., Popescu-Pelin, G., Socol, G., 2021. Degradation behavior of polymers used as coating materials for drug delivery—a basic review. *Polymers (Basel)*. 13. <https://doi.org/10.3390/polym13081272>
- Wadhwa, S., Paliwal, R., Paliwal, S.R., Vyas, S.P., 2010. Hyaluronic acid modified chitosan nanoparticles for effective management of glaucoma: Development, characterization, and evaluation. *J. Drug Target.* 18, 292–302. <https://doi.org/10.3109/10611860903450023>
- Wang, Y., Xu, X., Gu, Y., Cheng, Y., Cao, F., 2018. Recent advance of nanoparticle-based topical drug delivery to the posterior segment of the eye. *Expert Opin. Drug Deliv.* 15, 687–701. <https://doi.org/10.1080/17425247.2018.1496080>
- Weng, Y., Liu, J., Jin, S., Guo, W., Liang, X., Hu, Z., 2017. Nanotechnology-based strategies for treatment of ocular disease. *Acta Pharm. Sin. B* 7, 281–291.

<https://doi.org/10.1016/j.apsb.2016.09.001>

Wildburger, N.C., Lin-Ye, A., Baird, M.A., Lei, D., Bao, J., 2009. Neuroprotective effects of blockers for T-type calcium channels. *Mol. Neurodegener.* 4, 1–8.

<https://doi.org/10.1186/1750-1326-4-44>

Williams, D.L., 2008. Oxidative Stress and the Eye. *Vet. Clin. North Am. - Small Anim. Pract.* 38, 179–192. <https://doi.org/10.1016/j.cvsm.2007.10.006>

Wolf, C., Gramer, E., Müller-Myhsok, B., Pasutto, F., Reinthal, E., Wissinger, B., Weisschuh, N., 2009. Evaluation of nine candidate genes in patients with normal tension glaucoma: A case control study. *BMC Med. Genet.* 10, 91.

<https://doi.org/10.1186/1471-2350-10-91>

Wong-riley, M., 2010. Energy metabolism of the visual system. *Eye Brain* 99–116.

Wu, H.J., Wu, C., Niu, H.J., Wang, K., Mo, L.J., Shao, A.W., Dixon, B.J., Zhang, J.M., Yang, S.X., Wang, Y.R., 2017. Neuroprotective Mechanisms of Melatonin in Hemorrhagic Stroke. *Cell. Mol. Neurobiol.* 37, 1173–1185.

<https://doi.org/10.1007/s10571-017-0461-9>

Wu, X.S., Wang, N., 2001. Synthesis, characterization, biodegradation, and drug delivery application of biodegradable lactic/glycolic acid polymers. Part II: Biodegradation. *J. Biomater. Sci. Polym. Ed.* 12, 21–34. <https://doi.org/10.1163/156856201744425>

Yadav, M., Schiavone, N., Guzman-Aranguez, A., Giansanti, F., Papucci, L., Perez de Lara, M.J., Singh, M., Kaur, I.P., 2020. Atorvastatin-loaded solid lipid nanoparticles as eye drops: proposed treatment option for age-related macular degeneration (AMD). *Drug Deliv. Transl. Res.* 10, 919–944. <https://doi.org/10.1007/s13346-020-00733-4>

Yagami, T., Ueda, K., Sakaeda, T., Itoh, N., Sakaguchi, G., Okamura, N., Hori, Y.,

- Fujimoto, M., 2004. Protective effects of a selective L-type voltage-sensitive calcium channel blocker, S-312-d, on neuronal cell death. *Biochem. Pharmacol.* 67, 1153–1165. <https://doi.org/10.1016/j.bcp.2003.11.005>
- Yamada, H., Chen, Y.N., Aihara, M., Araie, M., 2006. Neuroprotective effect of calcium channel blocker against retinal ganglion cell damage under hypoxia. *Brain Res.* 1071, 75–80. <https://doi.org/10.1016/j.brainres.2005.11.072>
- Yang, J.M., Su, W.Y., Leu, T.L., Yang, M.C., 2004. Evaluation of chitosan/PVA blended hydrogel membranes. *J. Memb. Sci.* 236, 39–51. <https://doi.org/10.1016/j.memsci.2004.02.005>
- Yang, X., Yu, X.W., Zhang, D.D., Fan, Z.G., 2020. Blood-retinal barrier as a converging pivot in understanding the initiation and development of retinal diseases. *Chin. Med. J. (Engl.)* 133, 2586–2594. <https://doi.org/10.1097/CM9.0000000000001015>
- Yang, Y., Jiang, S., Dong, Y., Fan, C., Zhao, L., Yang, X., Li, J., Di, S., Yue, L., Liang, G., Reiter, R.J., Qu, Y., 2015. Melatonin prevents cell death and mitochondrial dysfunction via a SIRT1-dependent mechanism during ischemic-stroke in mice. *J. Pineal Res.* 58, 61–70. <https://doi.org/10.1111/jpi.12193>
- Yeh, T.H., Hsu, L.W., Tseng, M.T., Lee, P.L., Sonjae, K., Ho, Y.C., Sung, H.W., 2011. Mechanism and consequence of chitosan-mediated reversible epithelial tight junction opening. *Biomaterials* 32, 6164–6173. <https://doi.org/10.1016/j.biomaterials.2011.03.056>
- Yi, C., Pan, X., Yan, H., Guo, M., Pierpaoli, W., 2005. Effects of melatonin in age-related macular degeneration. *Ann. N. Y. Acad. Sci.* 1057, 384–392. <https://doi.org/10.1196/annals.1356.029>
- Yu, Y., Feng, R., Li, J., Wang, Y., Song, Y., Tan, G., Liu, D., Liu, W., Yang, X., Pan, H.,

- Li, S., 2019. A hybrid genipin-crosslinked dual-sensitive hydrogel/nanostructured lipid carrier ocular drug delivery platform. *Asian J. Pharm. Sci.* 14, 423–434. <https://doi.org/10.1016/j.ajps.2018.08.002>
- Zanna, C., Ghelli, A., Porcelli, A.M., Karbowski, M., Youle, R.J., Schimpf, S., Wissinger, B., Pinti, M., Cossarizza, A., Vidoni, S., Valentino, M.L., Rugolo, M., Carelli, V., 2008. OPA1 mutations associated with dominant optic atrophy impair oxidative phosphorylation and mitochondrial fusion. *Brain* 131, 352–367. <https://doi.org/10.1093/brain/awm335>
- Zeng, J., Xu, X., Chen, X., Liang, Q., Bian, X., Yang, L., Jing, X., 2003. Biodegradable electrospun fibers for drug delivery. *J. Control. Release* 92, 227–231. [https://doi.org/10.1016/S0168-3659\(03\)00372-9](https://doi.org/10.1016/S0168-3659(03)00372-9)
- Zeng, L., Ma, W., Shi, L., Chen, X., Wu, R., Zhang, Y., Chen, Huaiwen, Chen, Hui, 2019. Poly(lactic-co-glycolic acid) nanoparticle-mediated interleukin-12 delivery for the treatment of diabetic retinopathy. *Int. J. Nanomedicine* 14, 6357–6369. <https://doi.org/10.2147/IJN.S214727>
- Zhang, H., Huang, X., Mi, J., Huo, Y., Wang, G., Xing, J., Gao, Y., 2014. Improvement of pulmonary absorptions of poorly absorbable drugs using Gelucire 44/14 as an absorption enhancer. *J. Pharm. Pharmacol.* 66, 1410–1420. <https://doi.org/10.1111/jphp.12274>
- Zhang, W., Li, X., Ye, T., Chen, F., Sun, X., Kong, J., Yang, X., Pan, W., Li, S., 2013. Design, characterization, and in vitro cellular inhibition and uptake of optimized genistein-loaded NLC for the prevention of posterior capsular opacification using response surface methodology. *Int. J. Pharm.* 454, 354–366. <https://doi.org/10.1016/j.ijpharm.2013.07.032>

- Zhang, W., Li, X., Ye, T., Chen, F., Yu, S., Chen, J., Yang, X., Yang, N., Zhang, J., Liu, J., Pan, W., Kong, J., 2014. Nanostructured lipid carrier surface modified with Eudragit RS 100 and its potential ophthalmic functions. *Int. J. Nanomedicine* 9, 4305–4315. <https://doi.org/10.2147/IJN.S63414>
- Zhao, Z., Lu, C., Li, T., Wang, W., Ye, W., Zeng, R., Ni, L., Lai, Z., Wang, X., Liu, C., 2018. The protective effect of melatonin on brain ischemia and reperfusion in rats and humans: In vivo assessment and a randomized controlled trial. *J. Pineal Res.* 65, 1–12. <https://doi.org/10.1111/jpi.12521>
- Zhao, Z., Ukidve, A., Krishnan, V., Mitragotri, S., 2019. Effect of physicochemical and surface properties on in vivo fate of drug nanocarriers. *Adv. Drug Deliv. Rev.* 143, 3–21. <https://doi.org/10.1016/j.addr.2019.01.002>
- Zhou, Y., Fang, A., Wang, F., Li, H., Jin, Q., Huang, L., Fu, C., Zeng, J., Jin, Z., Song, X., 2020. Core-shell lipid-polymer nanoparticles as a promising ocular drug delivery system to treat glaucoma. *Chinese Chem. Lett.* 31, 494–500. <https://doi.org/10.1016/j.ccllet.2019.04.048>
- Zhu, D., Zou, W., Cao, X., Xu, W., Lu, Z., Zhu, Y., Hu, X., Hu, J., Zhu, Q., 2022. Ferulic acid attenuates high glucose-induced apoptosis in retinal pigment epithelium cells and protects retina in db/db mice. *PeerJ* 10, 1–20. <https://doi.org/10.7717/peerj.13375>
- Zhukova, V., Osipova, N., Semyonkin, A., Malinovskaya, J., Melnikov, P., Valikhov, M., Porozov, Y., Solovev, Y., Kuliaev, P., Zhang, E., Sabel, B.A., Chekhonin, V., Abakumov, M., Majouga, A., Kreuter, J., Henrich-Noack, P., Gelperina, S., Maksimenko, O., 2021. Fluorescently labeled plga nanoparticles for visualization in vitro and in vivo: The importance of dye properties. *Pharmaceutics* 13.

<https://doi.org/10.3390/pharmaceutics13081145>

Zou, W., Liu, C., Chen, Z., Zhang, N., 2009. Preparation and characterization of cationic PLA-PEG nanoparticles for delivery of plasmid DNA. *Nanoscale Res. Lett.* 4, 982–992. <https://doi.org/10.1007/s11671-009-9345-3>

CHAPTER X: *Annexes*

List of Publications and Scientific Contributions

1. Publications

Coating Lacticaseibacillus rhamnosus GG in Alginate Systems: an Emerging Strategy Towards Improved Viability in Orange Juice.

Bonaccorso A., Russo N., **Romeo A.**, Carbone C., Grimaudo M.A., Alvarez-Lorenzo C., Randazzo C., Musumeci T., Caggia C. *AAPS PharmSciTech.*, 2021 Apr 5; 22(3):123.

<https://doi.org/10.1208/s12249-021-01996-x>

Ferulic Acid-Loaded Polymeric Nanoparticles for Potential Ocular Delivery.

Romeo, A.; Musumeci, T.; Carbone, C.; Bonaccorso, A.; Corvo, S.; Lupo, G.; Anfuso, C.D.; Puglisi, G.; Pignatello, R. *Pharmaceutics*, 2021, 13, 687.

<https://doi.org/10.3390/pharmaceutics13050687>

mPEG-PLGA Nanoparticles Labelled with Loaded or Conjugated Rhodamine-B for Potential Nose-to-Brain Delivery.

Craparo, E.F.; Musumeci, T.; Bonaccorso, A.; Pellitteri, R.; **Romeo, A.**; Naletova, I.; Cucci, L.M.; Cavallaro, G.; Satriano, C. *Pharmaceutics*, 2021, 13, 1508.

<https://doi.org/10.3390/pharmaceutics13091508>

Fluorescent Nanosystems for Drug Tracking and Theranostics: Recent Applications in the Ocular Field.

Zingale, E.*; **Romeo, A.***; Rizzo, S.; Cimino, C.; Bonaccorso, A.; Carbone, C.; Musumeci, T.; Pignatello, R. *Pharmaceutics*, 2022, 14, 955.

<https://doi.org/10.3390/pharmaceutics14050955>

* These authors contributed equally to this work.

Melatonin loaded hybrid nanomedicine: DoE approach, optimization and in vitro study on diabetic retinopathy model

Romeo A., Bonaccorso A., Carbone C., Lupo G., Anfuso C.D., Giurdanella G., Caggia C., Randazzo C., Russo N., Romano G.L., Bucolo C., Rizzo M., Tosi G., Duskey J.T., Ruozi B., Pignatello R., Musumeci T. *International Journal of Pharmaceutics*, 2022, 627, 122195

<https://doi.org/10.1016/j.ijpharm.2022.122195>

Multilevel statistical optimization: ion pair complexes with flunarizine dihydrochloride encapsulated in nanostructured lipid carriers for potential ocular delivery

In progress.

Electrospun nanofibers for melatonin ocular delivery

In progress.

2. Conference proceedings

Oral communications

Topical administration of melatonin-loaded lipid-polymer hybrid nanoparticles for posterior segment eye diseases.

NanoInnovation 2021 “YoungInnovation – Ophthalmic/Topical Delivery”, Facoltà d’Ingegneria Civile e Industriale, Sapienza Università di Roma, Via Eudossiana, 18, Roma, 21-24 September 2021. Invited Speaker

Melatonin-loaded hybrid nanoparticles for delivery to the posterior eye segment.

20th Advanced Course in Pharmaceutical Technology “Biologics in Therapy”, On-line, 27-29 September 2021.

Innovative nanoplatforms to improve melatonin ocular delivery.

XXI Scuola Dottorale in Tecnologia Farmaceutica "Strategie terapeutiche per le patologie vascolari: il ruolo della tecnologia farmaceutica", Dipartimento di Chimica e Tecnologie del Farmaco, Sapienza Università di Roma, 5-7 September 2022

Poster

Alginate-based microencapsulation for probiotics protection in orange juice matrix: a preliminary study.

Romeo A., Russo N., Grimaudo M.A., Alvarez-Lorenzo C., Musumeci T., Bonaccorso A., Carbone C., Randazzo C.L., Caggia C.

5th International Conference on Microbial Diversity, Catania, September 25th-27th, 2019. Poster presentation

Design of alginate based microcapsules for delivering of probiotic bacteria as functional supplement in fruit juice.

Bonaccorso A., **Romeo A.**, Russo N., Grimaudo M. A., Alvarez-Lorenzo C., Carbone C., Randazzo C. L., Caggia C., Puglisi G., Musumeci T.

CRS Italy Chapter 2019 Annual Workshop, Catania, November 7th-9th, 2019.

Mediterranean EO-NLC for potential intranasal delivery.

Cimino C., Bonaccorso A., **Romeo A.**, Musumeci T., Pignatello R., Carbone C.

12th World Meeting on Pharmaceutics, Biopharmaceutics and Pharmaceutical Technology, Vienna, Austria, May 11th-14th, 2021.

Polymeric Nanoparticles Delivering Ferulic Acid for Potential Ocular Application.

Romeo A., Musumeci T., Carbone C., Lo Faro M. J., Bonaccorso A., Cimino C., Anfuso C. D., Lupo G., Pignatello R.

XXVII Congresso Nazionale della Società Chimica Italiana 2021, On-line, September 14th-23th, 2021. Poster presentation

Nutraceuticals: new frontier for drug delivery application.

Bonaccorso A., Cimino C., Lombardo R., **Romeo A.**, Zingale E., Rizzo S., Carbone C., Musumeci T., Pignatello R.

Pharmaday 2022, Il Dipartimento incontra le Aziende, II edition, Catania, June 1st, 2022.

Novel mucoadhesive hybrid nanosystems for melatonin delivery to the posterior eye segment.

Romeo A., Bonaccorso A., Carbone C., Lupo G., Caggia C., Bucolo C., Milena R., Duskey J. T., Pignatello R., Musumeci T.

Pharmaday 2022, Il Dipartimento incontra le Aziende, II edition, Catania, June 1st, 2022. Poster presentation

Nanotechnology for ocular drug delivery: from design to characterization.

Zingale E., Cimino C., **Romeo A.**, Lombardo R., Bonaccorso A., Santonocito D. C., Carbone C., Musumeci T., Puglia C., Pignatello R.

Pharmaday 2022, Il Dipartimento incontra le Aziende, II edition, Catania, June 1st, 2022. Poster presentation

Nanofibers as a novel vehicle for melatonin ocular delivery.

A. Romeo, A. Bonaccorso, C. Carbone, A. Kazsoki, R. Zelkó, R. Pignatello and T. Musumeci. CRS Italy Local Chapter, Workshop 2022, Genova 7 – 9 October 2022. Poster presentation

Optimization of a novel mucoadhesive hybrid platform for topical melatonin delivery to the posterior eye segment: in vitro studies on a diabetic retinopathy model.

A. Romeo, A. Bonaccorso, G. Lupo, C. Caggia, J. T. Duskey, C. Bucolo, C. Carbone, R. Pignatello and T. Musumeci. AMYC-BIOMED 2022 Naples, 17-19 October 2022. Poster presentation